OPTICAL ANGULAR MOTION SENSOR

H. T. Braswell, et al

Chrysler Corporation

Prepared for:

Space and Missile Systems Organization

1 April 1975

SAMSO-TR-75-120

OPTICAL ANGULAR MOTION SENSOR PHASE ONE FINAL REPORT

Department of The Air Force

Headquarters Space and Missile Systems Organization

Los Angeles, California 90009

PREPARED UNDER CONTRACT NO. F04701-74-C-0062

BY CHRYSLER CORPORATION SPACE DIVISION

NEW ORLEANS, LOUISIANA

UNCLASSIFIED

SECURITY CLASSIFICATION OF THIS PAGE (When Data Entered)

REPORT DOCUMENTATION PAGE		READ INSTRUCTIONS BEFORE COMPLETING FORM
1 REPORT NUMBER SAMSO TR NO. 75-120	2 GOVT ACCESSION NO.	3 RECIPIENT'S CATALOG NUMBER AD-A011 592
4 TITLE (and Subtitle) Optical Angular Motion Sensor Phase One - Final Report		5 TYPE OF REPORT & PERIOD COVERED Technical Report 10-1-73 through 4-30-75 6 PERFORMING ORG REPORT NUMBER
7 AUTHOR(s) S. W. Paulson, et al		8 CONTRACT OR GRANT NUMBER(s) F04701-74-C-0062 new
9 PERFORMING ORGANIZATION NAME AND ADDRESS Chrysler Corporation Space Division New Orleans, Louisiana 70189		10 PROGRAM ELEMENT PROJECT, TASK AREA & WORK UNIT NUMBERS
11 CONTROLLING OFFICE NAME AND ADDRESS Department of the Air Force Headquarters Space and Missile Sys. Org. Los Angeles, California 90009		12 REPORT DATE 4-30-75 13 NUMBER OF PAGES 237
14 MONITORING AGENCY NAME & ADDRESS(if different from Controlling Office)		15 SECURITY CLASS (of this report) Unclassified 15a DECLASSIFICATION DOWNGRADING SCHEDULE

16 DISTRIBUTION STATEMENT (of this Report)

Distribution A - Unlimited

17 DISTRIBUTION STATEMENT (of the abstract entered in Block 20, if different from Report)

18 SUPPLEMENTARY NOTES

PRICES SUBJECT TO CHANGE

19 KEY WORDS (Continue on reverse side if necessary and identify by block number)

Triaxial Measurement	Polarization
Optical Angular Sensor	Angle Transfer
Alignment	5 Arc Seconds Accuracy

20 ABSTRACT (Continue on reverse side if necessary and identify by block number)

The Optical Angular Motion Sensor (OAMS) Program, Phase I, consisted of the design, fabrication, test and analysis of a Triaxial Angular Motion Sensor.

A brassboard system was fabricated and assembled. It included a transmitter, a receiver assembly and an electronics assembly. The alignment information was transmitted between the transmitter and receiver on three

DD FORM 1473 EDITION OF 65 IS OBSOLETE

UNCLASSIFIED

SECURITY CLASSIFICATION OF THIS PAGE (When Data Entered)

20. Continued.

discrete polarized light beams.

The preliminary design and parametric analysis review was performed on the Phase 0 Final Report, and the re-evaluation of this design furnished criteria for the basic design of the brassboard demonstration model.

The detail design and supporting analysis for the brassboard demonstration model includes electronics and optical components, thermal analysis, compensation circuitry and environmental stability to demonstrate the performance requirements. The selection of parts, materials and processes for the design and fabrication were in accordance with the required specifications.

The critical component testing and evaluation was performed on all components identified as critical to the sensor operation. These were the light emitting diodes, silicon photodetectors and the angle sensing crystals. These critical components were tested to show compliance with the sensor requirements. Testing also was performed on the optical components and their mechanical subassemblies to demonstrate the suitability over 0-140 degrees Fahrenheit temperature range.

The developmental testing was carried out on the brassboard demonstration model to evaluate the capability of the brassboard system to achieve the requirements and goals of the sensor specification.

The feasibility of utilizing polarization combined with the use of birefringent crystals for precision angular measurement was demonstrated. The brassboard system demonstrated that relative angular motion in roll, pitch and yaw could be performed to an accuracy of better than five arc seconds.

The polarization concepts utilized in the program resulted in an advancement in the state of the art in angular measurement. The non-imaging optical concept resulted in extremely small optical systems and the utilization of matched angle sensing crystals permitted translation of target within the field of view without developing a tracking error.

OPTICAL ANGULAR MOTION SENSOR

PHASE ONE

FINAL REPORT

CONTRACT NO. F04701-74-C-0062

PREPARED BY: H. T. BRASWELL, J. W. FONTENOT, L. L. HARTLEY, B. F. HEINRICH, W. E. MILLER, N. J. OCKMAN, S. W. PAULSON, J. R. TAYLOR

APPROVED BY: J. W. Fontenot APPROVED BY: Paul A. Weber USAF

DATE: 1 APRIL 1975 DATE: 1 MAY 75

DISTRIBUTION A - UNLIMITED

CHRYSLER CORPORATION SPACE DIVISION

NEW ORLEANS, LOUISIANA

SUMMARY

The Optical Angular Motion Sensor (OAMS) Program, Phase I, consisted of the design, fabrication, test and analysis of a Triaxial Angular Motion Sensor.

A brassboard system was fabricated and assembled. It included a transmitter, a receiver assembly and an electronics assembly. The alignment information was transmitted between the transmitter and receiver on three discrete polarized light beams.

The preliminary design and parametric analysis review was performed on the Phase 0 Final Report, and the re-evaluation of this design furnished criteria for the basic design of the brassboard demonstration model.

The detail design and supporting analysis for the brassboard demonstration model includes electronic and optical components, thermal analysis, compensation circuitry and environmental stability to demonstrate the performance requirements. The selection of parts, materials and processes for the design and fabrication were in accordance with the required specifications.

The critical component testing and evaluation was performed on all components identified as critical to the sensor operation. These were the light emitting diodes, silicon photodetectors and the angle sensing crystals. These critical components were tested to show compliance with the sensor requirements. Testing also was performed on the optical components and their mechanical subassemblies to demonstrate the suitability over 0-140 degrees Fahrenheit temperature range.

The developmental testing was carried out on the brassboard demonstration model to evaluate the capability of the brassboard system to achieve the requirement and goals of the sensor specifications.

The feasibility of utilizing polarization combined with the use of birefringent crystals for precision angular measurement was demonstrated. The brassboard system demonstrated that relative angular motion in roll, pitch and yaw could be performed to an accuracy of better than five arc seconds.

The polarization concepts utilized in the program resulted in an advancement in the state of the art in angular measurement. The non-imaging optical concept resulted in extremely small optical systems and the utilization of matched angle sensing crystals permitted translation of target within the field of view without developing a tracking error.

PREFACE

Chrysler Corporation Space Division (CCSD) submits this final report, which covers the work performed in compliance with the work statement of contract F04701-74-C-0062. This contract was issued by the Department of the Air Force, Headquarters Space and Missile Systems Organization (SAMSO), AF Unit Post Office, Los Angeles, California 90009.

The program included design, fabrication and testing of a 3-axis Optical Angular Motion Sensor (OAMS) brassboard demonstration model. This model is to be used in the triaxial measurements of alignment between two separated devices. It also included issue of critical item specifications, test and evaluation of critical components, temperature tests of brassboard, development and test of time division multiplex concept and extensive theoretical and actual performance analysis.

The authors acknowledge many helpful discussions with Messrs. M. Arck, J. Redman, S. Marcus, E. Farr and Dr. T. Kazangey of Aerospace Corporation, and Lt. G. Shaw of SAMSO.

TABLE OF CONTENTS

Section		Page
	DD FORM 1473	i
	SUMMARY	iv
	PREFACE	v
1.0	INTRODUCTION	1-1
2.0	OBJECTIVE	2-1
	2.1 General	2-1
	2.2 Design	2-6
	2.3 Summary of Results	2-6
	2.4 Applicable Documents	2-7
3.0	POLARIZATION TECHNIQUES	3-1
	3.1 Polarization	3-1
	3.2 Roll Axis	3-2
	3.3 Lateral Axis	3-4
4.0	RECOMMENDED CONCEPT	4-1
	4.1 Considerations	4-1
	4.2 Design Selection	4-1
	4.3 Conceptual Design	4-2
5.0	PARAMETRIC ANALYSIS	5-1
6.0	BRASSBOARD DESIGN TRADE-OFFS	6-1
	6.1 Operational Trade-Offs	6-1
	6.2 Performance	6-2
	6.3 Noise Equivalent Angle Versus Source Power	6-2
	6.4 Temperature Effects on NEA	6-2
	6.5 Thermo-Electric Coolers	6-2
	6.6 Goals Versus Requirements	6-2
	6.7 Cost	6-3
7.0	RELIABILITY AND LIFETIME	7-1
	7.1 Sources	7-1
	7.2 Optical Components	7-1
	7.3 Detectors	7-1
	7.4 Power, Weight and Size	7-1
8.0	BRASSBOARD DESIGN	8-1
	8.1 Preliminary Design and Analysis	8-1
	8.1.1 System Analysis	8-1
	8.1.2 System Equation	8-1
	8.1.3 Analysis Review	8-8
	8.1.4 LED Intensity Control Loop - General	8-10
	8.1.5 LED Intensity Control Loop Analysis	8-12
	8.1.6 Extension of Analysis to Lateral Channels	8-15
	8.1.7 Background Illumination and Detector Noise Considerations	8-19
	8.1.8 Noise Evaluation	8-20
	8.1.9 Background Illumination	8-26
	8.2 Optical Design	8-27
	8.2.1 Transmitter	8-27
	8.2.2 Receiver	8-31
	8.2.3 Off-Axis Imagery	8-37

TABLE OF CONTENTS

Section			Page
	8.3	Mechanical Design	8-38
		8.3.1 Mechanical Design - General	8-38
		8.3.2 Transmitter Design	8-38
		8.3.3 Receiver Design	8-44
		8.3.4 Thermal Analysis	8-45
	8.4	Electronic Design	8-49
		8.4.1 LED Drive and Control Loop	8-49
		8.4.2 Signal Processing Electronic	8-52
		8.4.3 Electronic Component Description	8-56
		8.4.4 Wiring Diagram and Circuit Board Layouts	8-63
	8.5	Component Testing	8-70
		8.5.1 Light Emitting Diodes	8-70
		8.5.2 Detectors	8-79
		8.5.3 Angle Sensing Crystals	8-88
		8.5.4 Optical Filters	8-88
		8.5.5 Wollaston Prism	8-95
	8.6	Subassembly Tests	8-98
9.0	SYSTEM TEST AND EVALUATION		9-1
	9.1	General	9-1
	9.2	Stability and Warmup Tests	9-1
		9.2.1 Stability	9-1
		9.2.2 Warmup	9-1
		9.2.3 Interference Between Channels	9-4
	9.3	Calibration	9-4
		9.3.1 General	9-4
	9.4	Accuracy Tests	9-7
		9.4.1 Cross Coupling Accuracy	9-7
		9.4.2 Extended Angular Range	9-7
		9.4.3 Light Level Control	9-7
		9.4.4 Translation	9-18
	9.5	Response Time	9-18
		9.5.1 Response Time System One	9-18
		9.5.2 Response Time System Two	9-18
	9.6	Background Radiation	9-18
	9.7	Input Power Tests	9-25
	9.8	General System Characteristics	9-25
		9.8.1 Weight and Dimensions	9-25
		9.8.2 Signal to Noise	9-25
		9.8.3 Power Consumption	9-25
	9.9	Temperature Effects	9-25
	9.10	Coordinate Relationships for System Evaluation and Application	9-33
		9.10.1 General Considerations	9-33
		9.10.2 Coordinate Transformation for System Evaluation	9-33

TABLE OF CONTENTS

Section		Page
10.0	CONCLUSIONS AND RECOMMENDATIONS	10-1
11.1	REFERENCES A D BIBLIOGRAPHY	11-1
Appendix A	Mueller Matrix Methods	
Appendix B	Far Field Irradiance of an LED and Lens Combination	
Appendix C	Electronic Time Sharing System	
Appendix D	Modulated LED Systems	
Appendix E	Error Analysis	
Annex	Technical Requirements	

FIGURES

Number		Page
3-1	Angle Sensing Crystal	3-3
8-1	Transmitter-Receiver	8-2
8-2	Simplified Block Diagram	8-5
8-3	LED Drive Signals	8-9
8-4	LED Drive Signal Block Diagram	8-13
8-5	Open Loop System Block Diagram	8-14
8-6	Open and Closed Loop System Block Diagrams	8-14
8-7	System Block Diagram	8-17
8-8	Transmitter Optical Design	8-28
8-9	LED Selection	8-29
8-10	Receiver Optical Design	8-32
8-11	Receiver Design Details	8-33
8-12	Immersion Lens	8-34
8-13	Ray Trace Results for 1^{o} Off-Axis Object	8-37
8-14	OAMS System Three Assemblies (SKC 835)	8-39
8-14A	OAMS Brassboard Hardware	8-40
8-14B	OAMS Transmitter and Receiver Hardware	8-41
8-15	Transmitter Mechanical Design (SKC 833)	8-42
8-16	Receiver Mechanical Design (SKC 834)	8-43
8-17	Calculated Temperatures Across Transmitter	8-47
8-18	Cross Section of Thermal Analysis Location	8-48
8-19	Electronic Subsystem Block Diagram	8-50
8-20	Electronic Schematic Pitch Channel (SKC 837-P)	8-64
8-21	Electronic Schematic Yaw Channel (SKC 837-Y)	8-65
8-22	Electronic Schematic Roll Channel (SKC 837-R)	8-66
8-23	Proposed LED Control Scheme	8-67
8-24	Electronic Power Supply Schematic (SKC 838)	8-68
8-25	Wiring Diagram (SKC 839)	8-69
8-26	Example of LED Profiles	8-74
8-27	Two Dimensional LED Profile	8-75
8-28	Relative LED Output Within Subtended Angle	8-76
8-29	Spectral Profile	8-77
8-30	LED Response to Drive Current	8-78
8-31	LED Temperature Dependence of LED Output and Efficiency	8-80
8-32	LED Warmup	8-81
8-33	LED Spectral Characteristics vs Forward Current	8-82
8-34	LED Reliability Data	8-83
8-35	LED Output Degradation vs Elapsed Time	8-84
8-36	Detector Output Drift with Temperature	8-85
8-37	Detector Offset and Drift	8-86
8-38	Amplifier Offset Voltage and Drift	8-87
8-39	Detector and LED Distortion	8-89

FIGURES

Number		Page
8-40	Detector and LED Frequency Response	8-90
8-41	Summary of Broadband Detector Noise	8-91
8-42	Detector Offset and Change with Temperature	8-92
8-43	Summary of Broadband Detector Noise	8-93
8-44	Relative Filter Transmisssion and Channel Interference	8-94
8-45	Roll Filter Spectral Transmission	8-96
8-46	Filter Characteristics	8-97
8-47	LED/Detector Temperature Response	8-99
8-48	Transmitter Subassembly Test	8-100
8-49	Receiver Subassembly Test	8-101
8-50	Temperature Effect on Transmission	8-102
8-51	Temperature Effect on Signal Amplitude	8-103
9-1	System Warm Up Time	9-5
9-2	Pitch Response and Calibration	9-9
9-3	Yaw Response and Calibration	9-10
9-4	Roll Response and Calibration	9-11
9-5	Pitch Response with Extended Range	9-14
9-6	Yaw Response with Extended Range	9-15
9-7	Roll Response with Extended Range	9-16
9-8	Change in DC Sum with Pitch Angle Only	9-17
9-9	Effect of Line of Sight Translation	9-19
9-10	Effect of Lateral Translation	9-20
9-11	System Response to Background Radiation	9-23
9-12	DC Sum Response to Background Radiation	9-24
9-13	System Response with Background Radiation at Various Angles	9-26
9-14	D.C. Sum Response with Background Radiation at Various Angles	9-27
9-15	Input Power Tests 0-36 Volts	9-28
9-16	Input Power Tests 24-33 Volts	9-29
9-17	Temperature Effect on Pitch Transmitter and Receiver	9-31
9-18	Temperature Effects on Pitch System	9-32
9-19	Coordinate System	9-34
9-20	Pitch Coordinates	9-36
9-21	Yaw Coordinates	9-36
9-22	Roll Coordinates	9-37

TABLES

Number		Page
8-1	OAMS Phase One Noise Measurements Range 25 Ft.	8-23
8-2	OAMS Phase One Noise Measurements Range 5 Ft.	8-24
8-3	Summary of OAMS Phase One Random Errors	8-25
8-4	Optical Components	8-35
8-5	OAMS Operating Ranges	8-52
8-6	OAMS Filter Characteristics	8-55
8-7	Electronic Units and Location Assignment	8-57
8-8	LED Characteristics	8-60
8-9	Component Testing Summary	8-71
8-10	LEDs in Evaluation	8-72
8-11	Summary of LEDs	8-73
9-1	System Test and Evaluation Outline	9-2
9-2	Stability and Warmup	9-3
9-3	Interference Between Channels	9-6
9-4	Transformation Equations	9-8
9-5	Calibration Error without Crosscoupling	9-12
9-6	Calibration Error with Crosscoupling	9-13
9-7	Translation Effect	9-21
9-8	Response Time	9-22
9-9	Noise on System Output Signals	9-30
9-10	Source of Errors	9-41
9-11A	Evaluation of Test Results	9-42
9-11B	Evaluation of Test Results	9-43
9-11C	Evaluation of Test Results	9-44
9-11D	Error Evaluation	9-45

1.0 INTRODUCTION

In many spacecraft applications, the angular alignment of one device with respect to another must be known precisely. If practical in the layout of the spacecraft, the two devices would be attached physically to a common rigid structure which would maintain the angular alignment between them. Under certain conditions, mechanical strains and differential thermal expansion as well as an appreciable separation between the two devices make the maintaining of alignment by physical restraint difficult if not impossible. Under these conditions, a third device is required to monitor continuously the angular motions of one or more of the devices with respect to the designated reference device.

There is presently no system capable of monitoring the relative alignment with sufficient accuracy for precision space applications. The Optical Angular Motion Sensor (OAMS) offers a solution. It will monitor angular deviations and can provide signals to permit corrections to be made for misalignments. The Phase 0 study performed under contract No. F04701-72-C-0389 resulted in the selection of polarized optical technology as the best candidate system to fulfill the requirements for accuracy, translation, response, environment and general requirements for adaptability to spacecraft application.

The development Phase I used the results obtained in Phase 0. The laboratory verification tests performed in Phase 0 were used as the basis for the OAMS brassboard demonstration model. The documentation and specifications that were produced during the Phase 0 study and used in the Phase I contract were:

Final Report - SAMSO TR-73-6

Performance Evaluation Test Plan - CEI No. 73-6-TP

Prime Item Development Specification - CEI No. 73-6

Critical Component Specifications

Silicon Photodetector - CEI No. 73-6-A

Emitting Source - Pitch Channel - CEI No. 73-6-B

Emitting Source - Yaw Channel - CEI No. 73-6-C

Emitting Source - Roll Channel - CEI No. 73-6-D

Angle Sensing Crystal - CEI No. 73-6-E

Potential areas of application for an OAMS system will give some insight as to the need for such an angle measuring device. Some important areas of application are:

a) Transfer reference alignment between guidance platform and tracking mounts

b) Alignment of communications satellite to earth

c) Alignment while tracking space targets

d) Angular monitoring of space objects

e) Transfer of alignment to mounts external to spacecraft

f) Transfer of alignment between tracker and pointing of high energy lasers

g) Missile aiming

h) Structure flexure monitoring

i) Earth limb roll measurement

This final report is intended to cover all requirements for analysis, design, development, fabrication, assembly, test and evaluation of the brassboard model of an Optical Angular Motion Sensor.

2.0 OBJECTIVE

2.1 General

The objective of Phase I was design, fabrication and testing of a 3-axis demonstration model of an Optical Angular Motion Sensor (OAMS). The model was classified as a brassboard configuration containing all components necessary for a complete OAMS system, although not necessarily packaged in their final shape and size. The design was also to go as far as practical toward the final configuration goal so that the transmitter and receiver could be calibrated, tested, evaluated and tested in a thermal environment.

2.1.1 Goals

The original requirements and goals of the program are detailed in the Annex of this report. The performance goals were a) angular deflection measurement to an accuracy of $\pm$ 1 arc second (3 axis 1 sigma), b) measurement range $\pm$1 degree about Line of Sight (LOS), and c) operation over a distance of 5 to 50 feet.

2.1.2 Engineering Tasks

The following major engineering tasks were performed.

a. Detail design and supporting analysis. Complete design and CI specifications for system.

b. Critical component testing and evaluation. Included temperature tests from 0 to 140°F.

c. Developmental tests.

2.1.3 Performance Requirements

The requirements and goals of the program are included in the Annex of this report. The following list defines the major performance parameters required for an OAMS system:

a. Functional characteristics

b. Performance characteristics

1. Measurement range
2. Calibration
3. Accuracy
4. Output signals
5. Saturation characteriscics
6. Response time
7. Operating distance
8. Temperature range

c. Mechanical interface

d. Functional interface

e. Optical interface

f. Volume

g. Weight

h. Multiple targets

i. Structure design

j. Nuclear survivability

2.1.4 Contract Data Requirements List

Documentation required for program

2.1.5 Amendment P0003 - Change of Specifications.

Testing to demonstrate suitability over 0-140°F for components and subassemblies.

2.1.6 Amendment P0004 - Material Cost Change

2.1.7 Amendment P0005 - Increased Tests & Evaluation and Extend Schedule

2.1.8 Amendment P0006

a. Design, build and analyze a single color LED multiplex system.

b. LED review and development and test of alternate single color sources.

2.1.9 Amendment P0007

Procure, test and evaluate new LED sources for pitch and yaw channels.

Perform brassboard testing with all control loops operating in at least one channel.

A summary of the results for each listed item follows:

Item 2.1.1: Complete design for performance as stated in a, b, and c. Due to LED power output limitations the range was reduced to 25 ft. by technical agreement. This distance met the requirements of the program but not the goal of 50 feet.

Item 2.1.2: Engineering Tasks completed:

a. Detail design

b. Critical component testing

c. Development tests

Item 2.1.3: Performance Requirements

a. Functional characteristics of the system met the general requirements of the OAMS system.

b. Performance characteristics met pitch and yaw prototype requirements. Roll signal to noise was high at 25 feet but subsequent improvements to the system reduced it to compare to the pitch and yaw channels.

The following primary requirements were:

1. Measurement range - The angular range met the goals of one degree in each axis.

2. Calibration - Calibration curves are generally a sine curve. They can be defined by a low order polynomial of less than six terms.

3. Accuracy - Systematic errors generally met the requirements of less than 5 arc seconds for the system at the $\pm$30 arc minute range. Dynamic error was between the requirements and the goal.

4. Output signals of the brassboard were generally 1 mv per arc second. This range was selected for ease of readout on the brassboard display. The output signals are adjustable

5. Saturation characteristic curves are figures 9.5, 9.6 and 9.7.

6. Response time of 10 hertz was met.

7. Operating distance was established at the required distance of 25 feet due to the output decrease in the LEDs of the pitch and yaw channels.

8. Temperature Range was 0-140°F and complete brassboard tests were performed. The performance was as expected except one channel became erratic below 32°F. This was attributed to some of the components not having been qualified to military specifications for this temperature range.

9. Power requirements were not a criteria for the brassboard.

c. Mechanical interface to be determined for prototype.

d. Functional interface to be determined for prototype.

e. Optical interface met requirements.

f. Volume of transmitter and receiver under prototype requirements. Electronics over prototype requirements. (Not required for brassboard).

g. Weight of transmitter and receiver within requirements. Electronics over prototype requirements. (Not required for brassboard).

h. Multiple targets - not applicable to brassboard.

i. Structure met mechanical and thermal requirements.

j. Nuclear survivability (study only).

Item 2.1.4: CDRL - All documents submitted.

The reports that were produced during the Phase I contract were:

General Test Plan (OAMS Brassboard) - CEI No. 73-6-TP, Rev. A

Critical Component Test Plans - CEI No. 73-6-CCTP

Configuration Prime Item Development Specification - CEI No. 73-6, Rev A

Configuration Item Critical Components Specifications:

Silicon Photodetector - CEI No. 73-6-A, Rev A

Emitting Source - Pitch Channel - CEI No. 73-6-B, Rev. A

Emitting Source - Yaw Channel - CEI No. 73-6-B, Rev. A

Emitting Source - Roll Channel - CEI No. 73-6-D, Rev. A

Angle Sensing Crystal - CEI No. 73-6-E, Rev. A

Final Technical Report - SAMSO TR-75-120

Item 2.1.5: Amendment P0003 - Specifications changes to 0-140°F for brassboard and tests performed over that temperature range.

Item 2.1.6: Amendment P0004 - Costs adjusted

Item 2.1.7: Amendment P0005 - Increased tests and evaluation. These were completed and were presented in final presentation and the tests reports are in section 8.5 and 9.0 of this report.

Item 2.1.8: Amendment P0006 - Completed design of single color multiplex. Fabricated breadboard of system. Rebuilt brassboard so that time division multiplex could be demonstrated. Demonstrated system at final TD presentation. Tested LEDs in time division multiplex mode. Selected, evaluated and purchased alternate source LEDs. Results in final report.

The test plans were updated as the program developed. The Prime Item Development Specification and the Critical Item Development Specifications were updated and reissued as tests and evaluations are completed during the test program.

The developmental tests on the demonstration model evaluated the model's ability to meet performance requirements of the contract, as described in this final report.

2.2 Design

The major design areas covered in Phase I were: Brassboard Design - Mechanical, Optical and Electronic. The design consisted of the following sub-assemblies and assemblies:

Light Emitting Diodes and Electronic Drivers

Silicon Photodetector and Preamplifier

Optical Subsystem - Transmitter

Optical Subsystem - Receiver

Transmitter Housing Assembly

Receiver Housing Assembly

Signal processing electronics packaged separately with interconnecting cables

Power Supply with Regulation Subsystem

Brassboard Optical Design

An optical analysis was performed for both transmitter and receiver assemblies.

Brassboard Electronic Design

Electronic block diagram, schematic diagrams and specifications were developed and analyzed from best performance criteria for signal-to-noise, accuracy, linearity, response, angular resolution and channel separation. The flight features required for extended operational life will include automatic light level gain control, LED balance control loop. The operational features of these AGC loops were verified on the brassboard model. Full automatic temperature control loops were not incorporated in the brassboard.

2.3 Summary of Results

2.3.1 Summary of Phase Zero Results

In the initial phase of the OAMS Program, concepts that could be used for angular measurement were identified and evaluated. A concept making use of the polarized nature of radiation and the interaction of polarized radiation in optical crystals was selected as the OAMS concept. The feasibility of the concept was proven analytically and demonstrated experimentally in the laboratory.

A preliminary design of an angular measurement system based upon the polarization concept was accomplished. The preliminary design included the generation of optical, mechanical and electrical drawings.

An OAMS system specification was generated and issued, critical components were identified and critical component specifications issued. These specifications, in combination with the schematics and drawings resulting from the preliminary design effort, served as a baseline for the development of an OAMS demonstration model.

The use of polarization techniques was evaluated for application to the problem. Three different polarization systems were analyzed for potential application to spacecraft requirements. Components, subsystems and systems were reviewed with an emphasis on ultimate spacecraft requirements and operational environment expected within a typical spacecraft.

The major considerations for the system were sensitivity, accuracy, performance, reliability, operating environment, weight, size, power required, vulnerability, operating life, maintenance, electro-magnetic interference, electromagnetic compatibility, achievement of goals and potential problem areas.

Since it was not practical to maintain or calibrate the equipment in orbit, consideration was made for automatic gain control (for light level changes) and automatic balance control.

The report included analytical studies of polarization approaches, signal-to-noise and noise equivalent angle, optical sources, detectors, modulation techniques, optical materials, thermal effects, signal processing, demodulation, channel separation and cross coupling effects between axes. Radiation effects on operational life and components were included in the study.

2.3.2 Performance Summary of Brassboard

The test results of the brassboard were generally within the prototype requirements. Translation errors were greater than expected. An analysis of this problem resulted in a redesign of the LED control loop to compensate for the variations in the energy profile of the LEDs while moving across the field of view. The new LED control loop is now installed in the brassboard.

The signal to noise ratio of the roll channel was lower than expected due to light levels. At 25 feet the resolution was below requirements but at 10 feet they were satisfactory. The internal optical system was degraded due to components variation from specifications. This situation was corrected during the program extension.

The Light Emitting Diodes in the pitch and yaw channels degraded during tests and in the brassboard tests. They are unsatisfactory for flight hardware and must be replaced by another type of LED.

2.4 Applicable Documents

The following documents were applicable to the OAMS Phase I Program.

Specifications:

Document No.	Date	
MIL-E-8983A	30 Nov. 71	Electronic Equipment, Aerospace Extended Space Environment, General Specification for
MIL-Q-9858A	16 Nov 63	Quality Program Requirements
USAF Specification Bulletin 515	3 Nov. 59	Control of Non-conforming Supplies
SAMSO CEI Spec. 73-6	31 Dec. 72	Prime Item Development Specification for an Optical Angular Motion Sensor
MIL-STD-891A	1 June 72	Contractor Part Control and Standardization Program
MIL-STD-1515	2 Oct. 72	Fasteners Used in the Design and Construction of Aerospace Mechanical Systems
SYGS Exhibit 10002 Revision 1	15 June 70 15 May 73	Nuclear Survivability
SAMSO-TR-73-6	31 Dec. 72	Optical Angular Motion Sensor Concept Definition and Preliminary Design Phase
Test Plan No. 73-6-TP	31 Dec. 72	Performance Evaluation Test Plan for the Engineering Prototype of an Optical Angular Motion Sensor

3.0 POLARIZATION TECHNIQUES

3.1 Polarization

Polarization is a property which defines the transverse nature of light electric waves. Fully polarized light is characterized by orientation of all the electric wave transverse planes in one direction. Unpolarized light is characterized by the transverse plane orientation being equally distributed in all directions. Partially polarized light is a combination of the two conditions.

Light or radiation is not fully defined until its stokes parameters are known. In 1852 G. G. Stokes defined four unique characteristics of light which fully describe its intensity and polarization components. The parameters are generally illustrated by the following vector referred to as the Stokes Vector.

$$\begin{bmatrix} S_0 \\ S_1 \\ S_2 \\ S_3 \end{bmatrix}$$

where S_0 - intensity of light (polarized and unpolarized)
S_1 - horizontal/(vertical) plane preference
S_2 - 45 degree/(-45 degree) plane preference
S_3 - right/(left) hand circular preference

These are the unique characteristics of polarized light that can be separated, identified and measured.

Each Stokes parameter has the dimension of intensity and applies to polarized light when treated as a quasi-monochromatic wave. Super-position techniques are used for wide optical bands not meeting the quasi-monochromatic condition by dividing it into a number of quasi-monochromatic wavelength bands. The parameter S_0 represents the total intensity. The parameter S_1 is equal to the excess in intensity of light transmitted by a polarizer that accepts linear polarization in the azimuth $\theta = 0$ degrees over the light transmitted by a polarizer that accepts linear polarization in the azimuth $\theta = 90$ degrees.

The parameter S_2 has a similar interpretation with respect to the azimuths $\theta = 45$ degrees and $\theta = 135$ degrees. Finally, the parameter S_3 is equal to the excess in intensity of light transmitted by a device that accepts right-handed circular polarization over the light transmitted by a device that accepts left-handed circular polarization. A positive Stokes parameter value indicates a horizontal, 45 deg., or right circular preference, whereas a negative value indicates its orthogonal component; that is, vertical, -45 degrees, or left circular preference.

The Stokes vector, in addition to defining polarized light characteristics also provides a useful tool for systematic analysis of polarized light. Through the use of Mueller matrices for polarized optical elements such as quarter-wave plates, polarizers, modulators, Wollastons and analogous components; it is possible to predict the resultant polarized light characteristics after passing through a series of these elements. Reference 1.

Techniques

Numerous polarization systems have been designed and built for measuring angles by means of measuring changing polarization parameters such as phase relationship. References 2, 3, 4, 5, 6, 7, 11.

The first phase of this study was the review of known polarization systems for adaptability to spacecraft requirements as outlined in the OAMS technical requirements for performance and design.

Earlier programs had utilized several modulation techniques which included rotating polarizers, oscillating crystals, Kerr cells, light choppers, electro-optical light modulators (EOLM), scanners, and source modulation.

Of this group, both the EOLM and source modulation have several advantages for use in OAMS system as such devices are static (non-moving). The polarization modulation technique can be demodulated with synchronous detection techniques offering excellent, narrow band, signal to noise characteristics. A disadvantage associated with the EOLM concept is the high operating voltage of the device. Modulation of the source with either continuous wave (CW) or pulses offers a low voltage system but results in more complex data handling subsystems. Reference 11.

A new system was developed which combines 2 LED sources multiplexed into a single modulated polarized light beam. This accomplished the advantages of the EOLM and low voltage modulation requirements of a spacecraft. This new system is described in detail in Appendix D. Further study of the various modulation concepts are performed in later stages of this study.

The next requirement was the projection of a polarized light beam from the transmitter with a defined polarization signature which will not change unless birefringence is introduced. This was accomplished by the use of birefringent crystals which establish and maintain the polarization characteristics as a function of the angular relationship of the light to the crystals.

3.2 Roll Axis

In the case of roll measurement about the line of sight, the modulated polarized light leaves the transmitter through a calcite crystal. This crystal orients the polarized light by means of the 2 optical axes of the crystal into a symmetrical distribution across the beam of light.

At the receiver, a matching crystal "senses" the polarization distribution on the beam of light and distributes this polarization according to the orientation of the planes of polarization. A roll between the transmitter and receiver will increase/or decrease the polarized light on each exit beam of the prism as a function of roll. The relationship of this polarization is sensed and distributed onto the two detectors by means of a Wollaston prism. The relative intensities on the two detectors are a measure of roll angle.

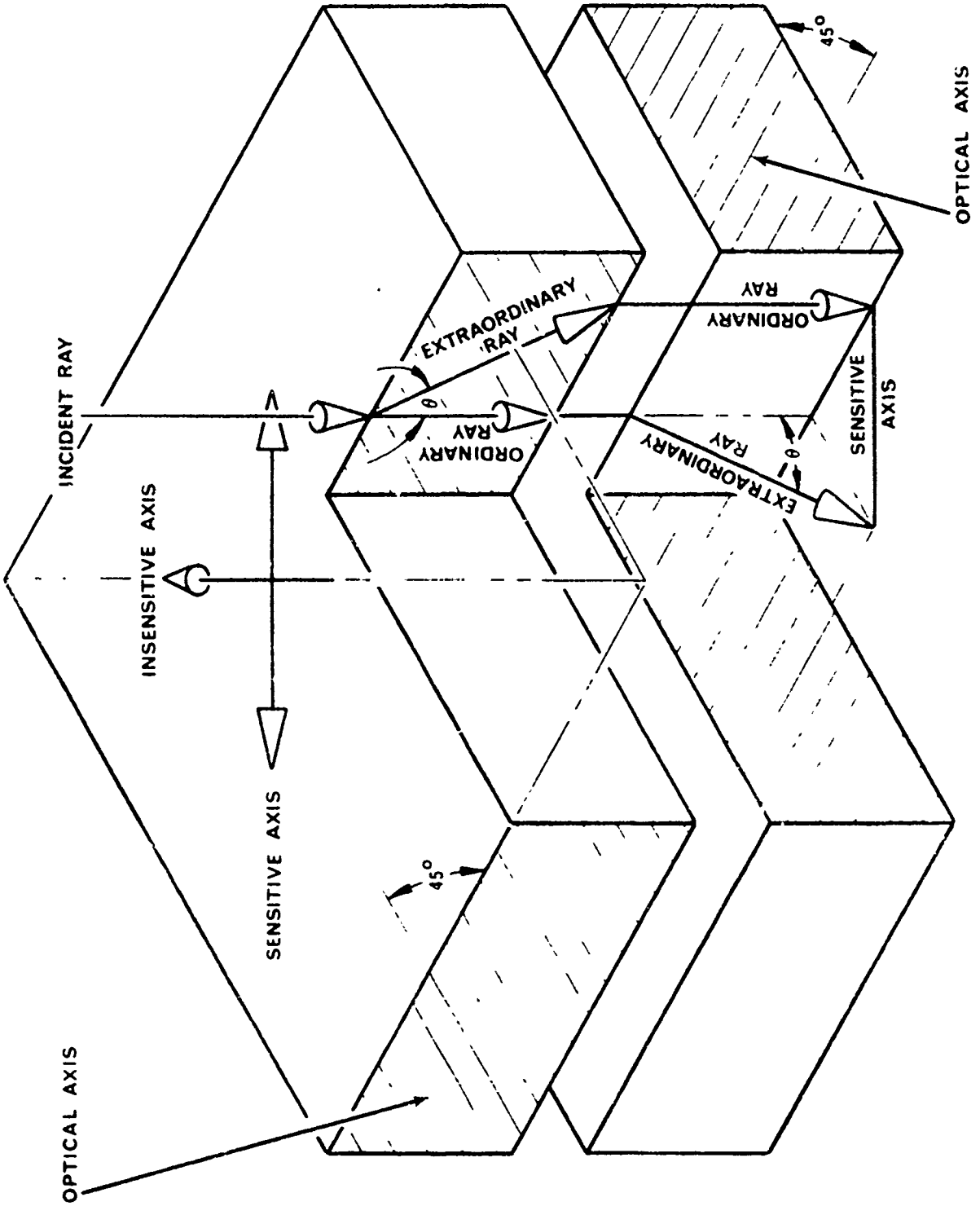
INCIDENT RAY
INSENSITIVE AXIS
SENSITIVE AXIS
OPTICAL AXIS
EXTRAORDINARY RAY
ORDINARY RAY
θ
45°
ORDINARY RAY
EXTRAORDINARY RAY
θ
SENSITIVE AXIS
45°
OPTICAL AXIS

A translation of the target across the light beam will not be sensed since the horizontal and vertical components of polarization are uniform across the entire cross section of the beam. Therefore, no change will occur at the prism and detectors due to lateral movement.

3.3 Lateral Axis

In the case of lateral axis sensing, polarization angle measuring concepts have been developed by Chrysler. The first axis consists of angle sensing crystals which were developed to introduce optical (polarization) phase shift between the ordinary and extraordinary rays as a function of the entrance angle of the light. The angle sensing crystals are two (2) identical birefringent crystals with the optical axis oriented at 45° to the surface of the crystal. The two crystals are turned at 90° to each other so that the extraordinary and ordinary rays of the polarized light passing through the first crystal were transposed in the second crystal as shown in Figure 3-1. Reference 11.

A zero optical phase shift between the E and O rays will occur for light perpendicular to the surface of the crystal. But for light not perpendicular, the phase retardation of the polarized light leaving the crystal will change as a function of the entrance angle. The crystals have one sensitive axis and one insensitive axis. The sensitivity of the angle sensing crystal is a function of the crystalline material and its thickness. Reference 6, 8, 9.

A matching crystal at the receiver, placed in opposition to the first crystal will compensate the angular retardation for small angular translation of the target within a projected cone of light. But it will sense and measure any relative angular change between the 2 crystals at any position in the cone of light.

The second axis is sensed in a manner identical to the first with the exception that the assembly is rotated exactly 90° to the first. The two channels are optically separated by differences in wavelength and optical filtering.

Analysis of various arrangements of these concepts are described in Appendices, A, D and E for application to the OAMS.

4.0 RECOMMENDED CONCEPT

4.1 Considerations

The three polarization/crystal concepts were analyzed and discussed in the Appendices of the Phase 0 report. Consideration was given to various combinations of crystals and includes multiplexing single sources with parallel light paths, and three discrete systems. An in-depth review of sources, detectors, modulation, demodulation and electronics was made and evaluated for operating life, packaging, reliability, signal to noise, weight, power required and other pertinent parameters.

The latest developments in Light Emitting Diodes (LEDs) were evaluated for lifetime, energy levels, efficiency, output geometry, size and applicability to the system. LEDs offer numerous advantages for spacecraft application and are discussed in detail. Tests and evaluations have been performed in the laboratory to determine actual performance characteristics. The latest developments in detectors were evaluated for sensitivity, detectivity, susceptibility to temperature, life and other important considerations. Modulation and demodulation were analyzed to determine the technique to be used in order to provide optimum system performance.

The hardware designs of both transmitter and receiver were considered for general applicability. The effects of thermal changes and gradients on the hardware were considered. The final design concept was predicated on the selection, test and evaluation of the components and subsystems.

After consideration of the analyses in appendix E and Section 8.1, the conclusion was reached that three discrete single color systems would have the probability of meeting the OAMS technical requirements with a minimum possibility of cross axis interference.

4.2 Design Selection

As a result of the work performed in this Phase I contract and experience applied from earlier programs, a design was selected which would meet all the program requirements. The design utilized selected polarized light and birefringent crystals to measure angular displacement. The design included a transmitter at the point of reference and a receiver at the target. The transmitter emits modulated, polarized light so that each axis (roll, pitch and yaw) has a discrete electro-optical system. The transmitted beams include discrete states which relate to each axis. The arrangement utilizes three distinct light paths—one for each axis. Two LED emitters alternately turn on and off for each individual channel. The light from each emitter is polarized differently. The sequence of light emitted is continuous wave and the LEDs for each channel operates at a discrete frequency and are filtered at the receiver. The polarized light then passes through an angle sensing crystal which orients the polarization state as a relationship to this crystal. The arrangement is shown in Figures E.1, E.2 and E.3 (Appendix E).

The transmitter consists of an assembly of six light emitting diodes, 6 light focusing lens, 3 polarizing prisms, 2 quarter wave plates and 2 angle sensing crystals in a single assembly. The three emitted light beams carry the triaxial angular information by their polarization states.

The receiver units are all within the cones of light projected by the transmitter. The unit contains three polarization sensing assemblies, one for each axis. The sensing assemblies consists of an angle sensing crystal (matched to the transmitter crystal), an optical filter for color separation, a Wollaston prism plus focusing lens and two silicon detectors.

The diagrams of the optical system are shown and analyzed in Section 8.2 and Appendix B and the electronics is shown and described in Section 8.4. Differential detection of each pair of detectors will display amplitude and polarity as a function of angular displacement. The sum of the two detectors operates as an Automatic Gain Control (AGC) for automatic light level control or automatic amplification control to compensate for light changes. Temperature compensation circuits for LEDs and detectors have been considered. A LED balance control loop maintains a balanced output of the two LEDs in each channel.

4.3 Conceptual Design

The following paragraphs discuss candidate design configurations which were considered for the OAMS requirements.

Systems Goals

The system requires the comparison of angular relationship between two points. The system must operate on a continuous basis and read out and display the angular position of the three angles (roll, pitch and yaw). The sensitivity and accuracy requirements and goals are defined in the Annex(Technical Requirements).

Power requirements must be reduced as far as possible and still maintain an acceptable signal to noise ratio. An effort to minimize system voltage requirements has been made for the spacecraft environment compatibility. The minimum Noise Equivalent Angle has been considered the operational design goal. The electrical system is being evaluated for Electro-Magnetic Interference (EMI) and Electro-Magnetic Compatibility (EMC).

Vulnerability to environment within the spacecraft is an important consideration in the electronic and opto-mechanical design. Optical materials have been evaluated for vulnerability, lifetime effects and environmental effects. The mechanical assembly has been designed to maintain stability and accuracy in the specified operational environments. The mechanical assembly considered, dominates size and weight considerations and is designed to minimize these parameters.

Concept Selection

System analysis is performed in Appendix E and Section 8.1 to determine and compare the advantages and disadvantages of different configurations and components. Several sources were evaluated and compared for efficiency, compatibility with requirements and general characteristics. Candidate detectors were compared, modulation and demodulation techniques were evaluated. Pulsed and Continuous Wave operation was compared and evaluated for accuracy and signal to noise. Automatic

Gain Control for light level compensation was evaluated, Automatic balance control for component aging compensation was considered, including the effects imposed by the detectors and electronic components characteristics. Detectors were evaluated on the basis of performance, detectivity, temperature sensitivity, noise and lifetime effects. Electronic components were evaluated for performance and compatibility.

The design analysis performed in Section 8.1 and the error analysis in Appendix E were performed prior to the fabrication of the brassboard and then updated and corrected after comparison with performance data as it became available.

5.0 PARAMETRIC ANALYSIS

The parametric analysis is presented in section 8.1. The error analysis for the system is shown in Appendix E. The modulated LED systems can use either one of two modulation techniques to produce one beam for each axis originating from three separate transmitting axes. These are discussed in Appendix D. Appendix E also discusses and analyzes the types and magnitudes of cross coupling in the system.

6.0 BRASSBOARD DESIGN TRADE-OFFS

Design trade-offs have been considered first from the standpoint of performance. These include measurement range, calibration, accuracy stability. Then size, power, weight, reliability and other critical areas were investigated.

6.1 Operational Trade-Offs

Performance is dependent on polarization and birefringent crystals to sense and measure angular displacement. Crystals that are commonly used for the elements are single crystal quartz and calcite. Both have good lifetime properties and will not deteriorate in a vacuum or dry air environment. Vulnerability to nuclear exposure is not known at this time, but under high radiation levels some discoloration and other effects may take place. Other birefringent materials such as sapphire, cadmium sulfide, cuprous chloride and magnesium fluoride have been investigated for this application, but offer no particular advantages.

Light emitting diodes are the most attractive source for a spacecraft application but in general other sources could be used such as laser, arc (Xenon or Zirconium), and incandescent (IR radiators). Sources were evaluated for power, temperature, size, energy, efficiency; lifetime and stability criteria. Several types have potential for this application, however, LEDs met overall requirements better than the others.

Source modulation offers many desirable design features and is considered to be a mandatory system requirement. Different modulation systems were evaluated but several were rejected due to high voltage requirements, moving parts, temperature susceptibility, non-uniform field of view and their electrical noise characteristics. A system was devised in which two LEDs operating alternately would result in a low voltage polarization modulation in continuous wave modes. Multiple color concepts have been analyzed and evaluated for application to this program. While color separation is attractive to reduce the probability of cross-coupling errors, it imposes special requirements on the sources. The sources must have relatively predictable optical characteristics, high energy output and small cross sectional area (for adequate focusing). Multicolor LED sources that met the OAMS Systems requirements were selected for the OAMS program. Multicolor LEDs were available but problems developed with G_A A_S P. Numerous detectors were evaluated for use in the system including photo-cells, photo-multipliers, various cooled detectors and various solid state sensors. The most ideal candidates are silicon diodes as these devices have high detectivity, low noise and can operate efficiently at 70°F ambient without the complexity of cooling.

The processing electronics area offers many trade-offs. Trade-off considerations include automatic gain control, automatic light level control, automatic aging control, automatic temperature compensation, among others which were evaluated during the course of this program.

6.2 Performance

Performance trade-off considerations focused upon the noise equivalent angle (NEA), the maximum distance between source and receiver, the angular magnitude of the transmitter radiation cone, system reliability and lifetime, the error in the angular measurement that can be achieved, and environmental effects upon the system performance. These trade considerations are influenced primarily by source power, linearity and stability requirements, the type of source modulation, the effect of temperature upon the source radiant output and detector noise, the NEP and responsivity of the detector, the alignment tolerance, the system thermal design and the cooling of the sources and/or detectors. The ultimate effects of these considerations result in tracking system sensitivity, accuracy and flexibility for extended life and reduced power, weight and size within the limitations imposed by the system measuring requirements.

In a latter stage of this program trade areas concerning the hardening of components and subsystems to nuclear weapon effects were briefly investigated. These trade-offs include additional circuit complexity versus lifetime and power requirements, selection of less vulnerable parts versus such parameters as gain, linearity, response characteristics and reliability, and hardening versus additional size and weight.

6.3 Noise Equivalent Angle Versus Source Power

Noise equivalent angle can be traded for source power, operating range capability, beam divergence and receiver aperture under all operating conditions.

6.4 Temperature Effects on Noise Equivalent Angle (NEA)

A change in temperature affects the optical power output and wavelength radiation of the LED sources, the responsivity and NEP* of the detectors, the bandpass of the optical filter. Also, in the electronics amplifiers, gain can change and active electrical bandpass filters can shift with temperature variations. This effect can be minimized by the use of high gain feedback amplifiers and temperature compensation networks. Shifts in wavelength of the radiant source can be compensated for by selection of a sufficiently broad bandpass for the optical filter. *Noise Equivalent Power

6.5 Thermo-Electric Coolers

A potentially advantageous application of the T. E. cooler is for cooling the detectors. Over the limited temperature range of operation of the OAMS system cooling of the detectors in order to reduce shot noise and improve responsivity is not warranted, as the resultant small performance improvement requires a substantial increase in power requirements.

6.6 Goals Versus Requirements

The results of the preceding studies indicate that the requirements listed in Annex (Technical Requirements) can be met in the initial prototype hardware. By the use of the latest LEDs for sources and silicon detectors the system NEA exceeds the requirements with sufficient margin to meet the goals listed in the referenced annex.

6.7 Cost

Cost of the system was considered in the design phase, stressing simplicity in mechanical fabrication, assembly and test. Electronic systems will utilize, wherever applicable, integrated circuits. Medium scale integration was investigated as a means of reducing costs. Components such as sources, optical elements and detectors utilized as far as possible, stock items, which eliminated excessive costs. Reliability, lifetime and maintainability are trade considerations that will affect the system cost. Assembly and test complexity procedures affecting costs were considered during the design phase.

7.0 RELIABILITY AND LIFETIME

7.1 Sources

An operational-lifetime in excess of 26,000 hours (3 years) with a shelf life of 5 years is a goal of the OAMS system development. Though no specific figure has been assigned for system reliability, the critical components from both a reliability and lifetime aspect are the sources. Therefore, source redundancy has been investigated during the course of the Phase I contract and is a major area of trade studies. Redundant sources are particularly attractive in view of the type of source that has been selected for this application, namely the LED. Statistical data on these devices up to the present time indicate that they have almost unlimited shelf life in certain wave lengths. Other trade areas that effect the sources are the radiant power output requirements, mode of operation (CW or pulsed), lifetime versus output power, power versus operational stability, temperature effects and cooling, and the resultant decrease in source power requirements through the use of lower NEP detectors. The effects of the nuclear environment on the sources will also eventually affect the trade studies.

7.2 Optical Components

The reliability and lifetime of the system's optical components is more affected by environmental considerations than any other parameters. The effect of the hard vacuum and nuclear environments will have to be investigated. The launch environment will also affect the optical components. Therefore, the ultimate reliability and life of these passive components will be dependent upon their capability of surviving and performing within specifications following the aforementioned environmental situations. Trade studies on these components hinge upon their environmental characteristics, methods of mounting and isolating material studies, size considerations and vulnerability in the nuclear environment.

7.3 Detectors

Reliability and lifetime data on silicon photodiode detectors are available from other programs. The available data on silicon PIN detectors have been accumulated and documented.

Past experience in the use of these devices indicate that they are very reliable and stable when properly operated. Lifetimes under normal operating conditions are in the tens of thousands of hour category. Trade studies have evolved about bias level, factors affecting noise during life and at elevated temperature operation, linearity as a function of bias, S/N capability as a function of bias, stability of response as a function of bias level, effects of load and the effects of high intensity levels upon life and performance. Reference 10.

7.4 Power, Weight and Size

Power tradeoffs have evolved considerations of source size and efficiency, operating range and beam divergence, translation capability and NEA. Since over

40 percent of the power required for system operation will be dissipated in the sources and source drives, a significant reduction in required power can be attained by the use of higher efficiency and smaller size sources. The processing electronics require approximately 150 watts. It is estimated that this power can be reduced by about 110 watts in a complete integrated circuit final design.

Weight and size considerations have been made primarily on the necessity of providing adequate mounting of the optical components, the prevention of excessive thermal gradients in the optical components and their mounting structures providing adequate heat sinking of the sources and allowing for packaging of the processing electronics.

TRANSMITTER UNIT

COMPONENT	WEIGHT POUNDS	SIZE - INCHES
Optical-Mechanical	10-1/2	5-5/8" Dia. x 6-3/8" long
Electronics	1/2	4-3/4" Dia. x 2" long

RECEIVER UNIT

COMPONENT	WEIGHT POUNDS	SIZE - INCHES
Optical-Mechanical	12-1/2	5-5/8" Dia. x 4-3/8" long
Electronics	1-1/2	4-1/2" Dia. x 2-1/2" long

8.0 BRASSBOARD DESIGN

8.1 Preliminary Design and Analysis

8.1.1 System Analysis

OAMS is basically an open loop measuring system which incorporates a number of closed loop subsystems to maintain stable parameters or calibration of the complete system.

The analysis of the system consists of the derivation of the open loop system equation expressing the effect at the output of all foreseeable system disturbances or perturbations. Next, each subsystem control loop is analyzed in its efficiency in reducing the perturbations.

The initial analysis concerns the roll channel, since it is the most basic of the three channels and its extension to the two lateral channels is straightforward.

8.1.2 System Equation

The polarization orientation of the two transmitter beams emerging from the Wollaston prism are assumed to be horizontal and vertical. The corresponding power (watts) at the receiver entrance pupil are denoted by I_H and I_V, respectively. The orientation of the receiver Wollaston prism at null is assumed to be 45° relative to the transmitter prism; see figure 8-1. The light received by a detector from each of the transmitter source is equal to the received flux, I_H or I_V, times the cosine squared of the angle between the source and the detector axis. The detector outputs (amps), 0_1 and 0_2, can be expressed as follows, where R is the detector responsivity, (amps/watt):

$$\text{Det. \#1} = 0_1 = R_1 I_V \cos^2(\theta_R + 45^\circ) + R_1 I_H \cos^2(\theta_R - 45^\circ)$$

$$= \tfrac{1}{2} R_1 (I_H + I_V) + \tfrac{1}{2} R_1 (I_H - I_V) \sin 2\theta_R$$

$$\text{Det. \#2} = 0_2 = R_2 I_V \cos^2(\theta_R - 45^\circ) + R_2 I_H \cos^2(\theta_R + 45^\circ)$$

$$= \tfrac{1}{2} R_2 (I_H + I_V) = \tfrac{1}{2} R_2 (I_H - I_V) \sin 2\theta_R$$

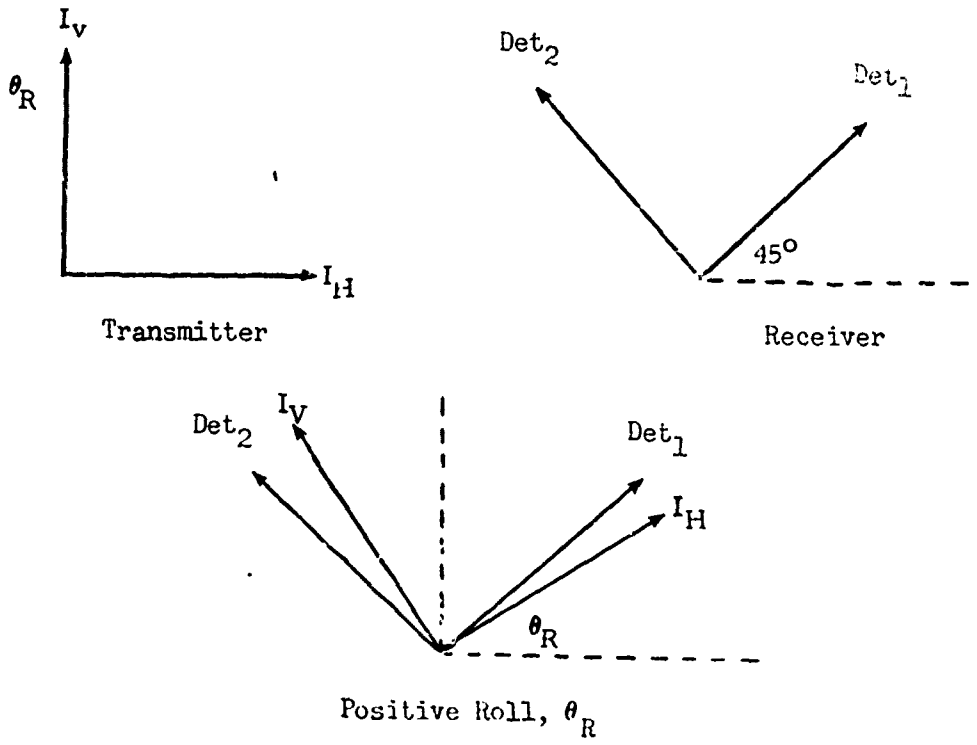

Figure 8-1. Transmitter-Receiver Polarization Orientations

Ideally, the responsivities of the two detectors should be equal. However, to account for small variations, the following notation will be used:

$$R_2 - R_1 = \Delta R \quad \text{and} \quad R_1 = R$$

The detector outputs are then:

$$\frac{2O_1}{R} = (I_H + I_V) + (I_H - I_V) \sin 2\theta_R$$

$$\frac{2O_2}{R} = (I_H + I_V) - (I_H - I_V) \sin 2\theta_R + S$$

$$= (1+\eta_R) \left[(I_H + I_V) - (I_H - I_V) \sin 2\theta_R \right]$$

The quantity, S ,is the detector unbalance error signal expressed in terms of the percent difference in responsivities, $(\Delta R/R) \times 100\%$:

$$S = \eta_R \left[(I_H+I_V) - (I_H-I_V) \sin 2\theta_R \right]$$

$$\eta_R = \Delta R/R$$

The OAMS signal processing requires the use of the difference and the sum of these two detector output signals. This difference and sum will be denoted by Δ and Σ, respectively. They are:

$$\Delta = O_1 - O_2 \qquad \Sigma = O_1 + O_2$$

$$\frac{2\Delta}{R} = 2(I_H-I_V) \sin 2\theta_R - S$$
$$= (2+\eta_R)(I_H-I_V) \sin 2\theta_R - \eta_R (I_H+I_V)$$

$$\frac{2\Sigma}{R} = 2(I_H+I_V) + S$$
$$= (2+\eta_R)(I_H+I_V) - \eta_R (I_H-I_V) \sin 2\theta_R$$

In OAMS each of the sources are sinusoidally modulated 180 degrees from each other:

$$I_V = \tfrac{1}{2} I_1 [1 - m_1 \sin\omega t]$$

$$I_H = \tfrac{1}{2} I_2 [1 + m_2 \sin(\omega t + \delta)]$$

where m_1 and m_2 are modulation indices and δ represents a phase error in the modulation. On making the substitutions:

$$\Delta I = I_2 - I_1 \qquad I_1 = I \qquad \eta_I = \Delta I/I$$

$$\Delta m = m_2 - m_1 \qquad m_1 = m \qquad \eta_m = \Delta m/m$$

one obtains

$$I_V = \tfrac{1}{2} I(1 - m \sin\omega t)$$

$$I_H = \tfrac{1}{2} I(1 + m \sin\omega t) + \tfrac{1}{2} mIE$$

$$mIE = \Delta I + (I\Delta m + \Delta I m + \Delta I \Delta m) \cos\delta \sin wt$$
$$+ (I+\Delta I)(m+\Delta m) \sin\delta \cos\omega t$$
$$- mI(1-\cos\delta) \sin\omega t$$

$$E = \frac{1}{m} \eta_I + (\eta_I + \eta_m + \eta_I \eta_m) \cos\delta \sin\omega t$$
$$+ (1+\eta_I)(1+\eta_m) \sin\delta \cos\omega t$$
$$\cdot (1-\cos\delta) \sin\omega t$$

$$= \frac{1}{m} \eta_I + P \sin\omega t + Q \cos\omega t$$

where $\eta_R = \frac{\Delta R}{R}$

$\eta_I = \frac{\Delta I}{I}$

$\eta_m = \frac{\Delta m}{m}$

$P = (\eta_I+\eta_m+\eta_I\eta_m)\cos\delta - (1-\cos\delta)$

$Q = (1-\eta_I)(1+\eta_m)\sin\delta$

Also

$(I_H-I_V) = mI(\sin\omega t + \frac{1}{2}E)$

$(I_H+I_V) = I(1+\frac{1}{2}mE)$

The difference and sum signals then become

$$\frac{2\Delta}{R} = mI(2+\eta_R)(\sin\omega t+\tfrac{1}{2}E)\sin 2\theta_R - \eta_R I(1+\tfrac{1}{2}mE)$$

$$\frac{2\Sigma}{R} = I(2+\eta_R)(1+\tfrac{1}{2}mE) - m\eta_R I(\sin\omega t+\tfrac{1}{2}E)\sin 2\theta_R$$

On substituting for E,

$$E = \frac{1}{m}\eta_I + P\sin\omega t + Q\cos\omega t$$

The differences and sum signals become

$$\frac{2\Delta}{R} = mI\left[(2+\eta_R)(1+\tfrac{1}{2}P)\sin 2\theta_R - \tfrac{1}{2}\eta_R P\right]\sin\omega t$$

$$+ mI\left[(2+\eta_R)\tfrac{1}{2}Q\sin 2\theta_R - \tfrac{1}{2}\eta_R Q\right]\cos\omega t$$

$$+ mI\left[(2+\eta_R)\left(\frac{1}{2m}\right)\eta_I\sin 2\theta_R - \frac{1}{m}(\eta_R)(1+\tfrac{1}{2}\eta_I)\right]$$

$$\frac{2\Sigma}{R} = I\left[(2+\eta_R)(1+\tfrac{1}{2}\eta_I) - \tfrac{1}{2}\eta_R\eta_I\sin 2\theta_R\right]$$

$$+ I\left[(2+\eta_R)\tfrac{1}{2}mP - m\eta_R(1+\tfrac{1}{2}P)\sin 2\theta_R\right]\sin\omega t$$

$$+ I\left[(2+\eta_R)\tfrac{1}{2}mQ - \tfrac{1}{2}m\eta_R Q\sin 2\theta_R\right]\cos\omega t$$

The difference and sum signals can now be written as

$$\frac{2\Delta}{R} = mIA\sin\omega t + mIC\cos\omega t + mIF$$

$$\frac{2\Sigma}{R} = IB + ID\sin\omega t + IG\cos\omega t$$

where the values of A, B, C, D, F, and G can be found from the two preceding equations.

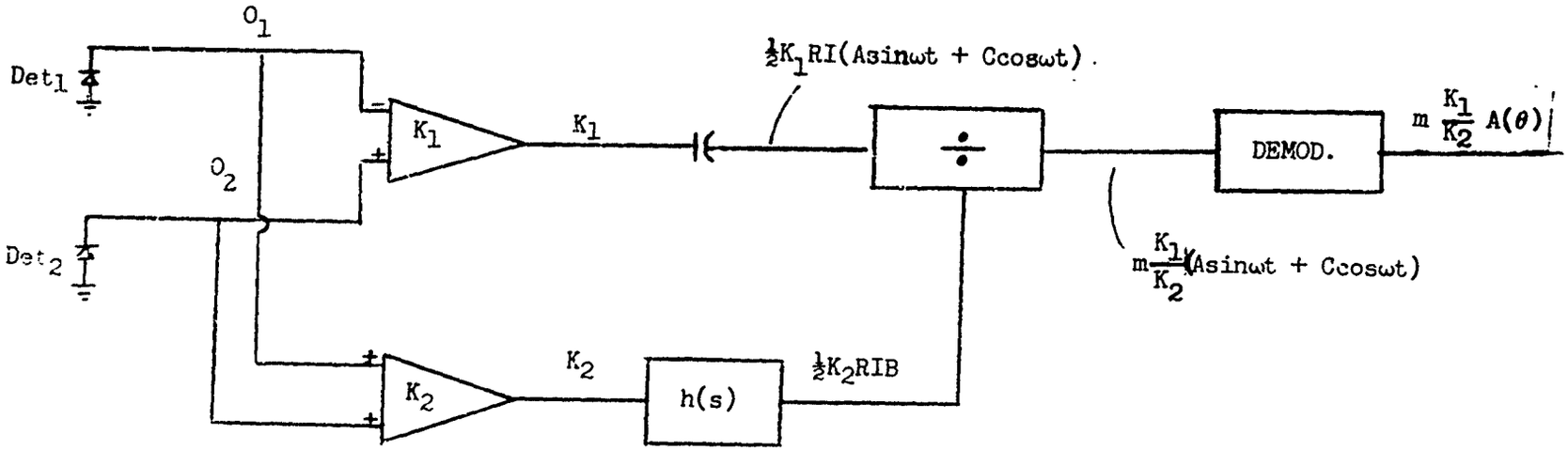

Figure 8-2, Simplified Block Diagram

A system block diagram consisting of the pertinent electronic processing elements is shown in figure 8-2. Amplifier K_1 represents the total gain of the preamplifiers and the differential amplifier. The blocking capacitor will remove the D.C. component of the difference signal. This difference signal then becomes the dividend signal for the divider. The sum signal is amplified by a low pass active network of D.C. gain K_2. The active filter attenuation at the signal frequency will be denoted by $h(\omega)$. The D.C. portion of the sum signal becomes the divider signal to the dividing module. The signal, V', emerging from the divider is

$$V' \quad V \frac{K_1\left(\frac{2\Delta}{R}\right)_{AC}}{K_2\left(\frac{2\Sigma}{R}\right)_{DC}} = \frac{mI\,[A\sin\omega t + C\cos\omega t]}{I\,[B+h(\omega)\,D\sin\omega t + h(\omega)\,C\cos\omega t]}$$

It it is assumed that the low pass filter in the sum circuit has sufficient high frequency attenuation,

$$h(\omega) \approx 0$$

and

$$\frac{K_2}{K_1} V' = m\frac{A}{B}\sin\omega t + m\frac{C}{B}\cos\omega t$$

For the present, it will be assumed that the synchronous demodulator will detect only the $\sin\omega t$ signal and ignore the quadrature component $m\frac{C}{B}\cos\omega t$. The output of the demodulator, V, can then be represented as

$$\frac{K_2}{K_1} V = m\,A/B$$

$$= m\,\frac{(2+\eta_R)\,(1+\tfrac{1}{2}P)\sin 2\theta_R + \tfrac{1}{2}\eta_R P}{(2+\eta_R)\,(1+\tfrac{1}{2}\eta_I) - \tfrac{1}{2}\eta_R\eta_I \sin 2\theta_R}$$

where

$$P = (\eta_I + \eta_m + \eta_I\eta_m)\cos\delta - (1-\cos\delta)$$

This can be written as

$$\frac{K_2}{K_1} V = m\,\frac{1+\tfrac{1}{2}P}{1+\tfrac{1}{2}(\eta_I-\Phi)}\sin 2\theta_R - \frac{m\,\eta_R\,P}{2(2+\eta_R)\,[1+\tfrac{1}{2}(\eta_I-\Phi)]}$$

$$\Phi = \frac{\eta_R\eta_I \sin 2\theta_R}{(2+\eta_R)}$$

Let

$$\frac{K_2}{K_1} V = m\,[1+u]\sin 2\theta_R - mv$$

where

$$u \cong \frac{1+\frac{1}{2}P}{1+\frac{1}{2}(\eta_I-\Phi)} - 1$$

$$= \frac{P-\eta_I+\Phi}{2+\eta_I-\Phi} \qquad \text{exact}$$

$$v = \frac{\eta_R P}{(2+\eta_R)\ (2+\eta_I-\Phi)} \qquad \text{exact}$$

$$P = (\eta_I+\eta_m+\eta_I\eta_m)\cos\delta - (1-\cos\epsilon)$$

The first term of amplitude $1+u$ represents the amplitude of the desired signal. If this term differs from unity, $u \neq 0$, the result is a change in scale factor. The percent change in scale factor or percent change in angular reading is therefore $u \times 100\%$.

The second term of amplitude, v, represents an output signal when the input angle, θ, is zero. Therefore, the amplitude of this term represents a shift in the position of null. The angular shift in null, $\Delta\theta$, is given by

$$m \sin 2\Delta\theta_R = mv$$

$$\Delta\theta_R \approx \tfrac{1}{2}v$$

Assuming the electronics can maintain a constant phase relationship between LED signals, $\delta = 0$, then

$$u = \frac{\eta_m+\Phi}{2+\eta_I-\Phi} \qquad \text{exact}$$

$$v = \frac{\eta_R(\eta_I+\eta_m+\eta_I\eta_m)}{(2+\eta_R)(2+\eta_I-\Phi)} \qquad \text{exact}$$

$$\Phi = \frac{\eta_R\eta_I \sin 2\theta_R}{(2+\eta_R)} \approx \tfrac{1}{2}\eta_R\eta_I(1-\tfrac{1}{2}\eta_R)\sin 2\theta_R$$

If only second order terms are retained, $\Phi = 0$, and

$$u = \tfrac{1}{2}\eta_m - \tfrac{1}{4}\eta_m\eta_I \qquad \text{2nd order}$$

$$v = \tfrac{1}{2}\eta_R(\eta_I+\eta_m) \qquad \text{2nd order}$$

If first order terms are retained

$$u = \tfrac{1}{2}\eta_m \qquad \text{1st order}$$

$$v = 0 \qquad \text{1st order}$$

8.1.3 Analysis Review

The change in scale factor, u, and the shift in null, v, are given by

$$u = \tfrac{1}{2}\eta_m(1-\tfrac{1}{2}\eta_I)$$

$$v = \tfrac{1}{2}\eta_R(\eta_I+\eta_m)$$

and the two LED light signals are

$$LED_i = I_i(1\pm m_i \sin t)$$

where η_I and η_m are the fractional differences between the intensities and the modulation indices of the two LED's:

$$\eta_I = \frac{I_2 - I_1}{I_1} \qquad \eta_m = \frac{m_2 - m_1}{m_1}$$

It can be seen that the change in scale factor , is (to 1st order) a function only of the difference in modulation index between the two LED's. In other words it is important to maintain the same ratio of A.C. drive signal to D.C. drive signal for each LED, i.e., $m_1 = m_2$ or $\eta_m = 0$. If this ratio is maintain the same in each LED, then the scale factor will remain unchanged even if the relative intensities, I_1 and I_2 of the two LED's change drastically. By obtaining the two LED drive signals from the same source as shown schematically in figure 8-3, a control dircuit to maintain the A.C. signals to the LED's or to control η_m, is unnecessary.

In this case the A.C. and the D.C. components of the two LED signals are derived from the same source, and hence the modulation index is the same in each case. This situation is presently maintain in the phase one electronics, although the details of the actual circuit differ from that of figure 8-2.

It is estimated that the modulation indices can be maintained easily to within 0.1%, or $\eta_m = .001$. This would correspond to a change in scale factor $(1/2)\eta_m$ or 0.9 arc seconds error at a full scale reading of 1800 arc seconds.

Next, consider the shift in the null position, v. Assuming that the modulation index is maintain constant, the shift in null is given by

$$\Delta\theta = \tfrac{1}{2}v = (1/8)\eta_R\eta_I$$

The shift is proportional to the product of the detector imbalance and the amplitude of the LED signal. It should be remembered that

$$\eta_I = \frac{I_2 - I_1}{I_i}$$

represents the <u>received</u> light unbalance. Two circumstances are envisioned which would change the relative levels of the received light: 1) due to aging, or some other cause, the conversion efficiency of one LED would change more than the other, 2) the light intensity pattern of each LED would be different at the receiver.

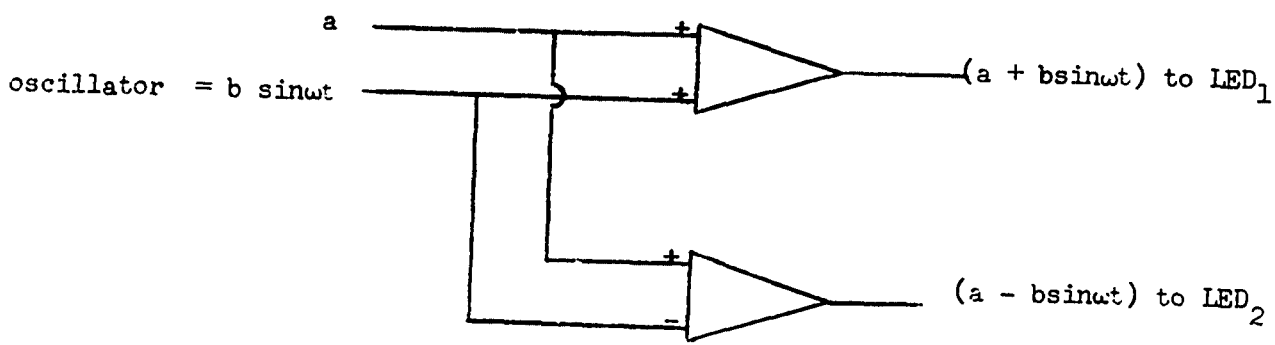

LED DRIVE SIGNALS = $a(1 \pm m \sin t)$

$m = b/a$

Figure 8-3, Led Drive Signal Derivation

Worst case considerations allow a possible estimated 10% variation in LED intensities. The detectors in OAMS are presently matched to 1%. This situation creates a shift in null of approximately

$$\Delta\theta = (1/8)\eta_R\eta_I = (1/8)(.01)(.1)$$

$$= 1.25 \times 10^{-4} \text{ rad}$$

$$= 25 \text{ arc seconds}$$

This error can be reduced by either of two methods, each of which involves the use of a control loop to adjust circuit parameters. One method is to monitor and adjust the detector unbalance, $\eta_R \rightarrow 0$. The second method and the most practical is to monitor and adjust the relative amplitudes of the two LED signals, $\eta_I \rightarrow 0$. This is described in the next section. If both detector unbalance, η_R, and LED unbalance η_I can each be maintained to 1%, the maximum shift in null would be

$$\Delta\theta = 1125 \times 10^{-5} \text{ rad}$$

$$= 2.5 \text{ arc seconds}$$

8.1.4 LED Intensity Control Loop - General

The drive currents and the light output of each of the LED's is of the form

$$LED_1 = I_1(1+m \sin\omega t)$$

$$LED_2 = I_2(1-m \sin\omega t)$$

Here it is assumed that, except for the 180° phase shift, each of the signals is derived from the same source, and therefore the ratio of A.C. to D.C. current, m, is the same in each LED. However I_1 and I_2 are functions of LED efficiency and of position in the transmitter field of view, and are therefore subject to variations. It is the requirement of the LED control loop to vary one of the LED signals such that the light amplitude of each of the LED's, as measured at the receiver, are equal, i.e.,

$$I_1 = I_2 \quad \text{and} \quad \eta_I = 0 \quad \text{at the receiver aperture}$$

This is accomplished in the following manner. It will be noted from the previous section that the sum signal in the receiver contains an A.C. component of magnitude

$$\Sigma_{AC} = \tfrac{1}{2}RID \sin\omega t$$

where

$$D = \tfrac{1}{2}(2+\eta_R)\, mP - m\eta_R(1+\tfrac{1}{2}P) \sin 2\theta_R$$

$$= \tfrac{1}{2}m\left[(2+\eta_R-\eta_R \sin 2\theta_R)(\eta_I+\eta_m+\eta_I\eta_m) - 2\eta_R \sin 2\theta_R\right]$$

Considering only first order terms and assuming $\eta_m = 0$

$$D = m(\eta_I+\eta_m)$$

$$= m\eta_I$$

Therefore, the A.C. component of the sum signal, Σ, is proportional to the LED urbalance.

$$\Sigma_{AC} = \tfrac{1}{2}mRI\eta_I$$

This signal is used as a control signal to vary the amplitude of the drive current to one of the LED's until $\Sigma_{AC} = 0$, at which point the LED intensities will be balanced (as seen by the receiver).

A detailed description and analysis of the control loop is contained in the following section. Here, the overall performance will be discussed.

Errors in the operation of the control loop will occur due to the fact that in the second order approximation, other circuit imbalances can also contribute to the A.C. component of the receiver sum signal. For example, to second order, the A.C. component of the sum signal is

$$\Sigma_{AC} = \tfrac{1}{2}mRI(\eta_I + \tfrac{1}{2}\eta_I\eta_R - \eta_R \sin 2\theta_R)$$

The important term is the last term, since it represents the minimum value of the control signal. Assuming the following system parameters:

$$\theta_{max} = .0175 = 1^o$$

$$\eta_R = .01$$

the last term becomes

$$\eta_R \sin 2\theta_R = 1.75 \times 10^{-4}$$

Therefore, the LED control loop cannot balance the LED's to an accuracy greater than

$$\eta_{I\ minimum} = 1.75 \times 10^{-4} = .0175\%$$

this represents a null shift of

$$\Delta\theta = \tfrac{1}{2}V = 1/8\,\eta_R\eta_I$$

$$= (1/8)(.01)(1.75 \times 10^{-4})$$

$$= .22 \times 10^{-6} \text{ rad}$$

$$= 0.045 \text{ arc seconds at } \theta = 1^o$$

It will be shown that the error in the lateral channel LED control loops is the same.

8.1.5 LED Intensity Control Loop Analysis

The OAMS LED control block diagram is shown in figure 8-4. The system clock oscillator provides the two A.C. drive signals to the LED's. The D.C. bias through the LED's is obtained from a reference voltage. The modulation index of each LED signal is, therefore, identical, even though the efficiencies of the LED's may differ.

LED number one receives the drive signal through a divider module. This divider is used as a variable gain amplifier in which the gain is proportional to a control signal at the divisor input.

The control signal is derived from the system sum signal, Σ ,

$$\Sigma = \tfrac{1}{2}RI\ (B+D\ \sin\omega t)$$

The sum signal is synchronously demodulated and filtered to provide only a D.C. signal, ϵ , equal to

$$\epsilon = \text{control signal}$$

$$= \tfrac{1}{2}K_3\ RID$$

$$= \tfrac{1}{2}K_3\ RIm\eta_I$$

where K_3 is the control loop gain.

The drive signal to the final LED is then

$$\frac{K_4 b(1-m\ \sin\omega t)}{C + \epsilon}$$

where C is the D.C. offset voltage applied to the divisor input of the divider module. This prevents division by zero when $\eta_I = 0$, and sets the operating points for the LED. The constant K_4 is the basic divider gain, i.e., K_4=10.0.

Since the control signal is small, the approximation

$$\frac{1}{1 + X} = 1-X$$

can be used, and the LED drive signal becomes

$$\frac{K_4 b}{C}(1 - m\ \sin\omega t) - \epsilon\frac{K_4 b}{C^2}(1 - m\ \sin\omega t)$$

$$= \text{steady state signal} + \text{control signal}$$

The use of the divider in the control circuit introduces an additional loop gain of b/c^2. The system can now be represented by a linear system in which the divider is replaced by a summation and an additional loop gain of b/c^2.

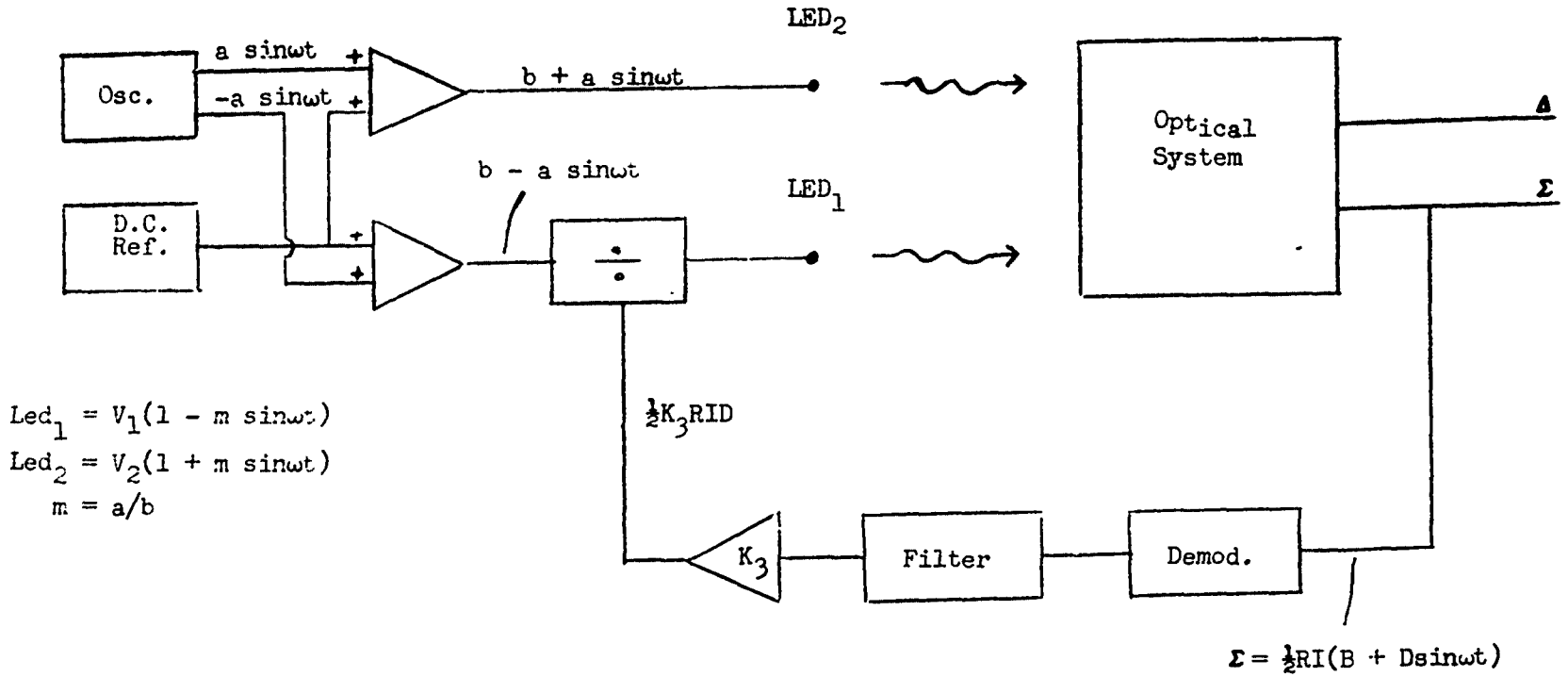

Figure 8-4, LED Control Loop Block Diagram

Considering only changes from a perfectly balanced LED system, it can be seen that a change in LED 1 signal amplitude dV_2 causes a change in the receiver sum signal $d\Sigma$. In general the system can be represented by block diagram, figure 8-5.

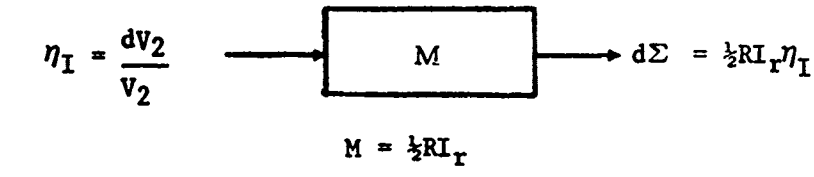

Figure 8-5. Open Loop System Block Diagram

The light intensity, I_r, contains the subscript to denote that it is the received light intensity which is to be used in this expression. The open loop transfer function, M, consists of the product of such factors as LED efficiency, detector responsivity, optical transmission and most importantly a function of range, since range will also affect the received light intensity. Therefore, for most OAMS applications, M, is a variable.

The open and closed loop systems and their respective A.C. sum error signals are shown in figure 8-6.

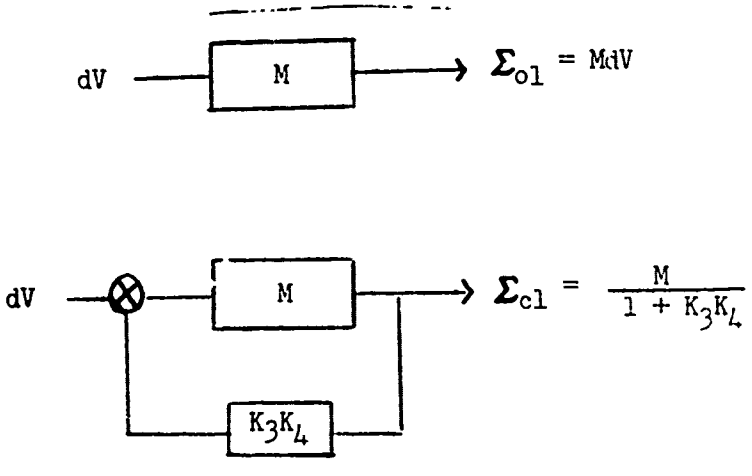

Figure 8-6. Open and Closed Loop System Block Diagrams

The reduction or improvement in the error signal is

$$\text{LED Control Loop Effectiveness} = \frac{\Sigma_{cl}}{\Sigma_{ol}} = \frac{\Delta m_{cl}}{\Delta m_{ol}}$$

$$= \frac{1}{1 + K_3 K_4 M}$$

where it must be remembered that the system transfer function M is a variable, depending on LED and detector efficiencies of transmitter-receiver separation.

Determination of M

The value of M for a given range will have to be determined experimentally by circuit voltage measurements. With the feedback loop disconnected, the two LED drive signals are adjusted until a zero A.C. sum signal is obtained. The A.C. drive voltage to LED #2 is then measured and recorded. Next a deliberate LED offset is introduced by changing the LED #2 drive signal, and recording the magnitude of the resultant A.C. sum signal. The value of M is therefore

$$M = \frac{\text{change in } \Sigma}{\text{change in LED \#2 drive voltage}} = \frac{d\Sigma}{dV_2}$$

A close approximation to M can be obtained by simply taking the ratio of the D.C. sum signal to the sum of the D.C. components of the LED drive signals.

$$M \cong \frac{\Sigma_{DC}}{2V}$$

In general M will be around unity, e.g., 0.5 to 5. The value of M needs to be found for only one transmitter/receiver operation. The values at other separations can be approximated by using the inverse square law. Also, since M is small, a relatively high loop gain, $K_3 K_4$, is required to significantly reduce the LED imbalance, i.e.,

$$\eta_{ICL} = \frac{1}{1 + K_3 K_4 M} \eta_{IOL}$$

$$K_3 K_4 M \gg 1$$

8.1.6 Extension of Analysis to Lateral Channels

In the lateral channels the light incident on each detector is given by

$$O_1 = R_1 \left[\tfrac{1}{2} I_H (1+\sin k\alpha) + \tfrac{1}{2} I_V (1-\sin k\alpha)\right]$$

$$O_2 = R_2 \left[\tfrac{1}{2} I_H (1-\sin k\alpha) + \tfrac{1}{2} I_V (1+\sin k\alpha)\right]$$

where

R = detector responsivity

k = optical gain of angle sensing crystal

α = relative angle between transmitter and receiver angle sensing crystals

Let $R_2 - R_1 = \Delta R \qquad R_1 = R$

and $$\eta_R = \frac{\Delta R}{R} = \frac{R_2 - R_1}{R_1}$$

The detector signals become

$$\frac{2O_1}{R} = (I_H+I_V) + (I_H-I_V) \sin k\alpha$$

$$\frac{2O_2}{R} = (I_H+I_V) - (I_H-I_V) \sin k\alpha + S$$

where

$$S = \eta_R [(I_H+I_V) - (I_H-I_V) \sin k\alpha]$$

This is exactly the same form as the equations for the light on the roll channel detector, except that the angular argument, $2\theta_R$, is replaced by $k\alpha$. Therefore, after making this substitution, the lateral channel error analysis becomes identical to the roll analysis.

The lateral channel output is

$$\frac{K_2}{K_1} V = m[1+u]\sin k\alpha - mv$$

where, as before

$$u = \frac{P-\eta_I+\Phi}{2+\eta_I-\Phi}$$

$$v = \frac{\eta_R P}{(2+\eta_R)(2+\eta_I-\Phi)}$$

$$P = (\eta_I+\eta_m+\eta_I\eta_m)\cos\delta$$

$$\Phi = \frac{\eta_R\eta_I \sin k\alpha}{(2+\eta_R)}$$

Or, if only second order terms are retained,

$$u = \tfrac{1}{2}\eta_m - \tfrac{1}{2}\eta_m\eta_I \approx \tfrac{1}{2}\eta_m$$

$$v = \tfrac{1}{2}\eta_R(\eta_I+\eta_m)$$

$$\Phi = 0$$

The change in output scale factor, u, is just as dependent on the modulation index on the roll channel, i.e., one-percent variation in indices is equivalent to one-half of one percent change in scale factor or 9.0 arc seconds error at 1800 arc seconds. As discussed in the roll channel, the modulation index for the LED's can be easily maintained to within 0.1% or less than one arc-second error at 1800 arc seconds.

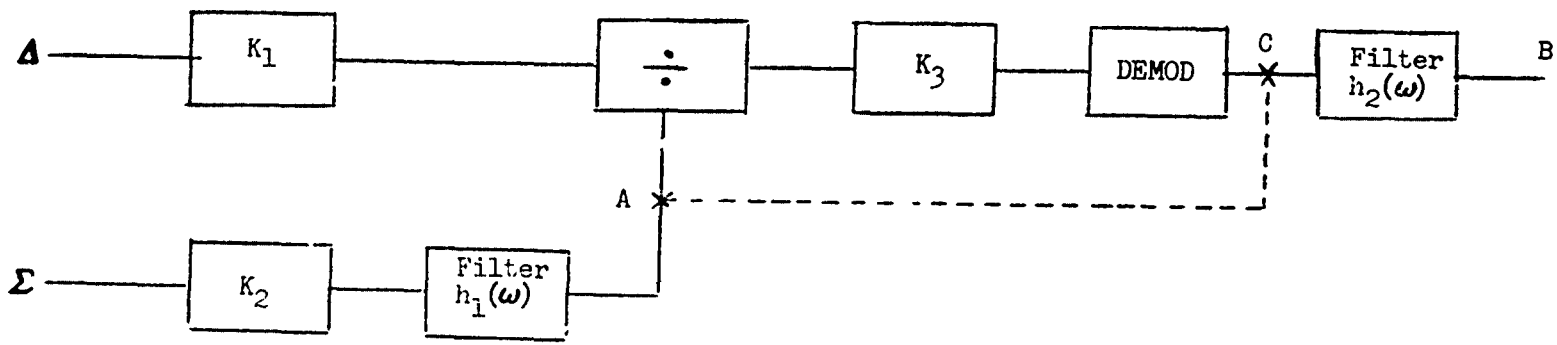

	K_1	K_2	K_3	$\frac{K_1 K_3}{K_2}$
PITCH	1	110.26	467	4.317
YAW	1	110.26	467	4.317
ROLL	100	110.26	162	1.470

Figure 8-7, System Electronic Gains

The shift in null position, $\Delta\alpha$, is found by

$$m \sin k\Delta\alpha = mv$$

$$\Delta\alpha \approx \frac{v}{k} = \frac{R\ I}{4k}$$

The null shift in the lateral channels is less than the shift in the roll channel by a factor of $(1/2)K \approx 30$ for OAMS.

Therefore, assuming an initial detector offset of one percent and an LED unbalance of 10 percent, the shift in null would be

$$\Delta\alpha = \frac{1}{(4)(30)} \quad (.1)(.01)$$

$$= 0.85 \times 10^{-5} \text{ rad}$$

$$= 1.75 \text{ arc seconds}$$

The requirement for an LED intensity control loop in the lateral channels is marginal. However, if an LED intensity control loop is incorporated into the lateral channels, the minimum unbalance then can be achieved (as calculated for the roll channel) is

$$\text{assuming } \alpha_{max} = .0175 = 1^{o}$$

$$\eta_R = .01$$

$$k = 60$$

$$\eta_{I\ minimum} = \eta_R \sin k\alpha_{max} \leq (1.01)(60)(.0175)$$

This represents a null shift of less than

$$\Delta\alpha = \frac{v}{K} = \frac{\eta_R \eta_{I\ min}}{4k}$$

$$= \frac{\eta_R}{4k} (\eta_R\ k\alpha\ max)$$

$$\frac{\eta_R^2}{4} \alpha_{max}$$

$$= \text{same as roll channel}$$

$$= .045 \text{ arc seconds}$$

The LED intensity control loop in the lateral channels has approximately the same ultimate accuracy as that of the roll channel, i.e., $\leq .045$ arc seconds. Due to the dependence on α, this error is actually a scale factor error, and .045 arc seconds error is the error at 1^{o}.

8.1.7 Background Illumination and Detector Noise Considerations

Assuming a background light intensity I_B entering the receiver aperture and two detectors each having a noise equivalent power, $N(f,\Delta f)$ watts/$Hz^{\frac{1}{2}}$, the output of each detector will be:

$$O_1' = O_1 + \tfrac{1}{2}R_1 I_B + R_1 I_N$$

$$O_2' = O_2 + \tfrac{1}{2}R_2 I_B + R_2 I_N$$

where

$$I_N = N(\Delta f)^{\frac{1}{2}} = I_N(f, \Delta f)$$

When the difference and the sum of the two detectors are taken, the resultant noise power will be the sum of the squares of the noise power output of each detector. The difference and sum signals will be

$$\Delta' = \Delta + \tfrac{1}{2}I_B(R_1 - R_2) + I_N \sqrt{R_1^2 + R_2^2}$$

$$\Sigma' = \Sigma + \tfrac{1}{2}I_B(R_1 + R_2) + I_N \sqrt{R_1^2 + R_2^2}$$

The output of the divider circuit will be

$$\frac{\Delta'_{AC}}{\Sigma'_{DC}} = \frac{\Delta_{AC} + I_{N\Delta}\sqrt{R_1^2 + R_2^2}}{\Sigma_{DC} \quad I_{N\Sigma}\sqrt{R_1^2 + R_2^2} + \tfrac{1}{2}I_B(R_1 + R_2)}$$

The different subscripts on I_N illustrate that, due to different bandwidths and center frequencies in the summation and difference electronics, the noise will be different in each case. The bandwidth of the difference amplifier circuit is in the tens of kilohertz. The summation amplifier circuit contains a D.C. low pass filter of 10 Hz bandwidth. Therefore, the two noise voltages will be different.

The divider output can be simplified:

$$\frac{\Delta'_{AC}}{\Sigma'_{DC}} = \frac{\tfrac{1}{2}mRIA \sin\omega t + I_{N\Delta}\sqrt{R_1^2 + R_2^2}}{\tfrac{1}{2}RIB + I_{N\Sigma}\sqrt{R_1^2 + R_2^2} + \tfrac{1}{2}I_B(R_1 + R_2)}$$

$$= \frac{mA \sin\omega t + 2\eta_{N\Delta}\sqrt{1 + (1+\eta_R)^2}}{B + 2\eta_{N\Sigma}\sqrt{1 + (1+\eta_R)^2} + \eta_B(2 + \eta_R)}$$

where

$$\eta_B = \frac{I_B}{I} = \frac{\text{background intensity}}{\text{signal intensity}}$$

$$\eta_{N\Delta} = \frac{I_{N\Delta}}{I} = \frac{\text{equivalent } \Delta \text{ noise intensity}}{\text{signal intensity}}$$

$$\eta_{N\Sigma} = \frac{I_{N\Sigma}}{I} = \frac{\text{equivalent } \Sigma \text{ noise intensity}}{\text{signal intensity}}$$

8.1.8 Noise Evaluation

For the moment, assume that the background illumination is zero, $I_B = \eta_B = 0$, and that the detector noise is small compared to the D.C. sum signal, $\bar{\eta}_{N\Sigma}$ B. The output of the divider is then

$$\frac{\Delta'_{AC}}{\Sigma'_{DC}} \approx \left[m \frac{A}{B} \sin\omega t + \frac{2\eta_{N\Delta}\sqrt{1+(1+\eta_R)^2}}{B} \right] \left[1 - \frac{2\ N\Sigma\sqrt{1+(1+\eta_R)^2}}{B} \right]$$

$$= \left[m \frac{A}{B} \sin\omega t + \epsilon_{N\Delta} \right] \left[1 - \epsilon_{N\Sigma} \right]$$

Since $A \approx 2 \sin K$, $B \approx 2$, and $\epsilon_{N\Delta}\epsilon_{N\Sigma} \approx 0$,

$$\frac{\Delta'_{AC}}{\Sigma'_{DC}} = m \left[1 - \epsilon_{N\Sigma} \right] \sin K\alpha \sin\omega t + \epsilon_{N\Delta}$$

The noise in the sum circuit, $\epsilon_{N\Sigma}$, creates a fractional change in scale factor, u ,

$$u = \epsilon_{N\Sigma} = \frac{2\,\eta_{N\Sigma}\sqrt{1+(1+\eta_R)^2}}{B}$$

$$\approx \sqrt{2}\ \eta_{N\Sigma}$$

$$= \frac{\sqrt{2}\ N(f_o, \Delta f_o)(\Delta f_o)^{\frac{1}{2}}}{I}$$

where, in OAMS, the summation noise is evaluated in a bandwidth of approximately 10 Hz, extending from zero Hertz to ten Hertz. This noise term will contain considerable 1/f noise and will probably have to be evaluated experimentally for each detector.

The noise in the difference circuit, $\epsilon_{N\Delta}$, creates a random shift in the position of null, $\Delta\alpha$, approximately equal to

$$m \sin k\alpha = \epsilon_{N\Delta}$$

$$\Delta\alpha = \frac{\epsilon_{N\Delta}}{mk}$$

$$= \frac{\sqrt{2}\ \eta_{N\Delta}}{mk}$$

$$= \frac{\sqrt{2}\ \ N\ (f_w, \Delta f_w)(\Delta f_w)^{\frac{1}{2}}}{mk}$$

In this case the noise is evaluated in a bandwidth, Δf_w, centered at the system oscillator frequency f_w. In general this noise, for equal bandwidth, will be much less than the noise in the sum signal since it does not contain the low frequency, 1/f, noise. This noise can usually be accurately predicted from vendor data on NEP, however, it is better to also measure this in the system to account for any other noise sources, i.e.,

$$\eta_{N\Sigma} = \frac{\text{noise voltage in } \Sigma \text{ signal}}{\text{average D.C. } \Sigma \text{ signal}} \times \frac{1}{\sqrt{2}}$$

$$\eta_{N\Delta} = \frac{\text{noise voltage at filtered output of demodulator}}{\text{average D.C. } \Sigma \text{ signal}} \times \frac{1}{\sqrt{2}}$$

In the OAMS circuit the measurement of $\eta_{N\Delta}$ and $\eta_{N\Sigma}$ is not straightforward due to the different gains and filter locations in the processing electronics. Figure 8-7 illustrates the block diagram.

The noise in the Σ circuit is amplified by K_4, filtered by $h_1(\omega)$ and, as shown in the analysis in this section, becomes an amplitude modulating signal for angular information. This modulation caused by the noise in demodulated and filtered, $h_2(\omega)$, along with the signal. The Σ circuit noise is therefore filtered twice, and the resultant noise spectrum given by

$$(\text{Detector noise spectrum}) \times h_1(\omega)\, h_2(\omega)$$

or the noise equivalent power incident on the detector, I_N, given by approximately

$$I_{N\Sigma} = N\,(\Delta f_o)^{\frac{1}{2}}$$

where Δf_o is the effective bandwidth of $h_1(\omega)\, h_2(\omega)$.

The equivalent Σ channel signal to noise ratio can be measured by measuring the signal to noise ratio at B in figure 8-7. For this measurement the connection indicated by the short AC is made and the Δ signal is grounded at D. The signal then appearing at B is the D.C. Σ signal plus the filtered noise.

$$(S/N)^{-1} = \epsilon_{N\Sigma} = \sqrt{2}\ \eta_{N\Sigma} = \frac{\text{noise at B}}{\Sigma_{DC} \text{ at B}}$$

The difference signal, Δ, is amplified by K_1 and K_2, demodulated at the channel frequency, and the demodulated signal filtered by $h_1(\omega)$. The resultant noise at B is, therefore, the amplified noise appearing in a bandwidth, Δf_1, centered about the system frequency. The bandwidth is the effective bandwidth of the demodulator and the filter $h_2(\omega)$.

This noise can be measured at B directly, since as shown in the analysis, the Δ circuit noise causes a shift in the position of null. The signal to noise ratio at the detector $(\eta_{N\Delta})^{-1}$ can be obtained from the noise measurement at B, since

$$\text{Noise at B (volts)} = \sqrt{2}\ PI_{N\Delta}\left(\frac{K_1 K_3}{K_2 RI}\right)$$

$$= \sqrt{2}\ \frac{K_1 K_3}{K_2}\,\eta_{N\Delta}$$

$$(S/N)^{-1} = \epsilon_{N\Delta} = \sqrt{2}\ \eta_N = \frac{K_2}{K_1 K_3} \quad (\text{Noise at B})$$

The effective shift in null is

$$\Delta\alpha = \frac{\sqrt{2}\,\eta_{N\Delta}}{mK}$$

$$= \frac{1}{m}\,\frac{K_2}{KK_1K_3} \times \text{(Noise at B)}$$

$$= \frac{\text{(Noise at B)}}{\text{(Scale Factor)}}$$

where

Scale Factor = volts/arc sec at B

$$= \frac{m\,K\,K_1K_3}{K_2}$$

Table 8-1 illustrates the noise measurements made on phase one OAMS at a range of 25 feet.

Effect of Noise on LED Control Loop

From the previous sections, the A.C. component of the sum signal or the LED control loop error voltage is (assuming $\eta_m = 0$)

$$\Sigma_{AC} = \tfrac{1}{2}mRI(\eta_I + \tfrac{1}{2}\eta_I\eta_R - \eta_R \sin k\alpha) + \text{Noise}$$

The noise is the detector (and system) noise appearing in the zero to ten Hz bandwidth of the sum amplifier circuit, which is

$$I_{N\Sigma}\sqrt{R_1^2 + R_2^2} = I\,\eta_{N\Sigma}$$

$$= \sqrt{2}\;\; N\,(f_o, \Delta f_o)(\Delta f_o)^{\frac{1}{2}}$$

which is predominently the detector (1/f) noise.

The control loop error voltage is

$$\Sigma_{AC} = \tfrac{1}{2}mRI\eta_I + \tfrac{1}{2}mRI(\tfrac{1}{2}\eta_I\eta_R - \eta_R \sin k\alpha + \eta_{N\Sigma})$$

The last term with the parenthesis is an undesired control voltage and the minimum possible value of η_I is

$$\eta_{I(\text{minimum})} = \tfrac{1}{2}\eta_I\eta_R - \eta_R K\alpha + \eta_{N\Sigma}$$

$$\approx \eta_{N\Sigma} - \eta_R K\alpha$$

Since the noise term is of random polarity, the negative sign should be considered positive to indicate the maximum value of the undesired control voltage. The error represents a shift in null of

$$= \frac{\eta_R\eta_{I(\text{minimum})}}{4K}$$

$$= \frac{\eta_R\eta_{N\Sigma}}{4K} + \frac{\eta_R^2}{4}\alpha$$

The effect of the noise on the control loop is reduced if the detectors are matched.

Table 8-1. OAMS Phase One Noise Measurements

Range = 25 Feet

Δ Signal

	OUTPUT NOISE[1] mv (peak)	$\eta_{N\Delta}$[2]	EQUIVALENT NULL SHIFT sec (peak)	CHANNEL TIME CONSTANT sec
PITCH	±1.5	1.57×10^{-4}	±1.5	.045
YAW	±3.0	3.03×10^{-4}	±3.0	.045
ROLL	**±12.0	3.84×10^{-5}	**±12.0	**.63

**Subsequent system signal to noise imprcvements reduced noise on roll channel and decreased time constant to .045.

Σ Signal

	Σ_{DC} volts	Σ_{NOISE} (TO FREQ) mv	$\eta_{N\Sigma}$	EQUIVALENT CHANGE IN SCALE FACTOR ±%	ERROR AT 1800 SEC. ±sec
PITCH	-3.814	±2.0	$3.5o \times 10^{-4}$	.052	.93
YAW	-2.654	±1.5	4.00×10^{-4}	.057	1.02
ROLL	-4.820	±1.5	2.20×10^{-4}	.031	.56

NOTE 1: Low frequency components - under 2 Hz predominated higher frequency (grass) was less than 0.6 mv rms.

NOTE 2: $\eta_{N\Delta} = \frac{mK}{2}\Delta\alpha$

Table 8-2. OAMS Phase One Noise Measurements

Range = 5.0 Feet

Δ Signal

	OUTPUT NOISE[1] mv (peak)	$\eta_{N\Delta}$	EQUIVALENT NULL SHIFT sec (peak)	CHANNEL TIME CONSTANT sec
PITCH	± 1.0	1.01×10^{-4}	± 1.0	.045
YAW	± 0.5	5.05×10^{-5}	± 0.5	.045
ROLL τ=.045	± 3.0[4]	1.00×10^{-5}	± 3.0[4]	.045
ROLL[2] τ=.63	± 0.5	1.68×10^{-6}	± 0.5	.63

Σ Signal

	Σ_{DC} volts	Σ_{NOISE} mv	$\eta_{N\Sigma}$	EQUIVALENT CHANGE IN SCALE FACTOR $\pm$%	ERROR AT 1800 SEC. $\pm$sec
PITCH	-3.190	± 1.5	3.32×10^{-4}	.047	.85
YAW	-3.05	± 0.5	1.15×10^{-4}	.016	.29
ROLL	-12.0[3]	± 2.0	1.18×10^{-4}	.017	.30

NOTE 1: Low frequency components under 2 Hz predominated higher frequency (grass) was less than 0.6 mv rms

NOTE 2: Low pass filter connected to system output

NOTE 3: Σ amplifier saturated at close range - noise measured at edge of fov.

NOTE 4: Data was taken before system improvements in signal to noise ratio of roll channel.

Table 8-3. Summary of OAMS Phase One Random Errors

Range = 25 Feet

	NEA AT NULL	RANDOM CHANGE IN SCALE FACTOR	TOTAL NEA AT 1800 SEC.
PITCH	± 1.5 sec	± .052 %	± 2.45 sec
YAW	*3.0	.057	*4.02
ROLL	*12.0	.031	*12.56

*Subsequent signal to noise improvements reduced these figures.

Range = 5.0 Feet

PITCH	± 1.0 sec	± .047 %	± 1.85 sec
YAW	0.5	.016	0.79
ROLL τ=.045	3.0	.017	3.30
ROLL τ=.63	0.5	.017	0.80

NEA = NOISE EQUIVALENT ANGLE

NOTE: Predominate noise errors are due to noise between 0 and 2 Hz. Figures shown are peak readings within an observation time of approximately 10 seconds on an oscilloscope. Measurement accuracy is ±0.5 mv peak due to scope noise.

8.1.9 Background Illumination

Assuming zero noise, the output of the demodulator is

$$\frac{\Delta'_{AC}}{\Sigma_{DC}} = \frac{m \sin k\alpha}{1+\frac{1}{2}\eta_B(2+\eta_R)}$$

$$\approx m\,[1-\tfrac{1}{2}\eta_B(2+\eta_R)]\ \sin k\alpha$$

$$= m\,[1-u]\sin k\alpha$$

Background illumination will cause a fractional change in the scale factor, ,

$$= \tfrac{1}{2}\eta_B\ (2+\eta_R)$$

$$\approx \eta_B$$

The fractional change in scale factor is equal to the ratio of background radiation entering the receiver aperture, $I_B\ (\lambda)$ to the signal radiation, I, entering the receiver aperture. Only the background radiation falling within the bandpass of the optical filter is to be considered in this ratio. The expected background illumination on the spacecraft is expected to be low level and have a small effect on the AGC. However, if higher levels become a problem A.C. demodulation will eliminate the effects.

8.2 Optical Design

8.2.1 Transmitter

The transmitter optical design is shown in figure 8-8. An objective lens is used to collimate the light emitted from the LED. One-half of the light from each LED is transmitted in the appropriate polarization mode, by the Wollaston Prism. This linearly polarized light is then changed to circular by the quarter wave plate. The light from one LED is right-hand circularly polarized as it leaves the quarter wave plate, while the light from the alternate LED is left-hand circularly polarized as it leaves the wave plate. These two light forms are then changed to elliptical as they pass through the angle sensing crystal (ASC).

In principle the transmitter optical design is straightforward. A simple collimator is required to image the light emitting area at infinity, the focal length of the collimator being adjusted to provide the desired field of view (FOV) or angular beam spread. The design is somewhat complicated by the fact that as a unit, the LED's are not Lambertian emitters, and the brightness or intensity as a function of angle of emission differs greatly from unit to unit. Also, it has been found that the emitting area is not of uniform brightness. Dark spots are not uncommon.

It is possible to calculate the far field intensity of the LED-lens combination, if the LED brightness is known. However, this involves numerical integration of the LED intensity pattern. This was done for two of the LED's, pitch and roll channels, with varying degrees of accuracy. The details are shown in appendix B.

The results are summarized in figure 8-9. The LED incremental area, d_A^1, and flux density E', is imaged in the far field as area dA and flux density E. By using geometrical optical relationships and LED emission parameters as shown in the appendix, the flux density, E, at the receiver can be calculated:

$$E = \frac{P_T}{A} \frac{G(\alpha)}{G(\frac{\pi}{2})} \frac{1}{\sin^2\alpha} \left(\frac{D}{2S}\right)^2$$

where P_T/A is the average power density over the emitting area, D is the diameter of the collimating lens and S is the range. The terms $G(\alpha)/G(\pi/2)$ is the fraction of the total emitted energy collected by the collimating lens. This is an increasing function of α, or the angle subtended by the detector as seen by the lens. The term $1/\sin^2\alpha$ represents a loss in flux density due to the magnification of the optics. As the focal length of the lens becomes shorter (α increases) the energy from the source is spread over a larger area, thus decreasing the flux density.

It is seen that there are two competing effects in the optimum choice of collimator focal length or α (α is proportional to 1/f). In other words, the collimator focal length must be chosen for each LED such that

$$\frac{G(\alpha)}{G(\frac{\pi}{2})} \quad \frac{1}{\sin^2\alpha}$$

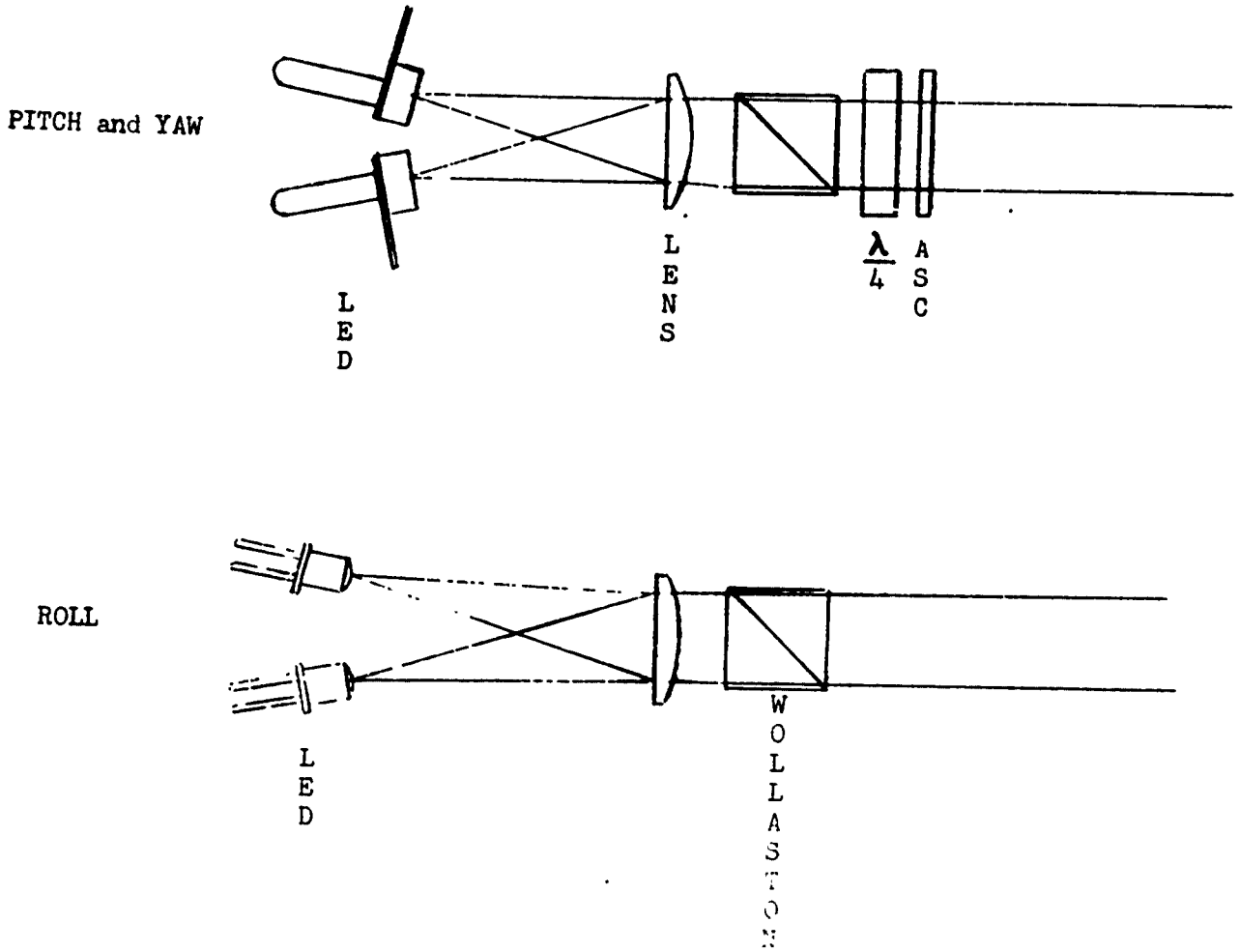

Figure 8-8, OAMS TRANSMITTER OPTICS

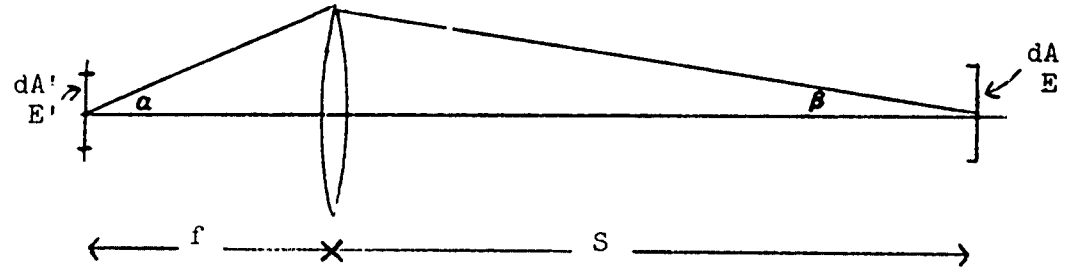

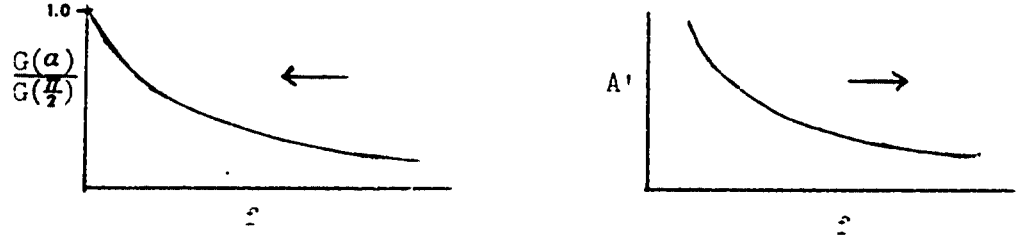

LED	IRRADIANCE at 50 ft. calculated	measured
TISLH3 .94	0.10 μw/cm²	0.06 μw/cm²
GE SSL-55C .94	0.2 μw/cm²	0.27 μw/cm²

$$E = E'(\alpha)/m^2 \qquad m = \sin\alpha/\sin\beta$$

$$\sin\beta = D/2S$$

$$E = \frac{E'(\alpha)}{\sin^2\alpha}\left(\frac{D}{2S}\right)^2$$

$$= \frac{P_T}{A}\,\frac{G(\alpha)}{G(\pi/2)}\,\frac{1}{\sin^2\alpha}\left(\frac{D}{2S}\right)^2$$

Figure 8-9, Summary of LED Selection Parameters

is a maximum. An additional constraint on the focal length is that the focal length not be so long that the field of view is less than the system requirement (approximately 3.0 degrees).

The quantity, G (α), must be obtained empirically for each LED and the optimum focal length calculated. Fortunately, the function to be maximized is quite broad in that it is not strongly dependent on focal length, or α. Indeed, for a Lambertian source

$$\frac{G(\alpha)}{G\left(\frac{\pi}{2}\right)} \quad \frac{1}{\sin^2\alpha} = 1$$

and the far field flux density is independent of collimator focal length.

Unfortunately, the data supplied by the manufacturer is usually not sufficient to calculate G (α), and the laboratory equipment and procedure required to measure G (α) is so extensive, that it is more straightforward to simply measure the far field intensity with a number of different focal length collimators. In most cases the emission is Lambertian to the extent that the selection of focal length is not very critical, the far field intensity variation being around ten to twenty percent for relatively large changes in collimator focal length. In most cases the focal length is determined more by the diameter of the emitting area and the desired field-of-view.

In figure 8-9 is shown the results of the irradiance calculations compared to the measured result for two LEDs. The Texas Instruments TI SLH3 calculation was made with the assumption of Lambertian emission. The GE-SSL55C calculations were made from measurements of G (α) as shown in the appendix.

In summary, the calculations and laboratory measurements indicate that an important LED selection criteria should be P_T/A or the emitted energy density at the emitting surface. In the case of a Lambertian emitter or an emitter in which the brightness does not vary greatly (fifty percent) over the emitting area this would be the only criteria. However, some LEDs have been found with vary greatly from a Lambertian source. These LEDs have significant "dark" areas on the emitting surface. In fact some of the LEDs are primarily edge emitters surrounded by a circular reflector which reflects the light forward. In such cases the effective radiating area is unknown and generally varies from unit to unit due to very loose internal tolerances. In such cases an approximation of the energy can be made by using the average energy density across the reflector ($P_T/\pi r^2$, r = reflector radius). This in general gives a conservative estimate of the available power output.

8.2.2 Receiver

The receiver optical design is shown in figure 8-10 and table 8-4 which gives the dimensions of the elements. The first element is the angle sensing crystal (ASC). This element is omitted in the roll channel and is replaced by a plane window. The angle sensing crystal is two millimeters thick, which provides an optical "gain", K=60, at the nominal system wavelength. (The gain does not vary significantly over the different channel wavelength. The Wollaston prism is next, followed by an interference filter. Off-the-shelf filters were selected for each channel such that the transmission versus wavelength characteristics provided the least cross coupling between channels. The elements up to and including the filter are plane-parallel components having zero power and do not enter significantly into the optical design. The system stop is located at the rear surface of the objective lens. The preceding elements are large enough so that there is no vignetting over the field of view, $\pm 1^{\circ}$.

Emerging from the Wollaston Prism are two collimated beams separated by $15^{\circ} \pm 0.5^{\circ}$. The plano convex lens and the immersion lenses (technically these are secondary lenses) image the aperture stop onto the detector. This arrangement insures that the detector is uniformly illuminated for any object position within the field of view. The details of the objective and immersion lens are shown in figure 8-11 and 8-12.

The focal point of the objective coincides with the radius of curvature of the immersion lens, and the immersion lens does not introduce additional aberrations into the system, for near on axis imagery. For moderate off-axis objects, the light strikes the immersion lens at near normal incidence.

The spherical aberration and coma of the plano-convex objective lens is easily calculated from the following equations:

$$TSA = .073 \frac{f}{(F\#)^3} = \frac{.073\ (50)}{(2)^3} = .45 \text{ mm}$$

$$\text{coma} = \frac{\theta}{16(N+2)} \frac{f}{(F\#)^2} = \frac{.148\ (50)}{16(3.52)\ (4)} = .0328 \text{ mm}$$

$$\theta_{max} = 8.5^{\circ} = .148 \text{ rad}$$

The optimum lens shape for the objective should be the Minimum Spherical Shape. However, for an object at infinity a plano-convex lens with the curved surface facing the infinite conjugate, the spherical aberration is only 9.0 percent larger. The coefficient in the above equation is .073 as opposed to .069 for the Minimum Spherical Shape. The coma of the plano-convex shape is slightly smaller than indicated in the equation.

As a rough estimate of the performance of the system, one can assume that the spot size on the detector will increase by an amount equal to the sum of the spherical aberration and coma. Since the system is designed about a nominal 2.0 mm spot size (assuming perfect imagery), the aberrations will increase the spot size to 2.49 mm, which is just within the 2.50 actual detector diameter.

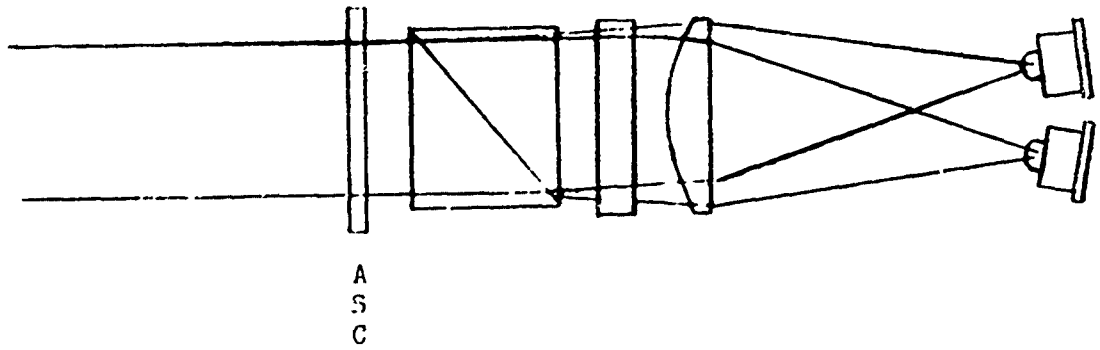

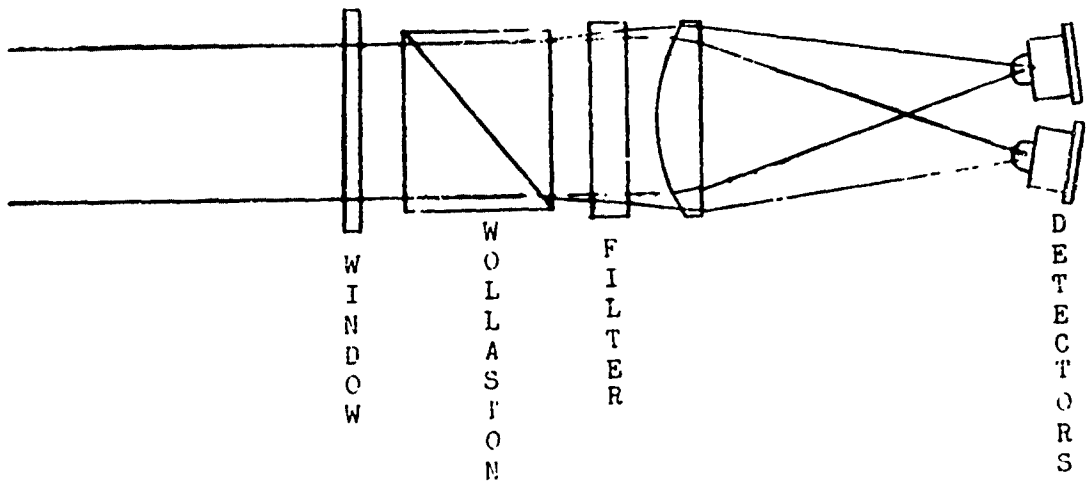

Figure 8-10, OAMS RECEIVER OPTICS

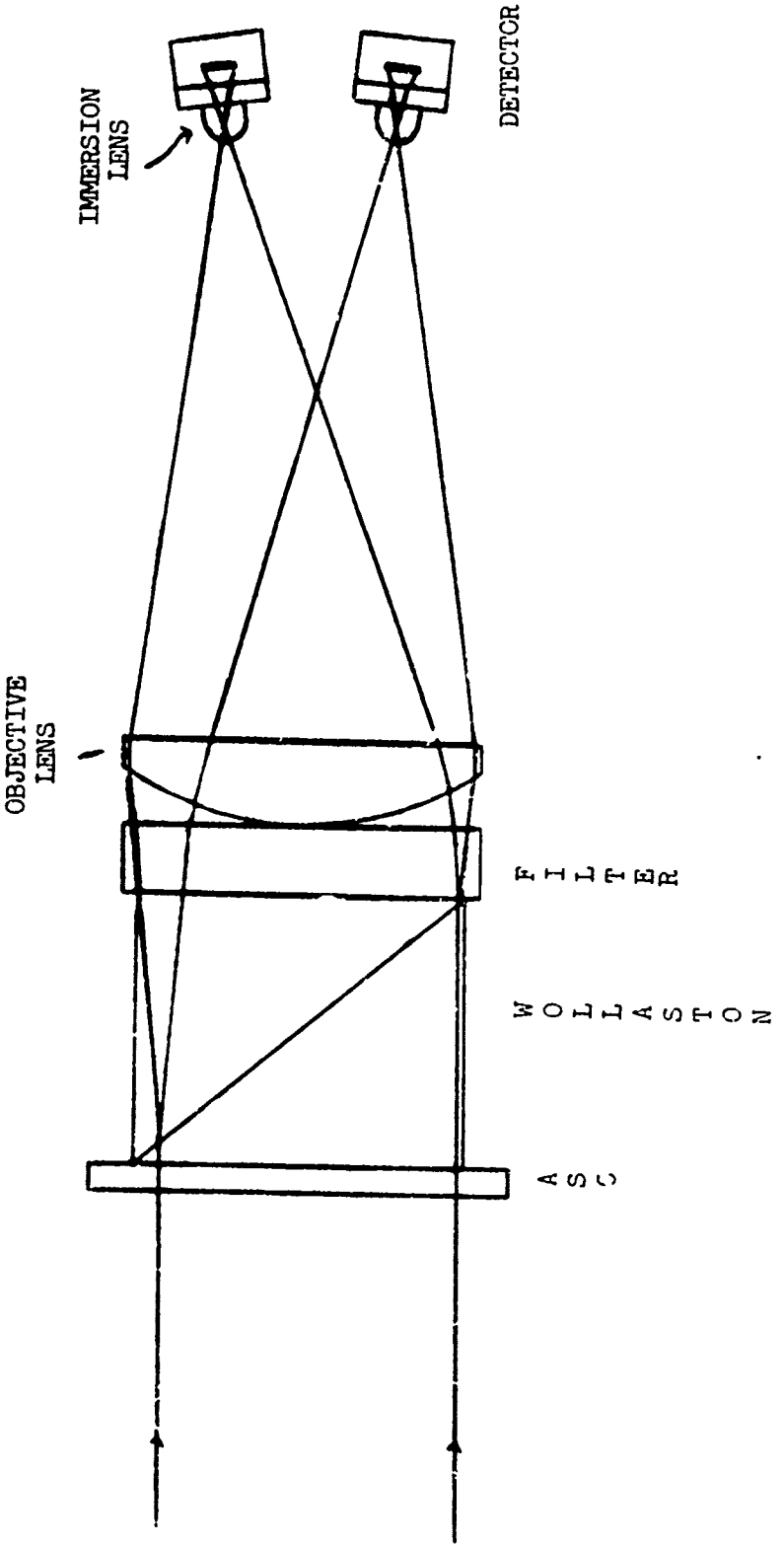

Figure 8-11, Details of Receiver Optics

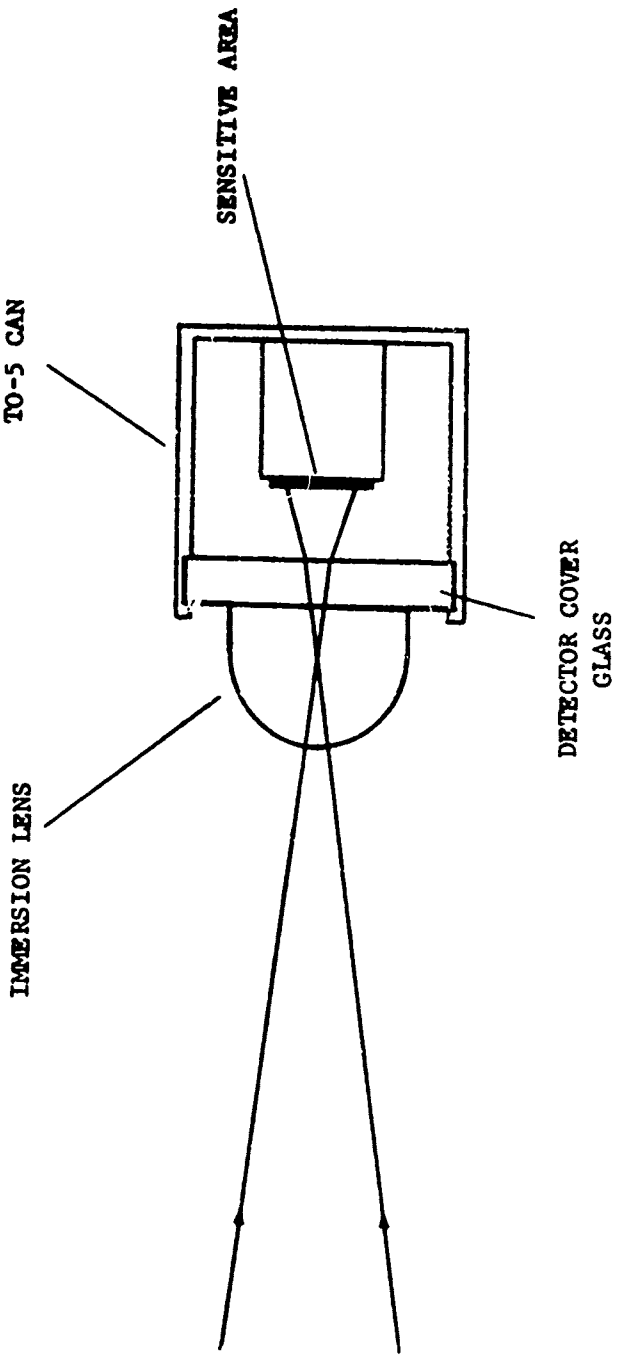

Figure 8-12, DETAILS OF IMMERSION LENS - DETECTOR ASSEMBLY

Table 8-4. OAMS Optical Components

RECEIVER

COMPONENT	SIZE	THICKNESS	CURVATURE	COMMENTS
Plane Window	32 mm dia.	2.0 mm	-	Roll only, BK-7
ASC	32 mm dia.	2.0 mm	-	Pitch and Yaw only, Quartz
Wollaston	25 x 25 mm	23 mm	-	Calcite, 15°
Filter	27 mm dia.	6.0 mm	-	
Aperture Stop	13 mm dia.	-	-	
Objective Lens	27 mm dia.	7.0 mm	F.L.=50 mm	
Immersion Lens	3.66 mm dia.	2.25 mm	R=1.83 mm	BK-8
Detector	2.5X2.5 mm	-	-	UDT-PIN-50

TRANSMITTER

COMPONENT	SIZE	THICKNESS	CURVATURE	COMMENTS
Plane Window	22 mm dia.	2.0 mm	-	Roll Only, BK-7
ASC	22 mm dia.	2.0 mm	-	Pitch and Yaw only, Quartz
Lens:				
Pitch	20 mm dia.	6.0 mm	F.L.=40 mm	
Yaw	20 mm dia.	6.0 mm	F.L.=40 mm	
Roll	20 mm dia.	7.0 mm	F.L.=50 mm	
λ/4 Plate:				Cemented Mica
Pitch	22 mm dia.	5.5 mm	-	7960A
Yaw	22 mm dia.	5.5 mm	-	8610A
Wollaston	15X15 mm	20 mm	-	Calcite, 20°
LED :				
Pitch	-	-	-	T.I.-SLH3 λ = 8,000
Yaw	-	-	-	T.I.-SLH4 λ = 8,600
Roll	-	-	-	G.E.-SSL55C λ= 9,500

Note: All optics, except detector, LED and immersion lens, are coated for less than 1.5% reflection, 0.8 to 0.95 microns.

However, the situation is actually much better than indicated by the rough estimate, as long as the spherical aberration of the objective lens is under-corrected. If the marginal focus of the objective lens is placed at the center of curvature of the immersion lens, all of the light from the objective lens will fall within the design diameter of 2.0 mm on the detector. Spherical aberration in the objective would in effect cause only a slight redistribution of light within the 2.0 mm circle. The extra 0.5 mm design margin is considered to be more than ample to accommodate manufacturing tolerances.

8.2.3 Off Axis Imagery

The coma of the objective lens, as shown by the preceding calculations, is negligible in comparison to the spherical aberrations and detector size. Therefore it is sufficient to consider only the on-axis configuration shown in figure 8-13. In the figure are shown the results of a ray trace for the upper and lower marginal rays from the objective lens. The object is at infinity and 1.0 degrees from the system axis. These rays strike the detector at radii of 1.004 and .645 mm respectively. Hence, even for off-axis objects the light still falls within the nominal design radius of 1.0 mm for the detector.

The above discussion assumed the use of an immersion lens in which the detector is bonded onto the rear surface of the lens. However, the detectors used in OAMS, UDT-PIN-5D, were mounted within a TO-5 can with a nominal 0.050 (-0 +.016) inch thick cover glass for protection. The actual detector surface is positioned .107 $\pm$ .012 inches below the inside surface of the cover glass. To account for the cover glass thickness and the air space, the ideal immersion lens thickness was shortened to that shown in the table. The immersion lenses were bonded to the detector cover glass with Summer's Lens Bond, type M-62.

A difficulty can be anticipated in this arrangement due to the relatively loose tolerances on the detector cover glass and spacing. Indeed, the manufacturer indicated that the type of glass was left to the discretion of their supplier. A number of detector cover glasses received by Chrysler could be seen to have distinct curvatures. The loose detector tolerances caused considerable difficulty in initial alignment.

The goal in the alignment procedure was to maintain the light intensity on the detector constant to within one-percent as the transmitter was moved within the receiver field of view. Because of the uncertainty in the separation and thickness of the components in the detector-immersion lens assembly, the goal could not be met without reducing the aperture. In future instruments the cover glass should be specified within closer tolerances or ideally removed entirely. In the present system this alignment trade-off between field of view uniformity and aperture size, resulted in a 40 to 50 percent intensity reduction.

NOT TO SCALE

y_1 = 1.004 mm
y_2 = 0.645 mm
$y_1 = y_2$ = 1.000 ON AXIS

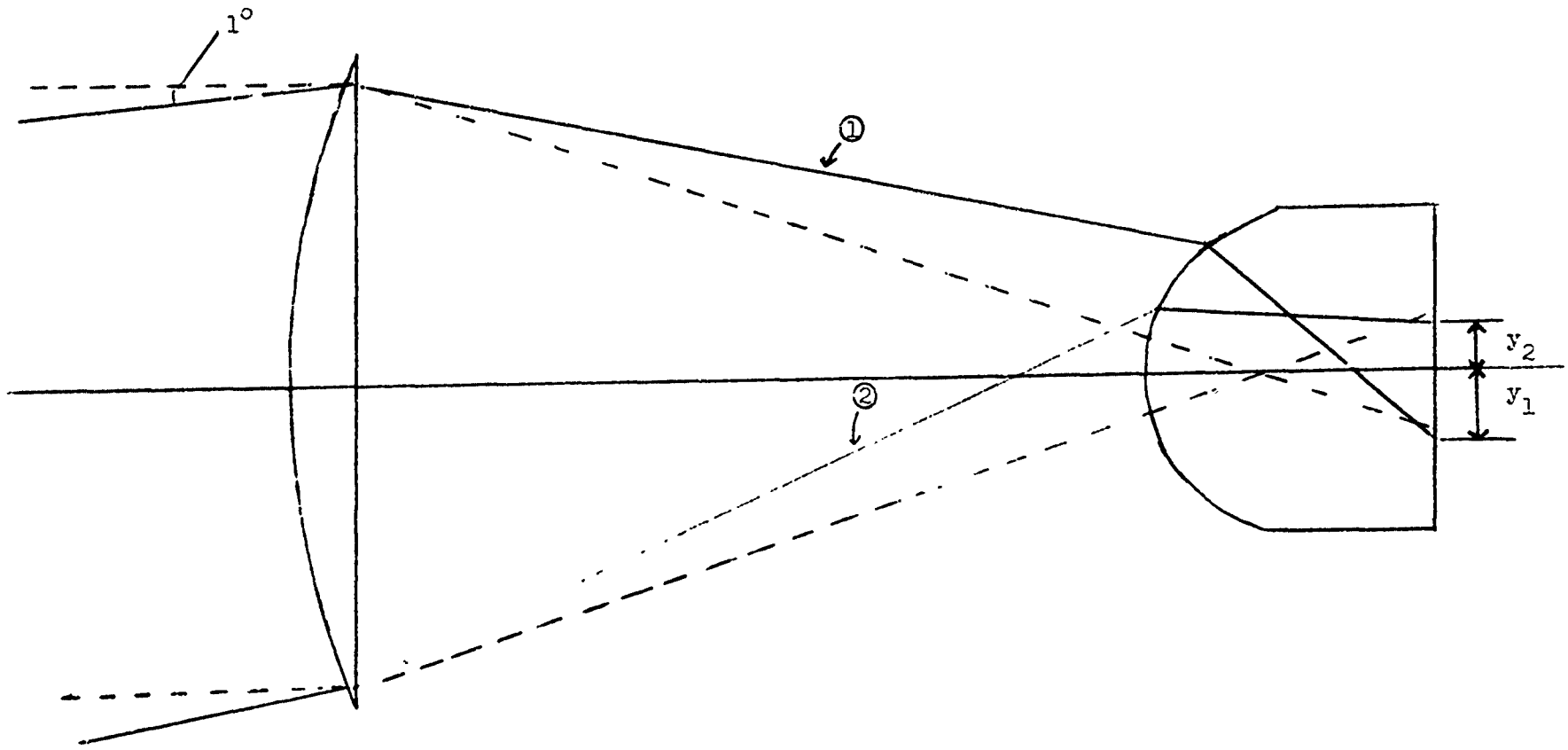

Figure 8-13, Summary of Receiver Ray Trace Results

8.3 Mechanical Design

8.3.1 Mechanical Design - General

Three assemblies are required for the sensor, a transmitter, a receiver and electronic unit, the units being positioned remote to each other as shown in figure 8-14. The transmitter and receiver mechanical assemblies are shown in figures 8-15 and 8-16. These assemblies each contain an optical package and an electronics package; the electronics package can be removed from the optical package without changing any optical component alignment.

The transmitter and receiver assemblies are hermetically sealed and the sealed containers will be purged with an inert gas prior to filling to a low pressure. Therefore, components of the transmitter and receiver assemblies would not be exposed to space vacuum conditions. This will prevent an outgassing from surrounding components or from the optical components themselves to affect the quality of the optical components. Outgassing on lens and angle sensing crystal faces would cause image blur and light transmission loss.

The reference surfaces (optical) are aligned with an autocollimator for the transmitter and receiver assemblies. The two assemblies are clamped to their respective reference platforms or positions, and autocollimated to each other to give a parallelism accuracy between the reference surfaces of $\pm$0.001 inch.

The required thermal stability that is necessary to obtain the accuracy of alignment is provided in the mechanical and structural configuration. This configuration has characteristics that allow a single unit construction matching capability. The multi-component mounts are positioned in cylindrical holders to ease the optical axis alignment problem. The thermal control of the sensor is accomplished by passive methods using the structural material (aluminum alloy) and, if needed, thermal coatings to give the derived amount of conduction and radiation as a means of heat transfer.

The angle sensing crystals which are the critical optical elements are so constructed that the two axes that are 90° apart have the same thermal gradient. Therefore, the temperature range requirement will have no effect on the angle sensing crystal measuring stability, provided that the elements of the angle sensing crystal are mounted together. This assures a uniform distribution of temperature.

8.3.2 Transmitter Design

The main transmitter housing is bored out from a one piece block of aluminum, into which the angle sensing crystals are hard mounted for the three channels. The shoulder, to which the angle sensing crystals are butted, have been machined and lapped to 8-12 micro inches, into this shoulder is the "O" ring groove which allows the compression of the "O" to completely fill the volume of the groove when the angle sensing crystal bottoms on the housing shoulder. Behind the angle sensing crystal is the quarter wave plate, spaced between these elements is a teflon shim or washer. This subassembly is clamped together by a threaded lock ring. The complete assembly is backed-up by a wave spring washer. The amount of compression that is applied to the complete assembly through the wave spring washer to allow the angle sensing crystal to bottom onto the lapped surface of the main housing is provided by the housing of sub-assembly holding the Wollaston prism and the light sources. This pre-assembled unit is positioned in the main housing and

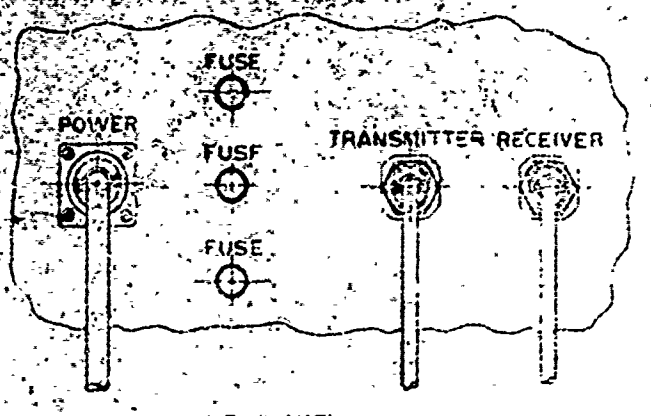

REAR VIEW

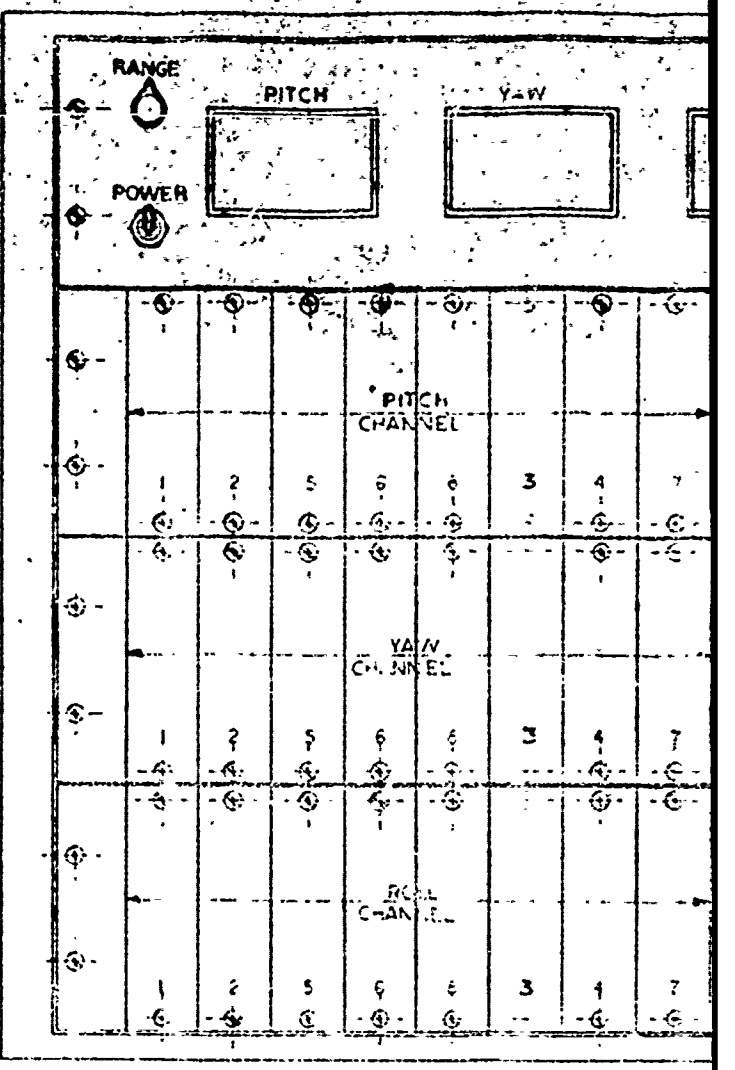

ELECTRONIC FRONT PAGE

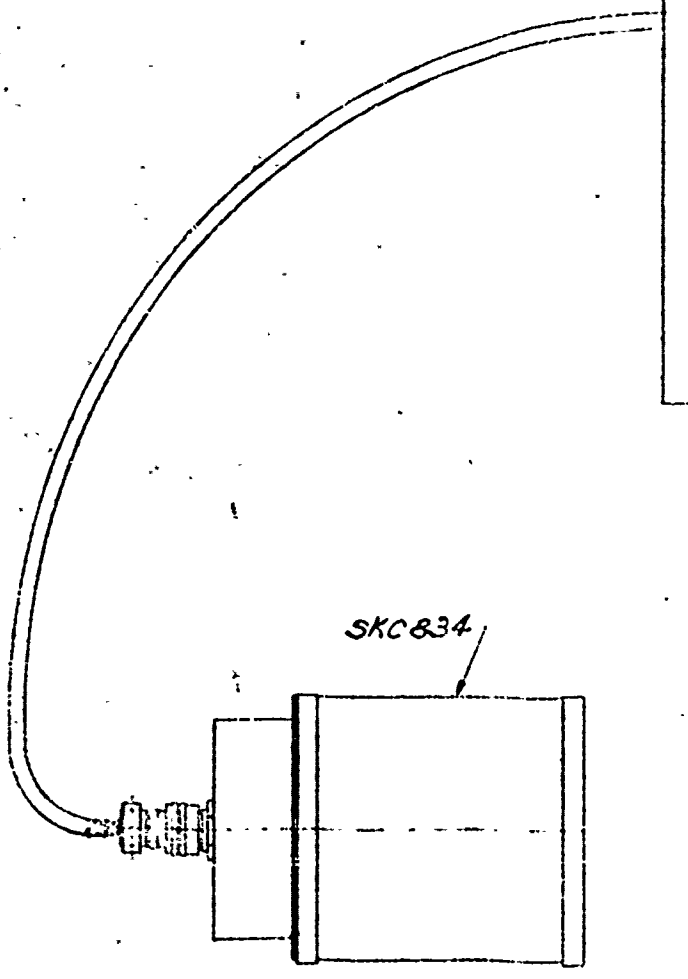

RECEIVER

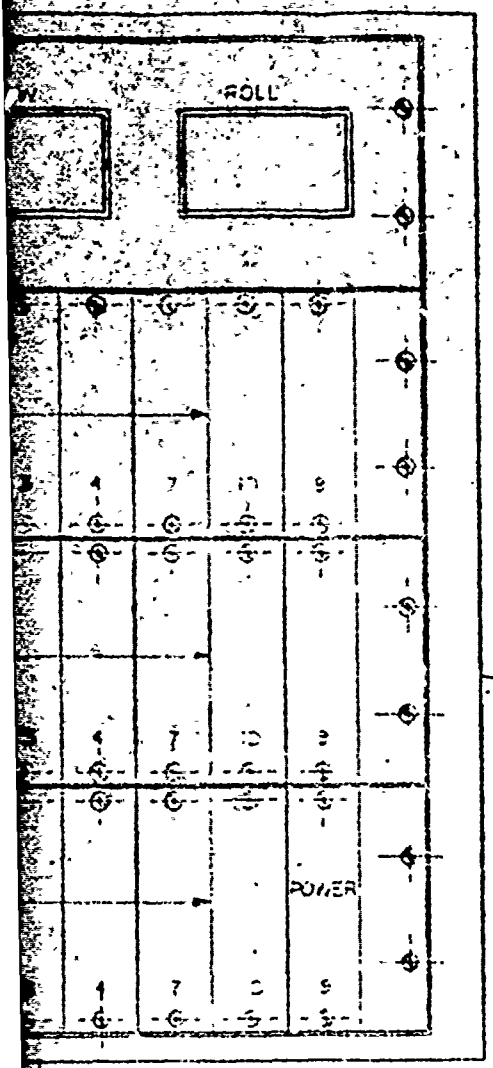

B-1 LIGHT EMITTING DIODE DRIVER BOARD
B-2 SIGNAL DIFFERENTIAL AMPLIFIER BOARD
B-3 SIGNAL DEMODULATION BOARD
B-4 DIFFERENTIAL-AMPLIFIER-LOW PASS FILTER BOARD
B-5 AUTOMATIC GAIN CONTROL BOARD
B-6 LED BALANCE DEMODULATION BOARD
B-7 LED BALANCE LOW PASS FILTER BOARD
B-8 SQUARE WAVE REFERENCE BOARD
B-9 POWER SUPPLY BOARD
PRE-AMPLIFIER BOARD IN RECEIVER

AGE

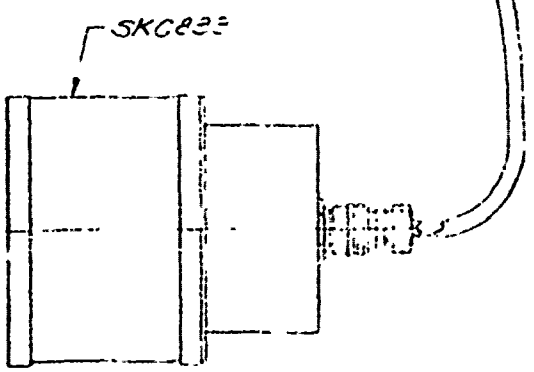

TRANSMITTER

THIS IS A REDUCED PRINT

OARE SYSTEM ENGINEERING BREADBOARD MODEL			
FIGURE 8-14		5-6-74	SKC 835

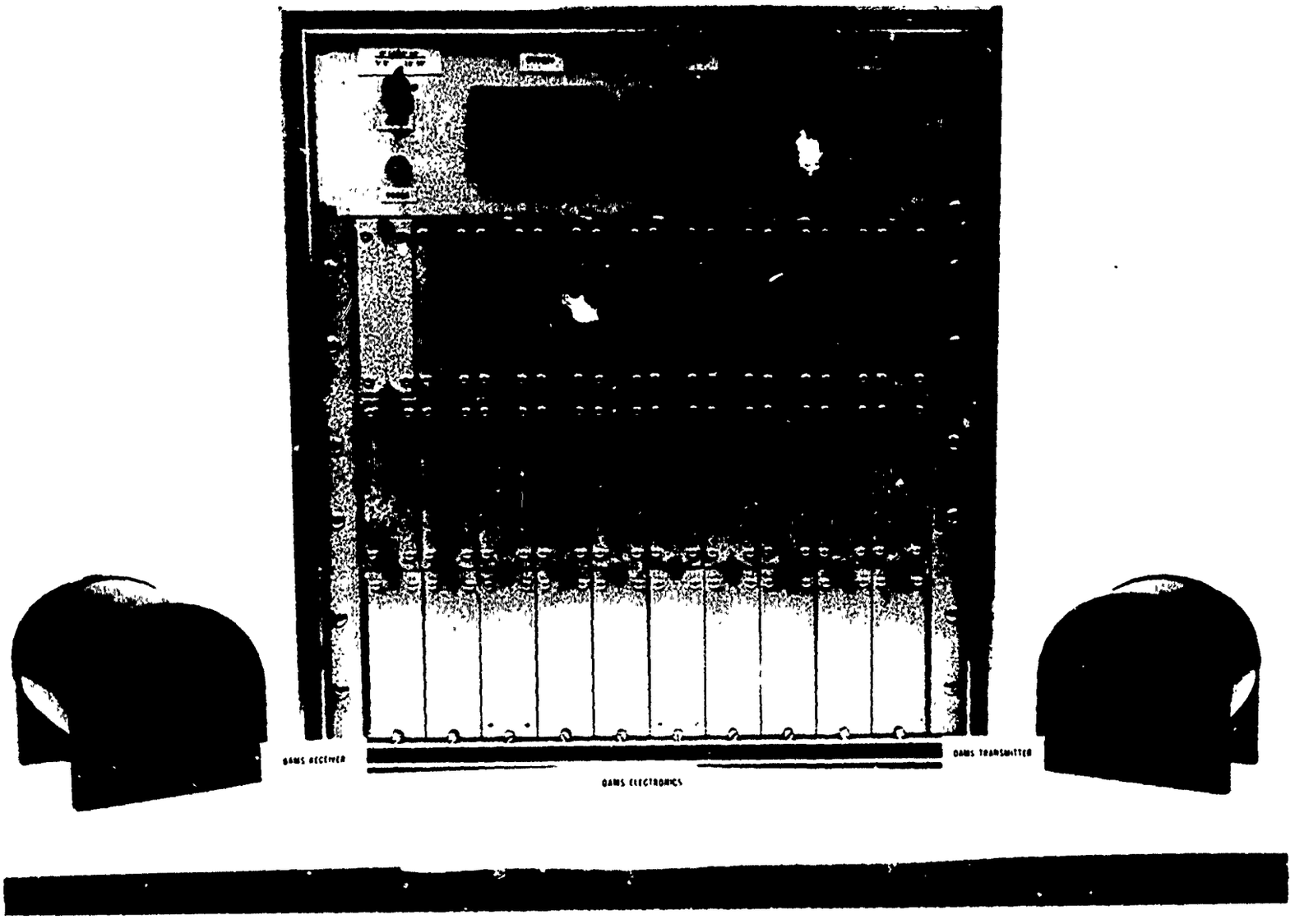

Figure 8-14A OAMS Brassboard Hardware

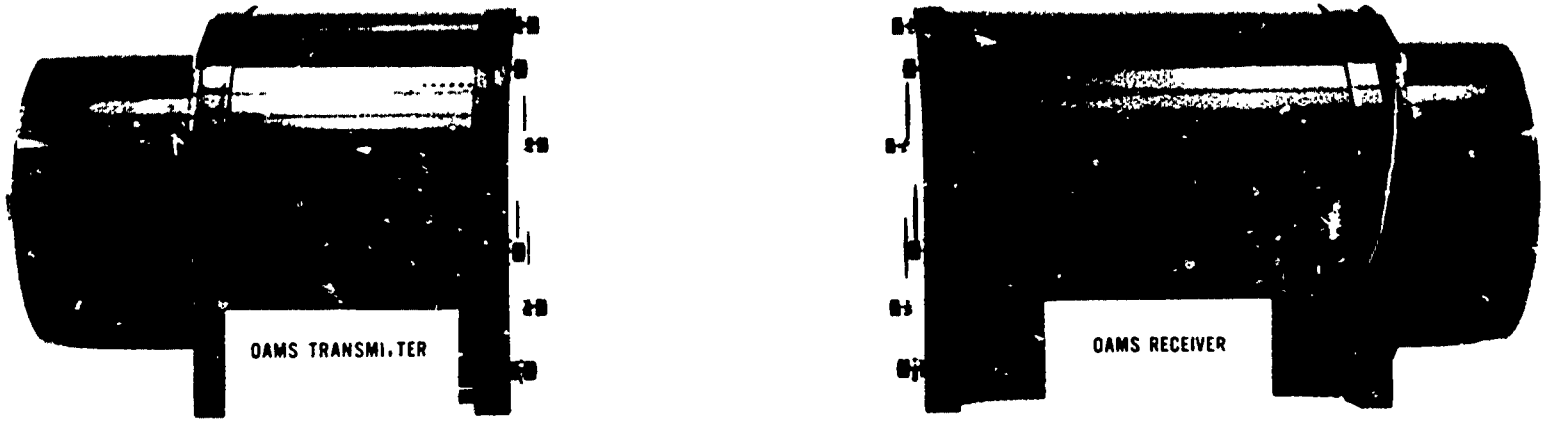

Figure 8-14B OAMS Transmitter and Receiver

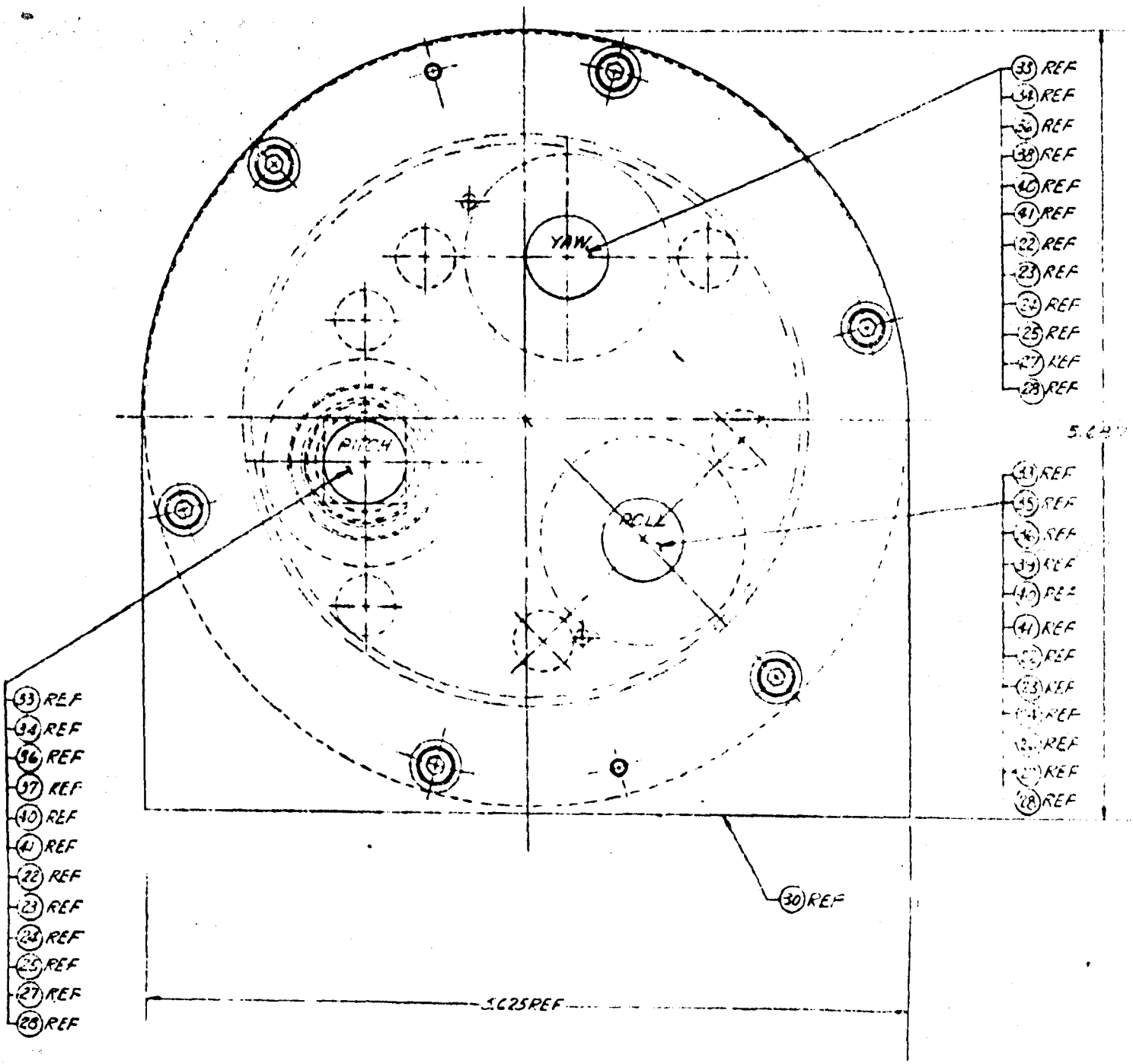

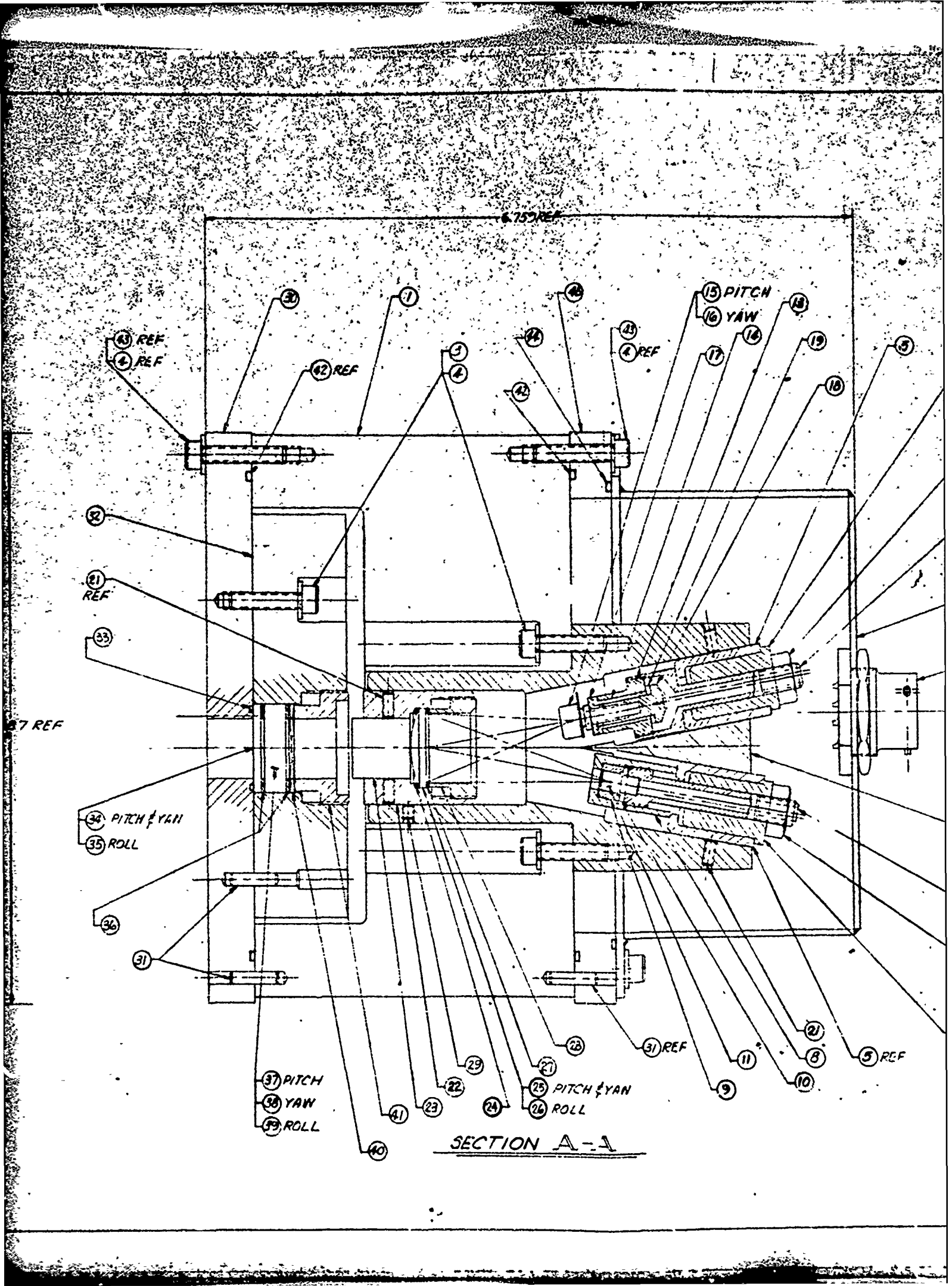
6.75 REF
30
1
46
15 PITCH
16 YAW
18
43 REF
4 REF
42 REF
3
4
44
43
4 REF
17
14
19
5
42
16
32
21 REF
33
7 REF
34 PITCH & YAW
35 ROLL
36
31
28
31 REF
21
11
8
5 REF
29
27
37 PITCH
38 YAW
39 ROLL
22
41
23
24
25 PITCH & YAW
26 ROLL
9
10
40

SECTION A-A

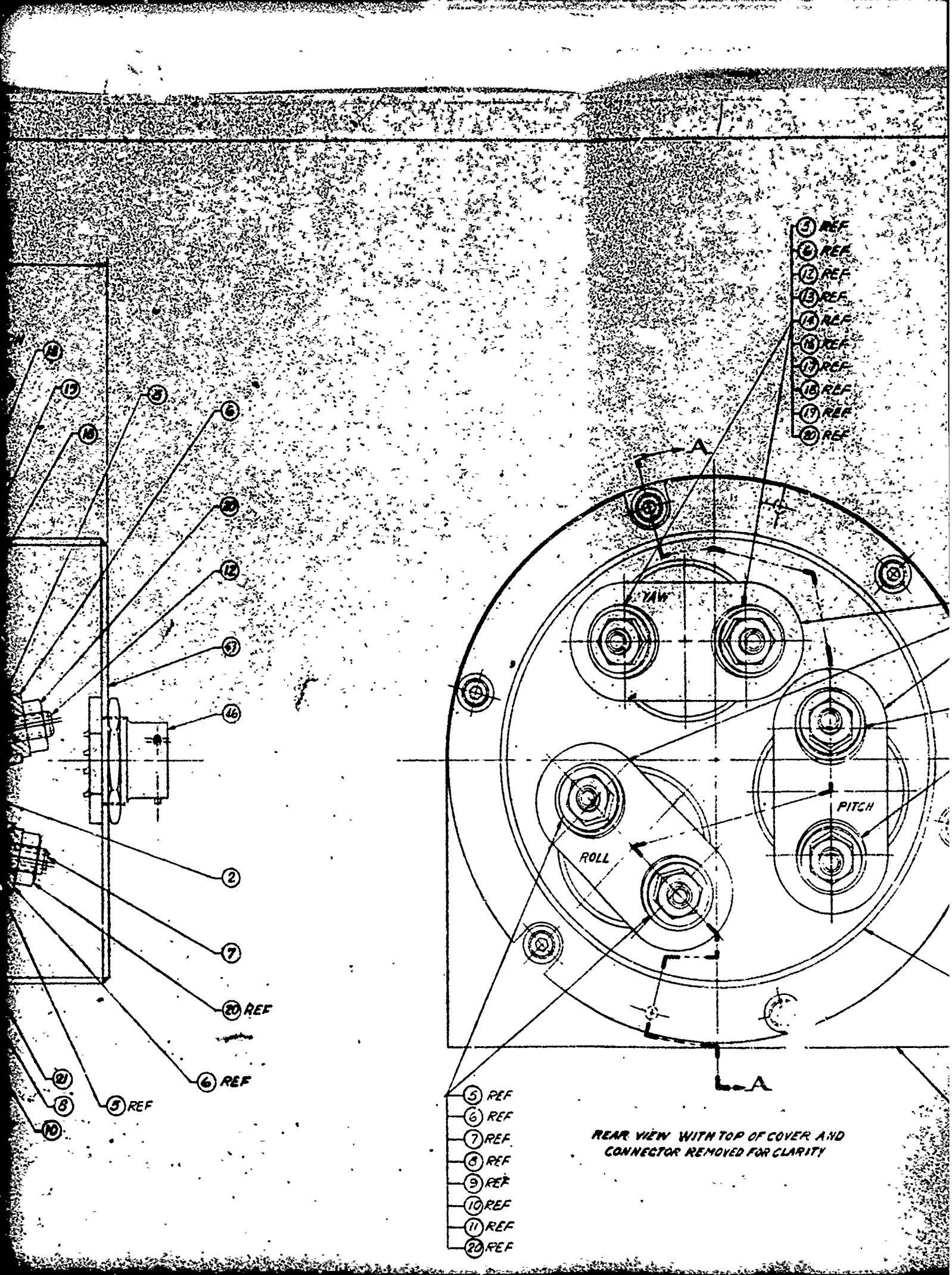

REAR VIEW WITH TOP OF COVER AND CONNECTOR REMOVED FOR CLARITY

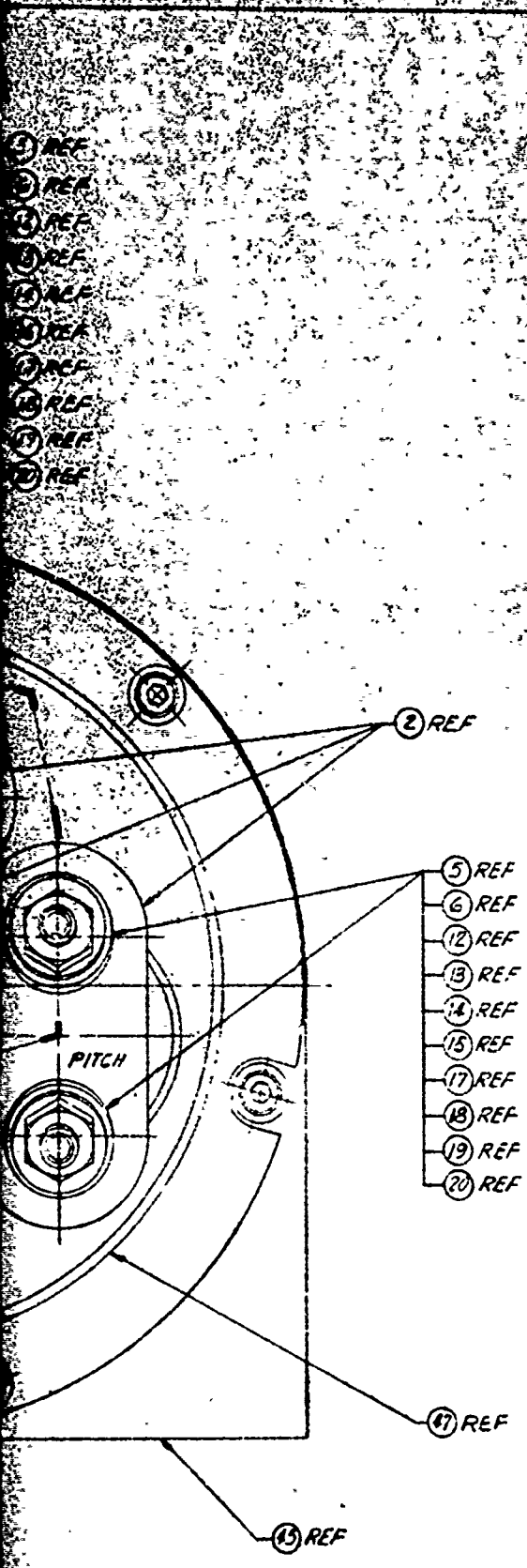

AND
ITY

ASSY NUMBER SKC835

PARTS LIST

ITEM NO	QTY REQD	SUB ASSY	PART NUMBER	DESCRIPTION	REMARKS
1	1	—	SKC828	HOUSING-TRANSMITTER	
2	3	—	SKC784	HOUSING	
3	5	—	[illegible]	SOCKET HD CAP SCREW	MATL: STAINLESS STEEL
4	21	—	[illegible]	WASHER-TYPE A PLAIN	
5	6	—	SKC796	BUSHING	
6	4	—	SKC793	ECCENTRIC	
7	2	—	SKC794	SHAFT	
8	2	—	SKC795	L.E.D. HOLDER	
9	2	—	SKC797	INSULATOR-SLEEVE	
10	2	—	SKC796	INSULATOR-WASHER	
11	2	—	SGL55C	L.E.D.-ROLL	GENERAL ELECTRIC CO
12	4	—	SKC787	SHAFT	
13	4	—	SKC791	L.E.D.-HOLDER	
14	4	—	SKC789	INSULATOR-BUSHING	
15	2	—	T.I.-SLH-3	L.E.D.-PITCH	TEXAS INSTRUMENTS
16	2	—	T.I.-SLH-4	L.E.D.-YAW	" "
17	4	—	SKC792	WASHER	
18	4	—	SKC788	NUT L.E.D.	
19	4	—	SKC790	INSULATOR-WASHER	
20	6	—	250-28 UNF-2A	NUT	
21	30	—	#4-40 UNC-2A-L.25	HEX-SOCKET SET SCREW	MATL: STAINLESS STEEL
22	3	—	SKC786	HOLDER-WOLLASTON PRISM	
23	3	—	15MM 30 20°	WOLLASTON PRISM	K. LAMBRECHT
24	3	—	SKC800	WASHER-LEVEL	
25	2	—	01LPX081	LENS-PLANO CONVEX	OPTICAL INDUSTRIES
26	1	—	01LPX107	LENS-PLANO CONVEX	" "
27	3	—	SKC799	WASHER PLAIN	
28	3	—	SKC801	NUT	
29	9	—	#4-40 UNC-2A-L.125	HEX-SOCKET SET SCREW	
30	1	—	SKC819	PLATE-FRONT	
31	6	—	.125 DIA x .500	DOWEL	MATL: CRES
32	1	—	SKC818	PLATE-ASSY & WAVER MTG	
33	3	—	S-181	"O" RING	PARKER SEAL CO.
34	2	—	22.2 MM DIA	ANGLE SENSING CRYSTAL	K. LAMBRECHT
35	1	—	22.2 MM DIA	PLATE WINDOW	BLOOMER RESEARCH
36	6	—	SKC816	WASHER-PLAIN	
37	1	—	22.2 MM DIA 795A	1/4 WAVE PLATE - YAW	K. LAMBRECHT
38	1	—	22.2 MM DIA 795A	1/4 WAVE PLATE - PITCH	K. LAMBRECHT
39	1	—	SKC820	SPACER-ROLL	
40	3	—	580-35-1	WAVE WASHER	SEASTORM MFG Co. INC
41	3	—	SKC817	NUT-ASSY & WAVER MTG	
42	2	—	2-014	"O" RING	PARKER SEAL CO.
43	12	—	#8-32 UNC-2A x .875	SOCKET HD CAP SCREW	
44	1	—	2-042	"O" RING	PARKER SEAL CO.
45	1	—	SKC827	PLATE-TRANSMITTER END	
46	1	—	UTO7C-12-4OP	CONNECTOR	BENDIX CORP.
47	1	—	SKC828	COVER-TRANSMITTER END	

THIS IS A REDUCED PRINT

TRANSMITTER, ENGINEERING BRASSBOARD MODEL (GAMA)		
FIGURE 8-15	3-1-74	SKC835

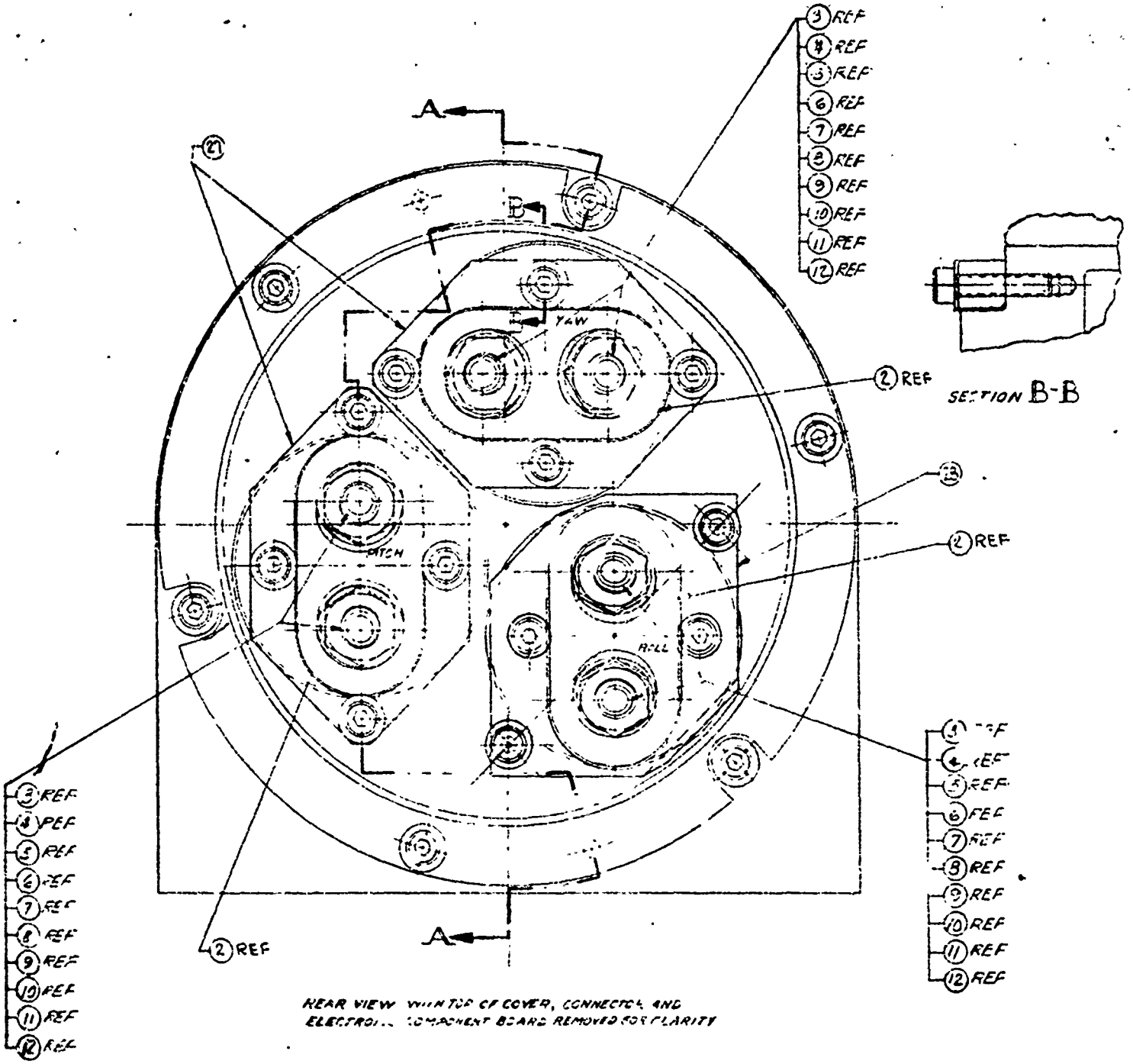

REAR VIEW WITH TOP OF COVER, CONNECTOR AND ELECTRONIC COMPONENT BOARD REMOVED FOR CLARITY

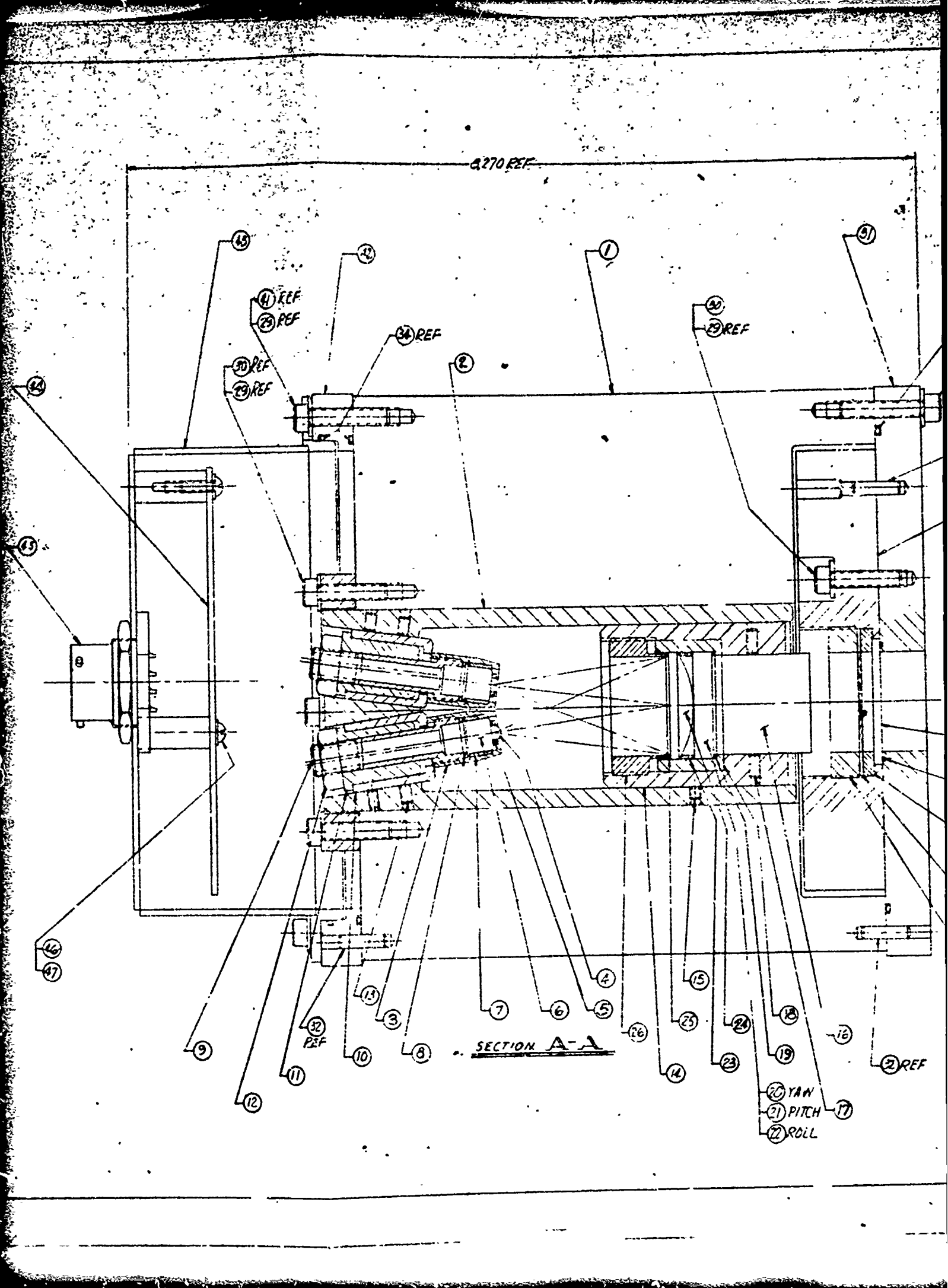
@270 REF
45
42
1
31
41 REF
29 REF
34 REF
30 REF
29 REF
30
29 REF
2
44
43
46
47
4
15
13
7
6
5
3
26
25
24
18
16
32 REF
9
10
8
SECTION A-A
14
23
19
22 REF
12
11
20 YAW
21 PITCH
22 ROLL
17

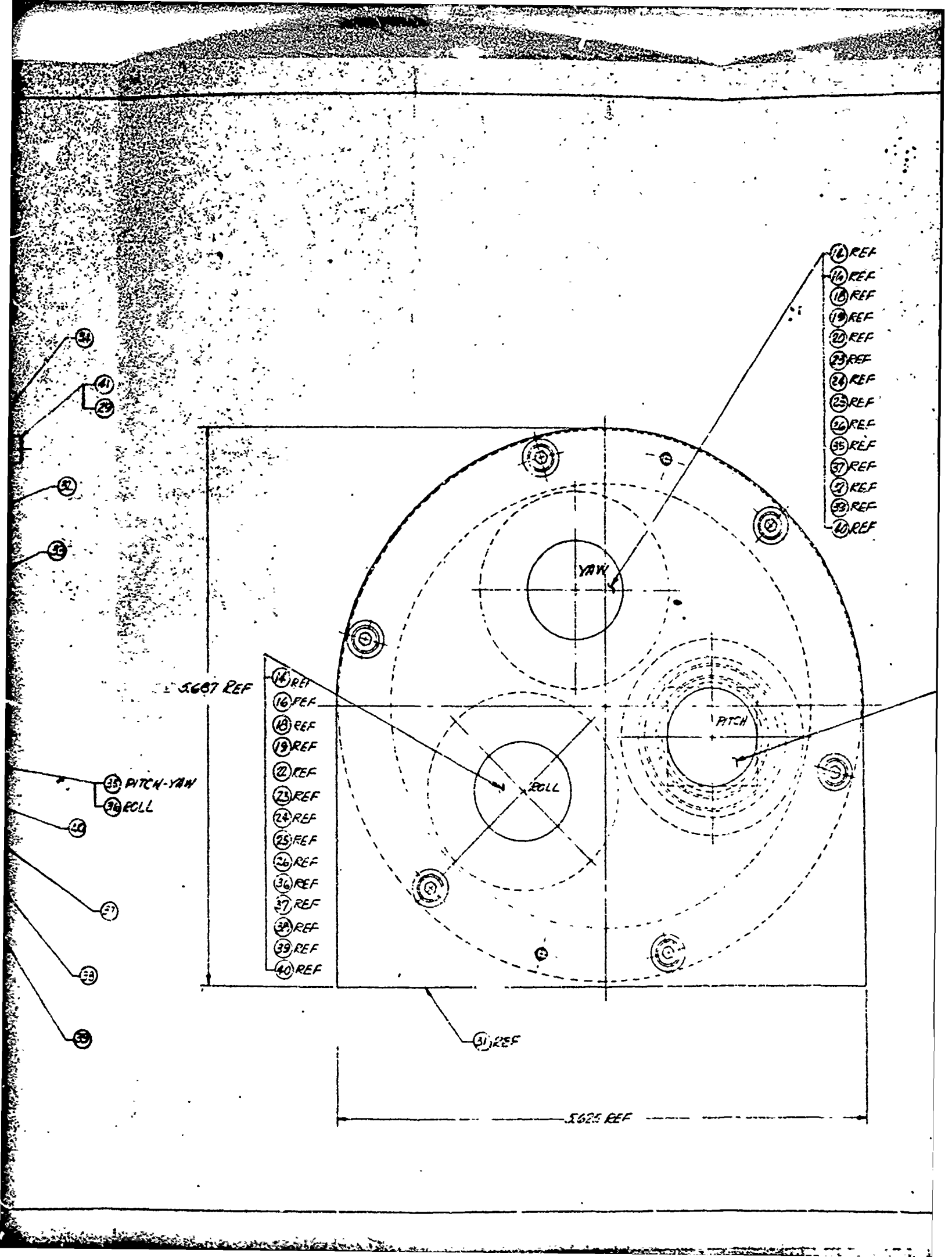
14 REF
16 REF
18 REF
19 REF
20 REF
23 REF
24 REF
25 REF
26 REF
35 REF
37 REF
41 REF
33 REF
40 REF
YAW
PITCH
ROLL
34
41
29
32
28
35 PITCH-YAW
36 ROLL
20
27
38
39
14 REF
16 REF
18 REF
19 REF
22 REF
23 REF
24 REF
25 REF
26 REF
36 REF
37 REF
38 REF
39 REF
40 REF
5.687 REF
31 REF
5.625 REF

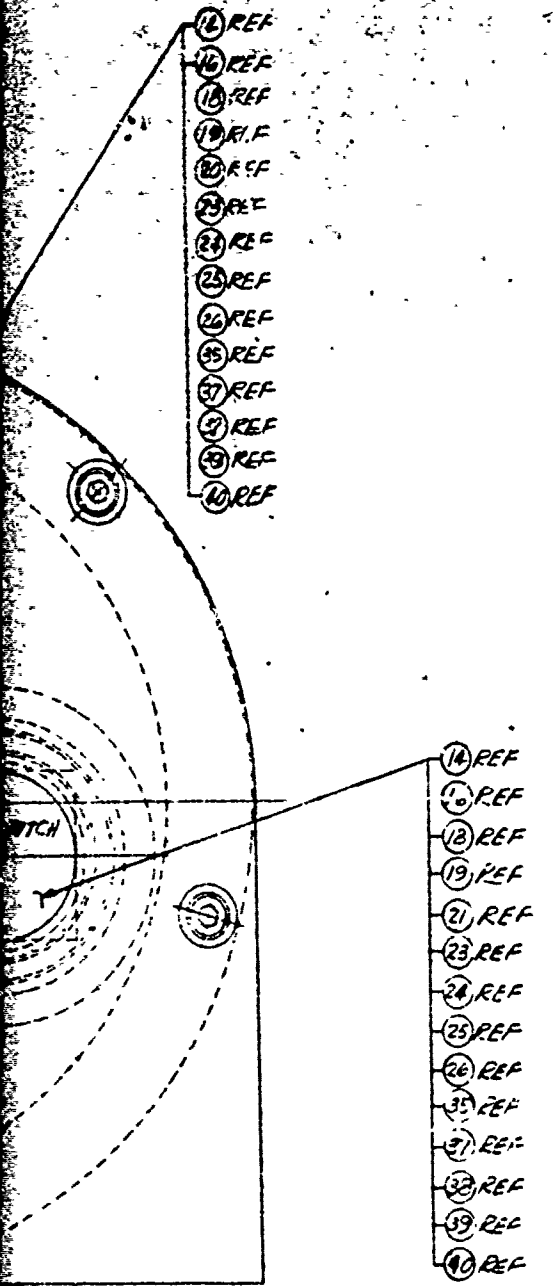

REVISIONS

NEXT ASSY NUMBER SKC235

PARTS LIST

ITEM NO.	QUTY REQD	SUB ASSY	PART NUMBER	DESCRIPTION	REMARKS
1	1	—	SKC826	HOUSING-RECEIVER	
2	3	—	SKC814	HOUSING-DETECTOR	
3	6	—	SKC802	HOLDER-DETECTOR	
4	6	—	[illegible]	IMMERSION LENS	BLOOMER RESEARCH
5	6	—	SKC832	RING-DETECTOR LENS MTG	
6	6	—	UDT FND/SDP	DETECTOR	UNITED DETECTOR TEC.
7	6	—	SKC807	INSULATOR-BUSHING	
8	3	—	SKC806	INSULATOR-WASHER	
9	6	—	SKC803	SHAFT	
10	6	—	SKC804	BUSHING	
11	6	—	SKC805	ECCENTRIC	
12	6	—	NAS-2[illegible]ZA	NUT	MATL: STAINLESS STEEL
13	12	—	#4-40 UNC-2A x .375	HEX SOCKET SET SCREW	MATL: STAINLESS STEEL
14	3	—	SKC813	HOLDER-LENS SUBASSEMBLY	
15	9	—	#4-40 UNC-2A x .125	HEX SOCKET SET SCREW	MATL: STAINLESS STEEL
16	3	—	25MM SCIE	WOLLASTON COMPENSATOR	K. LAMBRECHT
17	12	—	#4-40 UNC-2A x .250	HEX SOCKET SET SCREW	
18	3	—	SKC811	CUP-LENS FILTER	
19	3	—	SKC808	WASHER-SPACER	
20	1	—	22.2MM Dia 7425	FILTER-YELLOW CHANNEL	
21	1	—	" " 7750	FILTER-RED CHANNEL	
22	1	—	" " 7830	FILTER-IR CHANNEL	
23	3	—	SKC810	SPACER	
24	3	—	OIL P/108	LENS-PLANO CONVEX	OPTICAL INDUSTRIES INC
25	3	—	SKC809	WASHER-SPACER	
26	3	—	SKC812	NUT-LENS HOLDER/MIR	
27	2	—	SKC815	FLANGE-DETECTOR MOUNTING	
28	1	—	SKC836	RANGE-DETECTOR HOUSING	
29	27	—	#8 NARROW	WASHER-TYPE B PLAIN	MATL: STAINLESS STEEL
30	15	—	#8-32 UNC-2A x .750	SOC HD CAP SCREW	MATL: STAINLESS STEEL
31	1	—	SKC 824	PLATE-SECONDARY FRONT	
32	6	—	.125 DIA x .520	PANEL	MATL: CRES
33	1	—	SK-823	PLATE-DETECTOR MOUNTING	
34	9	—	S-140	O-RING	PARKER SEAL CO
35	2	—	1.250 DIA	SAPHIRE PLATE-MIRROR	K. AMBRECHT
36	1	—	1.250 DIA	ZONE WEDGE-ROLL	BLOOMER RESEARCH INC
37	3	—	SK-821	SPACER	
38	3	—	[illegible]-71-1	WAVE WASHER	SERVICEMASTER INC.
39	3	—	SKC 822	NUT-RING	
40	3	—	S-[illegible]	O-RING	PARKER SEAL CO
41	2	—	#832 UNC-2A x .875	SOC HD CAP SCREW	MATL: STAINLESS STL
42	1	—	SKC833	PLATE-RECEIVER REAR	
43	1	—	SKC830	COVER-RECEIVER END	
44	1	—	SK[illegible]	GASKET-END PLATE	
45	1	—	[illegible]	CONNECTOR	BENDIX CORP
46	3	—	#4 NARROW	WASHER-LOCK STEEL	MATL: STAINLESS STEEL
47	3	—	#4-40 UNC-2A x .375	[illegible]	MATL: STAINLESS STEEL

THIS IS A REDUCED PRINT

RECEIVER ENGINEERING SPECIFICATION MODEL (CAMS)

FIGURE 3-16

SKC 834 1-1

locked in position with screws, using dowel pins as guides, against the back face of the main housing. The wave spring washer is compressed to give the angle sensing crystal the hard mounting against the lapped surface. The Wollaston collimating lens and light source is a pre-aligned assembly unit and is positioned to the main housing and is used to apply the pressure onto the wave spring washer and positions the angle sensing to apply the pressure onto the wave spring washer and positions the angle sensing crystal. One of these assemblies, with its angle sensing crystal and quarter wave plate, is used for each of the three axes (see figure 8-15). This assembly has provision to align the Wollaston prism, collimating lens and the light emitting diodes (LED's). This mechanical adjustment is required to allow for tolerances in the Wollaston divergence angle (off-the-shelf Wollaston have $\pm 2^{o}$ tolerance on divergence angles). The adjustments for the Wollaston prism are line of sight positioning and roll. The LED and its collimating lens have mechanical movement adjustments relative to each other. The collimating lens is used as the fixed reference, and the LED can be adjusted along the line of sight for focusing the collimating lens on the light emitting area in the LED. The light emitting area is not necessarily equally spaced around the mechanical center line; to adjust for this the LED is mounted in two eccentric sleeves. This allows the LED to be rotated until the light emitting area centerline is positioned on the optical axis. When the adjustments have been completed, a sleeve and jam nut lock the assembly in position. The LED's are mounted directly in a special sleeve that will allow the heat generated to be conducted away to the main housing.

8.3.3 Receiver Design

The main receiver housing is bored out from a one piece block of aluminum, into which the angle sensing crystals are hard mounted for the three channels (figure 8-16). The shoulder for the angle sensing crystal is machined and lapped to 8- 12 micro inches; into this shoulder is the "O" ring groove which allows the compression of the "O" to completely fill the volume of the groove when the angle sensing crystal bottoms on the housing shoulder. This sub-assembly is clamped together by a threaded lock ring. This complete assembly is backed-up by a wave spring washer. The amount of compression that is applied to the complete assembly, through the wave spring washer to allow the angle sensing crystal to bottom onto the lapped surface of the main housing, is provided by the housing of the sub-assembly holding the Wollaston prism, objectives lens, field stop, and detection and its field lens. This pre-assembled unit is positioned in the main housing. It is locked in position with screws, using dowel pins as guides, against the back face of the main housing. The wave spring washer is compressed to give the angle sensing crystal the hard mounting against the lapped surface. One of these assemblies with its angle sensing crystal is used for each of the three axes; see figure 8-16. This assembly has provision to align the prism with its objective lens to the detector and its field lens. This mechanical adjustment is required to allow for tolerances in the prism divergence angle (off-the-shelf Wollaston prisms have $\pm 2^{o}$ tolerance on divergence angles). The adjustments for the Wollaston prism and its objective lens are axial and roll.

The detector and its field lens have mechanical adjustments for movement relative to each other. The field lens is used as the fixed reference, and the detector can be adjusted along the line of sight for focusing the field lens on the active area of the detector. The active area is not necessarily equally spaced around the mechanical center line. To adjust for this the detector is mounted in two eccentric sleeves. This allows the detector to be rotated until the active area center line is positioned on the optical axis. When the adjustments have been completed, a sleeve and jam nut lock the assembly in position.

8.3.4 Thermal Analysis

Several thermal analysis have been performed on Phase I design to evaluate the potential for indicated alignment errors caused by thermal stress distortions of both the transmitter and receiver instrument packages.

In general, the thermal distortion analyses indicated the following:

1. Temperature gradients along the instrument center axis are most likely to produce beam misalignment problems. The primary cause of these gradients is severe heating or cooling to the face of the instrument.

2. Non-symmetric heating or cooling of the instrument package is a secondary source of beam misalignment.

3. Internal heating sources will not produce significant crystal or beam alignment problems.

4. Using the available environment data, the instrument packages will not require special thermal environment isolation procedures. However, additional spacecraft mounting design and environment information is required to clearly define the amount of angular distortion that will result from imposed thermal transients.

Since a clear definition of a typical instrument installation environment was not provided, a detailed CINDA* analysis was only able to include thermal distortions due to internal heat sources. Internal instrument heating is due to the Light Emitting Diodes (LED) total power consumption (0.5 watts each). Only a small portion of the total LED power is transmitted out of the instrument as light. For a conservative analysis the light emitted was ignored. These preliminary results indicated that, considering a worst case of non-symmetic internal heat (i.e., one channel not operating), less than 0.1 arc second of crystal misalignment should result. To establish the actual crystal deflection from this heat source, will require a more extensive combined thermal and stress analysis which is currently planned for the future contract work.

A "First order" heating analysis was performed for several external situations that may cause thermal deflection of the face plate assembly holding the crystals. The analysis did not apply any mechanical restraints to the thermal expansion deflections that were predicted from external heat sources. The following results were indicated:

*CINDA - Chrysler Improved Numerical Differencing Analyzer Computer Program

1. Uniform hot or cold instrument body temperatures ($0^{o}F$ to $140^{o}F$) will not cause a significant crystal misalignment since all of the main body materials are of a common material.

2. Steady state heating or cooling to the instrument face or on mounting brackets will cause beam misalignment. Direct sunlight exposure to the instrument face (0.125 BTU/Ft^2-Sec.) will cause a crystal misalignment of less than 0.1 arc second with the instrument centerline.

3. A steady external total heat source applied on the instrument face of 4.14 BTU/Ft^2-Sec. will cause one arc second misalignment (the maximum allowable) of each crystal with respect to the instrument centerline and a 1.7 arc second misalignment of the crystals with each other. Currently there is no known satellite heat source of this magnitude.

4. Transient thermal environments will produce the most complex alignment problems. These require a combined thermal and stress analysis. A preliminary transient analysis indicated that high frequency transients (the order of 1 CPS) will not penetrate the instrument and that transients requiring more than a day to complete will not influence crystal alignment. Transient effects will be analyzed more extensively with CINDA during the Phase II program.

In general, the OAMS instrument package is a very stable thermal package. It is anticipated, however, that additional thermal stress evaluations be performed during future design studies as additional mounting hardware and installation thermal environments become better established. Figure 8-17 shows the calculated temperatures across the transmitter assembly at ambient. Figure 8-18 shows cross section at which these calculated values were obtained.

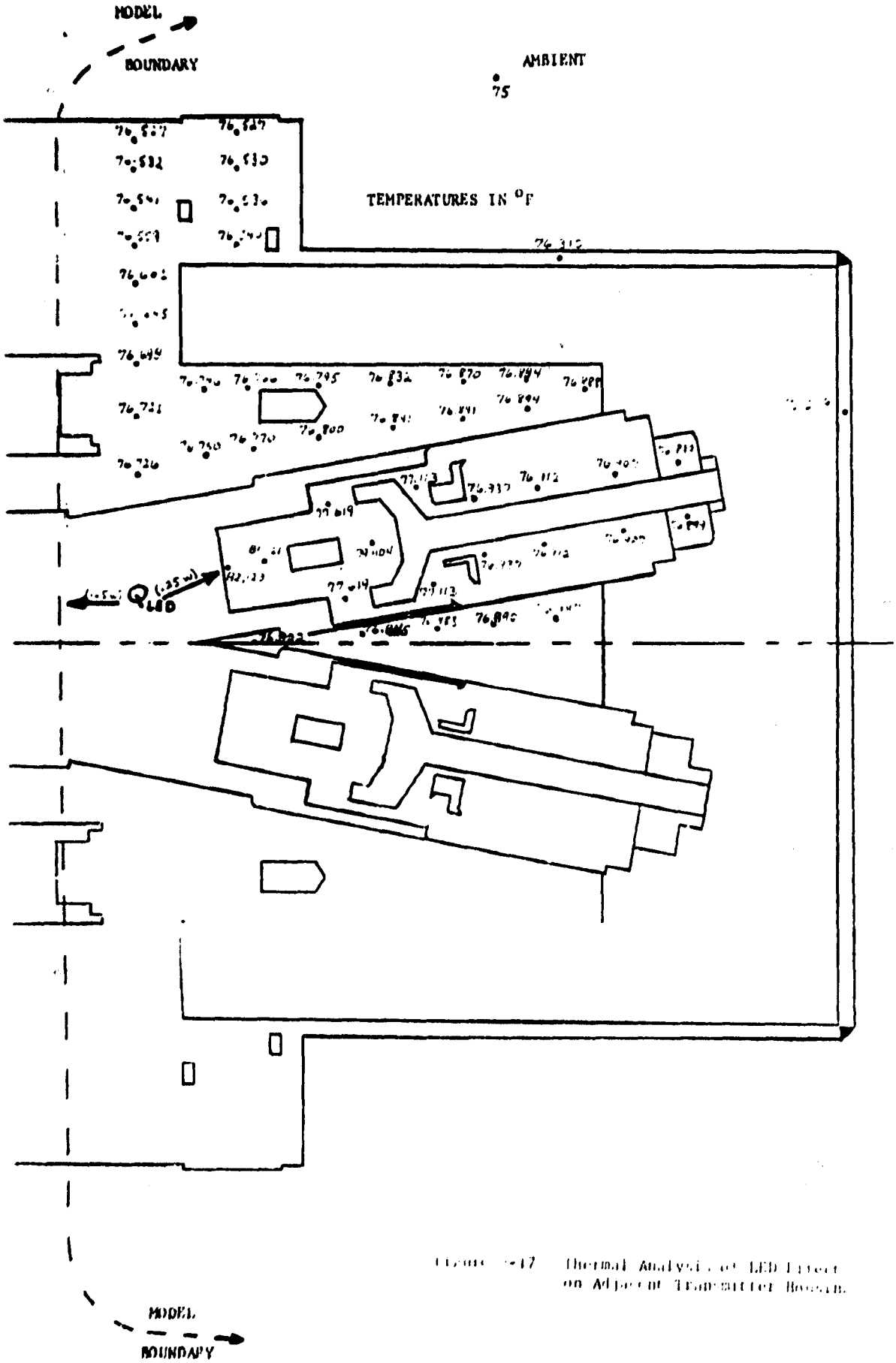

Figure 4-17 Thermal Analysis of LED Effect on Adjacent Transmitter Bocom.

Transmitter Rear View

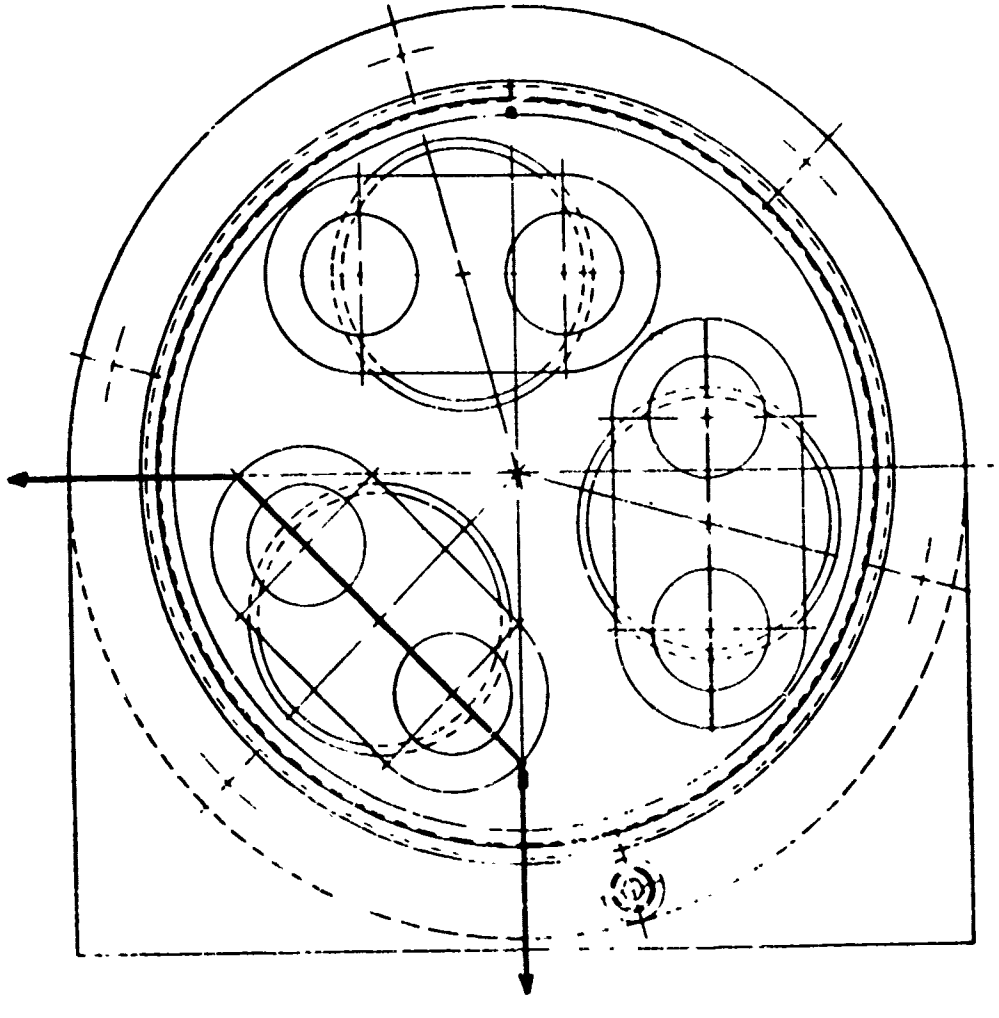

Figure 3-18 Location of Cross Section for Thermal Analysis

8.4 Electronic Design

The Optical Angular Motion Sensor Electronic Subsystem consists of three channels operated on an analog basis with three distinct frequencies of 925, 1850 and 3700 hz for roll, yaw and pitch, respectively. Each channel is integrated with three independent optical subsystems for the purpose of measuring relative angular displacement between two points in a 3-axis coordinate system. The composite system is a precision measurement device that converts small angular deflections (arc seconds) in roll, yaw and pitch between a reference point and a remote point into an electrical output. Basically, the electronics for each channel perform two functions; namely, 1) to provide the input to the system in the form of an intensity modulated light source about a quiescent level and 2) to detect this polarized modulated light source as a function of angular displacement and range, and process the resulting signal to yield an electrical output proportional to angular rotation.

With the aid of the block diagram shown in figure 8-19 and schematic drawings (Figures 8-20, 8-21 and 8-22) a comprehensive description of the functional operation of the OAMS electronic is presented. The electronic subsystem description will be subdivided into the following two subgroups: 1) LED Drive and Control Loop and 2) Signal Processing Electronic. These two subgroups will be identified and their functional operation and relationship upon each other described. Since all three channels are essentially identical (except for amplifier gain values, operating frequencies and low pass filters in the roll channel) this section will wherever practical address itself to a common description as indicated by the block diagram. Each block is assigned a numerical number for identification within the text. Following these two subsections, an electronic component description in Subsection 8.4.3 will describe the individual units and their application for the OAMS electronics.

8.4.1 LED Drive and Control Loop

Two light emitting diodes (LED), located in the transmitter, provide the input light source for each channel. Each diode pair is selected to emit energy in three different spectral regions to prevent cross coupling the light sources between channels. In both the transmitter and receiver the principle of duality was employed to increase system reliability and signal-to-noise ratio (SNR). The modulation frequency of operation for each channel are one octave apart. This provides additional immunity to channel cross talk since even harmonics are cancelled with the aid of the synchronous demodulator (9) and the differential amplifier (10). Odd harmonics from the roll channel frequency may enter the pitch channel, but are significantly attenuated by the optical filters and the action of the demodulator and differential amplifier combination.

NOTE: 1. DIAGRAM TYPICAL FOR PITCH, YAW AND ROLL.

2. SOLID LINES REPRESENT ELECTRICAL SIGNAL PATH

3. DASHED PORTION REPRESENTS MECHANICAL INTERFACE

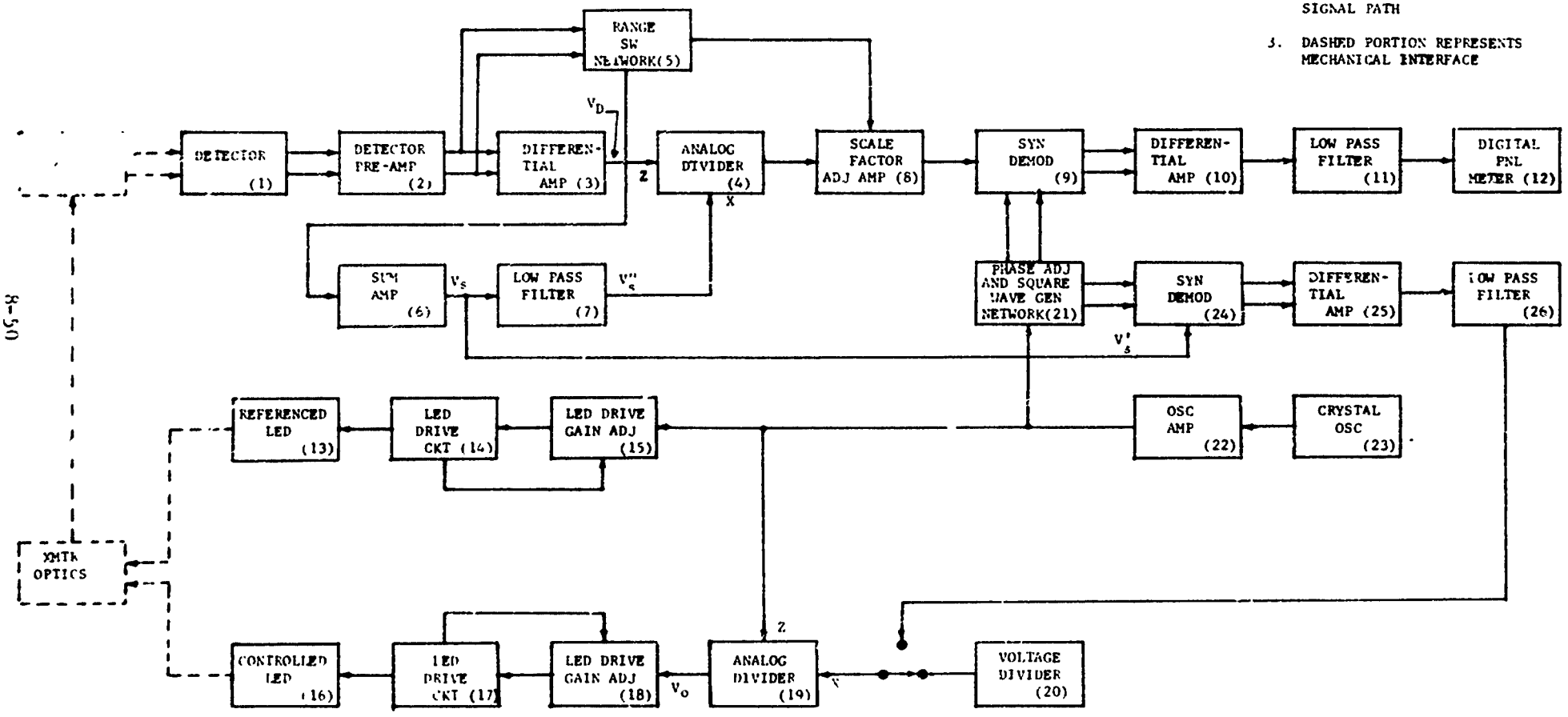

FIGURE 8-19 OAMS ELECTRONICS SYSTEM BLOCK DIAGRAM

The LED drive paths are similar except that one LED is used as reference (13) and the other controlled (16) through the action of the analog divider (19). The quartz crystal oscillator supplies the sinusoidal signal used in driving a three stage composite transistor circuit (cathode follower type action) with the LED connected between the positive 15 volt supply and the transistor's common collector tie point. In this application the LED diode and the third-stage-power transistor (Q_1 or Q_2) must be biased, by choosing the proper load line, such that the LED diode and transistor are compatible in their operation. In this case the diodes are always forward biased (a.c. as well as d.c.) and the maximum a.c. amplitude is bounded to prevent driving the transistor into saturation. The a.c. signal amplitude and d.c. bias current for the referenced LED (13) is fixed, however, this adjustment must be within a range whereby the a.c. and d.c. components of the controlled LED (16) can be effective (that is controllability of the modulation index) when controlling the level of light intensity seen at the detector outputs. Once the LED d.c. balance, as seen by the detector, are ascertained the bias d.c. current through the controlled and referenced LED is fixed per this design.

The analog divider (19) performs two basic functions in controlling LED output signal; namely, 1) to perform a 180 degree phase inversion on the a.c. signal and 2) to control the drive signal amplitude. The divider output is described by equation 8.4-1 where Z is the a.c. component (dividend) and X is a d.c. component (divisor). The X component is the controlling parameter and

$$V_o = -10 \frac{Z}{X} \qquad (8.4\text{-}1)$$

at this time is temporarily derived from a voltage divider (20). The primary reason for this action stems from the recent error analysis of Subsection 8.1 and Appendix E, whereby LED a.c. balance control alone will not be sufficient especially over long life cycles. As shown in the error analysis, LED modulation balance control requires, that both the d.c. quiescent (i_b) and the a.c. (i_m) current levels of the drive transistor be automatically adjusted. Otherwise a first order (primary) error will occur if i_m is the only controlled variable, therefore, causing the modulation ratio (m) of the controlled LED to shift away from that of the referenced LED (see equation E-50). Without control of i_b and i_m significant scale factor and null shift errors will result. Also, at or near LED balance the a.c. sum signal for controlling purposes is normally small relative to harmonics, noise generated signals and portions of the signal that are not cancelled due to signal distortion and small phase shifts. Because these unwanted signals masked the desired a.c. signal used for control purposes and consequently aggravated LED balancing via the synchronous demodulator (24), a band pass filter centered at the respected channel frequency is required. Because of these two problems and lack of time in designing three band pass filters, it was decided to use open loop control for LED a.c. balancing. The voltage divider setting was selected such that the a.c. sum signal's (output of summing amplifier (6) magnitude is minimal at system angular null. This effectively balances the LED light intensity output, however, this method does not compensate for light intensity shifts, as seen by the detector, due to angular motions in pitch, yaw and roll nor does it allow for changes in detector/LED responsivity degradations. Figure 8-23 is a proposed electronic block diagram that depicts an approach that is being incorporated in the brassboard for evaluation purposes.

Since the synchronous demodulator (24), differential amplifier (25) and low pass filter (26) applications are essentially the same as the signa

processing electronics subsystem, their operational description will be considered later in Subsection 8.4.4. The only exception is that the output of the low pass filter (26) is magnitude limited at -0.714 volts to avoid saturating the output of analog divider (19).

8.4.2 Signal Processing Electronic

The function of this circuit is to operate on two electrical signals, which are proportional to the light sources seen by the two detectors (1), such that the electrical output of the low pass filters (11) represents a relative difference in angle between the transmitter and target. The electronics required for this process is identified in figure 8-19 as Blocks 1 through 11. The operation of the optics of the light source impinging on the detectors is described in the System Analysis (Section 8.1) and OAMS Error Analysis (Appendix E).

The two silicon photodiodes (1) (two per channel) are operated in a photovoltaic mode (without d.c. biasing) where low noise equivalent power (NEP) capability is achieved. The signals from each detector (see figure E-6 and E-7) are preamplified (2) by low noise operational amplifiers and fed to the differential amplifier (3) and the range switch network (5). Should an angular difference exist between the transmitter and receiver, two a.c. signal components (d.c. blocked by capacitors located in Block 3) are applied to the differential amplifier. Since both signals are 180 degrees out of phase, the composite output signal (V_D) is effectively the sum of both input signals. This action doubles the signal level and cancels out common-mode noise components. The general differential amplifier output, V_D, is shown in equation 21, Appendix E. The term V_D (also Y) is the dividend for the analog divider (4). The divisor (X) for the analog divider (4) is obtained by the use of range switch network (5), summing amplifier (6) and low pass filter (7).

The range switch network consists of resistors which are selected according to the longitudinal distance between the transmitter and receiver. The OAMS is required to operate in four distinct longitudinal ranges (see Table 8-5).

Table 8-5 OAMS Operating Ranges

POSITION	RANGE
1	5 - 8 ft.
2	8 - 15 ft.
3	15 - 28 ft.
4	28 - 50 ft.

As a basis the OAMS range switch resistor network is calibrated according to the nearest longitudinal distance within each range. Since the summing amplifier requires two input signals (Detector 1 and 2), two input resistors are required for each position (see Figures 8-20, 8-21 and 8-22). These resistors in conjunction with the respective feedback resistor (R_9) determine the close-loop gain

(G_s) of the summing amplifier. The gain (G_s) within each range is selected such that the low pass filter (7) output will not drive the analog divider into saturation as long as the longitudinal distance is held above the next lowest range. Equations 8.4-2 through 8.4-6 describe the rationale for calculating these resistor values shown on the electrical schematics.

$$\frac{V_s}{G_{sj}} = (P_d)\ (R_d)\ (R_i)\ (G_p) \qquad (8.4\text{-}2)$$

where: V_s = voltage output of summing amplifier
P_d = power impinging on the detector (watts)
R_d = responsivity of detector (amp/watts)
R_i = shunt resistor across detector (ohms)
G_p = voltage gain of preamplifier (volt/volt)
G_{sj} = voltage gain of summing amplifier (volt/volt) at j range

If P_d equals intensity time solid angle, then

$$P_d = I_d \frac{A_d}{r_j^2} \qquad (8.4\text{-}3)$$

where: I_d = intensity on detector (watts/steradians)
A_d = receiver entrance aperture (ft^2)
r_j = smallest longitudinal range (ft)

Substituting equation 8.4-3 into 8.4-2 yields

$$\frac{V_s}{G_{sj}} = \frac{C_i}{r_j^2} \qquad (8.4\text{-}4)$$

where C_i equals ($I_d\ A_d\ R_d\ R_i\ G_p$) a proportionality constant.

Since V_s, r_{15} and G_{s15} are known for switch Position 3, all other gain values G_{s5}, G_{s8}, and G_{s28} and the resulting input resistors are calculated as shown.

$$\frac{V_s r_5^2}{G_{sj}} = \frac{V_s r_{15}^2}{G_{s15}}$$

$$G_{sj} = \frac{G_{s15} r_5^2}{r_j^2} \qquad (8.4\text{-}5)$$

If $G_{sj} = \frac{R_9}{R_{at\ j\ ft}}$ and $G_{s15} = \frac{R_9}{R_{at\ 15\ ft}}$

then by substituting these values in equation 8.4-5 the desired resistor value is obtained with equation 8.4-6.

$$R_{at\ j\ ft} = (R_{at\ 15\ ft}) \frac{r_{15}^2}{r_j^2} \qquad (8.4\text{-}6)$$

Note that $R_{at\ j\ ft}$ is the resistor value calculated at the new range.

The close-loop gain for each range is selected by the use of a four-position, break-before-make, ganged switch when rotated to the proper position enables the selection of the required resistor combination. The two signals from the detectors are fed to the summing amplifier (6) via the range switch network to the input resistor pair calculated by equation 8.4-6. These two signals are summed to yield the sum voltage, V_s, as described in equation E-20 of Appendix E. This voltage consists of a d.c. and a.c. component. The d.c. component is a function of the total light intensity. The a.c. signals consist of the fundamental and harmonic components plus electrical noise signals. The fundamental signal is a function of the LED imbalance as seen at the sum amplifier output. This a.c. signal (V') is fed to the synchronous demodulator (24) for use in LED a.c. balance control. The low pass filters (7) remove the a.c. signal from V_s and supplies a d.c. voltage, V_s'', as defined in equation E-36. These four pole, unity gain Butterworth, active filter transfer functions are shown in Table 8-6. The composite voltage transfer function for all filters are obtained as shown in equation 8.4-7.

$$H(s) = H_1(s)\ H_2(s) \tag{8.4-7}$$

where $H_1(s)$ and $H_2(s)$ are the component transfer functions. It should be noted that the filters in Block 26 are composed of a two pole Butterworth in series with a first order passive-phase-lead network. These filters are followed by a noninverting amplifier with gains of 32.1 for pitch and 21.0 for yaw and roll.

With V_D as the dividend and V_s'' as the divisor the analog divider (4) effectively normalizes the difference signal, V_D, for general variation in light intensity for a given angular position. The light intensity changes may be due to 1) detector and LED responsivity degradation, 2) non-uniformity in LED light pattern, and 3) change in range. This action of the divider on the difference signal is termed automatic gain control (AGC).

The normalized signal from the divider is fed to the scale-factor-adjust amplifier. This amplifier is a noninverting feedback amplifier with a close-loop voltage gain (G_f) as shown in equation 8.4-8.

$$G_f = \frac{R_1 + R_{f\ at\ j\ ft}}{R_1} \tag{8.4-8}$$

where $R_{f\ at\ j\ ft}$ is the feedback resistor found in the range switch network and R_1 is a constant 10 K ohm resistor for all three channels. Using equation 8.4-5 and substuting equation 8.4-8 for the gain yields the following scale-factor-adjust-resistor equation:

$$R_{f\ at\ j\ ft} = \frac{r_j^2}{r_{15}^2}\ (R_1 + R_{f\ at\ 15\ ft}) - R_1 \tag{8.4-9}$$

Note that $R_{f\ at\ 15\ ft}$ was determined by physically varying the feedback resistor until the desired scale factor was obtained. All of these feedback resistors are connected to the range switch, S_1, and are arranged with the sum amplifier resistor (equation 8.4-6) into groups, according to range, that are manually selected by rotating switch S_1.

TABLE 8-6. OAMS FILTER CHARACTERISTICS

BLOCK NO.	TRANSFER FUNCTION		CORNER FREQUENCY		DAMPING RATIO
	$H_1(s)$	$H_2(s)$	rad/sec	hz	
7 (Pitch, Yaw & Roll)	$\frac{3948.2}{s^2+116.1s+3948.2}$		62.8	10	0.924
11 (Pitch & Yaw Only		$\frac{3948.2}{s^2+48.1s+3948.2}$	62.8	10	0.383
11 Roll)	$\frac{9.914}{s^2+5.814s+9.914}$		3.14	0.501	0.924
		$\frac{9.868}{s^2+2.405s+9.868}$	3.14	0.499	0.383
26	$\frac{3948.9}{s^2+88.85s+3948.9}$		62.84	10	0.707
		$\frac{s+386.7}{s+3089.36}$	386.7 and 3089.4	61.6 and 491.7	- -

Because the roll channel has an optical angular sensitivity of 2 versus 60 for the lateral channels, larger roll differential amplifier (3) and scale-factor-adjust amplifier (8) gains are required. The amplified a.c. signal from the scale-factor-adjust amplifier (8) is proportional to the angular difference between the transmitter and receiver. This a.c. signal is fed to the synchronous demodulator (9) where two identical voltage follower amplifier stages are each slaved to the ON-OFF state of a grounded collector transistor. Two square wave signals, that are the complement of each other and derived from the phase adjust and square wave generator network (21), each drive the base of one transistor. The frequency of the square wave signals is the same as its corresponding channel frequency and is phase adjusted by an RC phase-lag circuit located in the phase adjust and square wave generator network (21). Each square wave signal turns ON and OFF its respective transistor such that one amplifier input is grounded (transistor ON) while the other amplifier is allowed (transistor OFF) to pass a half cycle of the a.c. signal. The resulting half wave rectified signals from each amplifier path are subtracted from each other by the differential amplifier (10). The resulting signal fed to the low pass filter (11) is a full-wave-rectified signal whose polarity is dependent upon whether the angular difference is positive or negative. The action of the synchronous demodulator and differential amplifier combination is to provide additional immunity to channel cross coupling and to generate a full-wave rectified signal whose magnitude is proportional to the angular difference. The differential amplifier provided unity gain since the required gain from the scale-factor-adjust amplifier (8) was sufficient for this application.

The low pass filter (11) for pitch and yaw channels are similar to the one described in equation 8.4-7 and Table 8-6. However, for the roll channel a four pole Butterworth filter whose corner frequency is at one-half hz was also designed to improve the SNR for long range tests. This filter is required to minimize the low frequency noise whose magnitude at null is approximately $\pm$ 30 mv peak-to-peak (as seen with a 10 hz filter) at a distance of 25 feet. The magnitude of this noise is proportional to channel signal strength which is directly related to longitudinal distance between the transmitter and receiver. In the lateral channels this phenomenon was held to within $\pm$1.5 mv (p-p) in pitch and $\pm$3.0 mv (p-p) in yaw because of the additional angular sensitivity. At a longitudinal distance of 5 feet the low frequency noise in all three channels was low as shown in Table 8-2 of the System Analysis Section. The filtered d.c. signal from each channel is fed to its respective digital panel meter (12) which is used to read data and monitor channel status.

8.4.3 Electronic Component Description

The purpose of this subsection is to describe in more detail the individual units that are used in the OAMS electronic subsystem. The previous sections described the function operations and rationale required in the electronic subsystem while this subsection will be less general and will focus on the specific applications and type components found in these units. Basic operational features, such as operational amplifier operation, etc., will not be covered. Each unit may contain one or several of the networks or circuits identified in the block diagram of figure 8-19. These units are either located on circuit boards, housed within the chassis, or in the receiver and transmitter subassemblies as shown on the schematic drawings (Figures 8-20, 8-21 and 8-22). This schematic also lists the part number of the individual components. For description purposes each unit will be categorized according to whether its function is related to: a) LED drive and control loop, b) signal processing

TABLE 8-7. ELECTRONIC UNITS AND LOCATION ASSIGNMENT

GROUP ASSIGNMENT	UNIT NAME	LOCATION	BOARD NO.
A. LED Drive and Control Loop	1. System Oscillator	Chassis	-
	2. LED Drive and Amplifier	Circuit Board (CB) and Chassis	B1
	3. Referenced and Controlled LED	Transmitter	-
	4. Synchronous Demodulator and Differential Amplifier	CB	B6
	5. Low Pass Filter	CB	B7
B. Signal Processing Electronic	1. Detector and Preamplifier	Receiver	-
	2. Differential Amplifier, AGC Analog Divider and Scale Factor Adjust Amplifier	CB	B2
	3. Summing Amplifier and Filters	CB	B5
	4. Range Switch Network	Chassis	-
	5. Synchronous Demodulator	CB	B3
	6. Output Differential Amplifier and Filters	CB	B4
	7. Digital Panel Meters	Chassis	-
C. Common to A and B	1. Phase Adjust and Square Wave Generator Network	CB	B8
	2. Power Supply	CB & Chassis	B9

electronic, or c) common to both a and b. The unit group assignment is shown in Table 8-7 and the description that follows will discuss each unit in the order allocated.

8.4.3.1 LED Drive and Control Loop Units

System Oscillator Unit

The basic synchronous oscillator source is a crystal controlled frequency device made by the Bulova Watch Company, Electronics Division. The output frequencies are: 925 Hz, 1850 hz and 3700 hz (all derived from a common oscillator source). The output voltage at each frequency is a sinusoidal, 1V RMS ±2% signal, that is stable to ±0.1%/day over a temperature range of -20°C to 60°C. The d.c. supply voltage required is a ±15 volt source with ±1% regulation.

LED Drive and Amplifier Unit

This unit contains the drive circuitry for both the controlled and referenced LED's. The oscillator amplifier is a non-inverting circuit with operational amplifier (A_5). This circuit provides impedance buffering between the oscillator and the driver circuits plus signal gains of 1.55, 1.32 and 1.4 in pitch, yaw and roll, respectively. This signal is applied to two parallel paths where one path is for the referenced LED and the other for the controlled LED. Both paths perform similar functions except that in the controlled LED path an analog divider is used for phase inversion and gain control of the drive circuit a.c. signal.

The analog divider is a product of Analog Devices, Inc., Model No. 427K. This is a precision type device with the following characteristics:

1) Maximum input voltage for rated accuracy is ±10.5 V

2) Full scale accuracy is 0.2%

3) Scale factor error is ±0.05%

4) Output noise is 50 μV rms

5) Supply source at rated performance is ±14.7 to 15.3 V

6) Temperature range at rated performance is 0°C to 70°C

The output of the divider is fed into a two stage non-inverting circuit with LM121 precision preamplifier (A_1 or A_3) driving a 741 amplifier (A_2 or A_4). The LM121 preamplifier operated with the general purpose operational amplifier (741 or LM118) drastically decreases d.c. errors and also improves SNR. Further, the added d.c. gain of the LM121 decreases the closed loop gain error. This type of two stage amplifier circuit is used extensively in the CAMS electronic. This circuit, for all three channels, had different gain values as shown in Figures 8-20, 8-21 and 8-22. The output of the two stage amplifier circuit (either path) inturn drives the three stage composite transistor circuit shown in the schematic. The final (third) stage power transistor (Q1 or Q2) located on the chassis drives the LED.

Referenced and Controlled LED Units

These LEDs are located in the transmitter. The diodes selected for this phase of UAMS are shown in Table 8-8.

Synchronous Demodulator and Differential Amplifier Unit

This a.c. error signal from the summing amplifier (B5), which represents LED imbalance, is applied to a non-inverting circuit (amplifier A_1) that has a gain of 19.2. This signal is then applied to two voltage followers, two-stage, amplifier circuit that are operated in parallel. Each voltage follower (A_2 and A_3 or A_4 and A_5) operate on either the negative or positive half cycle of the a.c. error signal and are slaved to the grounded collector transistor circuit (Q_{1A} or Q_{1B}). The square wave signal, driving these transistors through either diode D_1 or D_2, are complement of each other, thus determining which half cycle of the a.c. signal is rectified. The rectified a.c. signal from each path is fed into the differential amplifier stages of A_6 and A_7 where they are combined to yield a full-wave rectified signal at terminal J6-15.

Low Pass Filter Unit

The full-wave rectified signal at terminal J7-10 (from J6-15) is applied to the first-order zero/third order pole (1/3) filter (see Table 8-6). The active Butterworth filter consists of amplifiers A_1 and A_2 and the passive phase lead network consists of components R_6, R_7 and C_5. The resulting filtered output is applied to the non-inverting amplifier stages of A_5 and A_6 where gains of 21 for pitch and yaw and 32 for roll are obtained. Finally, diode D_1 and voltage divider (R_{12} and R_{13}) limits the signal at -0.714 volt to prevent driving the controlled analog divider into saturation.

8.4.3.2 Signal Processing Electronic Units

Detector and Preamplifier Unit

The detector and preamplifier unit located in the receiver is a dual circuit whose output is fed to the differential and summing amplifier circuits. The detectors are a product of United Detector Technology, Part No. PIN-5DP. The preamplifier circuit is a current-to-voltage converter with operational amplifier A_1 and A_2. A_1 and A_2 are the mono OP-05 series made by Precision Monolithics Incorporated. These amplifiers are for low signal level applications and feature low noise voltage, small offset voltage temperature drift and with long term stability. The output of each amplifier circuit is fed to an emitter follower transistor stage (Q_3 and Q_4) for impedance and buffering purposes.

Differential Amplifier, AGC Analog Divider and Scale Factor Adjust Amplifier Unit

The input signal to this unit is from the emitter follower via a shielded cable and is routed to terminals J2-10 and J2-11. Capacitor C_1 and C_2 block the d.c. components and allow the a.c. components to be differenced by the circuits containing A_1 and A_2. The differenced signal is applied to the Z terminal of the analog divider (same type as that discussed in 8.4.4.3) and a negative d.c. sum signal via terminal J2-12 is applied to the divider's X terminal. The normalized output from the divider is in turn applied to the non-inverting circuit that contains operation amplifier A_3 and A_4. This non-inverting circuit

TABLE 8-8. LED CHARACTERISTICS

MFG.	PART NO.	CENTER WAVE LENGTH	CONTINUOUS POWER RATING @ 25°C	CHANNEL
Texas Inst.	SLH3	800 n m	8 mw @ 200 m a	Pitch
Texas Inst.	SLH4	860 n m	8 mw @ 200 m a	Yaw
G. E. Co.	SSL55C	950 n m	14 mw @ 300 m a	Roll

nm = 1×10^{-9} meter

mw = milliwatt

is used to adjust the channel's scale factor for four ranges as described in 8.4.3. The output signal is in turn fed to the synchronous demodulator via terminal J2-15.

Summing Amplifier and Filters Unit

The detector preamplifier input signal is also routed via the shielded cable to the range switch assembly and then applied to terminals J5-14 and 15 when the range switch is in position 3 of Board B_5. These two signals are summed by the inverting circuit that contains operational amplifiers A_1 and A_2. The output from this summing circuit is applied to the four pole Butterworth filters and to terminal J6-11 of board B_6. The four pole filter characteristics are shown in table 8-6. The first second-order filter contains operational amplifiers A_3 and A_4 while the other second-order filter contains the amplifier pair A_5 and A_6. The filter output at terminal J5-18 is routed to the X input of the analog divider located on board B_2.

Range Switch Network

This network enables selection of the proper scale factor gain and summing amplifier gain. This is performed by a four position switch for all three channels by switching a resistor from each of three sets of four (R_3 thru R_6) for scale factor purposes and switching two resistors from each of three sets of eight (R_1 thru R_8) for sum gain purpose. For example R_5 located on the range switch and R_5 and R_6 on Board 5 are selected for range Position No. 3.

Synchronous Demodulator Unit

The synchronous demodulator of L_3 operates similarly to that described in 8.4.4.5. The only exception is the absence of a non-inverting circuit between C_5 and the junction with R_2 and R_7.

Output Differential Amplifier and Filter Unit

The two half-wave rectified input signals from the synchronous demodulator via terminals J4-10 and 11 are applied to the unity gain differential amplifier circuit containing A_1 and A_2. The polarity of the differenced signal is dependent upon whether the angular difference is positive or negative. The differenced signal (full-wave rectified) is applied to the first active Butterworth filter (see Table 8-6, $H_1(s)$) which contains A_3 and A_4. The second Butterworth filter, $H_2(s)$, contains A_5 and A_6.

The roll channel difference amplifier and filter each contain one stage of operational amplifier since the 1/2 cycle filter has good noise rejection properties, therefore, does not require the preamplifier stages shown in pitch and yaw. The roll filter transfer functions $H_1(s)$ and $H_2(s)$ are shown in Table 8-6. The rationale for selecting a 1/2 cycle filter is contained in 8.4.3.

Digital Panel Meters

The output signal from the filters located on board B_4 are applied to the panel meters via terminals J4-15. Three analog-to-digital panel meters (one per channel) are employed for the purpose of monitoring the

angular difference between the transmitter and receiver. The model number is AN2544, a product of Analogic. The meter accuracy is 0.01% at 25°C. The display has 5 digits with provisions for programmable decimal point selection. Operating temperature range is -10°C to +45°C. Supply voltage is either 117 or 234 Volt, 50/60 Hz.

8.4.3.3 Units Common to Both LED Control and Signal Processing

Phase Adjust and Square Wave Generator Network Unit

The purpose of this unit is to convert sinusoidal oscillator input signals from terminal J1-11 of Board B_1 into two complemented square wave signals that are in phase with the primary signals to the synchronous demodulators contained in B_3 and B_6. The input signal from terminal J8-10 is applied to the voltage follower circuit containing amplifier A_1. The output of the voltage follower furnishes a signal to two parallel and identical paths (one for the signal processing demodulator and the other for the LED control loop demodulator). Each path contains an RC phase-lag circuit (ex. R_3, R_5 and C_1), a voltage follower (A_2) and an a.c. coupled open-loop amplifier (A_4 and A_5). The double shunt limiter consisting of diode pairs (D_1, D_2 or D_3, D_4) provides the voltage drop across amplifier terminals 3 and 4. This voltage drop is a function of the diode's forward voltage and the signals are complemented by reversing the input terminals of the amplifiers. Two sets of square wave and complemented signals are thus generated.

System Power Supply

The power supply operates from a nominal +28 VDC source and supplies regulated ±15 VDC to the system. In the description of the power supply, reference will be made to the power supply schematic Figure 8-24.

First to be described will be the +15V section. Transistors Q11 and Q12 and transformer T2 along with an associated RC network of R1, R20, C1 and C2 make up its inverter stage which has a 115 volts rms, 400 Hertz output. This output is stepped down in voltage through transformer T4 to approximately 24 volts rms which is applied to the diode bridge rectifier consisting of diodes D5 through D12. The bridge output supplied across filter capacitor C3 forms the unregulated DC voltage supplied to the power transistors Q6, Q7 and Q8 and to the regulator V2. The collectors of these three transistors provide the regulated output to the +15 VDC buss. Filter capacitor C6 is also connected to this buss. Current limiting is provided by resistor R5 and the output level is set by the network of R2 and R3. The regulator sensing leads are connected to the supply and ground busses through card connector pins 17 and 18. Fuses F2 is provided for protection in the event of failure in the regulating section.

Next to be described will be the -15 VDC section. The inverter, stepdown transformer, diode bridge, filter capacitor and protective fuse are the same as for the +15 VDC section. Transformer T1 with transistors Q13 and Q14 and associated components make up the inverter. The step down transformer is T3. The diode bridge is composed of diodes D13 through D20. The filter capacitor for the bridge output is C9 and the protective fuse is F1.

The regulator is made up of reference V1 with amplifiers A1 and A2 and power transistors Q1, Q9 and Q10. Regulated voltage is applied as supply to amplifiers A1 and A2 by a pre-regulator made up of transistors Q2 and Q3, reference diode D3 and associated components. Supply output level is set with the network of R18 and R19. Sensing leads are connected to the power and ground busses through card connector pins 5 and 6. Current limiting is provided by R14 and transistor Q5. Over-voltage protection is provided in the event of regulator failure by the network consisting of diodes D3 and D4, transistor Q4 and associated resistors R21, R22 and R23. Filter capacitor C4 is connected from the supply buss to the ground buss.

Fuse F3 is the main fuse for both the plus and minus 15 VDC supply and is located in the line to the +28 volt source. In the final version, a network to protect this supply from transients would also be put in this line following the main fuse. A diode will protect against negative transients. An inductor followed by a large filter capacitor and a varistor will protect the supplies from positive transients.

Power Supply Modifications

Presently the OAMS brassboard uses approximately 150 watts of power from a +28 VDC supply. It is estimated that this quantity can be reduced to less than 36 watts as described in the following paragraphs.

First to be described will be the present system. The power required by the three channels without including the dissipation in the power supply is approximately 56 watts. Of this, the light emitting diodes and driver transistors together dissipate 18 watts, the driver resistors dissipate 18 watts and the remaining channel electronics dissipate about 20 watts. Power dissipated in the $\pm$15 VDC regulators is approximately 43 watts. The two saturating inverters have a no load dissipation of 21 watts each for a total of 42 watts for both. This sums up to 141 watts. The remaining 9 watts are dissipated in various networks throughout the system.

In the next system, the number of operational amplifiers will be reduced from a total of 135 to a total of 84. This will achieved by replacing each LM121/LM118 op-amp pair with a single Precision Monolithics OP-07A. Supply voltage to the op-amps will be reduced from $\pm$15 VDC to $\pm$7½VDC. This reduces the 20 watt requirement in the channel electronics to 5 watts. The 9 watts referred to as dissipated in various networks will be reduced to 2.25 watts. Voltage to the LEDs will be +7½VDC and voltage to the driver resistors will be -4V. This reduces the previous 36 watts required by the driver section to 13.8 watts while maintaining the same bias currents. This reduces the power required by the three complete channels of electronics from a total of 65 watts to a total of about 21.1 watts. This quantity must be increased only by enough for power supply loss in order to obtain the total input power required. Assuming an efficiency of 60% for the inverter and regulator together for an optimum system, 35.2 watts would be required from a +28VDC source.

8.4.4 Wiring Diagram and Circuit Board Layouts

Figure 8-25 shows the complete wiring diagram for the electronics unit and the interconnecting cables for the transmitter and receiver units. The circuit board layouts with the major components indicated by the reference numbers from the electronic schematic diagrams are shown in Figures 8-20, 8-21, and 8-22.

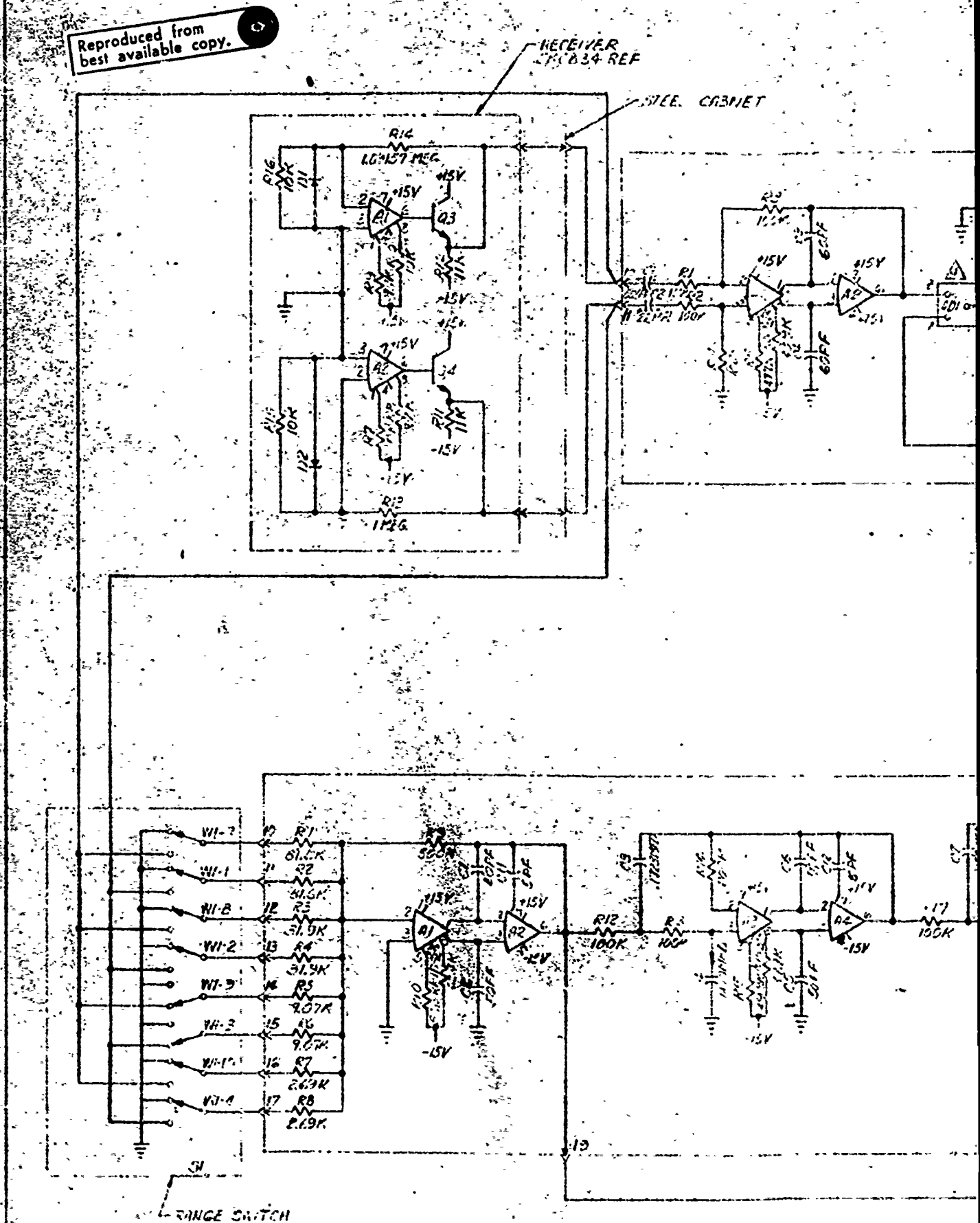

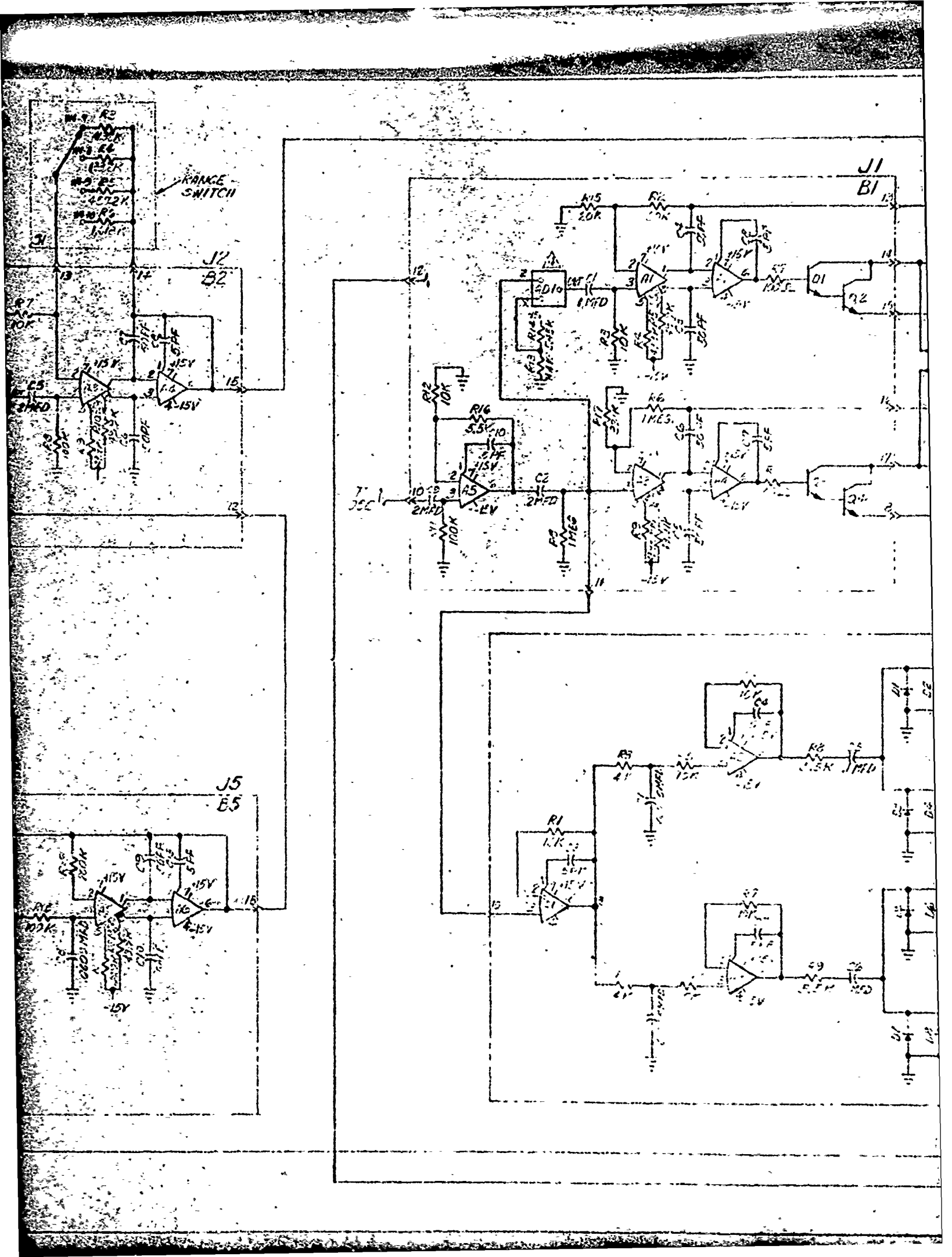
J1
B1
J2
B2
J5
B5
RANGE SWITCH
R1
10K
C5
2MFD
C1
1MFD
C2
2MFD
R16
5.5K
R17
3.3K
R6
1MEG.
R5
1MEG
R12
10K
R15
20K
R4
100K
A1
A2
A3
A4
A5
A6
A7
A8
A9
A10
D1
D2
+15V
-15V

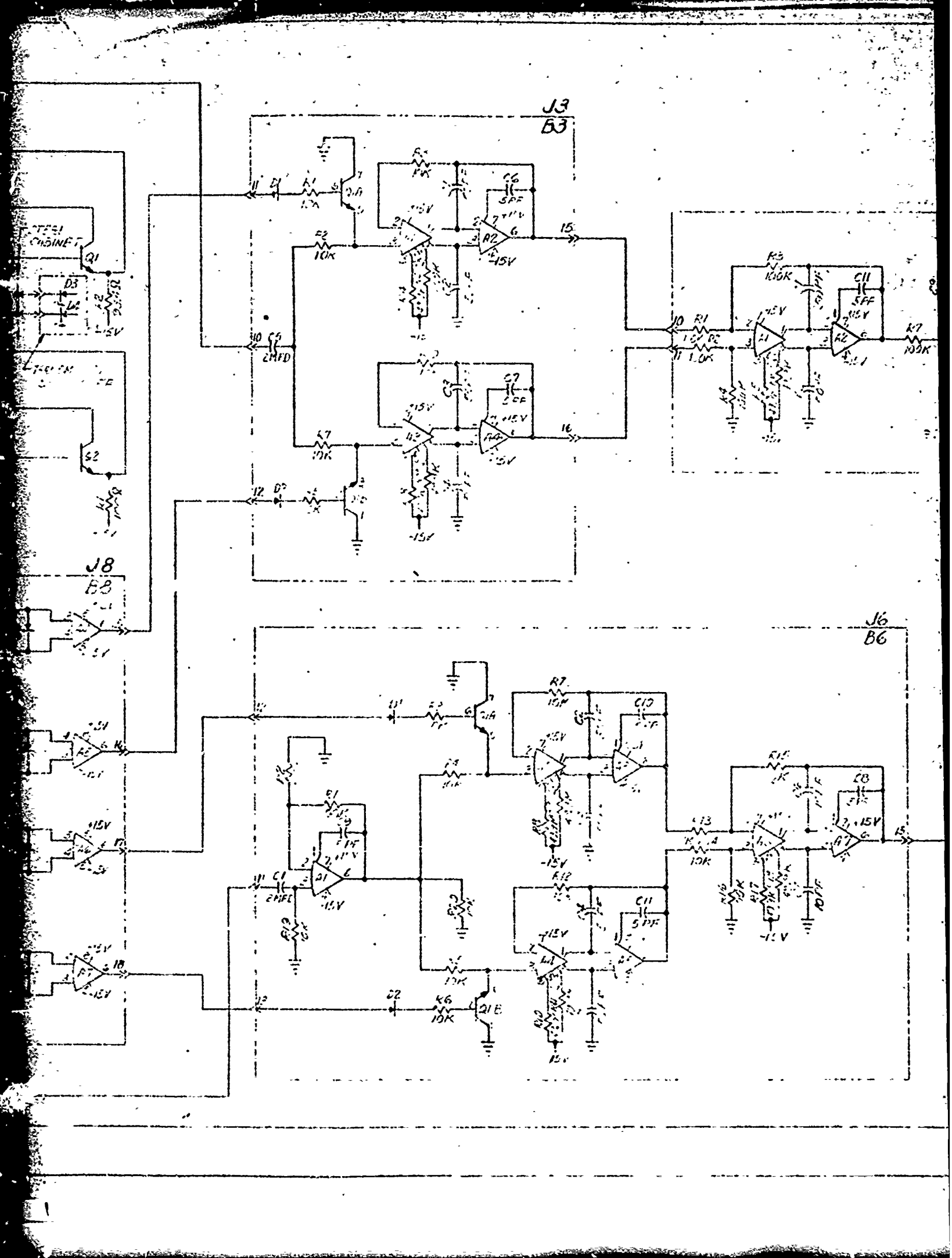
J3
B3
J8
B8
J6
B6
R1
R2
R3
R4
R5
R6
R7
R8
R9
R10
R11
R12
R13
C1
C2
C3
C4
C5
C6
C7
C8
C9
C10
C11
Q1
Q2
D1
D2
D3
10K
100K
15V
-15V
2MFD
5PF
5PFF
1.0K

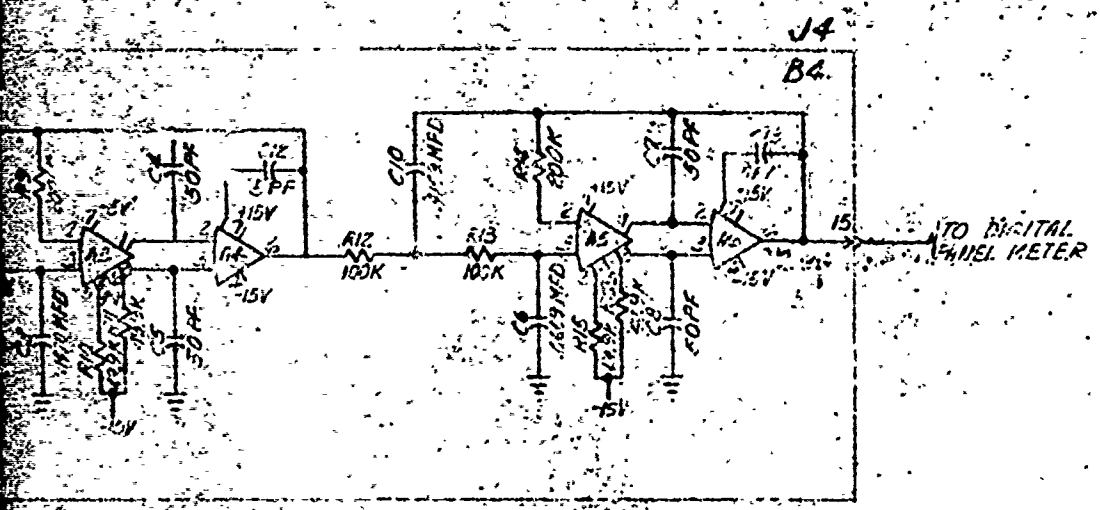

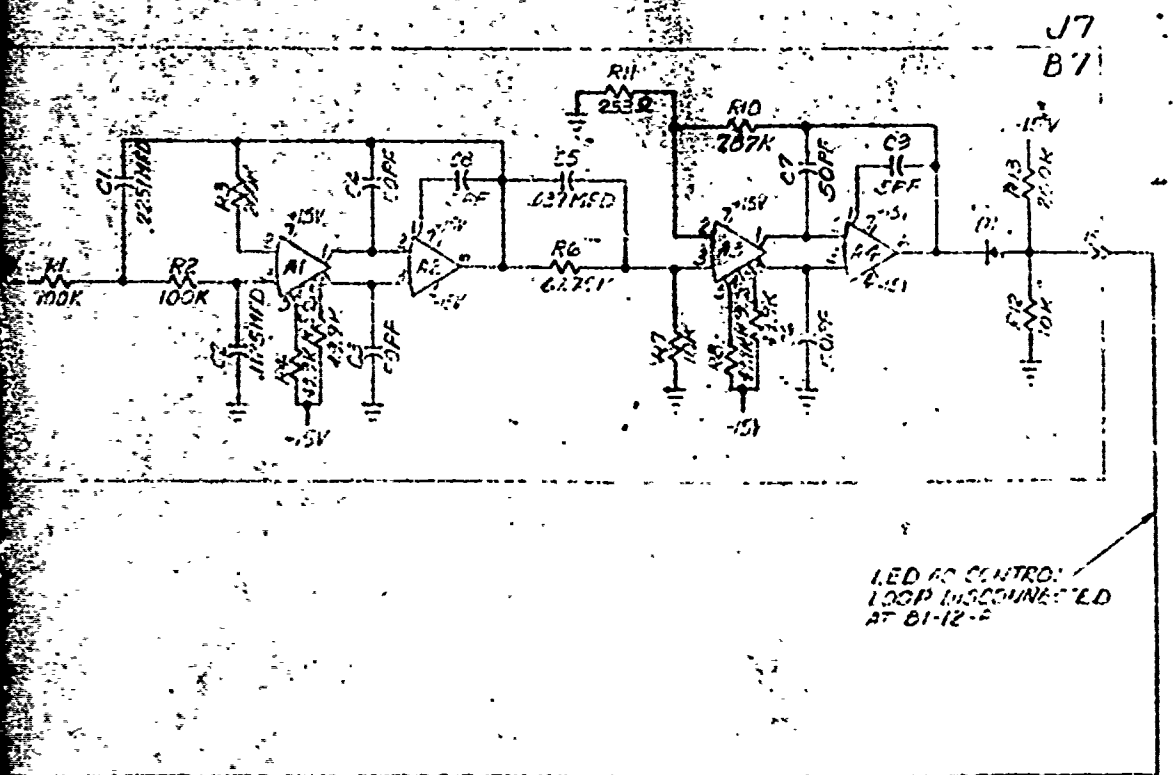

BOARD NO.	ITEM NO.	QUANTITY USED
B1	Q1, Q7	2
	Q2, R15	2
	Q3, R12	2
	R1, R5, R9, R10	4
	R6, R8	2
	R7	1
	A1, A3	2
	A2, A4	2
	A5	1
	C1	1
	C4	1
	C3, C6, C2	3
	Q1, Q5	2
	Q2, R4	2
	ADI	1
	R3	1
	R16	1
	R17	1
B2	R1, R5, R9, R10	4
	R6, R7, R8, R11	4
	A1, A3	2
	A2, A4	2
	C1, C2	2
	Q1, Q2	2
	ADI	1
	R8	1
B3	C1, C3, C5, C7	4
	C2, C4, C6, C8	4
	A1, A3	2
	A2, A4	2
	C9, C10	2
	Q1, Q2	2
	Q3, Q4, Q5, Q6	4
	C11, C12	2
F4	R1, R2, R3, R4, R5	5
	A1, A2, A3	3
	C1, C2, C3, C4, C5, C6	6
	R9	1
	C11, C12	2
	F1	1
	F2	1
	F10	1
B1	C3, R13	2
	C4, C5	2
	C6	1

1. [illegible]
2. [illegible]
3. [illegible]
4. [illegible]
5. ALL BOARDS ON -15V PIN [illegible]

PART NUMBER	DESCRIPTION	REMARKS
100S	RESISTOR	
[illegible]51003?F	"	
[illegible]51002F	"	
19.9K	"	
1 MEG	"	
[illegible]	"	
[illegible]S.1003F	"	
LM1458	AMPLIFIER	
741	"	
[illegible]125H	"	
1 MFD	CAPACITOR	
2 MFD	"	
50PF	"	
2N2222A	TRANSISTOR	
2N2132		
AD427K	ANALOG DIVIDER	
14.4K	RESISTOR	
543P		
5.5K		
51K		
RN55J1003E17	RESISTOR	
49.9K	"	
[illegible]1002B	"	
11K		⚠
LM1458?	AMPLIFIER	
741	"	
22 MFD	CAPACITOR	
2PF	"	
2MFD	"	
22PF	"	
AD427	ANALOG DIVIDER	
15PF	CAPACITOR	
[illegible]K	RESISTOR	
RN55J1002F		
49.9K		
LM1458	AMPLIFIER	
741		
220PF	CAPACITOR	
2 MFD		
1N4154	DIODE	
2N2222A	TRANSISTOR	
5PF		
[illegible]	RESISTOR	
	"	
49.9K	"	
100K		
LM1458	AMPLIFIER	
741	"	
[illegible]PF	CAPACITOR	
[illegible] MFD	"	
[illegible]PF	"	
.0039 MFD	"	
.1[illegible] MFD	"	
.159 MFD	"	
11K	RESISTOR	⚠
[illegible] MF	CAPACITOR	
2MFD		

▲ THIS PART IS LOCATED ON RECEIVER [illegible]

THIS PART IS [illegible] ON [illegible] AS #16

IS COMMON TO ALL [illegible] CHANNELS

DIVIDERS TO BE CONNECTED AS FOLLOWS [illegible] TRIMMED FOR NO OUTPUT OFFSET.

[illegible] OUTPUT

THIS SCHEMATIC WILL HAVE COMMON [illegible] No. 1, [illegible] GND PIN No 2

ASSY NUMBER SKC[illegible]

PARTS LIST

BOARD NO.	ITEM NO.	QTY. REQD.	PART NUMBER	DESCRIPTION	REMARKS
B5	R1,R2	2	71.5K	RESISTOR	
	R3,R4	2	[illegible]	"	
	R5,R6	2	1.07K	"	
	R7,R8	2	2.15K	"	
	R9	1	RN55J1003F	"	
	[illegible]	2	49.9K	"	
	[illegible]	3	[illegible]	"	
	A1,A2	2	200K	"	
	A1,A2,A5	3	LM1458	AMPLIFIER	
	A2,A4,A6	3	741	"	
	C1,C2,C5,C6	6	50PF	CAPACITOR	
	C3	1	[illegible] MFD	"	
	C4	1	.47 MFD	"	
	[illegible]	3	1PF	"	
	[illegible]	1	.47 MFD	"	
	[illegible]	1	.068 MFD	"	
	R10	1	37.15K	RESISTOR	
B6	R1	1	200K	RESISTOR	
	R2	1	5.5K		
	R3,R6	2	15K		
	[illegible]	6	RN55J1002F	"	
	[illegible]	6	49.9K	"	
	[illegible]	2	[illegible]	"	
	[illegible]	2	[illegible]	"	
	A1	1	AD427K	ANALOG DIVIDER	
	A5,A6	2	[illegible]	"	
	A2,A3,A7	3	[illegible]	"	
	C1	1	1 MFD	CAPACITOR	
	C2,C3,C7,C5	4	33PF	"	
	C6,C7	2	1.5K	"	
	C1,C2	2	1N4154	DIODE	
	Q1A,Q1B	2	2N2417	TRANSISTOR	
	C8,C9,C10,C11	4	5PF	CAPACITOR	
B7	R1,R3	2	RN55J1002F	RESISTOR	
	R4	1	33K	"	
	R5,R6,R8,R9	4	37.2K	"	
	R6	1	67.1K		
	R7	1	3K		
	R10	1	7.87K		
	A1,A2	2	LM1458	AMPLIFIER	
	A3,A4	2	LM[illegible]	"	
	C1	1	.225 MFD	CAPACITOR	
	C2	1	.015 MFD	"	
	C3,C4,C5,C7	2	50PF	"	
	C6	1	.027 MFD	"	
	C8,C9	2	5PF	"	
B8	R2,R3	2	4K	RESISTOR	
	R1,R4,R5	3	RN55J1002F	"	
	R6,R7	2	15K	"	
	R8,R9	2	[illegible]	"	
	A1,A2,A3	3	LM1458	AMPLIFIER	
	A4,A5,A6,A7	4	741	"	
	C1,C2	2	0.[illegible] MFD	CAPACITOR	
	C3,C4	2	1 MFD	"	
	[illegible]	2	1N4154	DIODE	
	[illegible]	2	5PF		
E[illegible]	[illegible]	1	[illegible]	[illegible]	
		1	2232		
E7	[illegible]	1	[illegible]		
	[illegible]	1	22.1K		
	[illegible]	1	[illegible]		
	[illegible]	1	[illegible]		
	[illegible]	1	[illegible]		
	[illegible]	1	[illegible]		
	[illegible]	1	[illegible]		
	[illegible]	2	[illegible]1002E		
	[illegible]	1			
	[illegible]	2	11K		
	[illegible]	1	1 MEG		
	[illegible]	1	[illegible] MEG		
	[illegible]	2	[illegible]	AMPLIFIER	
	[illegible]	2	[illegible]	[illegible]	
	[illegible]	2	[illegible]		
	[illegible]	1	[illegible]	[illegible]	
	[illegible]	2	[illegible]	[illegible]	
	[illegible]	2	[illegible]	LED	
E7	D1	1	1N4154	DIODE	

FIGURE 8-20

[illegible] ELECTRICAL SCHEMATIC FOR BREADBOARD [illegible]

CHRYSLER

SKC837-P

SHEET 1 of 1

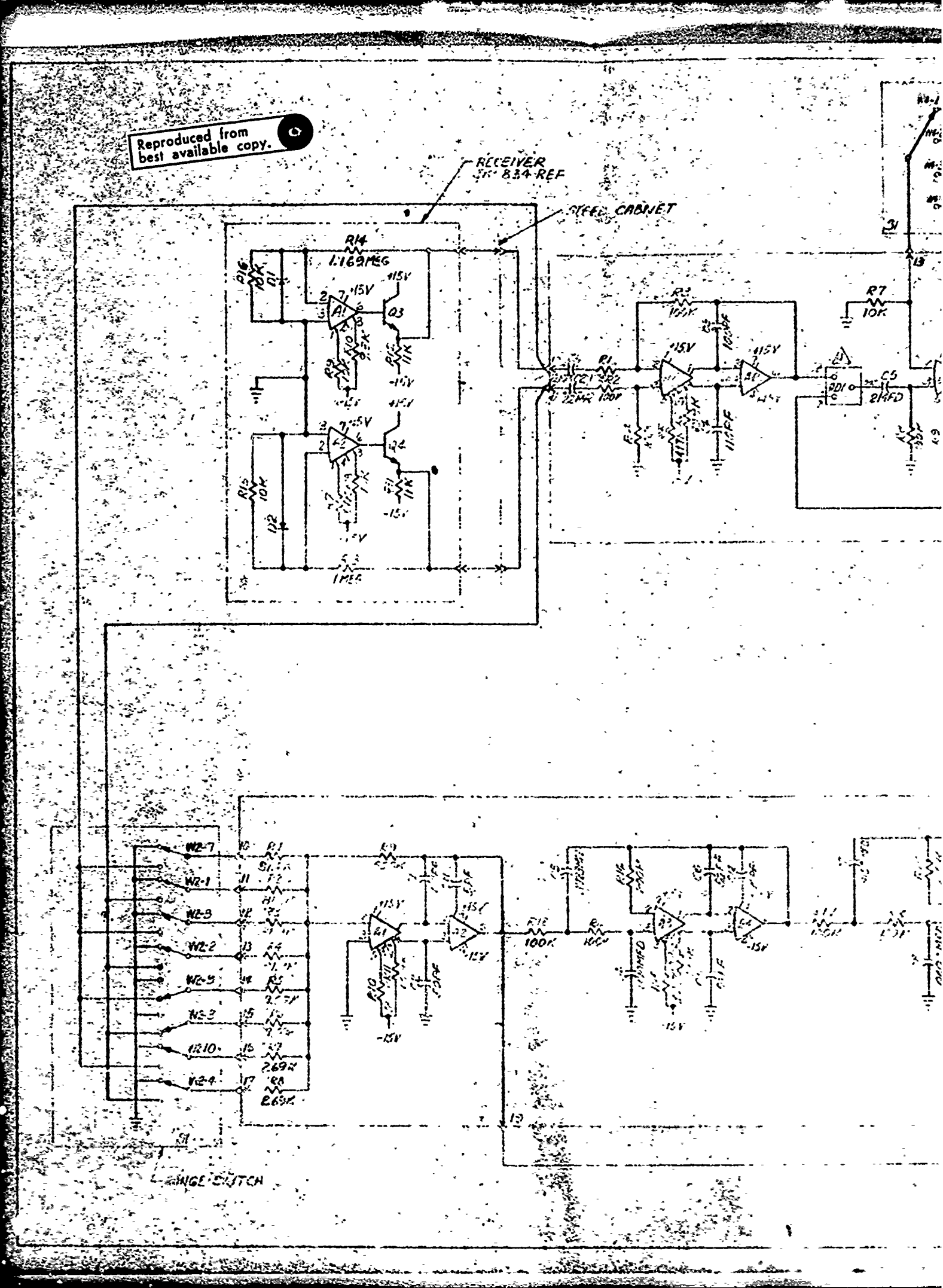

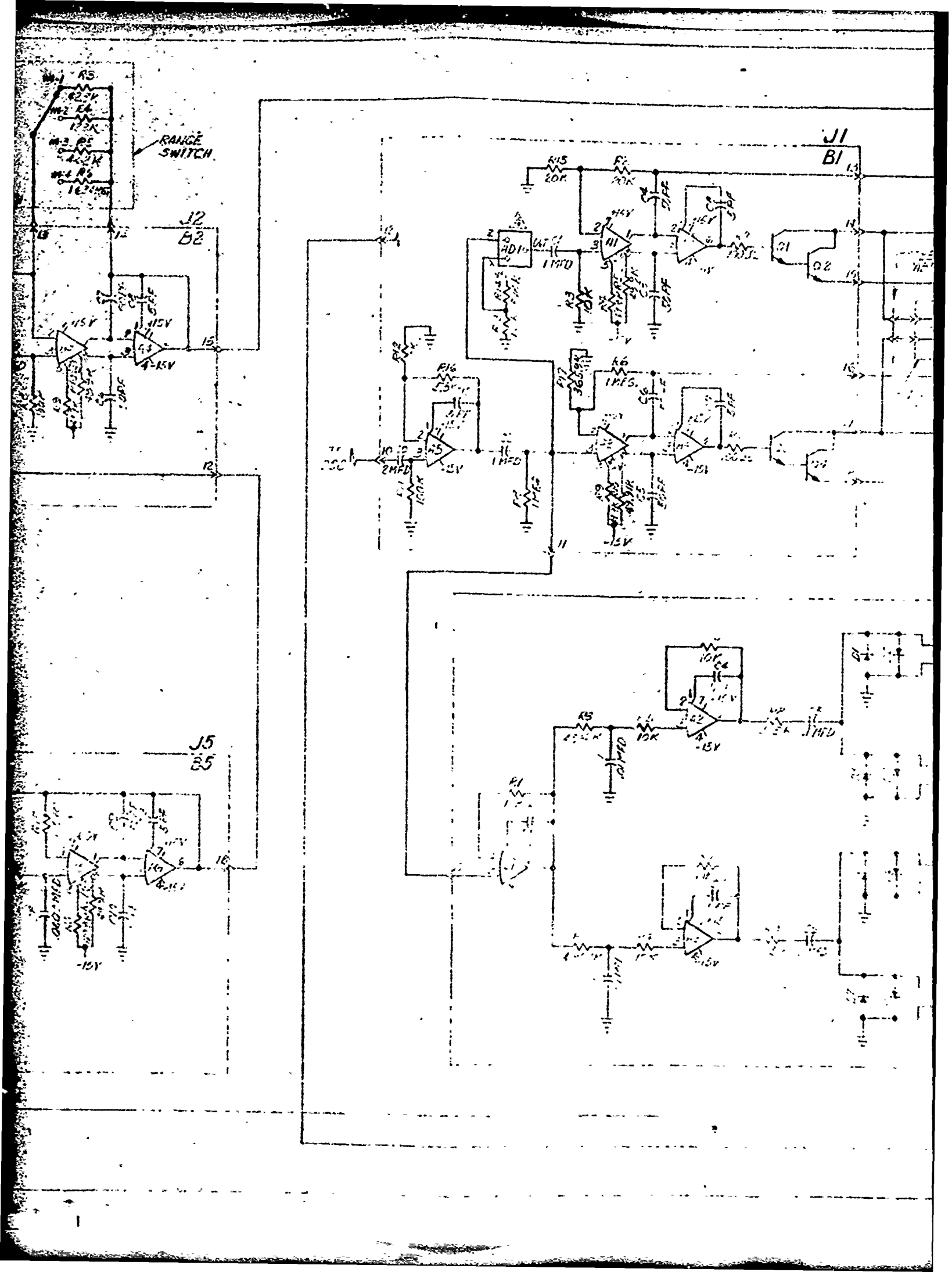
RANGE SWITCH
J1
B1
J2
B2
J5
B5
R5
R15
20K
R1
100K
1 MFD
R6
1 MEG.
2 MFD
10K
-15V
+15V

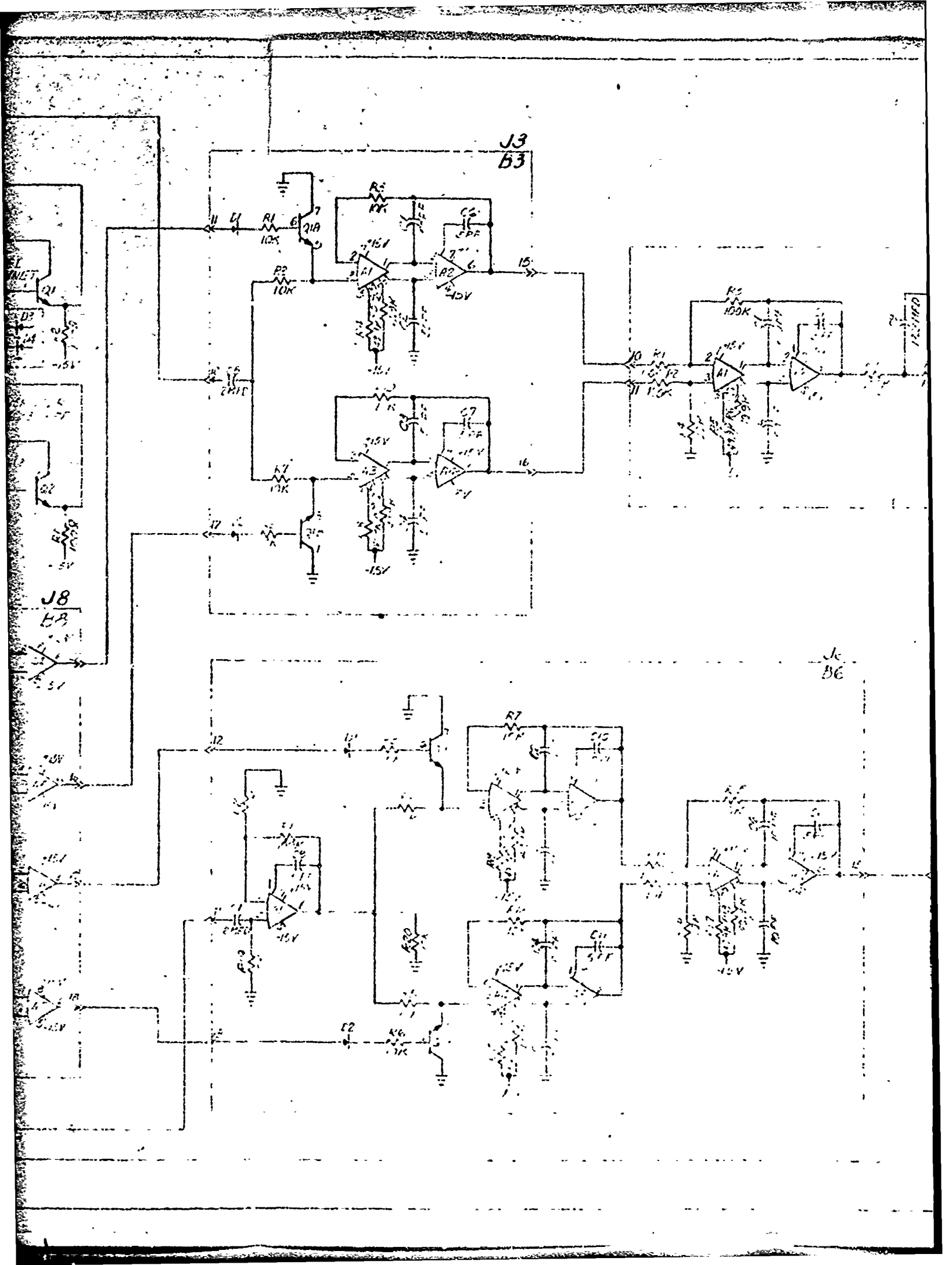
J3
B3
J8
B8
J4
B6
R1
10K
R2
10K
R3
100K
R4
1K
R5
1K
R6
1K
R7
1K
R8
1K
R9
1K
R10
1K
R11
1K
R12
1K
C1
C2
C3
C4
C5
C6
C7
C8
C9
C10
C11
C12
C13
C14
C15
Q1
Q2
Q3
Q4
Q5
Q6
Q7
Q8
Q9
Q10
Q11
Q12
Q13
Q14
Q15
Q16
Q17
Q18
Q19
Q20
Q21
Q22
Q23
Q24
Q25
Q26
Q27
Q28
Q29
Q30
Q31
Q32
Q33
Q34
Q35
Q36
Q37
Q38
Q39
Q40
Q41
Q42
Q43
Q44
Q45
Q46
Q47
Q48
Q49
Q50
Q51
Q52
Q53
Q54
Q55
Q56
Q57
Q58
Q59
Q60
Q61
Q62
Q63
Q64
Q65
Q66
Q67
Q68
Q69
Q70
Q71
Q72
Q73
Q74
Q75
Q76
Q77
Q78
Q79
Q80
Q81
Q82
Q83
Q84
Q85
Q86
Q87
Q88
Q89
Q90
Q91
Q92
Q93
Q94
Q95
Q96
Q97
Q98
Q99
Q100
Q101
Q102
Q103
Q104
Q105
Q106
Q107
Q108
Q109
Q110
Q111
Q112
Q113
Q114
Q115
Q116
Q117
Q118
Q119
Q120
Q121
Q122
Q123
Q124
Q125
Q126
Q127
Q128
Q129
Q130
Q131
Q132
Q133
Q134
Q135
Q136
Q137
Q138
Q139
Q140
Q141
Q142
Q143
Q144
Q145
Q146
Q147
Q148
Q149
Q150
Q151
Q152
Q153
Q154
Q155
Q156
Q157
Q158
Q159
Q160
Q161
Q162
Q163
Q164
Q165
Q166
Q167
Q168
Q169
Q170
Q171
Q172
Q173
Q174
Q175
Q176
Q177
Q178
Q179
Q180
Q181
Q182
Q183
Q184
Q185
Q186
Q187
Q188
Q189
Q190
Q191
Q192
Q193
Q194
Q195
Q196
Q197
Q198
Q199
Q200
Q201
Q202
Q203
Q204
Q205
Q206
Q207
Q208
Q209
Q210
Q211
Q212
Q213
Q214
Q215
Q216
Q217
Q218
Q219
Q220
Q221
Q222
Q223
Q224
Q225
Q226
Q227
Q228
Q229
Q230
Q231
Q232
Q233
Q234
Q235
Q236
Q237
Q238
Q239
Q240
Q241
Q242
Q243
Q244
Q245
Q246
Q247
Q248
Q249
Q250
Q251
Q252
Q253
Q254
Q255
Q256
Q257
Q258
Q259
Q260
Q261
Q262
Q263
Q264
Q265
Q266
Q267
Q268
Q269
Q270
Q271
Q272
Q273
Q274
Q275
Q276
Q277
Q278
Q279
Q280
Q281
Q282
Q283
Q284
Q285
Q286
Q287
Q288
Q289
Q290
Q291
Q292
Q293
Q294
Q295
Q296
Q297
Q298
Q299
Q300
Q301
Q302
Q303
Q304
Q305
Q306
Q307
Q308
Q309
Q310
Q311
Q312
Q313
Q314
Q315
Q316
Q317
Q318
Q319
Q320
Q321
Q322
Q323
Q324
Q325
Q326
Q327
Q328
Q329
Q330
Q331
Q332
Q333
Q334
Q335
Q336
Q337
Q338
Q339
Q340
Q341
Q342
Q343
Q344
Q345
Q346
Q347
Q348
Q349
Q350
Q351
Q352
Q353
Q354
Q355
Q356
Q357
Q358
Q359
Q360
Q361
Q362
Q363
Q364
Q365
Q366
Q367
Q368
Q369
Q370
Q371
Q372
Q373
Q374
Q375
Q376
Q377
Q378
Q379
Q380
Q381
Q382
Q383
Q384
Q385
Q386
Q387
Q388
Q389
Q390
Q391
Q392
Q393
Q394
Q395
Q396
Q397
Q398
Q399
Q400
Q401
Q402
Q403
Q404
Q405
Q406
Q407
Q408
Q409
Q410
Q411
Q412
Q413
Q414
Q415
Q416
Q417
Q418
Q419
Q420
Q421
Q422
Q423
Q424
Q425
Q426
Q427
Q428
Q429
Q430
Q431
Q432
Q433
Q434
Q435
Q436
Q437
Q438
Q439
Q440
Q441
Q442
Q443
Q444
Q445
Q446
Q447
Q448
Q449
Q450
Q451
Q452
Q453
Q454
Q455
Q456
Q457
Q458
Q459
Q460
Q461
Q462
Q463
Q464
Q465
Q466
Q467
Q468
Q469
Q470
Q471
Q472
Q473
Q474
Q475
Q476
Q477
Q478
Q479
Q480
Q481
Q482
Q483
Q484
Q485
Q486
Q487
Q488
Q489
Q490
Q491
Q492
Q493
Q494
Q495
Q496
Q497
Q498
Q499
Q500
Q501
Q502
Q503
Q504
Q505
Q506
Q507
Q508
Q509
Q510
Q511
Q512
Q513
Q514
Q515
Q516
Q517
Q518
Q519
Q520
Q521
Q522
Q523
Q524
Q525
Q526
Q527
Q528
Q529
Q530
Q531
Q532
Q533
Q534
Q535
Q536
Q537
Q538
Q539
Q540
Q541
Q542
Q543
Q544
Q545
Q546
Q547
Q548
Q549
Q550
Q551
Q552
Q553
Q554
Q555
Q556
Q557
Q558
Q559
Q560
Q561
Q562
Q563
Q564
Q565
Q566
Q567
Q568
Q569
Q570
Q571
Q572
Q573
Q574
Q575
Q576
Q577
Q578
Q579
Q580
Q581
Q582
Q583
Q584
Q585
Q586
Q587
Q588
Q589
Q590
Q591
Q592
Q593
Q594
Q595
Q596
Q597
Q598
Q599
Q600
Q601
Q602
Q603
Q604
Q605
Q606
Q607
Q608
Q609
Q610
Q611
Q612
Q613
Q614
Q615
Q616
Q617
Q618
Q619
Q620
Q621
Q622
Q623
Q624
Q625
Q626
Q627
Q628
Q629
Q630
Q631
Q632
Q633
Q634
Q635
Q636
Q637
Q638
Q639
Q640
Q641
Q642
Q643
Q644
Q645
Q646
Q647
Q648
Q649
Q650
Q651
Q652
Q653
Q654
Q655
Q656
Q657
Q658
Q659
Q660
Q661
Q662
Q663
Q664
Q665
Q666
Q667
Q668
Q669
Q670
Q671
Q672
Q673
Q674
Q675
Q676
Q677
Q678
Q679
Q680
Q681
Q682
Q683
Q684
Q685
Q686
Q687
Q688
Q689
Q690
Q691
Q692
Q693
Q694
Q695
Q696
Q697
Q698
Q699
Q700
Q701
Q702
Q703
Q704
Q705
Q706
Q707
Q708
Q709
Q710
Q711
Q712
Q713
Q714
Q715
Q716
Q717
Q718
Q719
Q720
Q721
Q722
Q723
Q724
Q725
Q726
Q727
Q728
Q729
Q730
Q731
Q732
Q733
Q734
Q735
Q736
Q737
Q738
Q739
Q740
Q741
Q742
Q743
Q744
Q745
Q746
Q747
Q748
Q749
Q750
Q751
Q752
Q753
Q754
Q755
Q756
Q757
Q758
Q759
Q760
Q761
Q762
Q763
Q764
Q765
Q766
Q767
Q768
Q769
Q770
Q771
Q772
Q773
Q774
Q775
Q776
Q777
Q778
Q779
Q780
Q781
Q782
Q783
Q784
Q785
Q786
Q787
Q788
Q789
Q790
Q791
Q792
Q793
Q794
Q795
Q796
Q797
Q798
Q799
Q800
Q801
Q802
Q803
Q804
Q805
Q806
Q807
Q808
Q809
Q810
Q811
Q812
Q813
Q814
Q815
Q816
Q817
Q818
Q819
Q820
Q821
Q822
Q823
Q824
Q825
Q826
Q827
Q828
Q829
Q830
Q831
Q832
Q833
Q834
Q835
Q836
Q837
Q838
Q839
Q840
Q841
Q842
Q843
Q844
Q845
Q846
Q847
Q848
Q849
Q850
Q851
Q852
Q853
Q854
Q855
Q856
Q857
Q858
Q859
Q860
Q861
Q862
Q863
Q864
Q865
Q866
Q867
Q868
Q869
Q870
Q871
Q872
Q873
Q874
Q875
Q876
Q877
Q878
Q879
Q880
Q881
Q882
Q883
Q884
Q885
Q886
Q887
Q888
Q889
Q890
Q891
Q892
Q893
Q894
Q895
Q896
Q897
Q898
Q899
Q900
Q901
Q902
Q903
Q904
Q905
Q906
Q907
Q908
Q909
Q910
Q911
Q912
Q913
Q914
Q915
Q916
Q917
Q918
Q919
Q920
Q921
Q922
Q923
Q924
Q925
Q926
Q927
Q928
Q929
Q930
Q931
Q932
Q933
Q934
Q935
Q936
Q937
Q938
Q939
Q940
Q941
Q942
Q943
Q944
Q945
Q946
Q947
Q948
Q949
Q950
Q951
Q952
Q953
Q954
Q955
Q956
Q957
Q958
Q959
Q960
Q961
Q962
Q963
Q964
Q965
Q966
Q967
Q968
Q969
Q970
Q971
Q972
Q973
Q974
Q975
Q976
Q977
Q978
Q979
Q980
Q981
Q982
Q983
Q984
Q985
Q986
Q987
Q988
Q989
Q990
Q991
Q992
Q993
Q994
Q995
Q996
Q997
Q998
Q999
Q1000

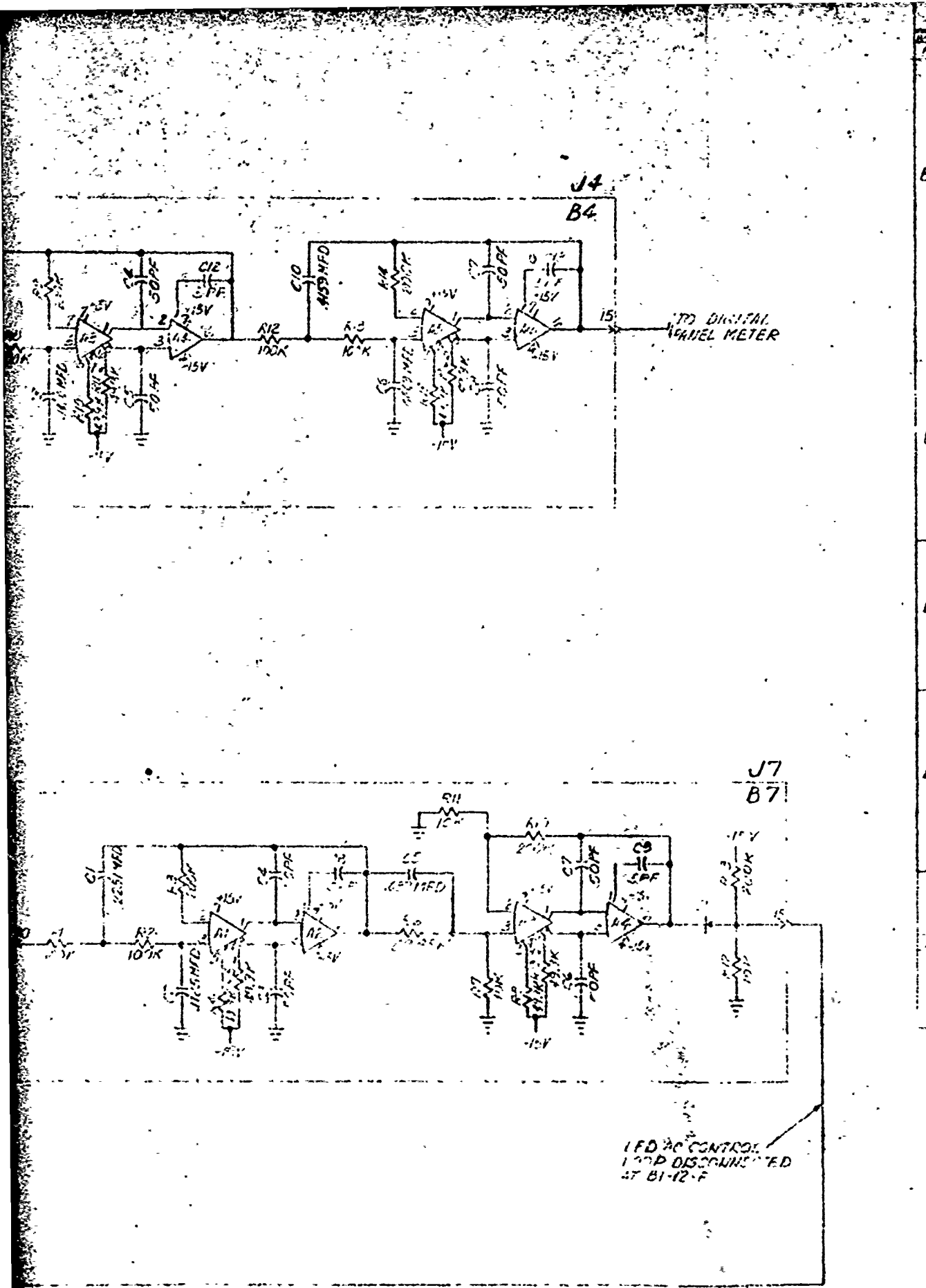

BOARD NO.	ITEM NO.	QTY USED
B1	R1, R7	2
	R2, R5	2
	R3	1
	R4, R5, R6, R8	4
	R6	2
	ST	1
	R1, R3	2
	C1, C4, C5	2
	C2	2
	C3, C4, C5, C6	4
	R1, R2	2
	C1, C2	2
	R4	1
	R5	1
	R16	1
	R12	1
	ST	1
B2	R13	1
	A1 R3	1
	C1	1
	C2	1
	R11	1
B3	R1a	2
	C1	2
	C6, C7	2
B4	A1	1
	C	1
	R	1
B1	R17	1
	R 3	1

SKC ... [illegible]

PARTS LIST

QTY REQD	PART NUMBER	DESCRIPTION	REMARKS
2	100Ω	RESISTOR	
2	RN55D1002F	"	
1	RN55D1002F	"	
4	49.9K	"	
2	1 MEG	"	
1	RN55D1003F	"	
2	LM311	AMPLIFIER	
2	741	"	
1	AD...	"	
2	1 MFD	CAPACITOR	
4	6.8PF	"	
2	2N2222A	TRANSISTOR	
2	2N2907	"	
1	...	DIODE, ZENER	
1	...	RESISTOR	
1	3.3K	"	
1	5.5K	"	
1	1K	"	
1	...	RESISTOR	
2	499K	"	
1	...	"	
1	11K	"	
2	LM...	AMPLIFIER	A
2	.22 MFD	CAPACITOR	
1	1... PF	"	
1	2 MFD	"	
1	...	"	
1	...	POTENTIOMETER	
1	...	CAPACITOR	
2	10K	RESISTOR	
[illegible]	[illegible]	[illegible]	
1	...	CAPACITOR	
1	...	RESISTOR	
2	5PF		
2	...	RESISTOR	
1	...	RESISTOR	
1	56.9K	RESISTOR	
2	11...	"	
1	...	CAPACITOR	
[illegible]	[illegible]	[illegible]	

PARTS LIST

BOARD NO.	ITEM NO.	QTY REQD	PART NUMBER	DESCRIPTION	REMARKS
	R1, R2	2	1.5K	RESISTOR	
	R3, R4	3	4.7K	"	
	R5, R6	2	9.07K	"	
	R7, R8	2	269K	"	
	R9	1	RN55D1502F	"	
	...	4	499K	"	
	...	4	RN55D1002F	"	
A5	...	2	200K	"	
	...	3	LM311 ...	AMPLIFIER	
	...		741	"	
	C1, C2 ...	6	30PF	CAPACITOR	
	...	1	.1 MFD	"	
		1	.47 MFD	"	
	...	3	6PF	"	
		1	4.7 MFD	"	
	...	1	.068 MFD	"	
	R...	1	38.3K	RESISTOR	
	R...	1	100K	"	
		1	5.5K	"	
		2	10K	"	
			RN55D1003F	"	
			22K	"	
			...	"	
A6		1	AD...	AMPLIFIER	
			...	"	
		1	2 MFD	CAPACITOR	
			...	"	
		1	2N3417	TRANSISTOR	
		4	5PF	CAPACITOR	
			RN55D1002F	RESISTOR	
	R...	2	100K	"	
		3	49.9K	"	
		1	63...	"	
A...	D1	1	1N4154	DIODE	
			...	AMPLIFIER	
			...	CAPACITOR	
			.01 MFD		
			6 PF		
			499	RESISTOR	
			...		
			.0033 MFD		
	...	1	200K		
	R...	1	4.7K		
	K1	1	1 ... MFD		
			OPO...		
	Q3, Q4		2N2222		
		1	...		

NOTES:
... FOR ... RECEIVER ...
ITEM ...
... TRANSMITTER ...
ITEM ...
... IS COMMON TO ...
VALUES ... SELECTED ... TEST
... USED FOR ... SELECT

... SCHEMATIC ...

FIGURE 8-21

ELECTRICAL ...

SKC-8378

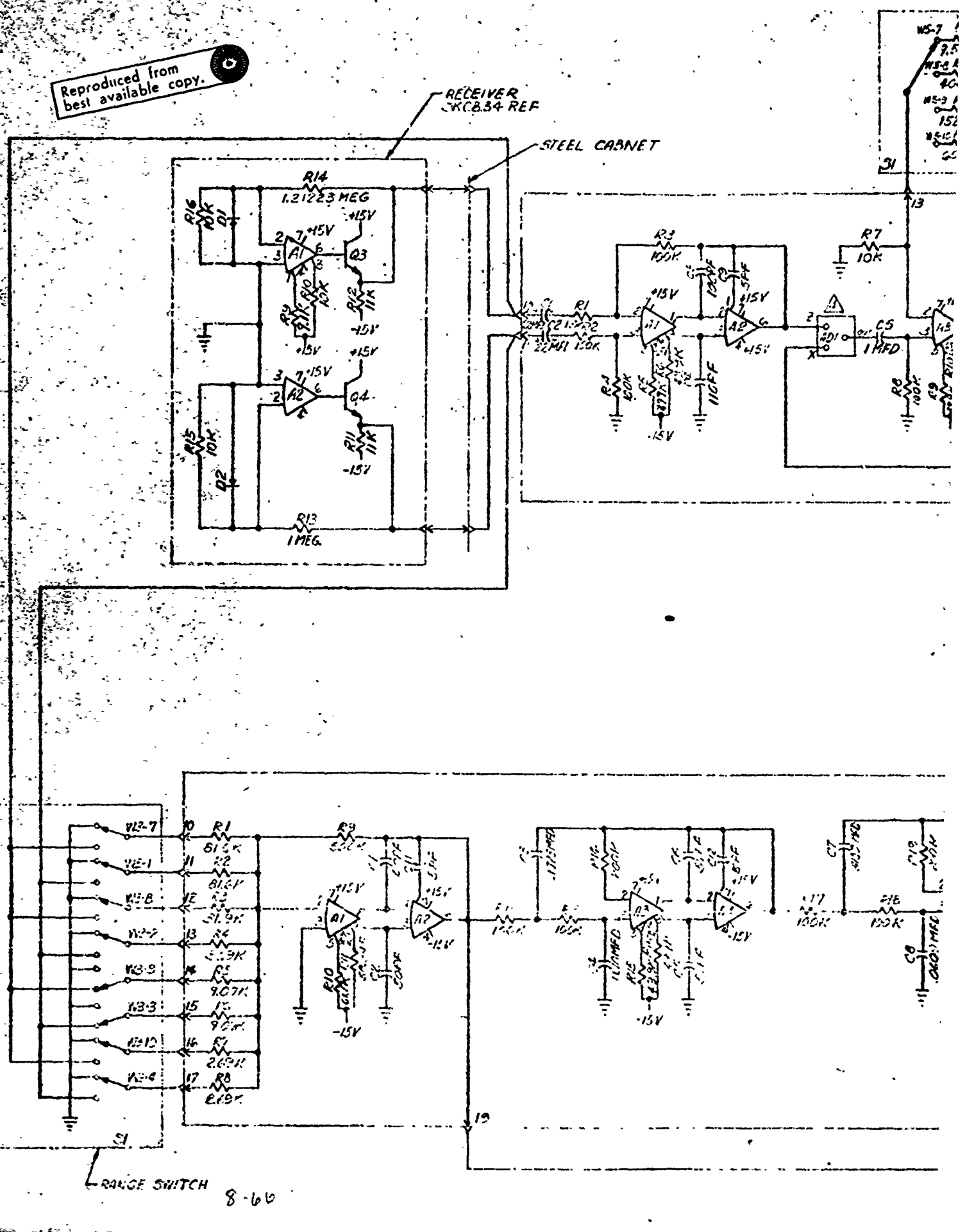

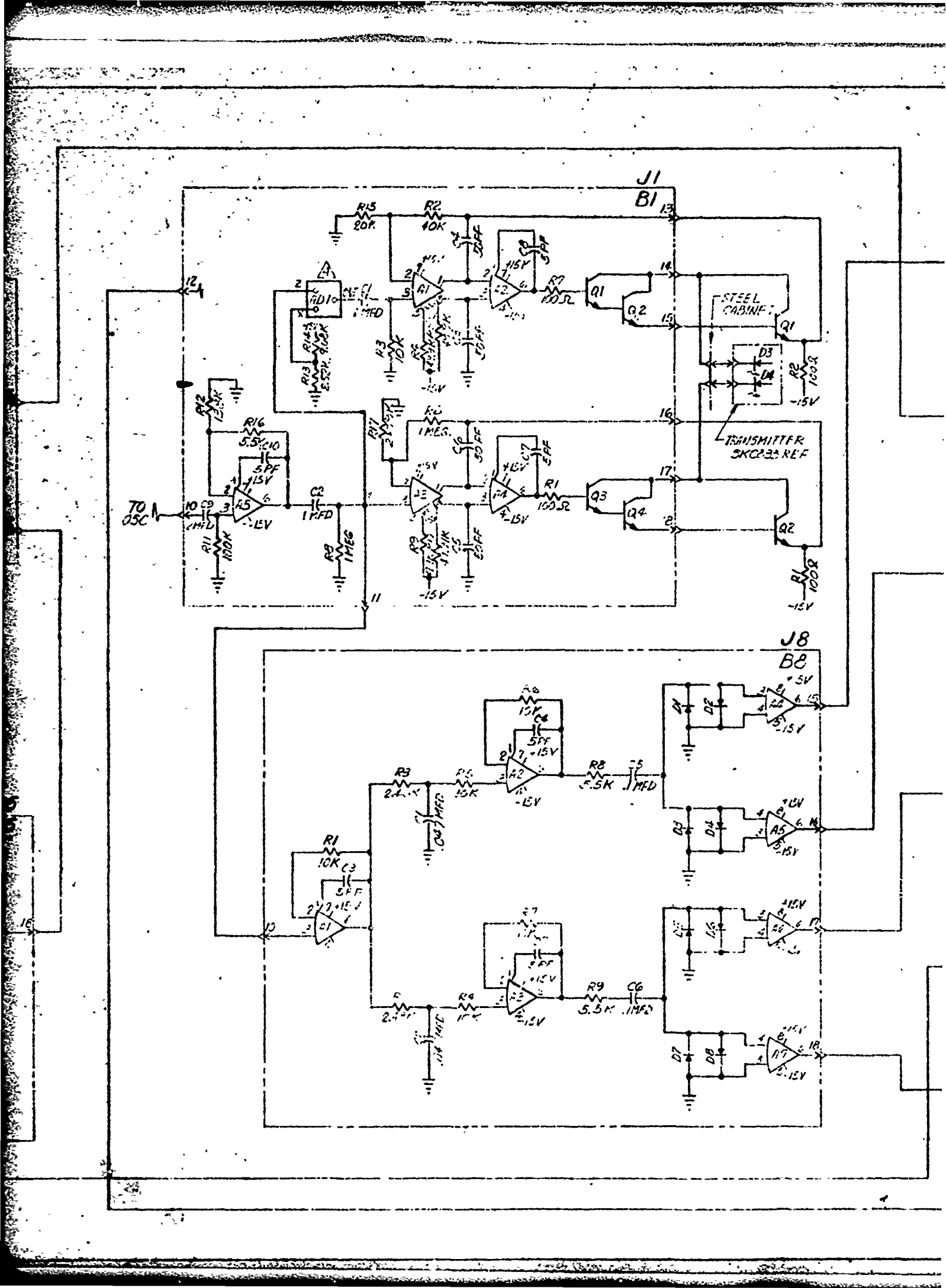
J1
B1
J8
B8
TO 05C
STEEL CABINET
TRANSMITTER SKC2-33 REF
R15 20K
R2 10K
R16 5.5K
R12 15.5K
R14 2.5K
R13 2.5K
R3 10K
R4 1MEG
R5 1MEG
R6 1MEG
R7 100Ω
R1 100Ω
R17 1MEG
R11 100K
R10 1MEG
R8 5.5K
R9 5.5K
C1 .1MFD
C2 1MFD
C3 5PF
C4 5PF
C5 .05MFD
C6 .1MFD
C7 5PF
C8 5PF
C9 .1MFD
C10 5PF
C11 .05MFD
C12 .1MFD
A1
A2
A3
A4
A5
A6
A7
A8
Q1
Q2
Q3
Q4
D1
D2
D3
D4
D5
D6
D7
D8
+15V
-15V

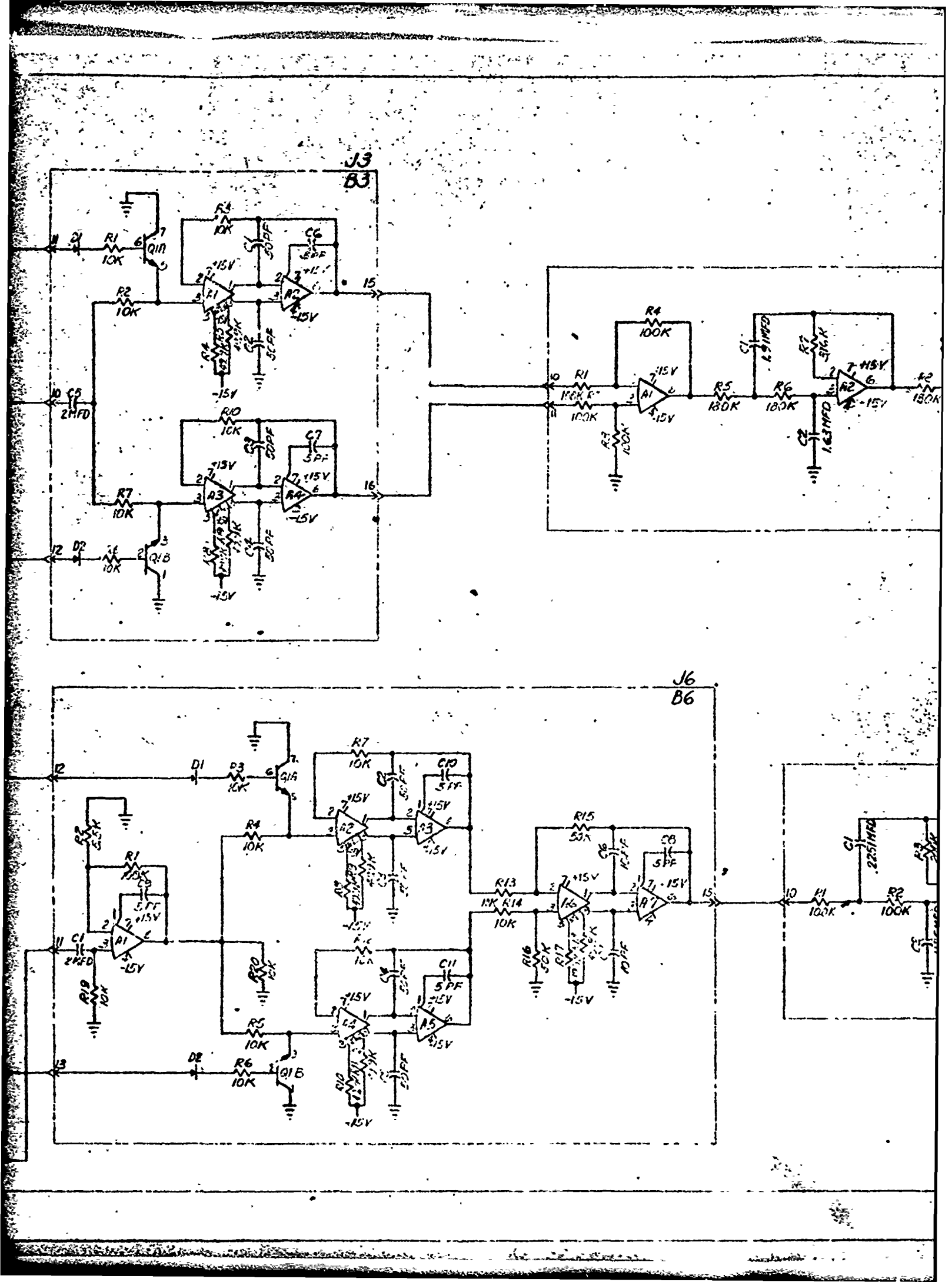
J3
B3
R4
10K
C6
5PF
+15V
R1
10K
Q1A
R2
10K
A1
A2
-15V
15
R3
100K
C4
50PF
C5
2MFD
R10
10K
C9
50PF
C7
5PF
A3
A4
R7
10K
Q1B
12
D2
R1
100K
A1
R4
100K
R5
180K
R6
180K
C1
.491MFD
R7
51K
A2
C2
1.63MFD
R2
180K
R3
100K
J6
B6
D1
R3
10K
Q1A
R7
10K
C10
5PF
A2
A3
R15
50K
C8
5PF
R13
10K
R14
10K
A6
A7
C1
.225MFD
R1
100K
R2
100K
R16
50K
R17
51K
C11
5PF
A4
A5
R5
10K
R6
10K
Q1B
D2
R19
10K
C1
2MFD
A1

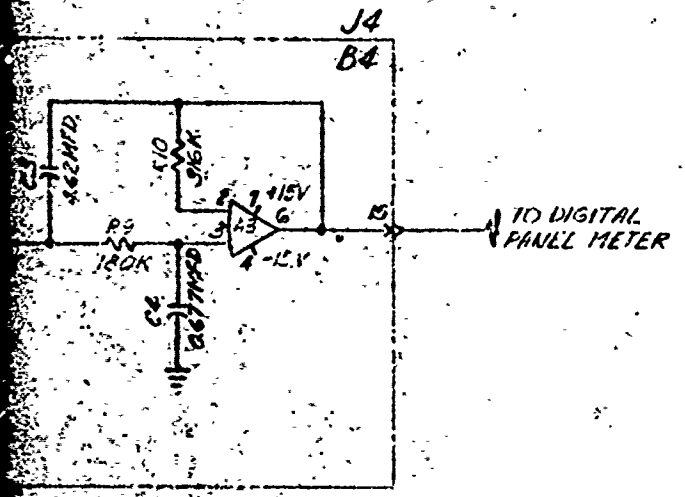

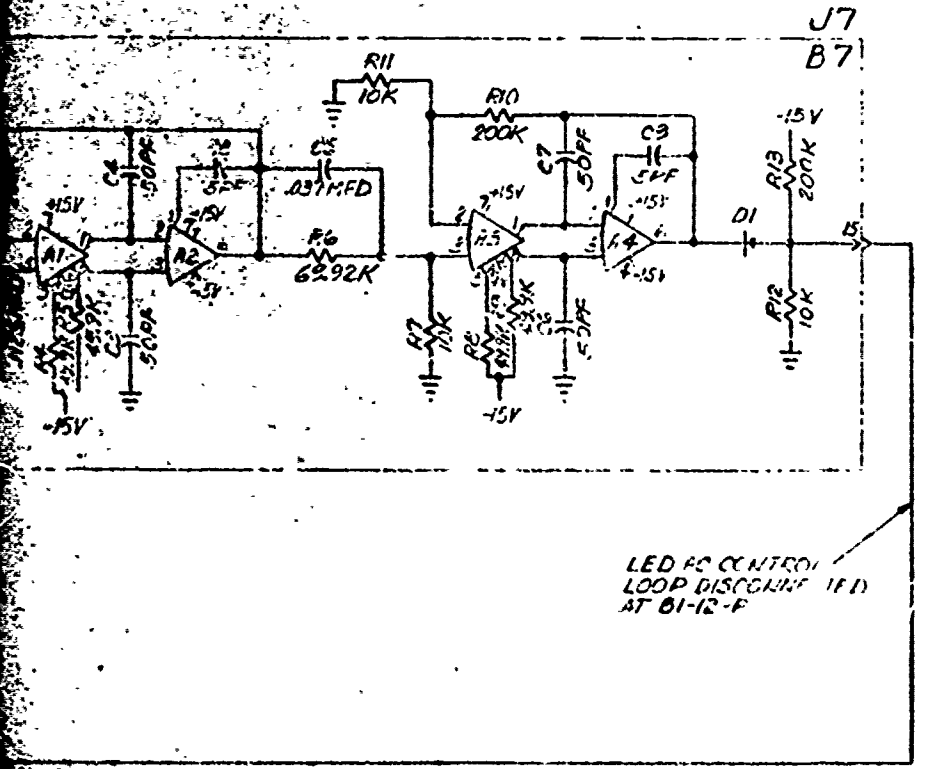

LED PC CONTROL LOOP DISCONNECTED AT B1-12-F

PARTS LIST

BOARD NO.	ITEM NO.	QUANTITY USED	PART NUMBER	DESCRIPTION
B1	R1, R7	2	100Ω	RESIS
	R15	1	RN-6B5120002F	"
	R3	1	RN-6B5110002F	"
	R4, R5, R9, R10	4	49.9K	"
	R6, R8	1	1 MEG	"
	P2	1	40K	"
	C1	1	RL-07-S1003F	"
	A1, A3	2	LM-121AH-883B	IMPRE
	A2, A4	2	741	"
	A5	1	AD533SH	"
	C11, C7	2	1 MFD	CAPAC
	R17	1	820.9K	"
	C8, C9, C10	3	50 PF	"
	C1, C6	2	2.21 MFD	CAPACI
	C2, C5	2	2.43 MFD	"
	A6	1	AD432TH	ANALOG
	R14	1	2.32K	RESIS
	"	1	2.06K	"
	R15	1	5.5K	"
	R16	1	13.8K	"
B2	R1, R3, R5, R8, R9, R10, R12	7	RN-6B5110002F	RESIS
	R2, R4	2	4.32K	"
	R11	1	RN-6B5-11002E	"
	R16, R17	2	11K	"
	A1, A3	2	LM121 AH-883	IMPRE
	A2, A4	2	741	"
	C1, C2	2	.82 MFD	CAPAC
	C3	1	180 PF	"
	C4	1	1 MFD	"
	C5, C6	2	4.7 MFD	"
	A5	1	AD432TH	ANALOG
	C7, C8	2	5 PF	CAPAC
B3	C1, C2	2	1K	"
	R1, R3, R5, R7	4	RN-6B5-11002F	"
	R2, R4	2	3.3K	"
	R6, R8	2	1 MEG	RESIS
	C1, C2	2	100 PF	CERAM
	C3, C4	2	1 MFD	"
	C5, C6	2	.1 MFD	"
	A1, A2	2	AD-534-JD	ANALOG
	C7, C8	2	5 PF	CAPAC
B4	R1, R2, R3, R4	4	1.0K	RESIS
	R5, R6, R9, R10	4	10K	"
	R7, R8	2	31.6K	"
	C1	1	1.91 MFD	CAPAC
	C2	1	1.63 MFD	"
	C3	1	4.62 MFD	"
	C4	1	0.69 MFD	"
	A1, A2, A3	3	741	"
B1	R1, R2	2	11K	RESIST
	C1	1	.1 MFD	CAPACI
	C2	1	2 MFD	"
B2	A1	1	LM-1-F	LINEAR

⚠1 PART NUMBER FOR THIS PART IS LOCA… SCHEM. ITEM #6.

⚠2 PART NUMBER FOR THIS PART IS LOCA… SCHEM. ITEM #11, #15, & #16.

⚠3 SWITCH SHOWN IS COMMON TO ALL …

⚠4 EIGHT ANALOG DIVIDERS TO BE CO… WITH R18 AND R19 TRIMMED FOR NO…

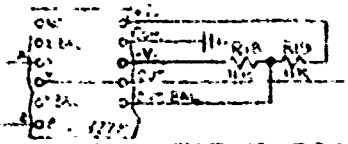

5. ALL BOARDS ON THIS SCHEMATIC H… -15V PIN No. 5 AND GND PIN No. 3

NEXT ASSY NUMBER
SKC 839

PARTS LIST

QUAN. REQ'D	PART NUMBER	DESCRIPTION	REMARKS
2	100 Ω	RESISTOR	
1	MRB3 200F	"	
1	MRB3 1002F	"	
4	499K	"	
1	1MEG	"	
1	40K	"	
1	MRB3 1003F	"	
2	TP 21 LM139	AMPLIFIER	
2	121	"	
1	A 3135H	"	
2	1 MFD	CAPACITOR	
1	2.2 0.9K		
4	50 PF	"	
2	2N 2222A	TRANSISTOR	
2	2N 3638	"	
1	MD 427K	MATCHED DIODE	
1	2.32K	RESISTOR	
1	200K	"	
1	2.5K	"	
1	13.8K	"	
5	MRB3 1003F	RESISTOR	
2	499K	"	
1	MRB3 1002F	"	
2	11K	"	
2	LM121 AH883	AMPLIFIER	
5	24	"	
2	.22 MFD	CAPACITOR	
1	100 PF	"	
1	1 MFD	"	
7	5 PF	"	
1	2N3417	MATCHED DIODE	
2	5 PF	CAPACITOR	
2	10K	RESISTOR	
4	MRB3 1002F	"	
2	332K	"	
2	LM121 AH883	AMPLIFIER	
5	24	"	
2	200K	CAPACITOR	
1	2 MFD	"	
2	IN4154	DIODE	
2	2N2060A	TRANSISTOR	
2	5 PF	"	
4	10K	RESISTOR	
2	100K	"	
2	3 KK	"	
1	1.91 MFD	CAPACITOR	
1	1.63 MFD	"	
1	4.62 MFD	"	
1	0.677 MFD	"	
3	.241	"	
2	11K	RESISTOR	A
2	5 PF	CAPACITOR	
1	2 MFD	"	
1	110 PF	CAPACITOR	

ER FOR THIS PART IS LOCATED ON RECEIVER DWG
TEM #6.
ER FOR THIS PART IS LOCATED ON TRANSMITTER DWG
TEM #11, #15, & #16.
SHOWN IS COMMON TO ALL THREE CHANNELS
LOG DIVIDERS TO BE CONNECTED AS FOLLOWS
AND R19 TRIMMED FOR NO OUTPUT OFFSET.

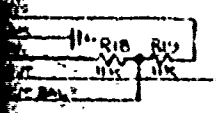

ON THIS SCHEMATIC WILL HAVE COMMON +15V ON No. 1,
AND GND PIN No. 8

PARTS LIST

CHAN. NO.	ITEM NO.	QUANT. REQ'D	PART NUMBER	DESCRIPTION	REMARKS
B5	R1, R2	2	81.6K	RESISTOR	
	R3, R4	2	31.9K	"	
	R5, R6	2	9.07K	"	
	R7, R8	2	26.1K	"	
	R9	1	MRB3 1500 3F	"	
	R10, R11, R20, R21	4	499K	"	
	R12, R13, R22, R23	4	MRB3 1003F	"	
	R14, R15	2	200K	"	
	U1, U2, U3	3	LM121 AH/883	AMPLIFIER	
	R16, R17, R18	3	121	"	
	C1, C2, C3, C4, C5	5	50 PF	CAPACITOR	
	C6	1	.172 MFD	"	
	C7	1	1.420 MFD	"	
	C8, C9, C10	3	5 PF	"	
	C11	1	.4153 MFD	"	
	C12	1	0.609 MFD	"	
	R19	1	81.1K	RESISTOR	
B6	R1	1	100K	RESISTOR	
	R2	1	5.5K	"	
	R3, R5, R15, R14	4	10K	"	
	R4, R6, R13, R16	4	MRB3 1102F	"	
	R7, R8, R9, R12	4	19.9K	"	
	R10, R11	2	50K	"	
	U1	1	CASD185H	AMPLIFIER	
	U2, U3, U4	3	LM121 AH/883	"	
	U5, U6, U7	3	LM119 AH/883	"	
	C1	1	2 MFD	CAPACITOR	
	C2, C3, C4, C5	4	50 PF	"	
	C6, C7	2	10 PF	"	
	D1, D2	2	IN4154	DIODE	
	Q1, Q2	2	2N3417	TRANSISTOR	
	C8, C9, C10, C11	4	5 PF	CAPACITOR	
B7	R1, R2	2	MRB3 1102F	RESISTOR	
	R3, R4, R5	3	5.11K	"	
	R6, R7, R9	3	49.9K	"	
	R8	1	62.1K	"	
	R10, R11, R12	3	40K	"	
	D1, D2	2	IN4154	DIODE	
	U1, U2	2	LM121 AH/883	AMPLIFIER	
	U3, U4	2	LM119 AH/883	"	
	C1	1	2 MFD	CAPACITOR	
	C2	1	1.1 MFD	"	
	C3, C4, C5, C7	4	50 PF	"	
	C6	1	.037 MFD	"	
	C8, C9	2	5 PF	"	
B8	R1	1	2.49K	RESISTOR	
	R2, R3, R5	3	MRB3 1002F	"	
	R4, R6, R7	3	10K	"	
	R8, R9	2	2.5K	"	
	U1, U2, U3, U4	4	LT1013M	AMPLIFIER	
	C1, C2, C3, C4	4	1.5 MM	"	
	C5, C6	2	0.047 MFD	CAPACITOR	
	C7, C8	2	.1 MFD	"	
	D1, D2, D3, D4	4	IN4154	DIODE	
	C9, C10	2	5 PF	"	
	R10	1	82.34K	RESISTOR	
	R11	1	75.5K	"	
	R12	1	100K	RESISTOR	
	R13	1	2.21K	"	
	R14	1	46.4K	"	
	R15	1	1525K	"	
	R16, R17	2	MRB3 1002F	"	
	R18	1	1K	"	
	R19, R20	2	11K	"	
	C11	1	1.2 MFD	"	
	C12	1	1.21 MEG	"	
	U5, U6, U7	3	OP-07A	AMPLIFIER	
	Q1, Q2	2	2N3416	TRANSISTOR	
	D5, D6, D7	3	IN4154	DIODE	
	D8, D9, D10	3	IN4154	DIODE	
B8	R3	1	2.49K	RESISTOR	

FIGURE 8-22

ROLL CHANNEL ELECTRONIC SCHEMATIC FOR BREADBOARD MODEL (FAMS)

SIZE D | SCALE | DATE 1-24-78 | SHEET

RECEIVED OCT 31 1978 | SKC 837-R

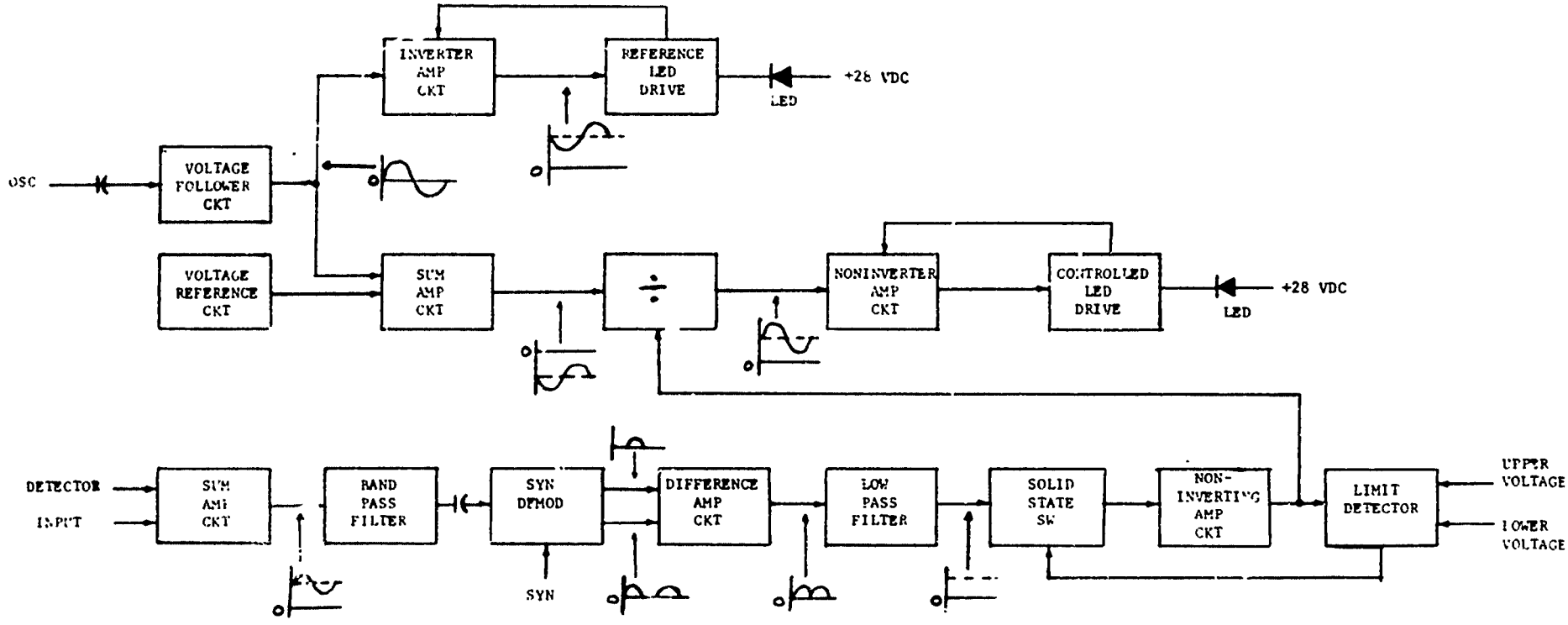

FIGURE 8-23 PROPOSED LED CONTROL SCHEME FOR OAMS

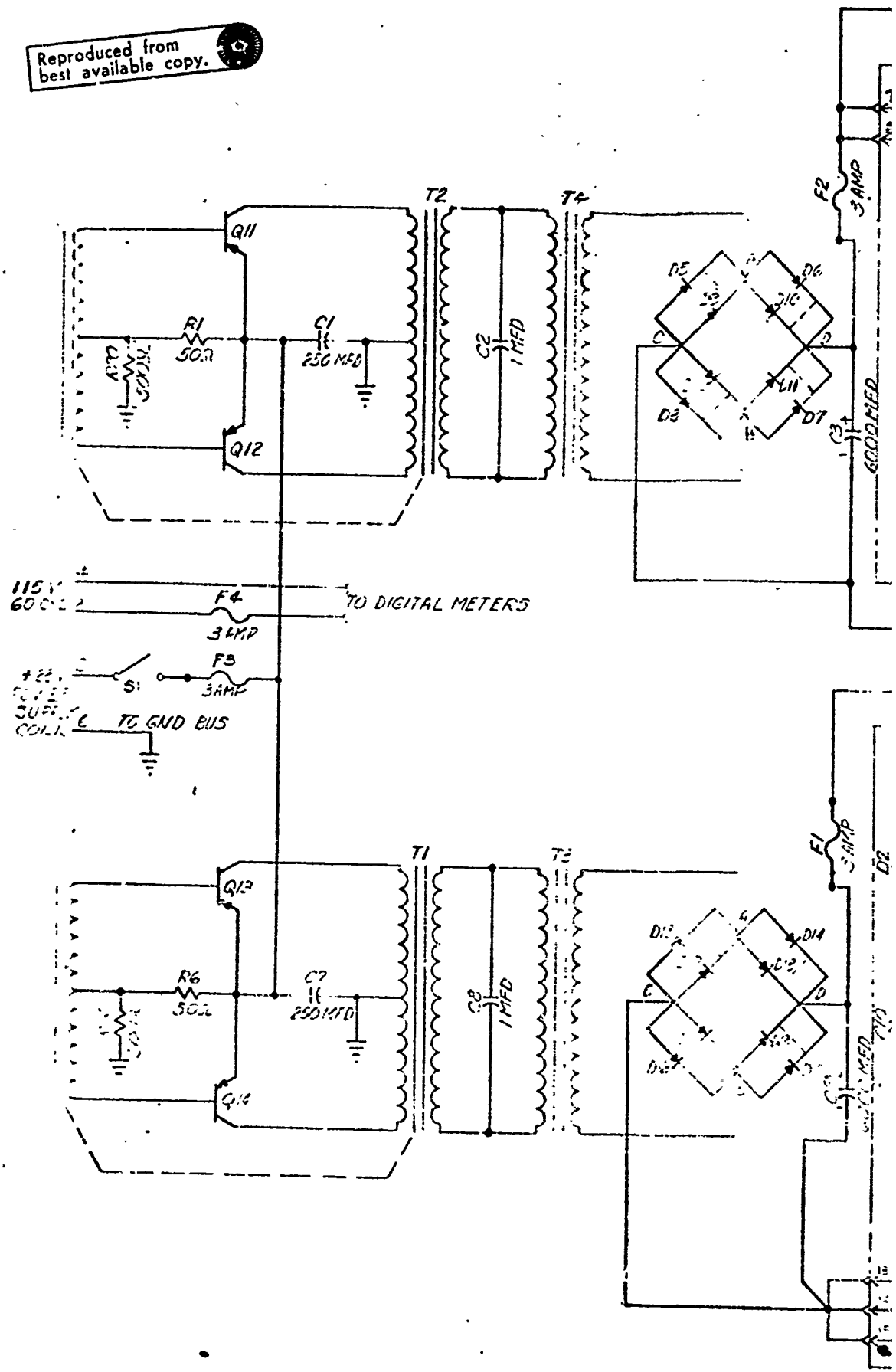

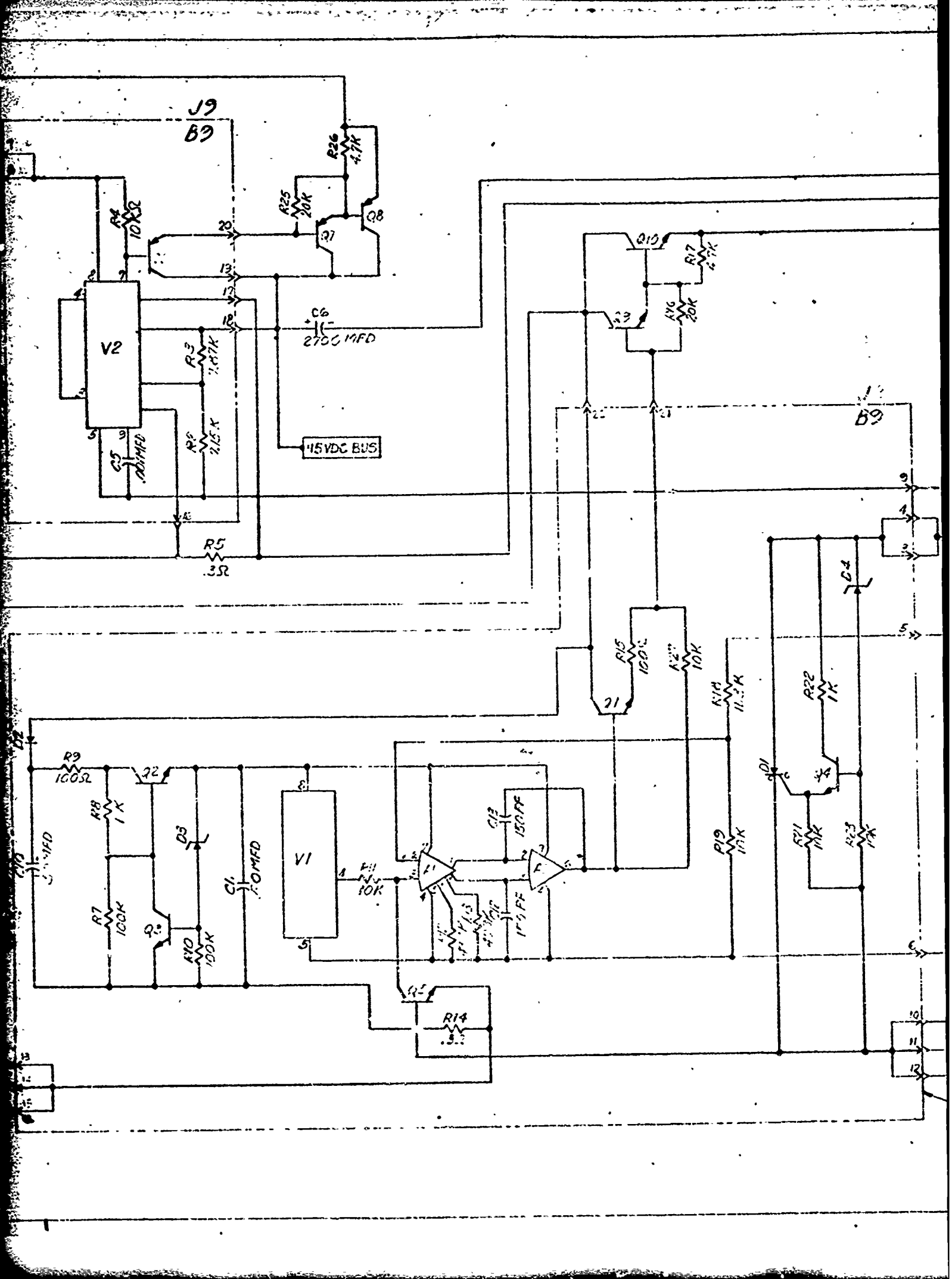
J9
B9
R26
4.7K
R25
20K
Q8
R4
10Ω
V2
R3
1.47K
R5
.3Ω
C5
.68MFD
R6
2.15K
C6
2700 MFD
+15VDC BUS
Q10
R17
4.7K
R16
20K
B9
C4
R15
100K
R21
10K
R24
11.3K
R22
1K
Q1
Q4
R11
11K
R23
1K
R19
17K
R9
100Ω
R8
1K
Q3
R7
100K
Q2
R10
100K
C1
.40MFD
V1
R11
10K
C12
150PF
C13
175PF
R14
.3Ω

PARTS LIST

BOARD NO.	ITEM NO.	QNTY REQ'D	PART NUMBER	DESCRIPTION	REMARKS
	R1, R6	2	50Ω	RESISTOR	
	R2	1	7.15K	"	
	R3	1	7.87K	"	
	R4	1	10K	"	
B9	R14	1	.35Ω	"	
	R7, R10	2	100K	"	
	R8, R22	2	1K	"	
	R9, R15	2	100Ω	"	
	R11, R23, R24, R27	4	10K	"	
	R12, R13	2	49.9K	"	
	R16, R25	2	20K	"	
	R17, R26	2	4.7K	"	
	R18	1	RNR65J1002F	"	
B9	R19	1	RNR65J1132F	"	
	R20, R21	2	500Ω	"	
	C1, C7	2	250 MFD	CAPACITOR	
	C2, C8	2	1 MFD	"	
	C3, C9	2	6000 MFD	"	
	C4, C6	2	2 150 MFD	"	
	C5	1	.22 MFD	"	
	C10, C11	2	50MFD	"	
B9	C12, C13	2	150 PF	"	
	Q1, Q3, Q4, Q5	4	2N2222A	TRANZISTOR	
	Q2	1	2N4237	"	
	Q6	1	2N-2564	"	
	Q7	1	2N4898	"	
	Q8	1	MJ2267	"	
	Q9	1	2N1486	"	HEAT SINK
	Q10	1	2N5067	"	HEAT SINK
	Q11, Q12, Q13, Q14	4	2N2146	"	HEAT SINK
B9	D1	1	2N4441	SILICON RECTIFIER	
	D2	1	1N4001	DIODE	
	D3, D4	2	1N4747A	"	
	D5, D6, D7, D8, D9, D10, D11, D12, D13, D14, D15, D16	12	1N4007	"	
	T1, T2	2	[illegible]	TRANSFORMER	
	T3, T4	2	[illegible]	"	
	U1, U2	2	[illegible]	ADJUSTABLE REGULATOR	
	F1, F2, F3	3	[illegible]	FUSE	
	S1	1	[illegible]	SWITCH	
	A1	1	LM121 AH/883	AMPLIFIER	
	A2	1	LM112 H/883	"	
	R5	1	.35Ω	RESISTOR	

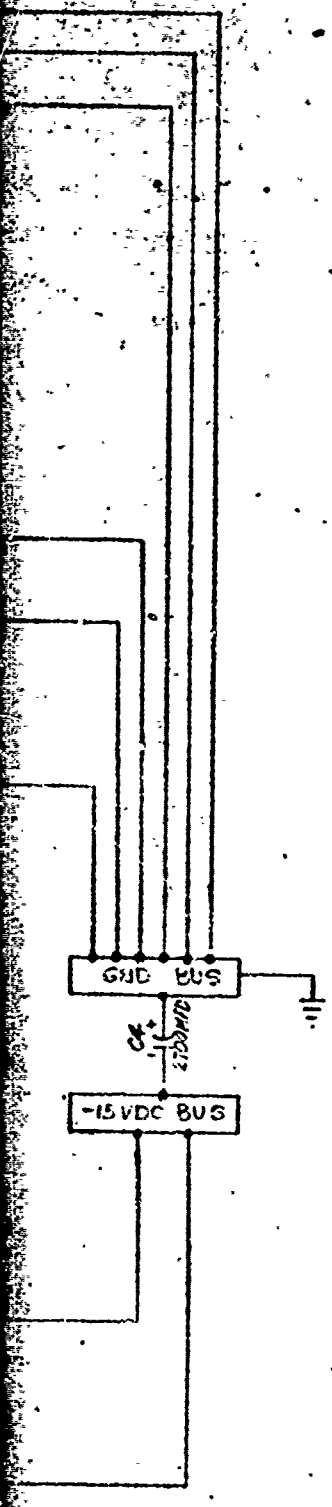

-B9 LOCATED IN ROLL CHANNEL RACK

POWER SUPPLY SCHEMATIC FOR BRASSBOARD MODEL (CAMS)	CHRYSLER CORPORATION
FIGURE 8-24.	SKC852
	SHEET 1 OF 1

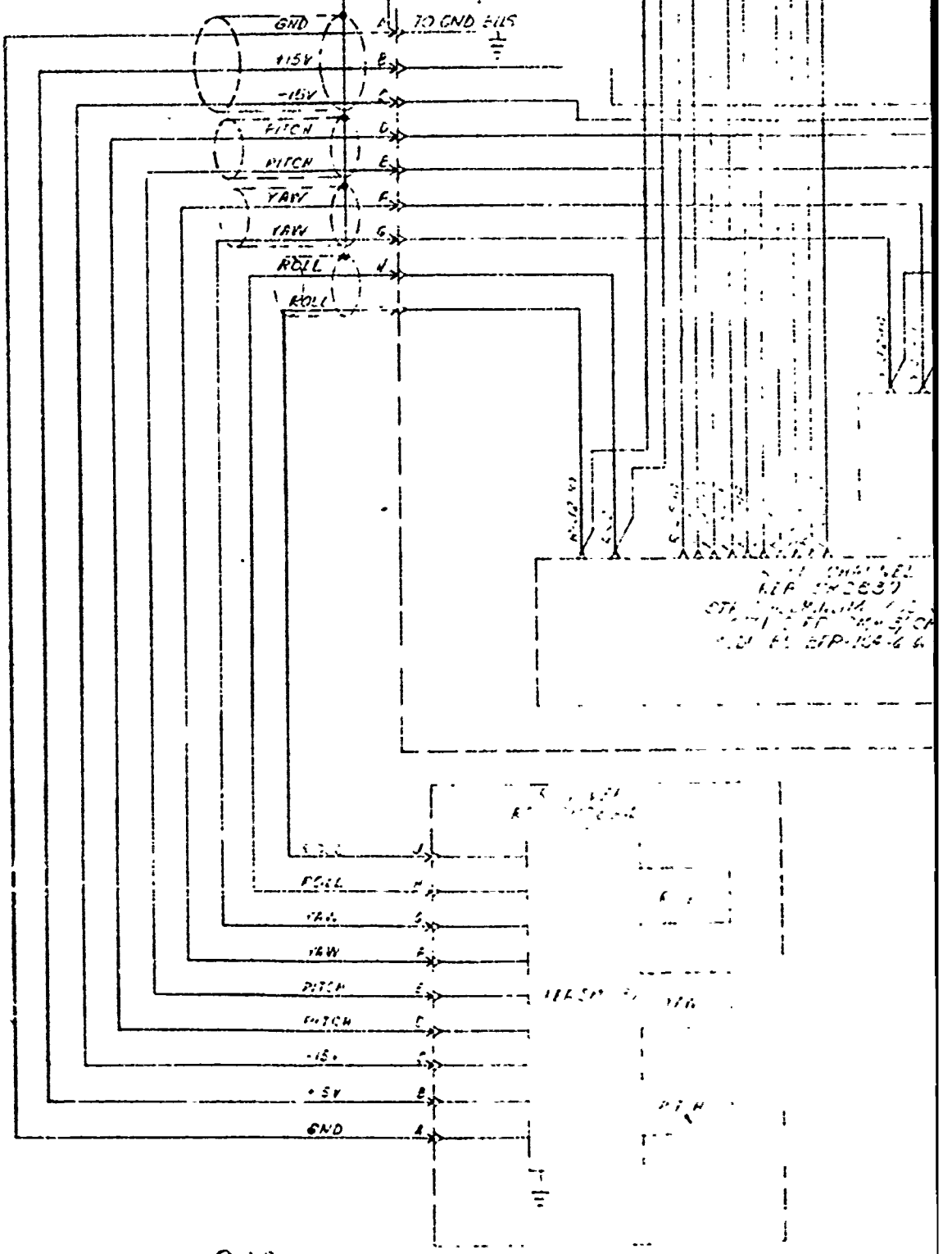

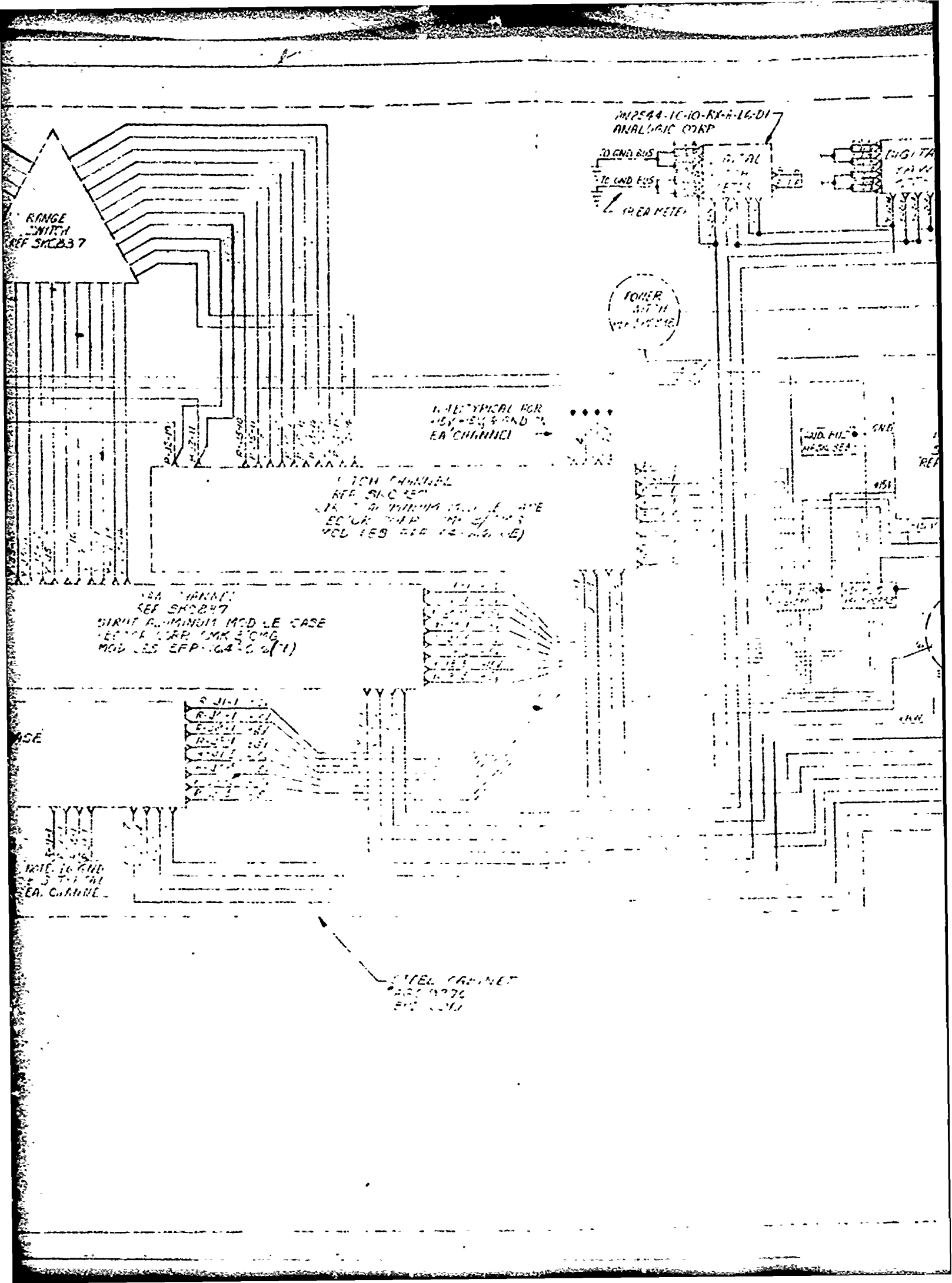
RANGE SWITCH REF SKC837
TO GND BUS
TO GND BUS
TOWER SWITCH
SEE SKC847
SEE SKC847
STEEL CABINET

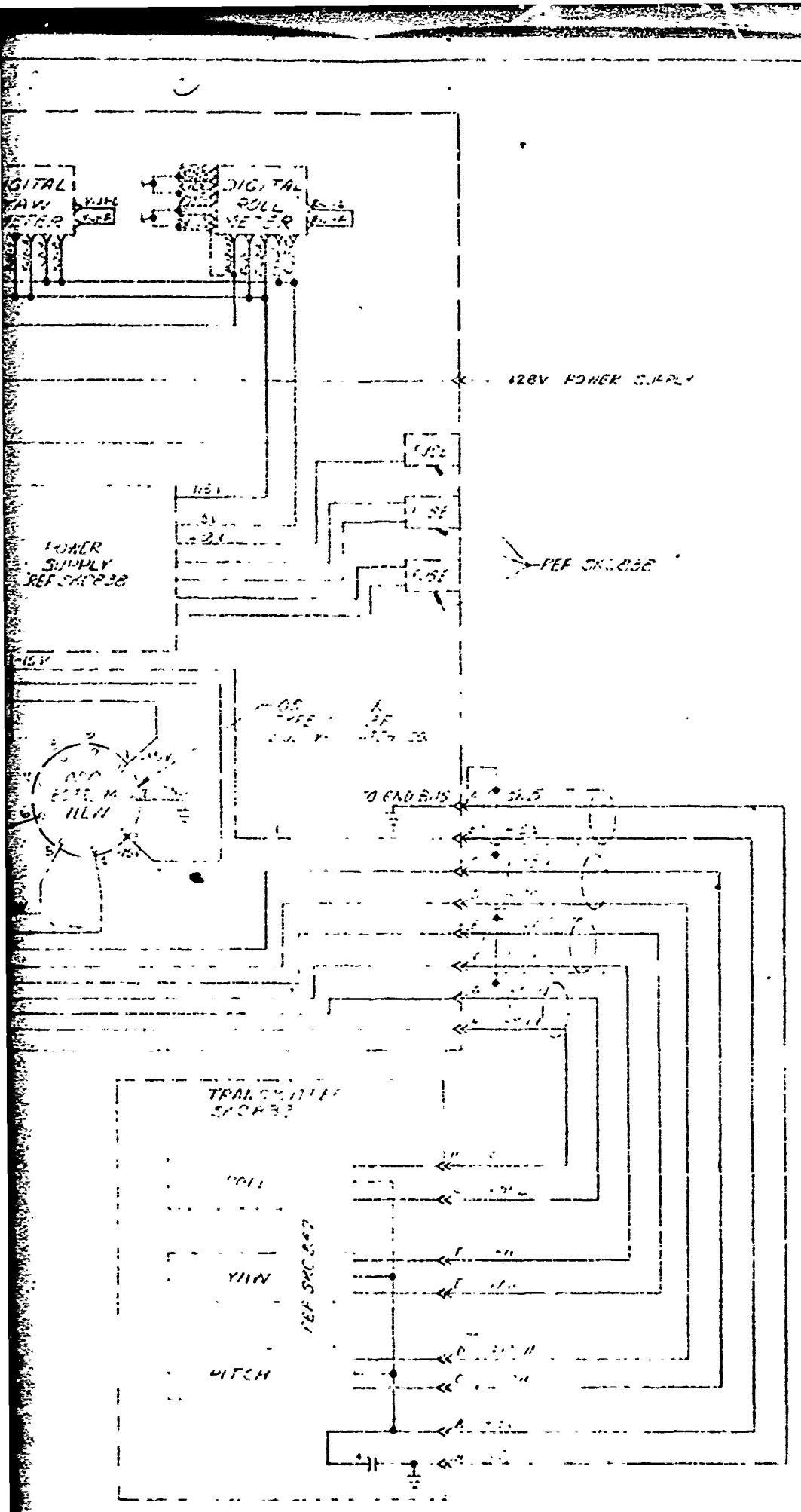
DIGITAL
YAW
METER
DIGITAL
ROLL
METER
+28V POWER SUPPLY
POWER
SUPPLY
REF SKC238
REF SKC238
TO RAD BUS
ROLL
YAW
PITCH
REF SKC 207

HEAT ASSEMBLY NUMBER
SKC635

WIRING DIAGRAM
FOR
BACKBOARD MODEL (SKC)

FIGURE 8-25.

CHRYSLER

8.5 Component Testing

Tests were conducted during OAMS Phase 1 development in order to evaluate components for their suitability to the OAMS application. The components tested include the critical components (LEDs, photodetectors and angle sensing crystals) as well as the Wollaston prism and optical filters. All of the work described in the critical component test plan was performed as shown in Table 8.9.

Two problem areas isolated during the component tests are marked with an asterisk in Table 8.9. The Texas Instrument (T.I.) LEDs degraded significantly during burn-in and the photodetector initially selected for use produced excessive noise and drift. Another problem reported earlier concerning the fact that the optical filters did not give the anticipated channel separation is no longer considered important based on the system test results. These problems will be described in more detail in the following summary of the tests along with an evaluation of their effect on system performance.

8.5.1 LEDS

Eighteen types of Light Emitting Diodes (LEDs) have been tested as part of an evaluation to determine the most suitable LEDs for the OAMS application and the best optical configuration. The LEDs tested are listed in Tables 8.10 and 8.11. Tests were performed to verify the specified values of power output, beam width at the half power points, spectral peak wavelength and half power bandwidth, frequency response, distortion and the change in these parameters over time and temperature changes.

Intensity profiles of the LEDs used in OAMS are shown in Figure 8.26. The SLH3 (λ_c = 800 nm) and SLH4 (λ_c = 860 nm) are used in the pitch and yaw channels respectively. These LEDs are made by Texas Instruments, Inc. The General Electric SSL-55C is presently used in the system roll channel. A replacement is now necessary for the SSL-55C because General Electric no longer offers this type of LED in its product line. A two dimensional intensity profile of the SSL-55C is shown in Figure 8.27. These profiles provide information on beam uniformity and can be used to determine the percentage of power which can be collected by an optical system with a given f/number as shown in Figure 8.28.

These profiles also show the variation in beam intensity which can be expected in the OAMS system and why the LED control loop is required to keep the LEDs balanced in intensity at any point in the beam.

A spectral profile of the OAMS LEDs is given in Figure 8.29. This information is important in evaluating the cross talk between channels which are separated by using optical bandpass filters.

The relation between output power and forward current for the SSL-55C is shown in Figure 8.30 for a particular heatsink and ambient temperature. This relationship must be considered for the extremes of ambient temperature in

TABLE 8.9
COMPONENT TESTING SUMMARY

	STATUS			
	SSL-55C	SLH4	SLH3	
LEDS				
TEST I - BURN IN	COMPLETED	COMPLETED*	COMPLETED*	REPORTED PREVIOUSLY, DECREASING OUTPUT
TEST II - NOMINAL CHARACTERISTICS	COMPLETED	COMPLETED	COMPLETED	DECREASING OUTPUT AND NON-UNIFORMITY
TEST III - STABILITY	COMPLETED	COMPLETED*	COMPLETED*	DECREASING OUTPUT
TEST IV - SPECTRAL CHARACTERISTICS	COMPLETED	COMPLETED	COMPLETED	
DETECTOR	UDT-600/PREAMP		UDT PIN-5DP	
TEST V - PRIMARY DET. CHAR.	COMPLETED*		COMPLETED	NOISE AND DRIFT
TEST VI - SECONDARY CHAR.	COMPLETED		(COMPLETED)	PIN-5DP RESULTS INFERRED FROM TESTING ON UDT-600
ANGLE SENSING CRYSTAL				
TEST VII - PRIMARY ASC CHAR.		COMPLETED		
TEST VIII- SECONDARY CHAR.		COMPLETED		
OPTICAL FILTER				
SPECTRAL TRANSMISSION CHAR.		COMPLETED		MORE CROSSCOUPLING THAN ANTICIPATED
WOLLASTON				
SIZE AND DEFLECTION ANGLES		COMPLETED		PHYSICAL DIMENSION AND DEFLECTION ANGLES ARE OUT OF SPEC.

* DEFINITE PROBLEM AREA

TABLE 8.11
SUMMARY OF LEDS FOR OAMS PHASE 1

		P (TOTAL POWER)	I_{MAX} (MAX. INTENSITY)*	EFFICIENCY (APPROX.)	λ_p (PEAK WAVELENGTH)	H.B.W. (HALF POWER SPECTRAL WIDTH)
GE SSL-55C	#9	10.7 M WATT	49.08 μW/STER.	2.23%	.9590 μM	510 Å
	#11	10.9	47.95	2.27%	.9615	510
	#1	10.0	51.89	2.08%	.9540	510
	#7	11.9	64.28	2.48%	.9465	445
	#2	9.8	41.06	2.04%	-	-
	#12	8.6	-	1.79%	-	-
T.I.SLH4	#2	4.39 MW(9.6MW)		3.14%	.8600 μM	200 Å(250Å SPEC)
	#3	2.25 (8.9)		2.93%	.862 (.8630)	220 Å(250Å SPEC)
	#4	(6.4)		(1.90%)	(.8570)	(250Å SPEC)
	#5	(6.4)		(1.75%)	(.8640)	(250Å SPEC)
T.I.SLH3	#1	3.37 MW(8.1MW)		2.28	.798 μM (.7950μM)	210 Å (250Å)
	#3	23.7 (22.1)		6.91%	.815 (.820)	240 Å (250Å)
	#4	(7.0)		(1.96%)	(.8010 μM)	(250Å SPEC)
	#5	(6.9)		(1.89%)	(.7990 μM)	(250Å SPEC)

(X) VALUES MEASURED BY T.I.
* MEASURED WITH A .051 CM^2 AREA Si DETECTOR AT 30 FEET, $\Omega = 5.57740^{-5}$ STER.

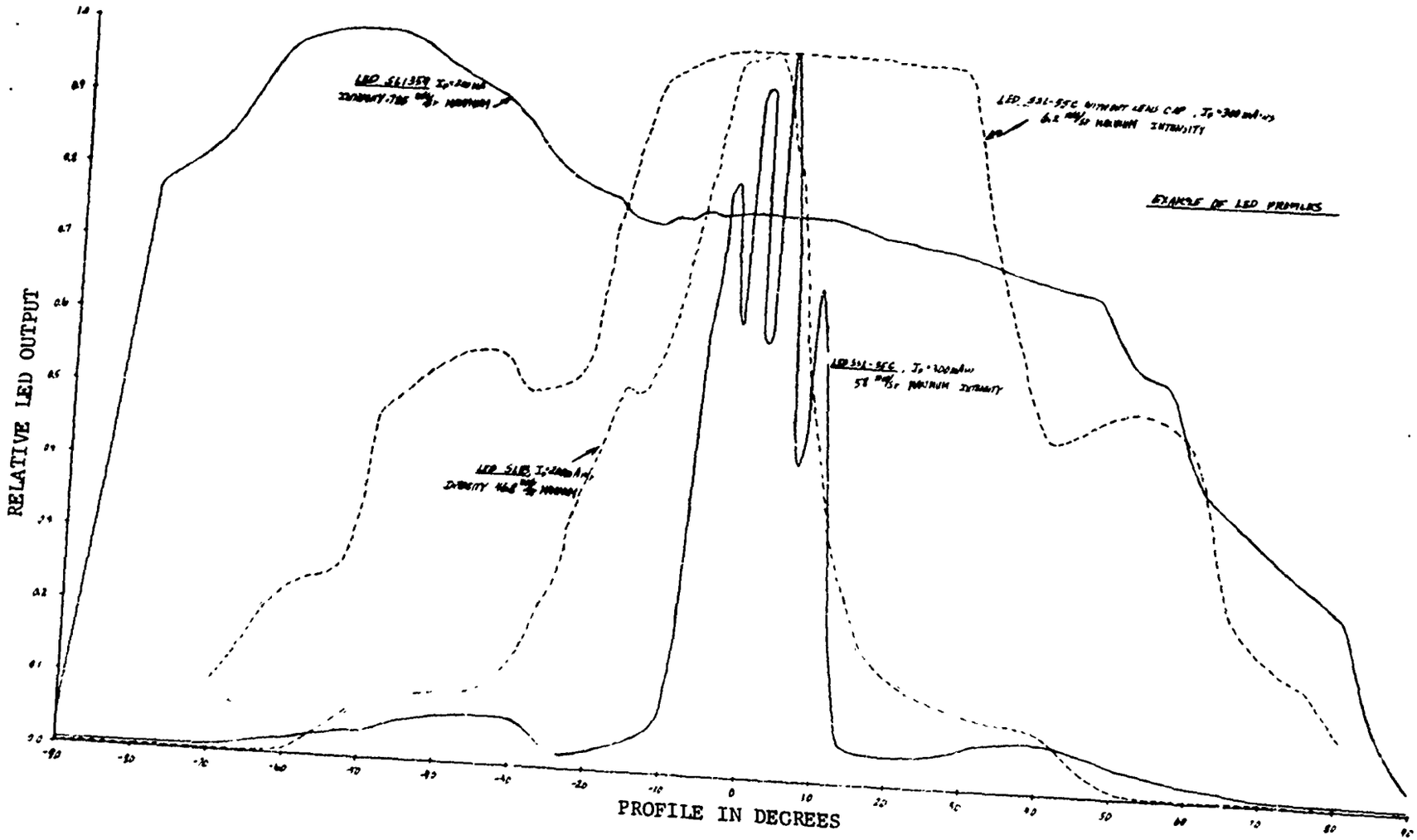

EXAMPLE OF LED PROFILES
FIGURE 8.26

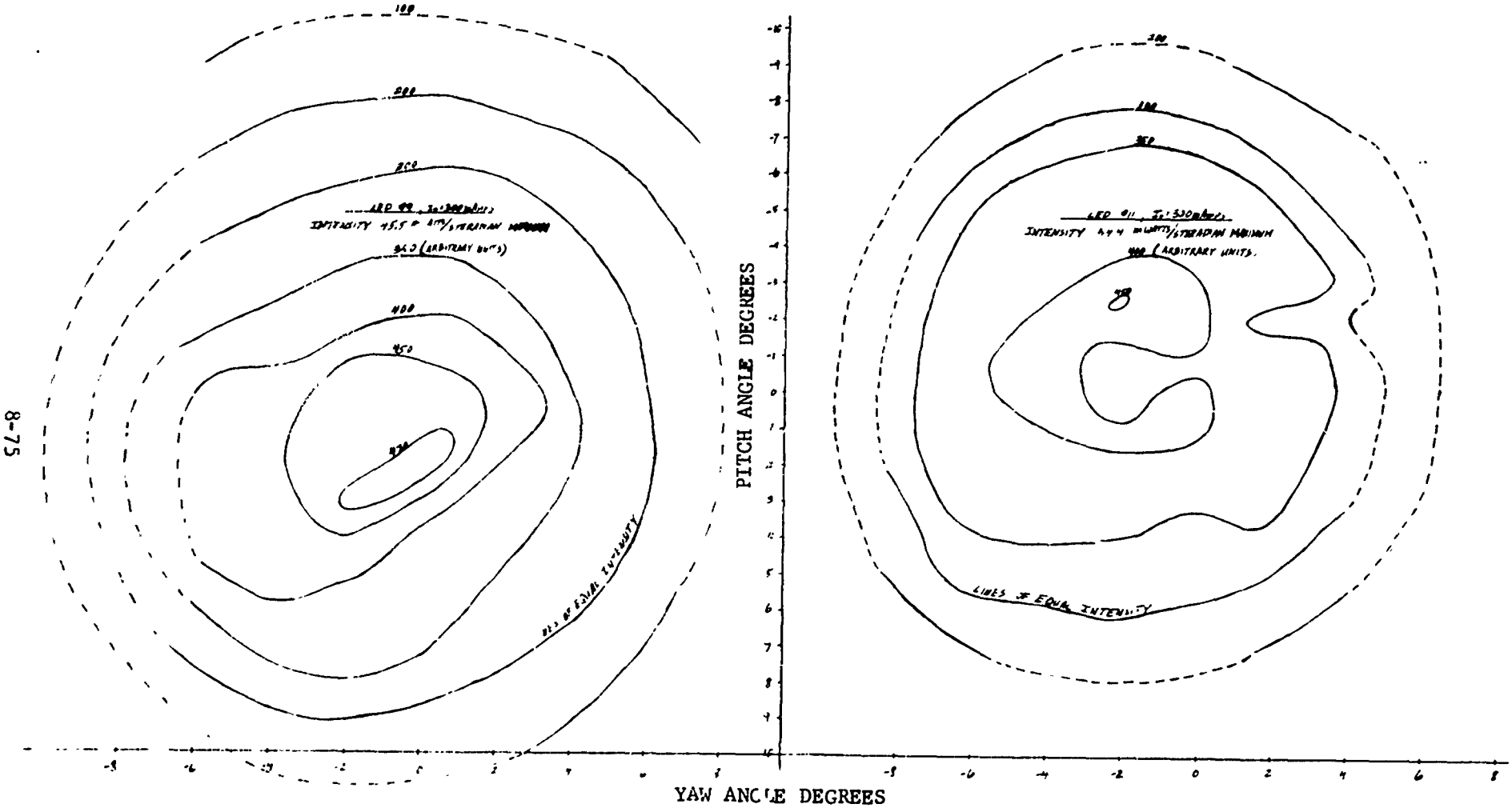

TWO DIMENSIONAL PROFILE OF TWO GE SSL-55C LED BEAMS

FIGURE 8.27

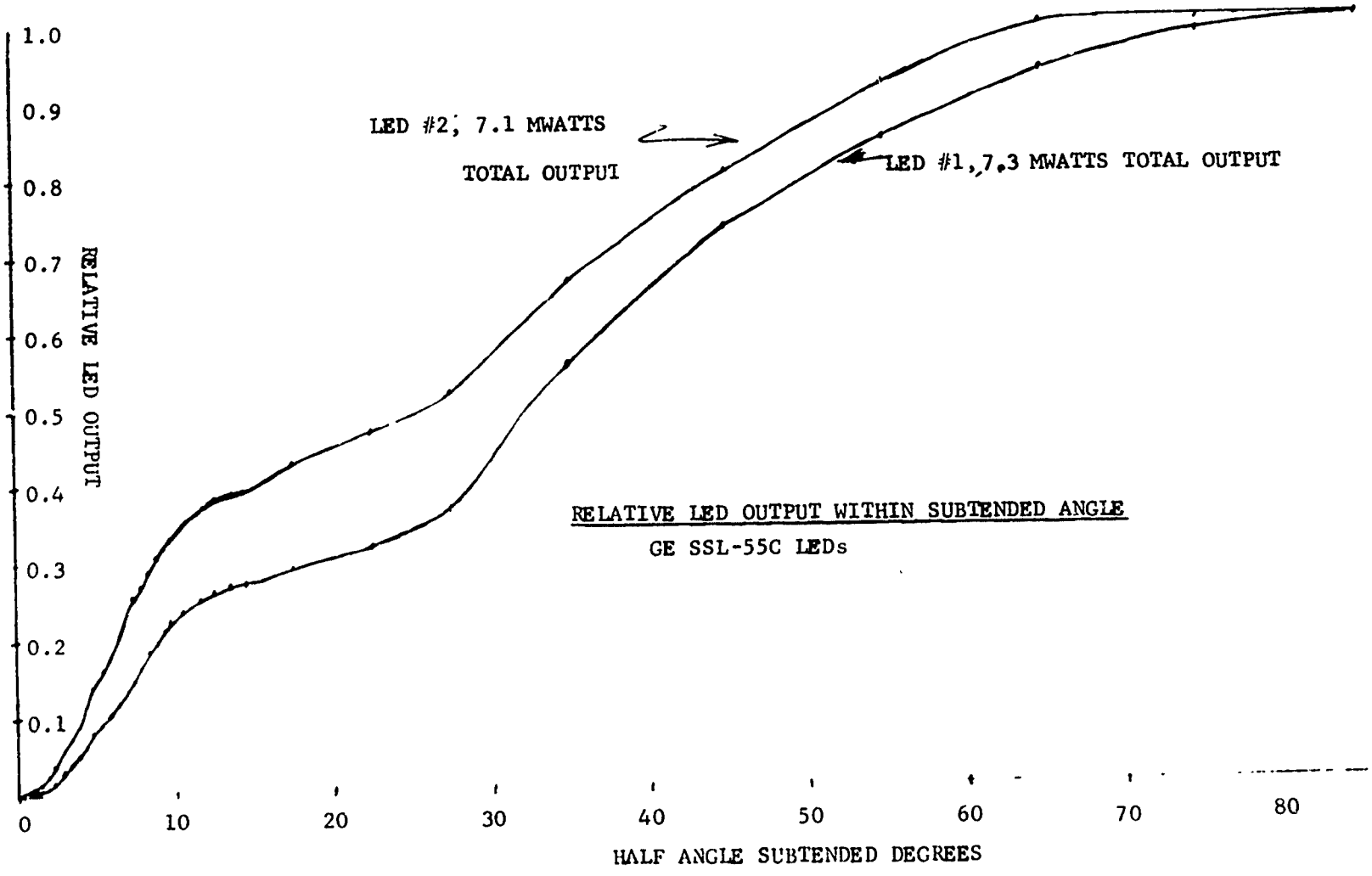
1.0
0.9
0.8
0.7
0.6
0.5
0.4
0.3
0.2
0.1
RELATIVE LED OUTPUT
LED #2, 7.1 MWATTS
TOTAL OUTPUT
LED #1, 7.3 MWATTS TOTAL OUTPUT
RELATIVE LED OUTPUT WITHIN SUBTENDED ANGLE
GE SSL-55C LEDs
0
10
20
30
40
50
60
70
80
HALF ANGLE SUBTENDED DEGREES

FIGURE 8.28

FIGURE 8.29

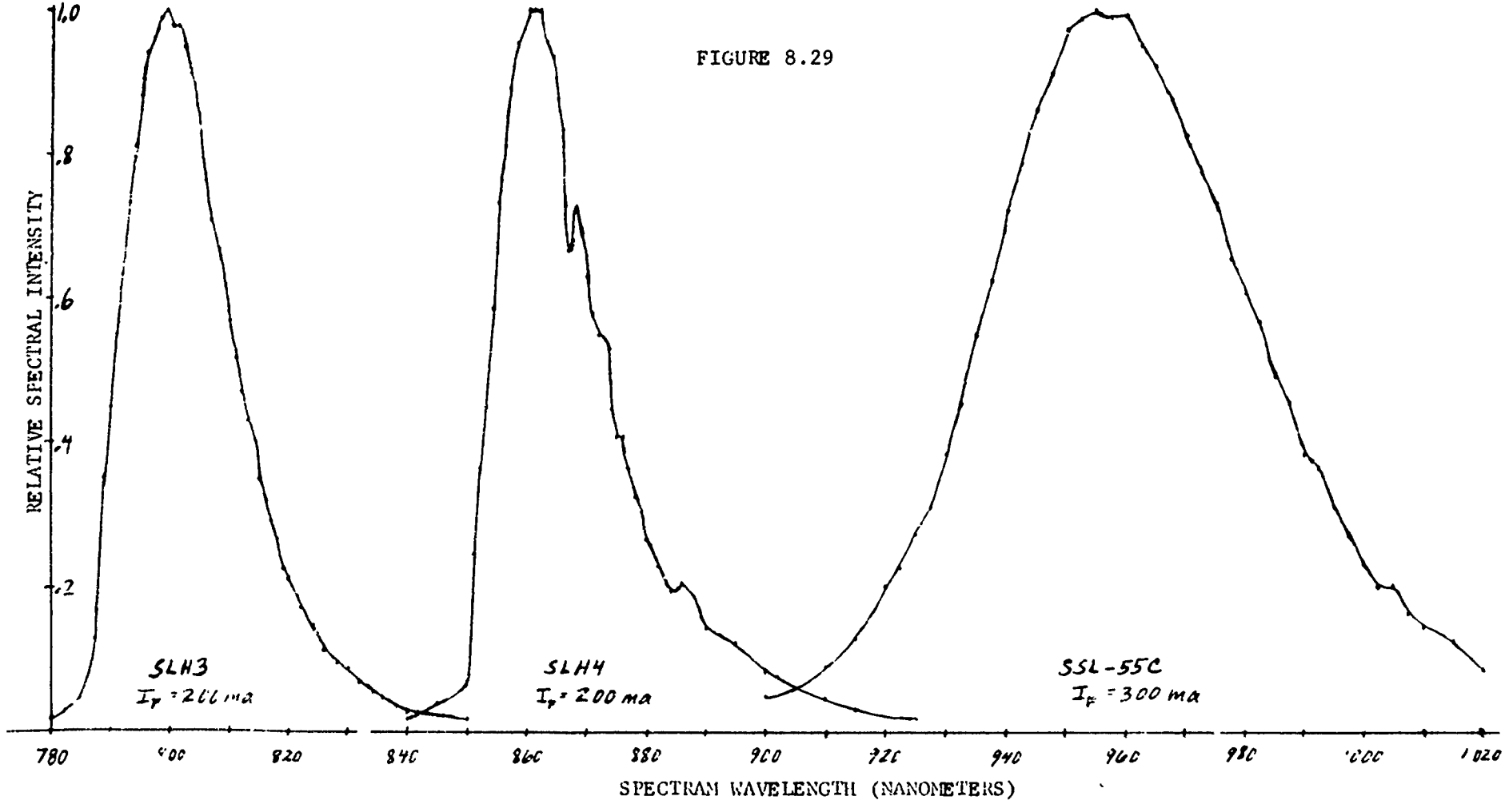

DATA TAKEN WITH A McPHERSON MODEL 235 SCANNING MONOCHROMETER

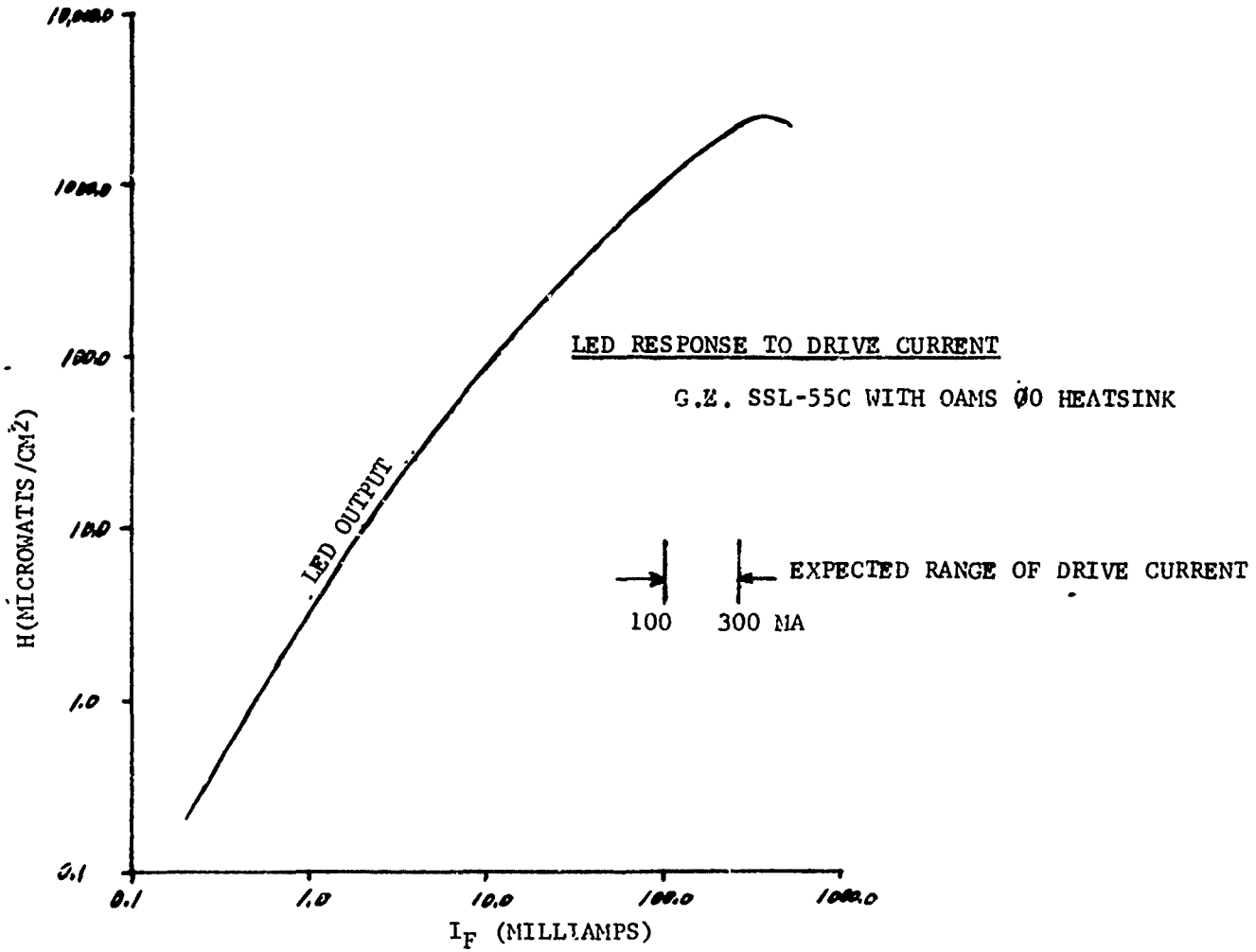
LED RESPONSE TO DRIVE CURRENT
G.E. SSL-55C WITH OAMS ØO HEATSINK
LED OUTPUT
EXPECTED RANGE OF DRIVE CURRENT
100
300 MA
H(MICROWATTS/CM²)
0.1
1.0
10.0
100.0
1000.0
I_F (MILLIAMPS)

FIGURE 8.30

which the LED must operate in order to avoid saturation or damage to the junction. The effect of temperature on SSL-55C output and efficiency is shown in Figure 8.31. A typical value for efficiency is -.3%/°F. The warm up time for an LED depends on its construction and heat dissipation of the heat sink. Figure 8.32 shows a typical LED output reaching stability after 5 minutes. The peak wavelength varies with forward current as shown in Figure 8.33. The spectral shift with temperature must be considered in evaluation of system crosstalk.

Frequency response and distortion were evaluated in the low frequency range of 10 to 10,000 Hertz. No significant distortion or attenuation with frequency response was observed over the temperature range of 0° to 140°F as long as the LED bias current value was below the saturation range.

Burn in tests are important in determining reliability characteristics for LEDs. The biggest degradation usually occurs in the first few hundred hours of operation. Burn in produces diodes with more stable performance and, in addition, allows more defective units to be separated because they are frequently characterized by more unstable performance. Burn in tests have been conducted on 74 LEDs representing six types of materials or manufacturers. Tests were conducted for periods between 200 and 500 hours at forward currents which were approximately half the maximum rated value. The standard commercial types (SSL-55C, FLV104 and MV4H), showed typical 5-10% output decrease. Figure 8.34 shows reliability data provided by General Electric on an LED very similar to the SSL-55C. The SLH3 and SLH4 diodes which had been selected for wavelength and packaged for the Chrysler Corporation requirements by Texas Instruments showed a 50%-90% output decrease in 200 hours of operation. This phenomenom was then verified by T. I. as shown in Figure 8.35 which lists the probable cause as contaminants in the crystal growing reactor. Further investigation revealed that Wright Patterson Air Force Avionics Laboratory had experienced a similar problem with LEDs from T. I. made of the same type of semiconductor material. This degradation of GaAsP devices was one of the two problem areas isolated during the component testing.

Texas Instruments has manufactured LEDs from GaAlAs material in the same wavelength region as the GaAsP. These devices have had much better reliability. Burn in tests at Chrysler indicated a typical degradation of 5% during 150 hours of operation. Several GaAlAs LEDs failed at one time during the burn in test due to what was thought to be an external factor in the test setup. T. I. has performed extensive testing of GaAlAs reliability with good results.

8.5.2 Detectors

A detector with a built in preamplifier was initially selected for the OAMS system. This offered the advantage of reducing capacitance and interference on the signal by minimizing the distance between the detector and preamplifier. The UDT-600 detector/preamplifier combination operating in the biased mode was determined in test to be very temperature sensitive. The dark current offset increased two orders of magnitude from 0°F to 140°F as shown in figure 8.36. Although compensation was possible, it would be difficult. Figure 8.37 shows the change in offset of the UDT 600 detector without the preamp in both the biased and unbiased mode. The detector offset in both modes was approximately the same value at low temperatures. It can be seen that the unbiased detector will require less temperature compensation. The temperature change in the preamplifier offset voltage is shown in figure 8.38. The noise and temperature characteristics of the preamp used in the UDT-600, the Teledyne Philbrick

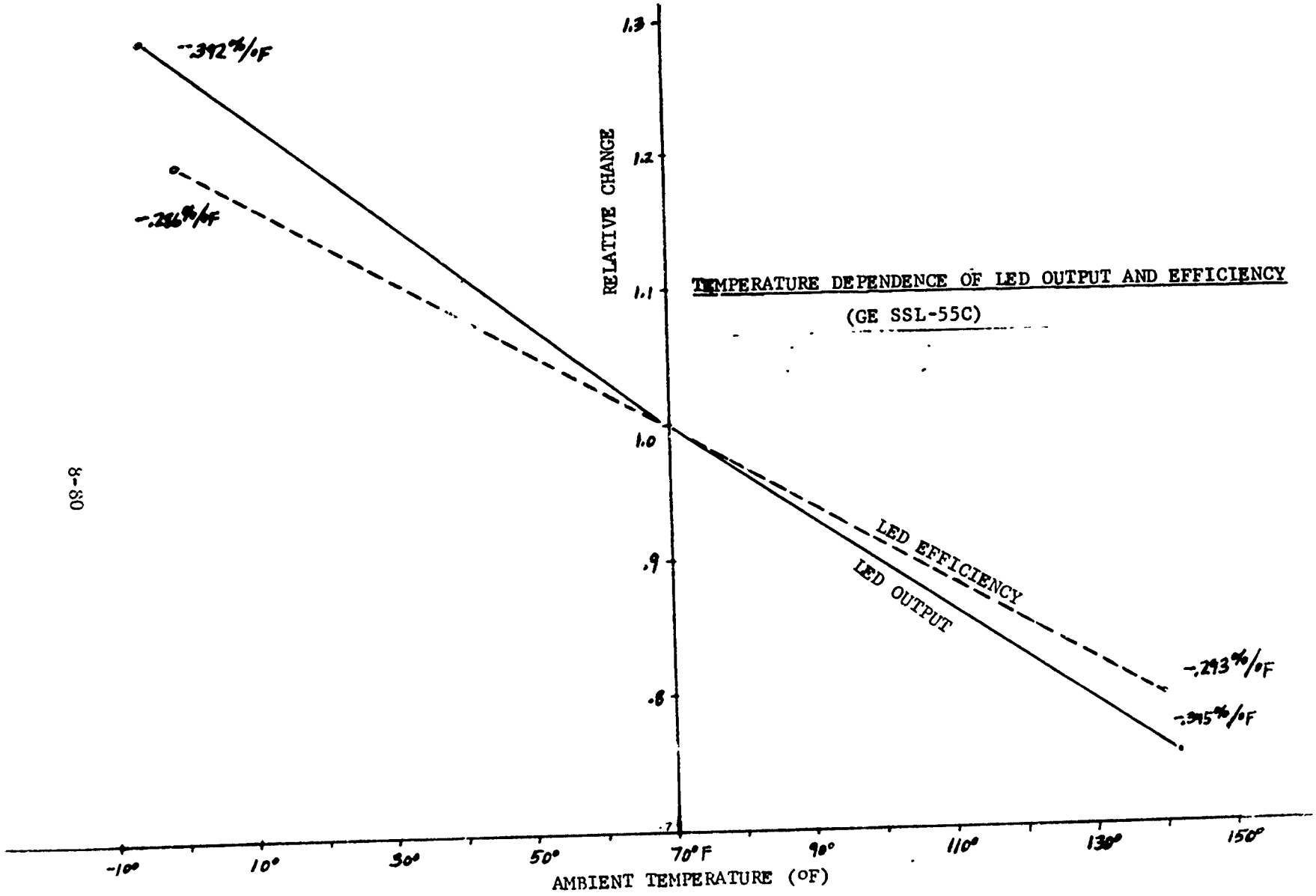
TEMPERATURE DEPENDENCE OF LED OUTPUT AND EFFICIENCY
(GE SSL-55C)
RELATIVE CHANGE
1.3
1.2
1.1
1.0
.9
.8
.7
-.392%/°F
-.286%/°F
LED EFFICIENCY
LED OUTPUT
-.293%/°F
-.345%/°F
-10°
10°
30°
50°
70°F
90°
110°
130°
150°
AMBIENT TEMPERATURE (°F)

FIGURE 8.31

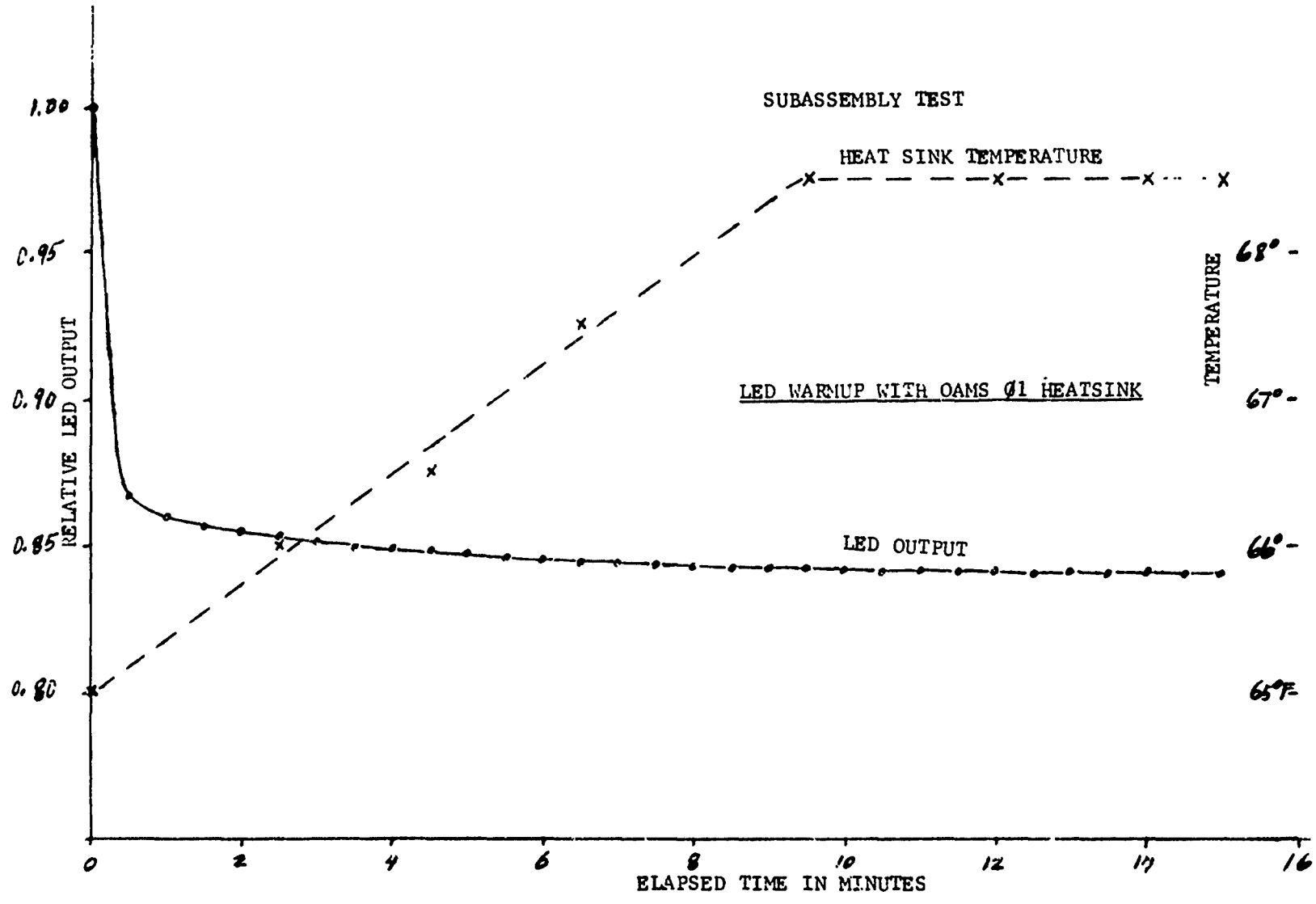
SUBASSEMBLY TEST
HEAT SINK TEMPERATURE
LED WARMUP WITH OAMS Ø1 HEATSINK
LED OUTPUT
RELATIVE LED OUTPUT
TEMPERATURE
1.00
0.95
0.90
0.85
0.80
68°
67°
66°
65°F
0
2
4
6
8
10
12
14
16
ELAPSED TIME IN MINUTES

FIGURE 8.32

SSL-55C #1 LED SPECTRAL CHARACTERISTICS VERSUS I_F

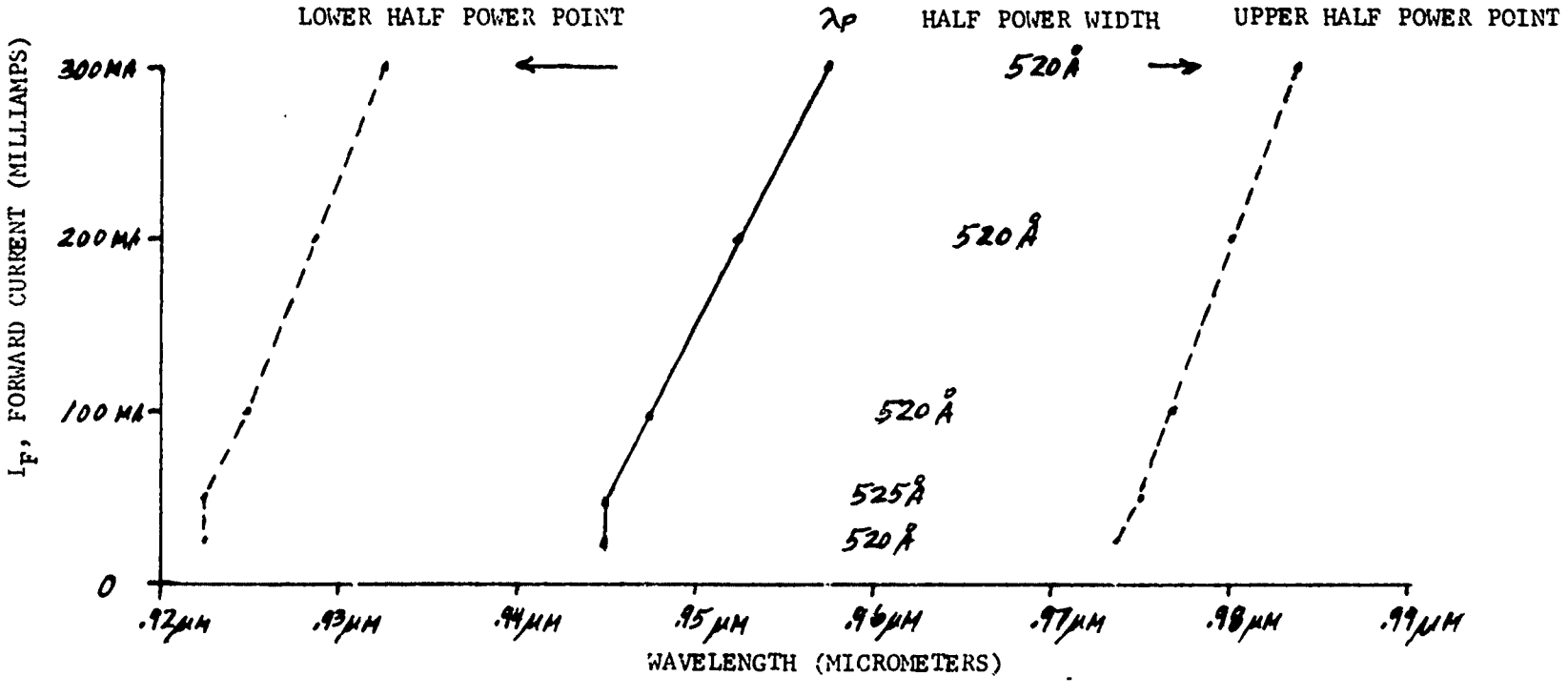

FIGURE 8.33

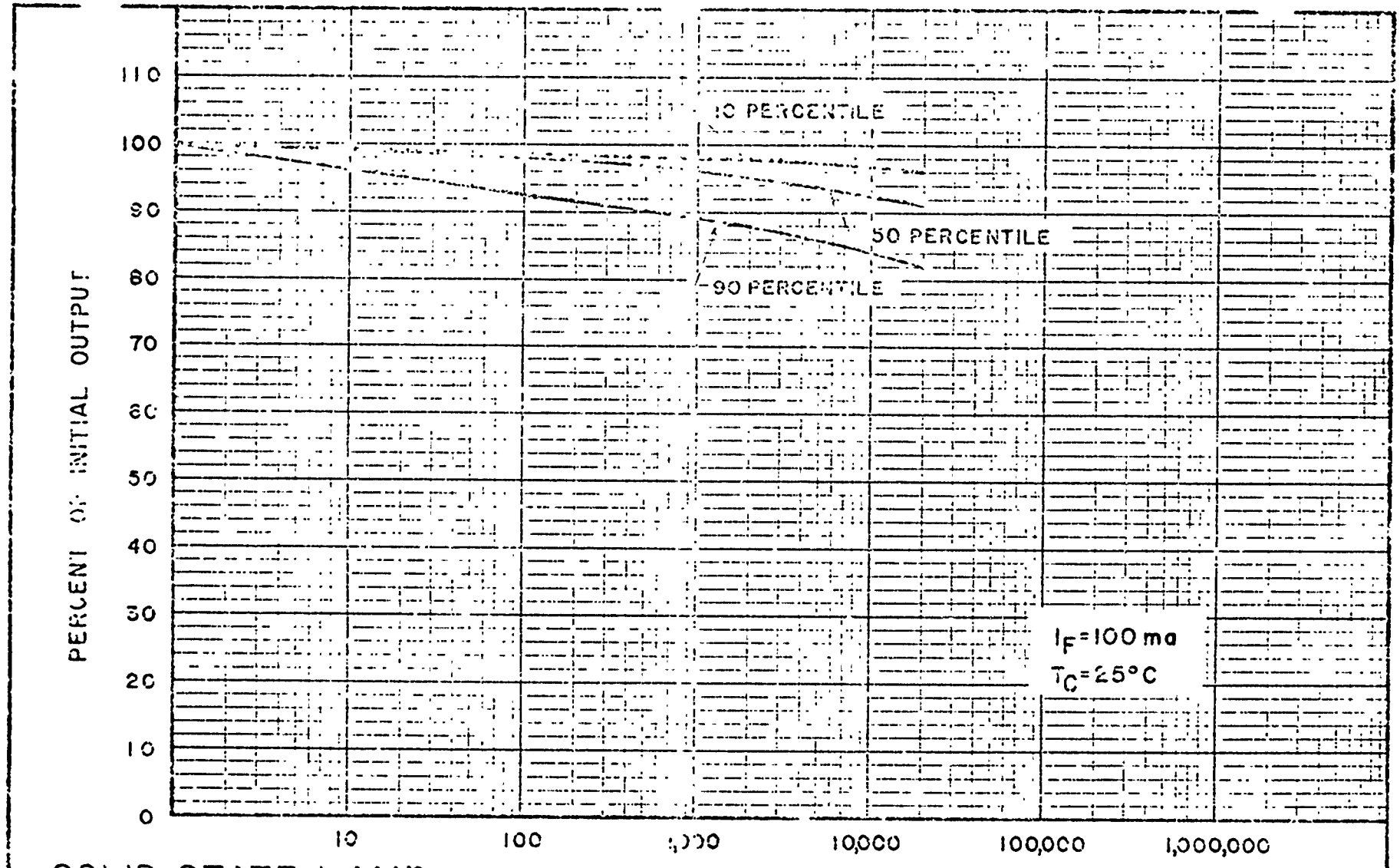

SOLID STATE LAMP
LIFE TEST DATA
SSL-5 (SAMPLE SIZE-14)

FIGURE 8.34

DATE APRIL 26, 1972
SCALE
DRAWN BY A T S
APPROVED BY JW H

GENERAL ELECTRIC
MINIATURE LAMP DEPARTMENT
NELA PARK · CLEVELAND 44112 · OHIO

SSL-A-1209

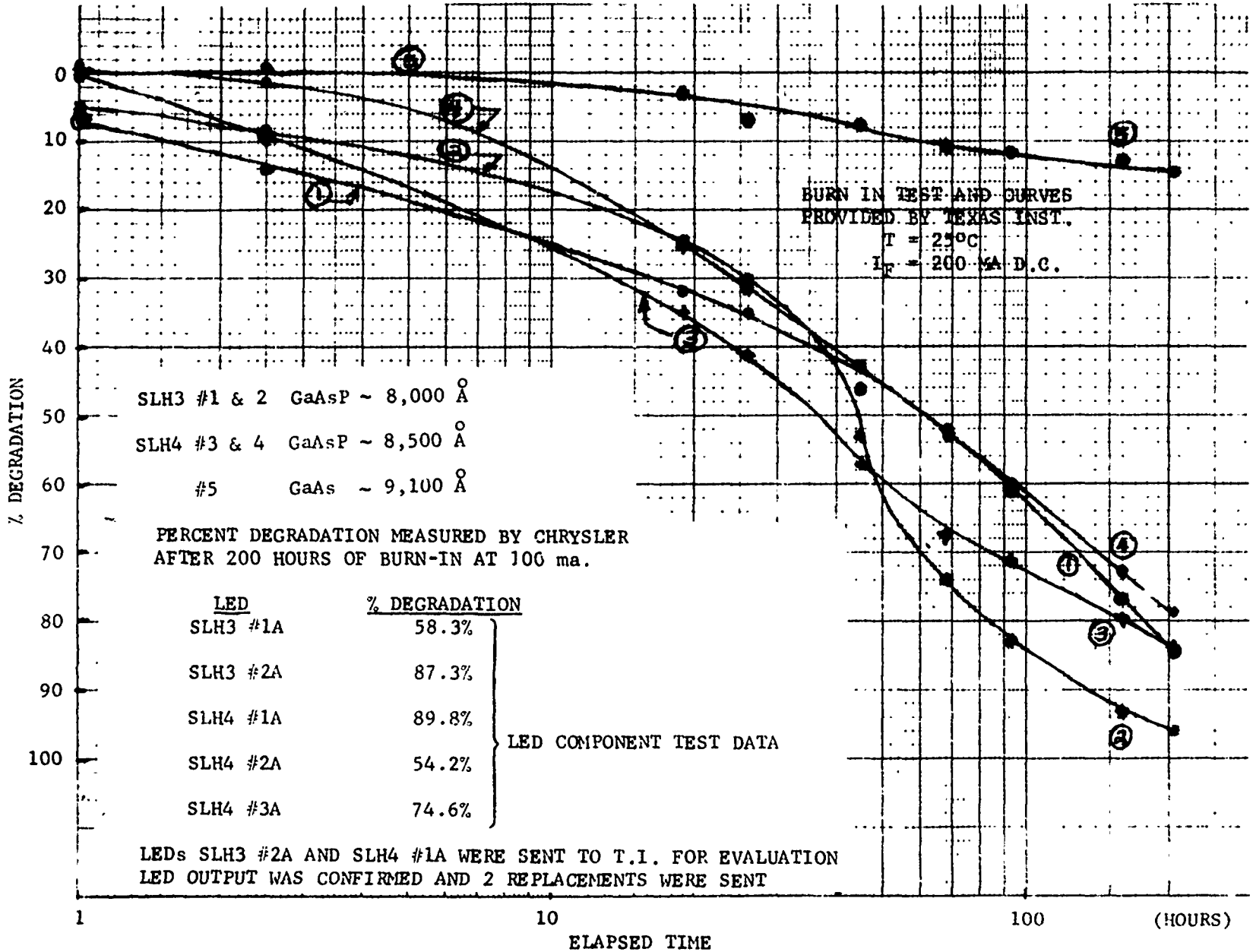
% DEGRADATION
0
10
20
30
40
50
60
70
80
90
100
1
10
100
(HOURS)
ELAPSED TIME
BURN IN TEST AND CURVES
PROVIDED BY TEXAS INST.
T = 25°C
I_F = 200 MA D.C.
SLH3 #1 & 2 GaAsP ~ 8,000 Å
SLH4 #3 & 4 GaAsP ~ 8,500 Å
#5 GaAs ~ 9,100 Å
PERCENT DEGRADATION MEASURED BY CHRYSLER
AFTER 200 HOURS OF BURN-IN AT 100 ma.
LED
% DEGRADATION
SLH3 #1A 58.3%
SLH3 #2A 87.3%
SLH4 #1A 89.8%
SLH4 #2A 54.2%
SLH4 #3A 74.6%
LED COMPONENT TEST DATA
LEDs SLH3 #2A AND SLH4 #1A WERE SENT TO T.I. FOR EVALUATION
LED OUTPUT WAS CONFIRMED AND 2 REPLACEMENTS WERE SENT

FIGURE 8.35

FIGURE 8.36

DETECTOR OUTPUT DRIFT
WITH TEMPERATURE

UDT-600 DETECTOR/PREAMPLIFIER
WITH R_F = 1.082 MEGOHM
NO INCIDENT RADIATION

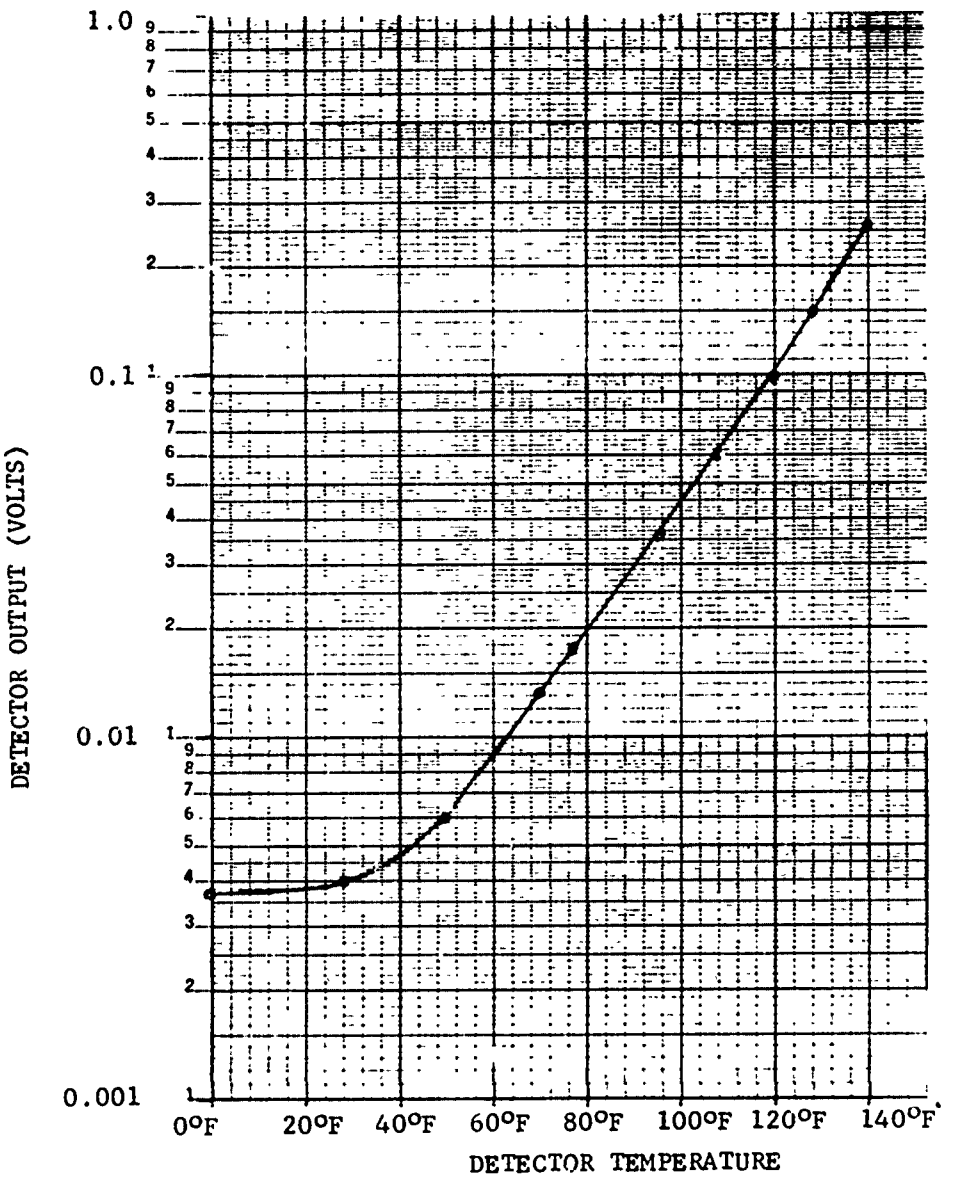

FIGURE 8.37

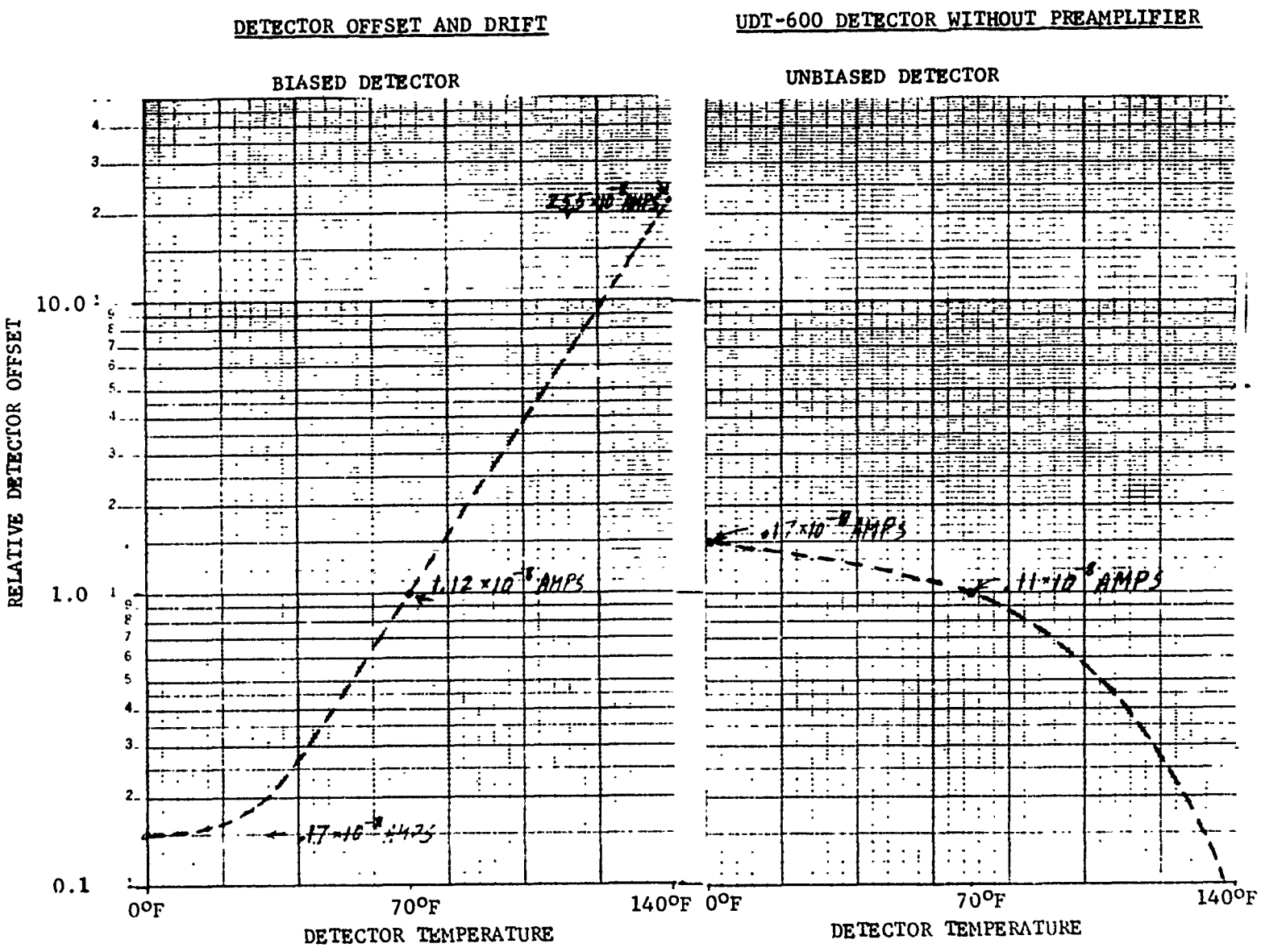
DETECTOR OFFSET AND DRIFT
UDT-600 DETECTOR WITHOUT PREAMPLIFIER
BIASED DETECTOR
UNBIASED DETECTOR
RELATIVE DETECTOR OFFSET
10.0
1.0
0.1
1.12 x 10⁻⁸ AMPS
11 x 10⁻⁸ AMPS
0°F
70°F
140°F
DETECTOR TEMPERATURE

FIGURE 8.38

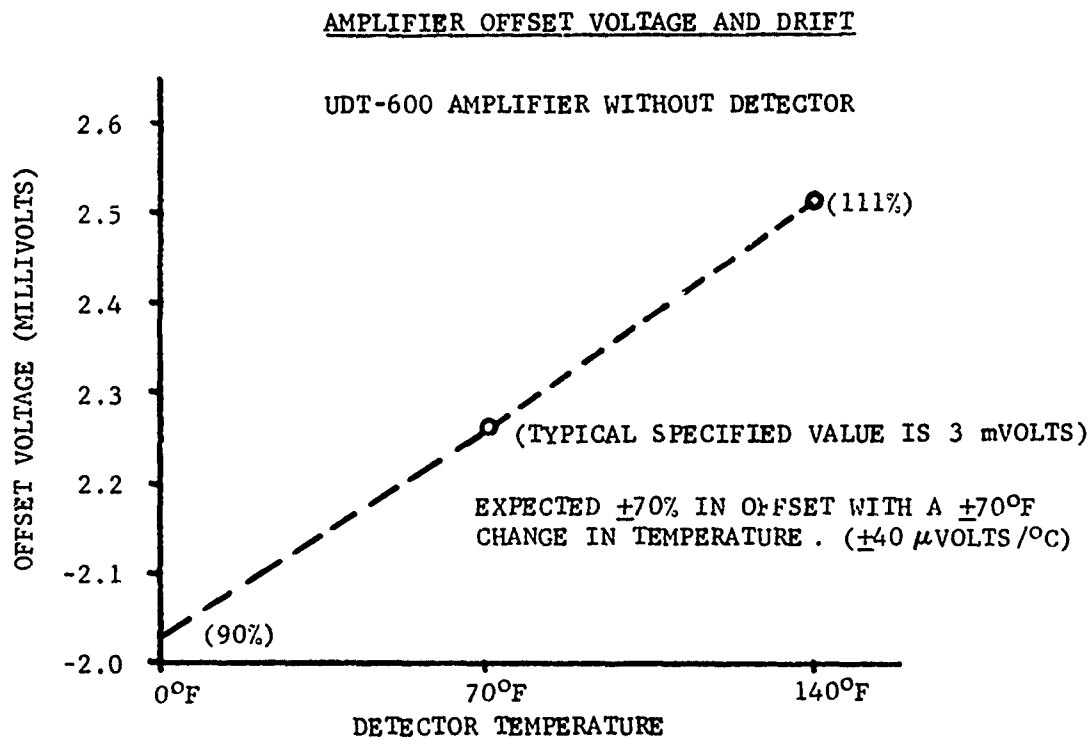
AMPLIFIER OFFSET VOLTAGE AND DRIFT
UDT-600 AMPLIFIER WITHOUT DETECTOR
OFFSET VOLTAGE (MILLIVOLTS)
2.6
2.5
2.4
2.3
2.2
-2.1
-2.0
(111%)
(TYPICAL SPECIFIED VALUE IS 3 mVOLTS)
EXPECTED ±70% IN OFFSET WITH A ±70°F
CHANGE IN TEMPERATURE . (±40 μVOLTS/°C)
(90%)
0°F
70°F
140°F
DETECTOR TEMPERATURE

1421, is not as good as others available as discrete components. The change in responsivity was ±20% with a ±70°F change in temperature. This was observed with or without the preamplifier and in both the biased and unbiased mode. Silicon detectors typically show only ±7% responsivity change over this temperature range as observed in tests on the RCA C30808 detector.

Distortion and frequency response are shown in figures 8.39 and 8.40 for the UDT-600 detector in the biased mode. Response and distortion were minimal throughout the OAMS operating region from 925 to 3700 herz. Temperature had no measurable effect on these parameters. The LED drive circuit limited the measurements to below 10,000 herz.

Detector noise was measured for the UDT-600 in the biased mode as shown in figure 8.41. The noise was divided into low frequency and high frequency. High frequency in this case was everything which could not be identified as low frequency below 20 herz. The dependence of low frequency noise with the level of incident radiation is also shown. The noise is within the detector specification at 70°F but increases significantly with temperature.

In order to reduce low frequency noise and the change in detector offset with temperature, the UDT PIN-5DP photovoltaic detector was used. The reduced temperature effect on detector offset current is shown in figure 8.42 and on the low frequency noise is shown in figure 8.43. The high frequency noise in the test setup is the combined effect of detector and an external amplifier. The effect of temperature on responsivity was about ±14% for a ±70°F change.

8.5.3 Angle Sensing Crystals

The fringe spacing in the fringe pattern produced by the angle sensing crystals was measured with light through a band pass filter centered at 630nm and then extrapolated to the operating wavelengths of the OAMS system. The period of the fringes at 800nm is 5.5°. At 860nm it is 5.9° and at 940nm it is 6.4°. This is in close agreement with the expected fringe spacing of the specified 1mm thick crystal.

The fringe pattern of an angle sensing crystal was monitored while the crystal was cycled in temperature from 0°F to 140°F to determine the change in the fringe period. Two detectors were positioned at the half intensity points of an adjacent fringe. There was no change in fringe spacing within the accuracy of the test which was approximately ±0.4% of the field of view or ±1 arc minute. A test setup to improve the accuracy would require a system as sensitive as the OAMS or a more adaptable temperature chamber. Further evaluation was conducted in the subassembly testing reported below.

8.5.4 Optical Filters

The optical interference filters were evaluated for transmission, cross channel interference and changes with temperature. Figure 8.44 shows the performance of the filters in the component test and the system test and gives the initial design estimate for comparison. The system tests are the most meaningful since they test the filters in the manner in which they are used in the system. The variation from design was primarily due to the inability to accurately express the LED spectral intensity from vendor specifications. Spectral data taken on LEDs at Chrysler, presented previously, show more long wavelength emission than anticipated.

DETECTOR (AND LED) DISTORTION OVER FREQUENCY AND TEMPERATURE RANGE

FIGURE 8.39

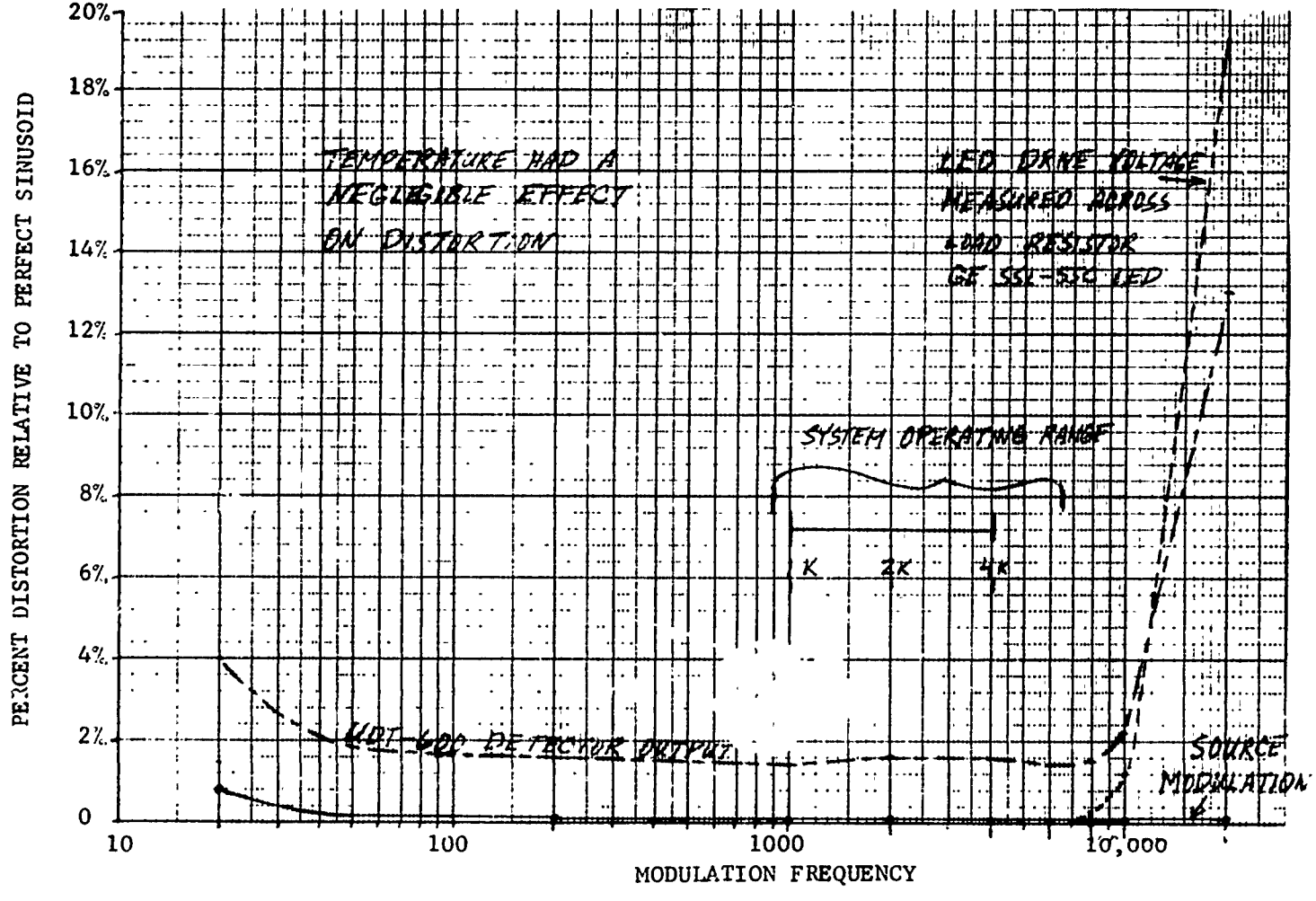

DETECTOR (AND LED) FREQUENCY RESPONSE

OVER FREQUENCY AND TEMPERATURE RANGE

TEMPERATURE HAD A NEGLIGIBLE EFFECT ON FREQUENCY RESPONSE OF DETECTOR

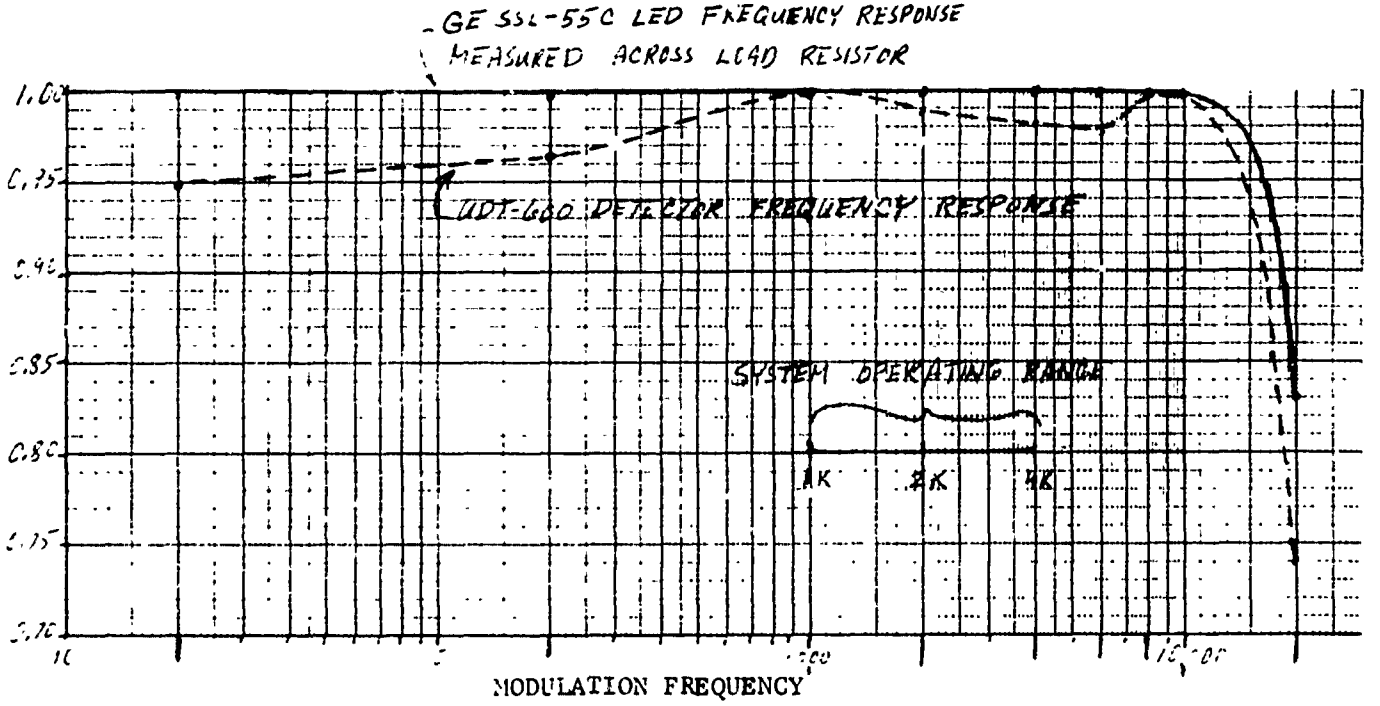

FIGURE 8.40

FIGURE 8.41

SUMMARY OF BROADBAND DETECTOR NOISE

UDT-600 WITH 1.08 MEGOHM RESISTANCE FEEDBACK
OPERATED ON BATTERY POWER SUPPLY

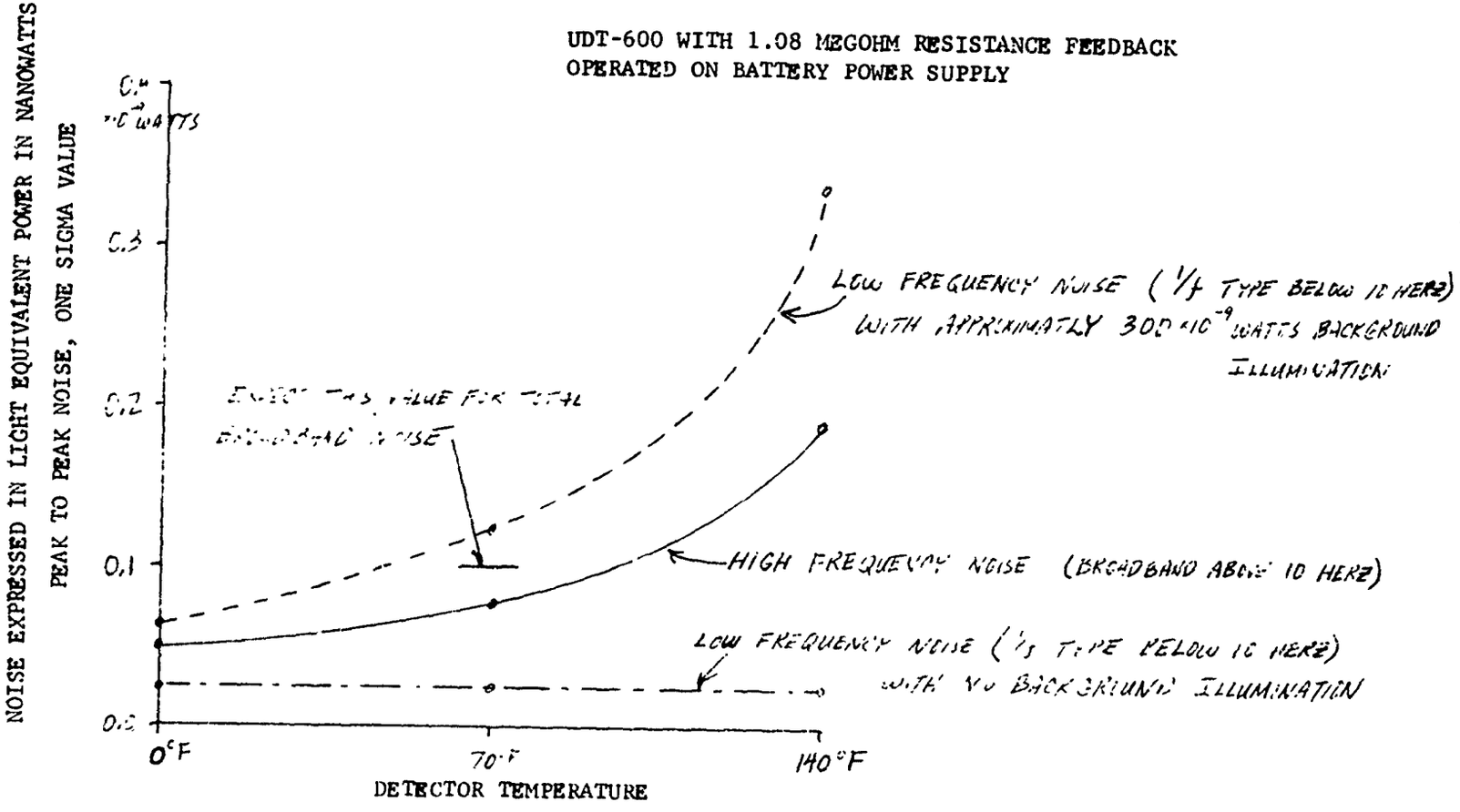

FIGURE 8.42

DETECTOR OFFSET AND CHANGE WITH TEMPERATURE

UDT PIN-5DP

UNBIASED DETECTOR

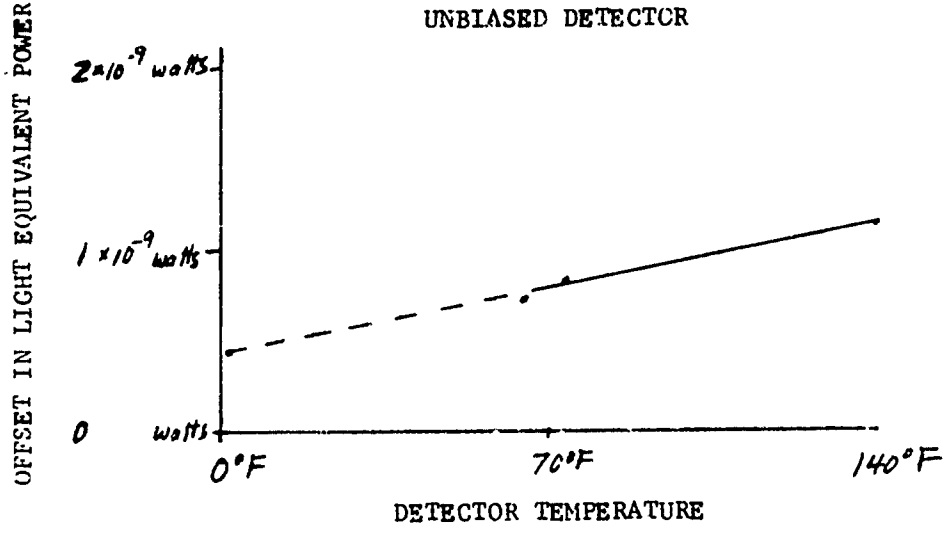

FIGURE 8.43

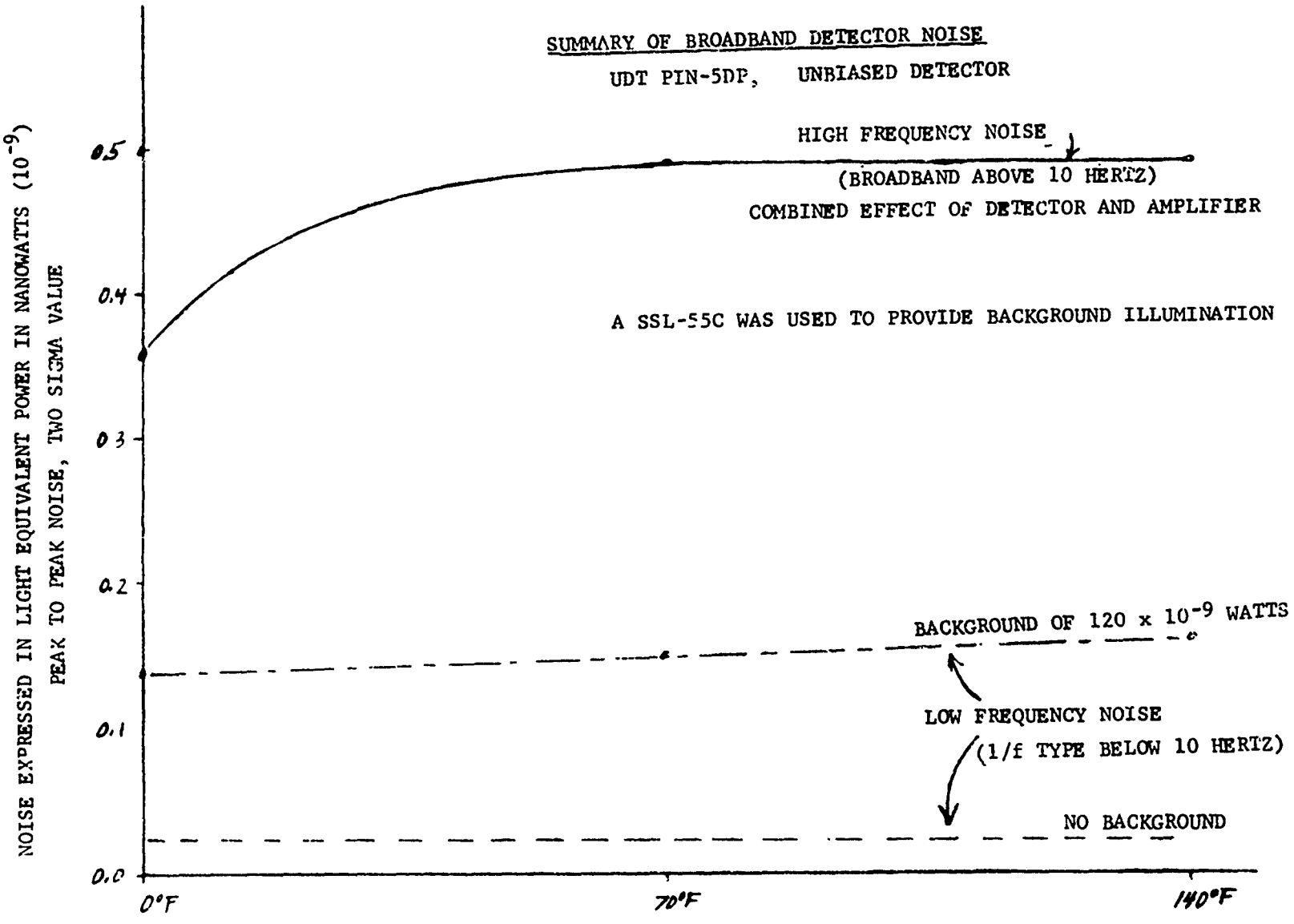
SUMMARY OF BROADBAND DETECTOR NOISE
UDT PIN-5DP, UNBIASED DETECTOR
HIGH FREQUENCY NOISE
(BROADBAND ABOVE 10 HERTZ)
COMBINED EFFECT OF DETECTOR AND AMPLIFIER
A SSL-55C WAS USED TO PROVIDE BACKGROUND ILLUMINATION
BACKGROUND OF 120 x 10-9 WATTS
LOW FREQUENCY NOISE
(1/f TYPE BELOW 10 HERTZ)
NO BACKGROUND
NOISE EXPRESSED IN LIGHT EQUIVALENT POWER IN NANOWATTS (10-9)
PEAK TO PEAK NOISE, TWO SIGMA VALUE
0.5
0.4
0.3
0.2
0.1
0.0
0°F
70°F
140°F

ABSOLUTE TRANSMISSION

LED	ROLL FILTER		YAW FILTER		PITCH FILTER	
	Component Test	Design Estimate	Component Test	Design Estimate	Component Test	Design Estimate
Roll LED	34%	32.8%	3.1%	.3%	.6%	.4%
Yaw LED	2.9%	.3%	35%	37%	1.8%	.4%
Pitch LED	8.8%*	.3%	2%	.3%	50%	24.1%

*Probable error in testing

RELATIVE TRANSMISSION

LED \ DETECTOR # (POLARIZATION)	ROLL FILTER				YAW FILTER				PITCH FILTER			
	SYSTEM TESTS		DESIGN ESTIMATE		SYSTEM TESTS		DESIGN ESTIMATE		SYSTEM TESTS		DESIGN ESTIMATE	
	1 (Horiz.)	2 (Vert.)	1 (Horiz.)	2 (Vert.)	1 (Horiz.)	2 (Vert.)	1 (Horiz.)	2 (Vert.)	1 (Horiz.)	2 (Vert.)	1 (Horiz.)	2 (Vert.)
Roll LED #1	45.8%	54.2%	50%	50%	.02%	.04%	.3%	.3%	.01%	.01%	.4%	.4%
#2	45.9%	54.1%	50%	50%	.03%	.04%	.3%	.3%	.01%	.01%	.4%	.4%
Yaw LED #1	1.2%	.04%	.3%	.3%	2.0%	98.0%	0%	100%	.11%	.01%	.4%	.4%
#2	.04%	1.6%	.3%	.3%	97.7%	2.3%	100%	0%	.01%	.07%	.4%	.4%
Pitch LED #1	.26%	.01%	.3%	.3%	.06%	2.3%	.3%	.3%	98.8%	1.16%	100%	0%
#2	.01%	.30%	.3%	.3%	1.64%	.05%	.3%	.3%	2.8%	97.2%	0%	100%

Figure 8.44 Filter Transmission

From this correction, it would be expected that the roll channel would have the most interference (3 times as much as initial design) and that was the case. Another factor was the difference in central wavelength and peak wavelength for the filters as shown in figure 8.45. Because the peak wavelength is close to the high frequency cutoff side of the filter, more of the higher frequency LED output from the adjacent channel will be transmitted.

The transmission of the filter varies with translation and angle as shown in figure 8.46. The angular effect must be considered in our system since an axial ray in our system will enter the filter at approximately 7.5° which corresponds to approximately 90% of maximum transmission at normal incidence.

The effect of temperature on transmission is shown in figure 8.50.

8.5.5 Wollaston Prism

The Wollaston deflection angles and physical dimensions were found to be slightly out of the specification Chrysler had applied in ordering them from the Karl Lambrecht Corporation. This deviation made the alignment and mounting of the optics difficult but should not have a significant effect on system performance.

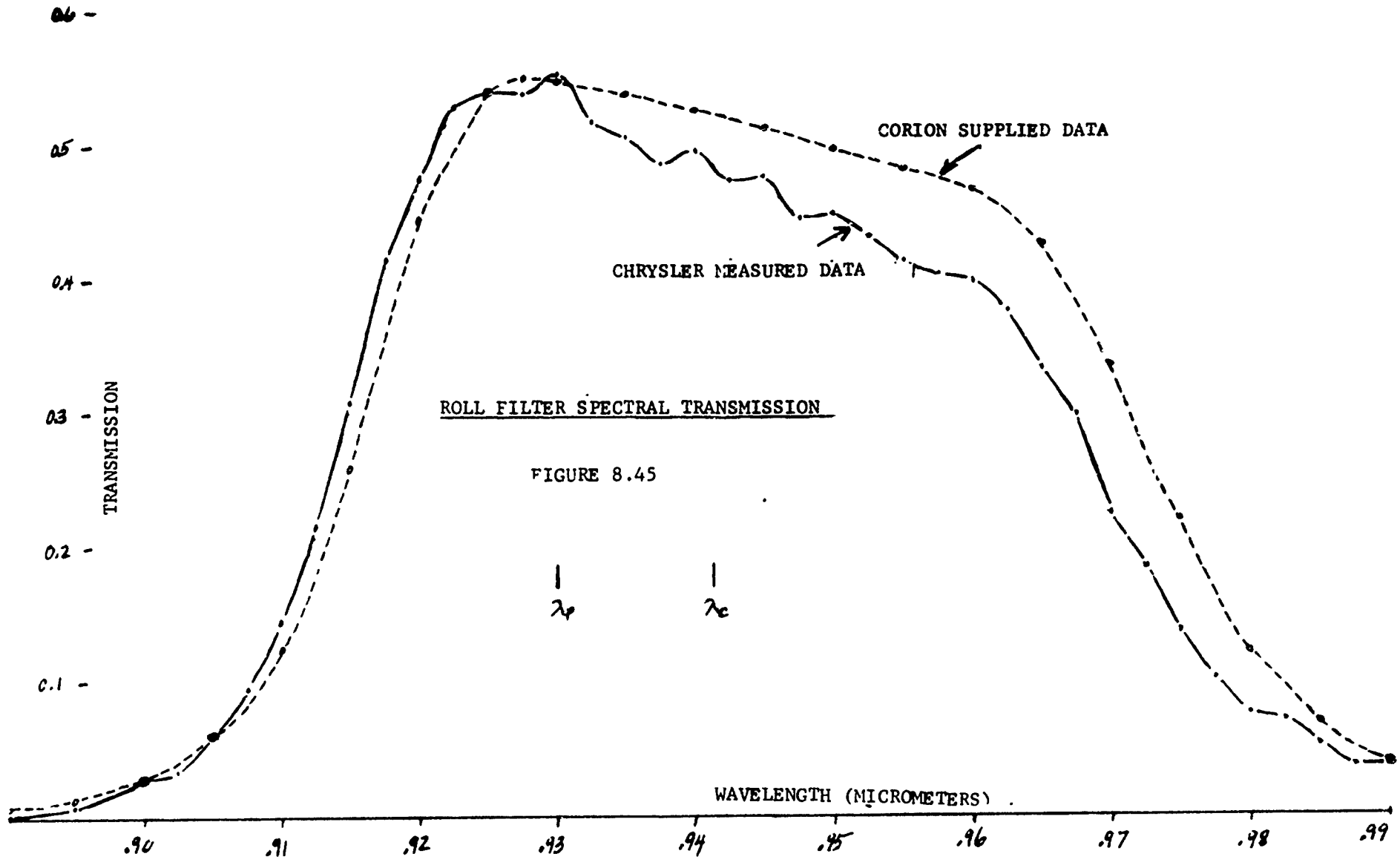

ROLL FILTER SPECTRAL TRANSMISSION

FIGURE 8.45

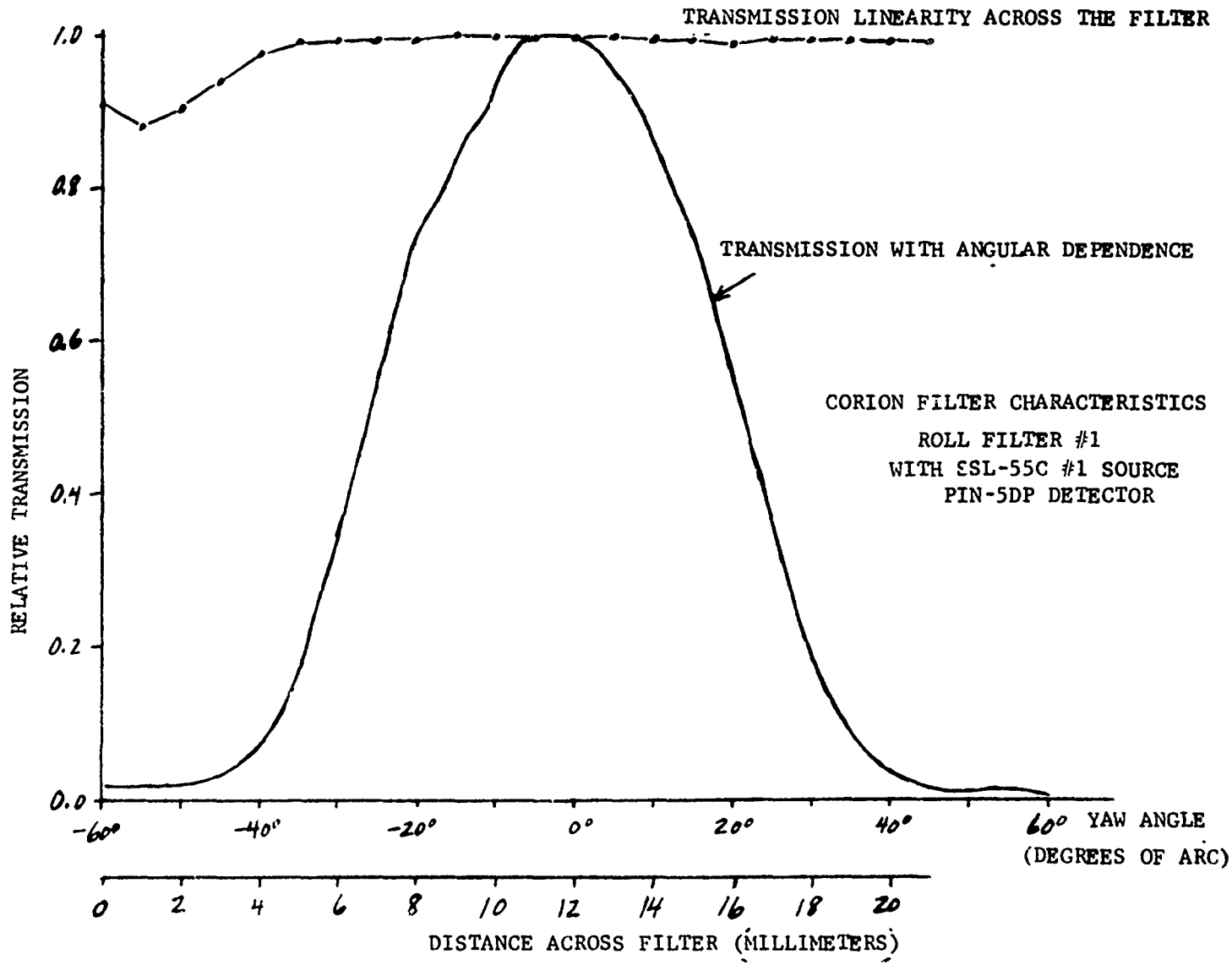
TRANSMISSION LINEARITY ACROSS THE FILTER
TRANSMISSION WITH ANGULAR DEPENDENCE
CORION FILTER CHARACTERISTICS
ROLL FILTER #1
WITH SSL-55C #1 SOURCE
PIN-5DP DETECTOR
RELATIVE TRANSMISSION
1.0
0.8
0.6
0.4
0.2
0.0
-60°
-40°
-20°
0°
20°
40°
60°
YAW ANGLE
(DEGREES OF ARC)
0
2
4
6
8
10
12
14
16
18
20
DISTANCE ACROSS FILTER (MILLIMETERS)

8.6 Subassembly Tests

The objective of the subassembly testing was to determine the temperature dependence of the optics by adding one optical component at a time to the OAMS mechanical assembly between temperature cycles. Figure 8.47 shows the individual and combined effects of the LED and detector temperature dependence. The effect of the other transmitter and receiver components (except the emersion lens and filter) is shown in figure 8.48 and 8.49 respectively. When the effect of the special filter is taken in account (Figure 8.50) the total effect on the OAMS signal amplitude is shown in figure 8.51. This change of about $\pm 30\%$ for $\pm 70^{\circ}F$ temperature change should be within the range of the system A.G.C., although an LED control loop is also expected to be required to keep the LEDs balanced during the large change in output power with temperature. There was no degradation in appearance or performance of any of the optical components or mounts during these tests. The immersion lens was not incorporated into these tests.

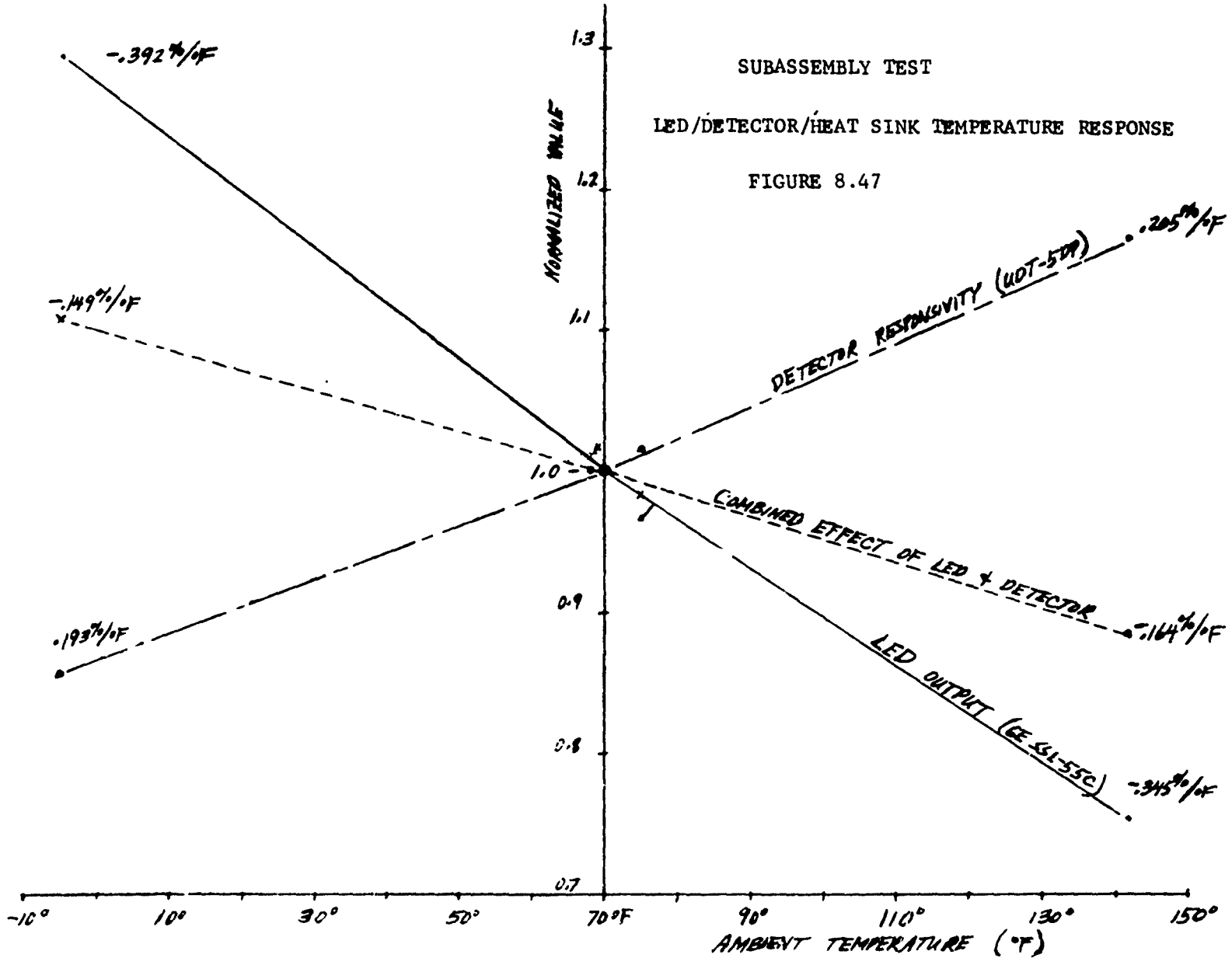

LED/DETECTOR TEMPERATURE RESPONSE

FIGURE 8.48

SUBASSEMBLY TEST

EFFECT OF TRANSMITTER COMPONENTS OTHER THAN LED

ON TRANSMITTER OUTPUT

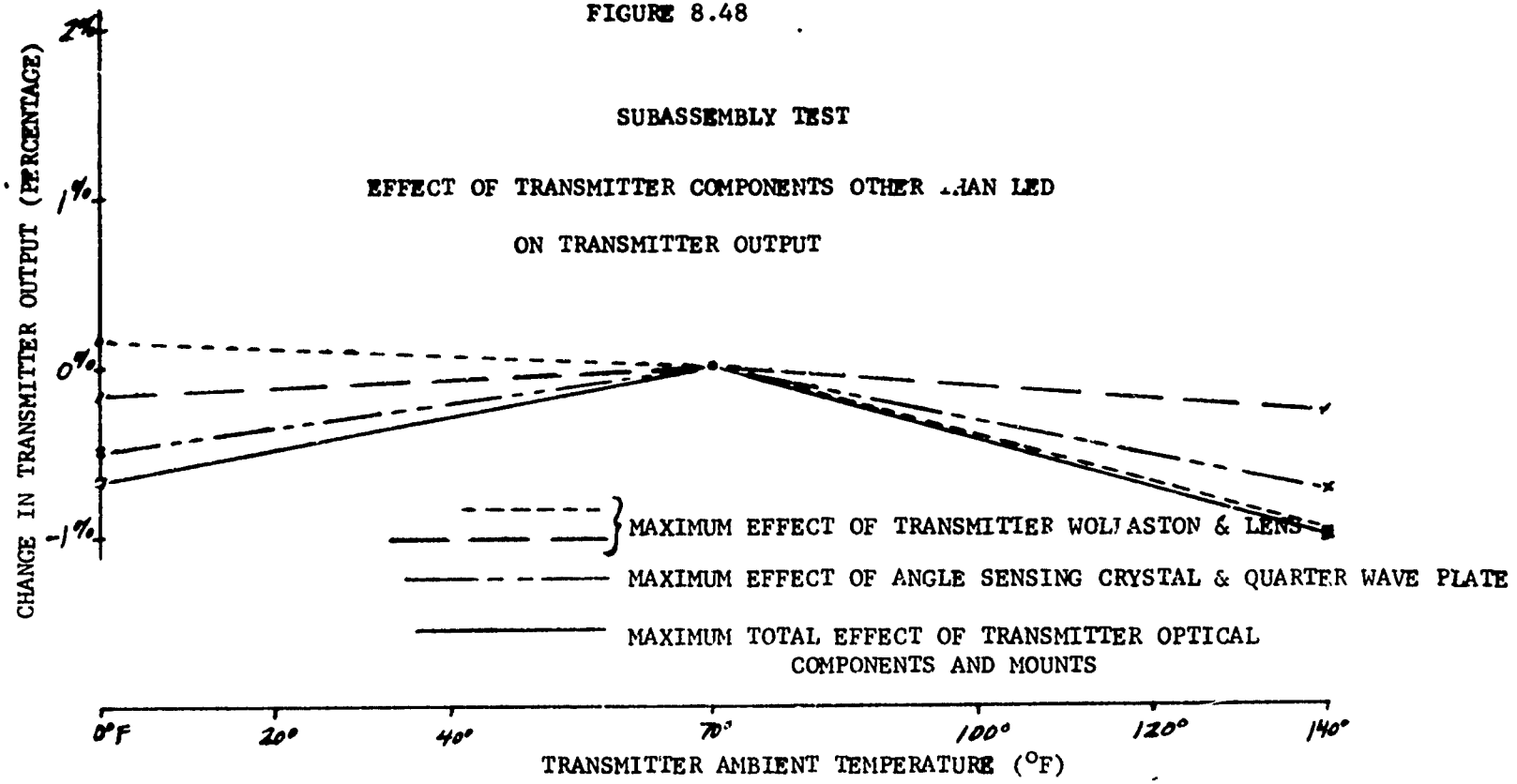

FIGURE 8.49

SUBASSEMBLY TEST

EFFECT OF RECEIVER COMPONENTS

OTHER THAN DETECTOR (AND FILTER)

ON RECEIVER OUTPUT

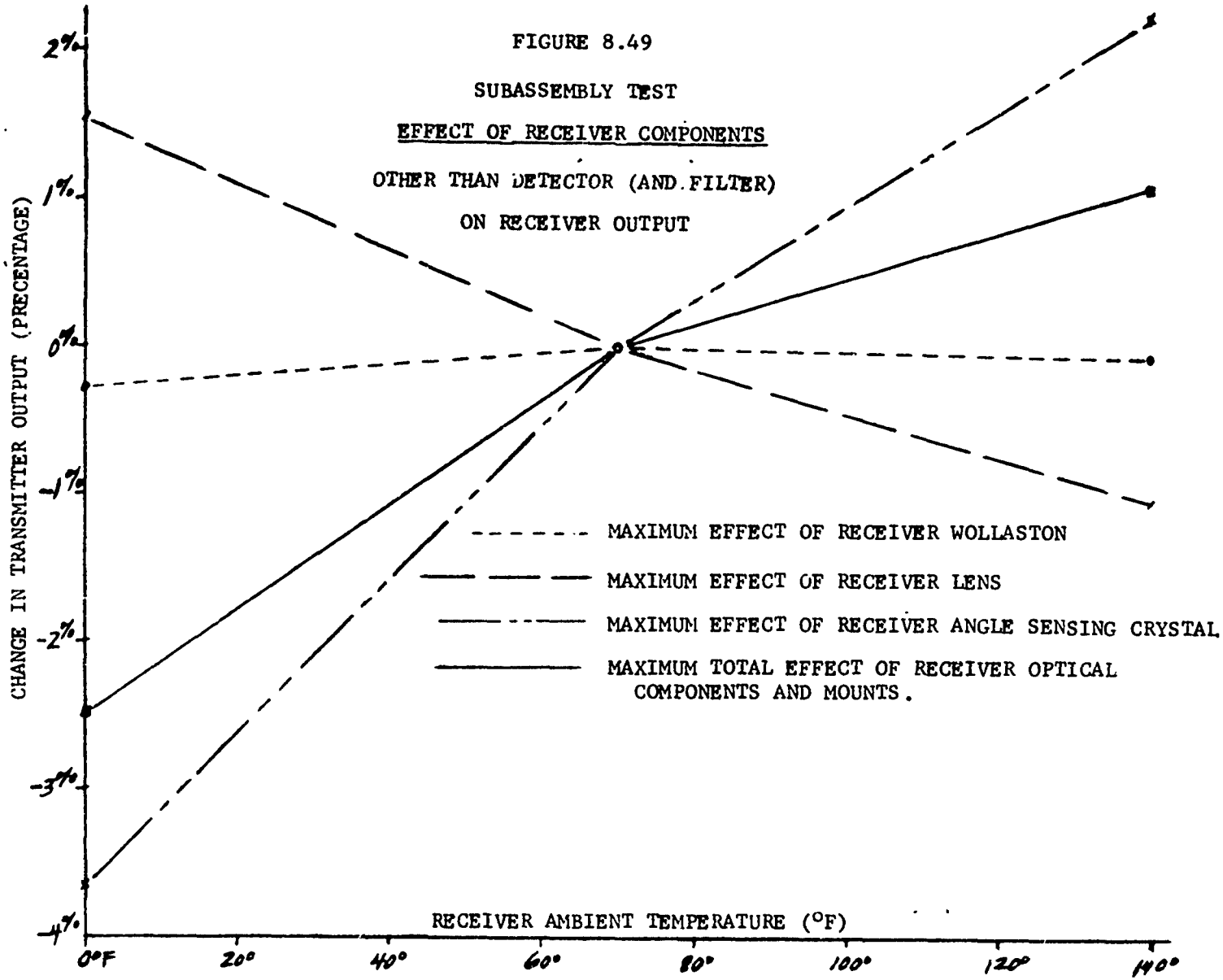

FIGURE 8.50

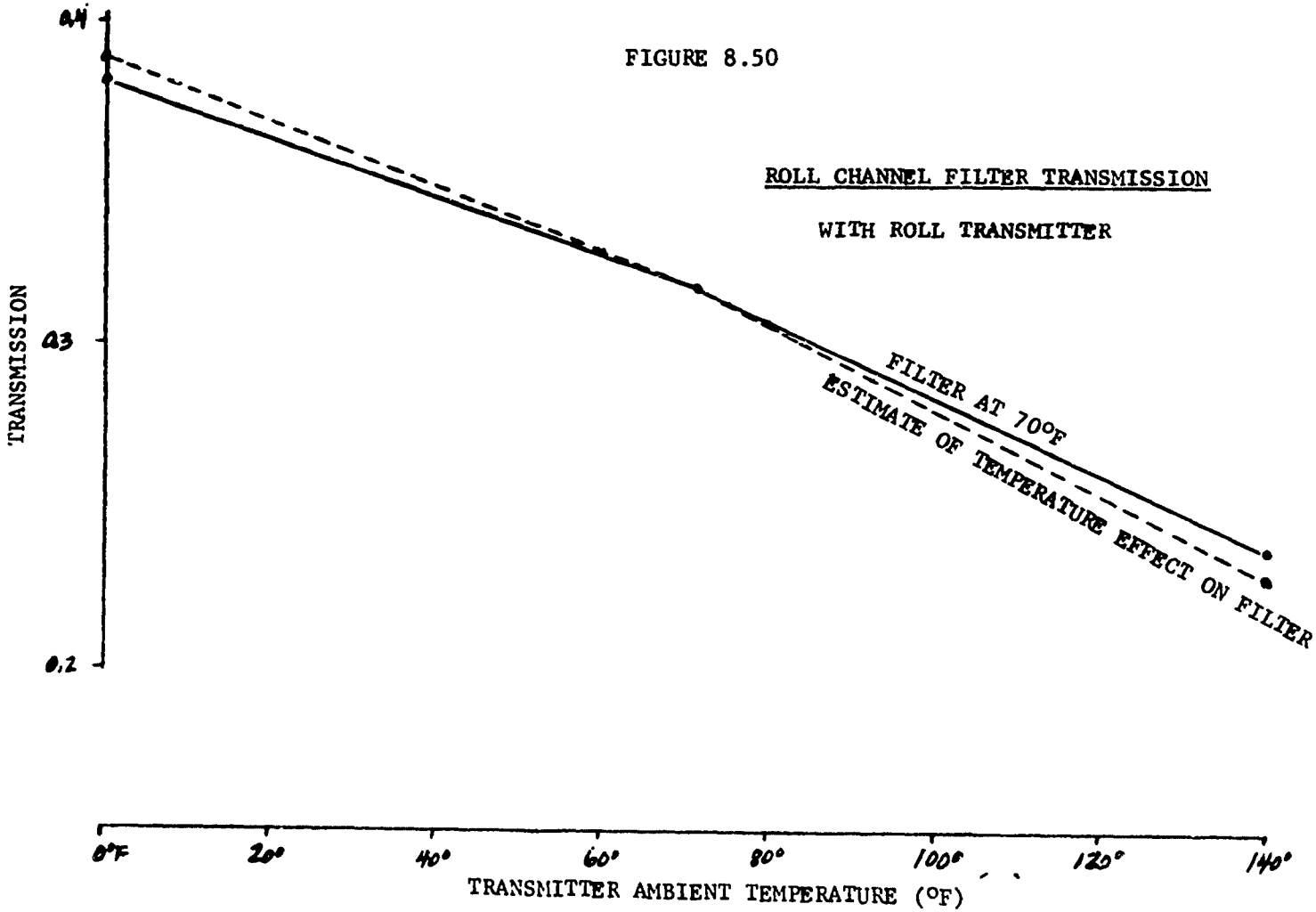
ROLL CHANNEL FILTER TRANSMISSION
WITH ROLL TRANSMITTER
TRANSMISSION
0.4
0.3
0.2
FILTER AT 70°F
ESTIMATE OF TEMPERATURE EFFECT ON FILTER
0°F
20°
40°
60°
80°
100°
120°
140°
TRANSMITTER AMBIENT TEMPERATURE (°F)

FIGURE 8.51

TEMPERATURE EFFECT ON OAMS SIGNAL AMPLITUDE

STATIC CONDITION WITH CONSTANT LED DRIVE CURRENT

ROLL CHANNEL SUBSYSTEM

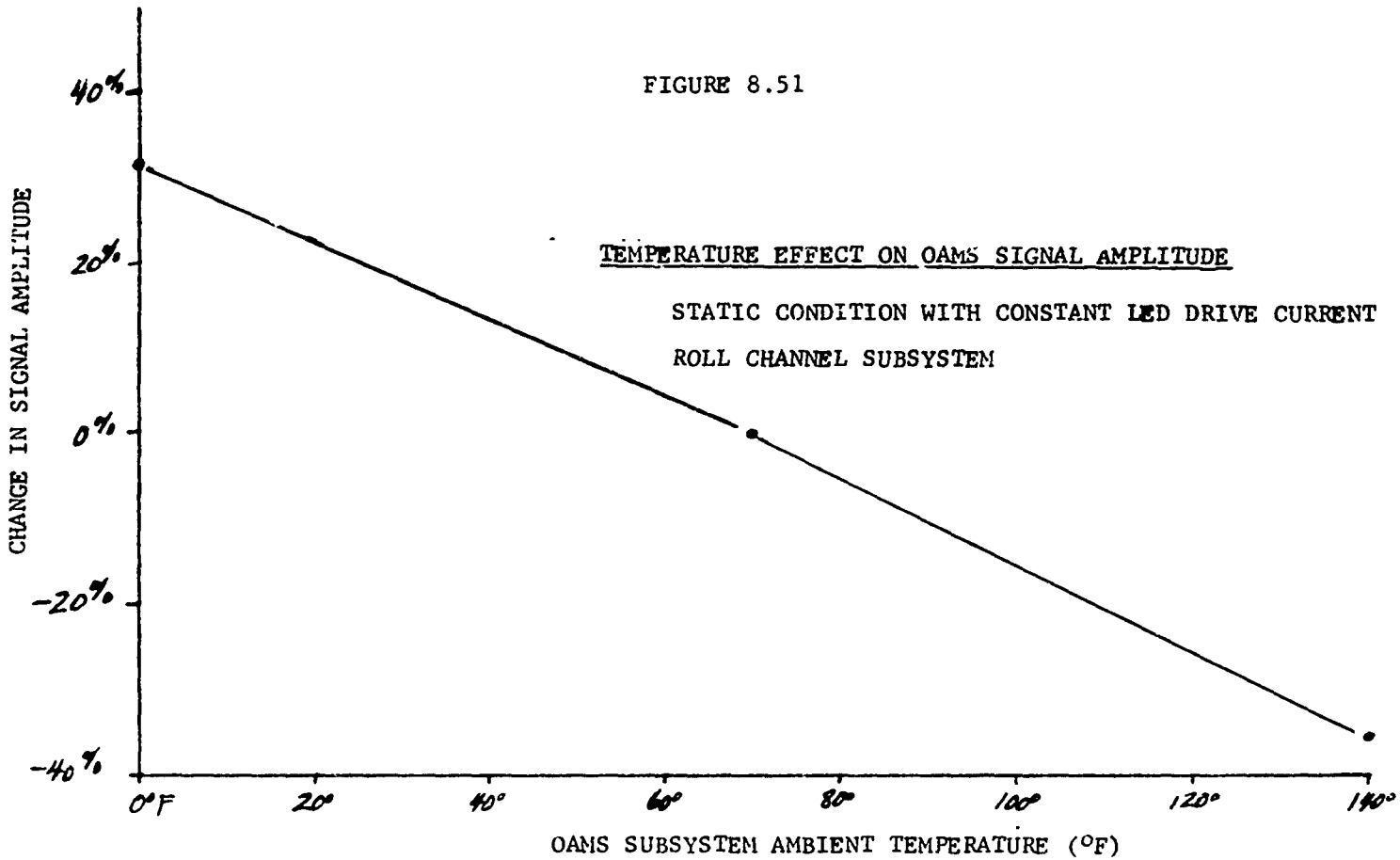

9.0 SYSTEM TEST AND EVALUATION

9.1 General

Tests were performed to determine system accuracy and stability and operating characteristics in evaluating the ability of the system to measure three axes angular motion between transmitter and receiver. The test program followed the General Test Plan TP73-6-TP revised 15 March 1974 except as noted below in the discussion of the tests.

The lifetime problem of the LEDs in the pitch and yaw channel, noted previously, limited the tests requiring long operating time such as the stability testing and light level control calibration. Temperature was maintained at 74°F ±4°F. Barometric pressure was controlled within 28.5 ± 4.5 inches of mercury. Relative humidity remained between 20 to 80 percent. Air turbulence and the fluorescent room lighting were not found to be an important factor on system performance. The tests are discussed in the categories shown in the Test Summary, Table 9.1.

All tests were conducted at a range of 25 feet, except where noted.

9.2 Stability and Warmup Tests

9.2.1 Stability

The stability was determined over a period of 3 hours. System instability is defined here as the total change in system output while the angles between transmitter and receiver are held constant and is shown in Table 9.2. The test was conducted for 1 hour at 0°, 0°, 0° input for pitch, yaw and roll angle respectively and 2 hours at .5°, .5°, .5° input angles. An instability related to a bad solder connection was isolated and corrected. No other instabilities were seen during the test program except at 0°F in the temperature tests described later. The time for stability tests had originally been scheduled for 40 hours but this was limited by the LED lifetime.

This test and the following test program indicate that the system has good short term stability. Long term stability was not determined but a high degree of stability would not be expected for this system since the LED control loop was not implemented to keep the LEDs balanced during their output degradation with time. It is estimated that the output of the LEDs in pitch and yaw dropped over 50% during the test program alone. The long term system stability will be affected by this accelerated aging process when uncompensated.

9.2.2 Warmup

The system warmup and recovery time was determined under a variety of conditions. The best and worst case warmup time is shown in Table 9.2

TEST	STATUS	COMMENTS
Stability and Warmup	Completed	Testing time shortened because of LED lifetime problem
System Calibration	Completed	Derived calibration curves
Accuracy Tests - Crosscoupling	Completed	
Extreme Range	Completed	
Light Level Control	Completed	Reduced evaluation test due LED lifetime problem
Translation	Completed	Full lateral range for goal. Line of sight movement was limited to ± 3 inches by test setup. Meets requirement (±1) but not goal (±5 inches)
Response Time	Completed	Step Angle simulated. Unable to rotate wedge at 10 Hz
Background Radiation	Completed	
Input Power	Partially Completed	Transients, ripple and reverse polarity power tests not performed.
General System Characteristics	Completed	
Temperature Tests	Completed	Test indicates need for LED control loop.
Test Summary	Completed	

Table 9.1. OAMS System Test and Evaluation Outline

STABILITY over a 3-hour period

	Pitch	Yaw	Roll
Total change in system output	4 m volt	4 m volt	20 m volt

The only observed instability was corrected by resoldering a connection on the detector preamp offset. No other instability was seen in 75 hours of system tests.

WARMUP and recovery time required for system to return to within 5 arc seconds of nominal value

	Pitch	Yaw	Roll
System warmup (worst case)	100 sec	10 sec	40 sec
System warmup (best case)	5 sec	2 sec	20 sec
LED warmup, system on (worst case conditions)	15 sec	2 sec	40 sec
Recovery from blocked beam	1 sec	1 sec	4 sec

Data averaged over 32 turn on events.

Table 9.2. Stability and Warmup

for each channel. The time was longer for stability at large angles. The warmup time is defined here as the time which the system takes to return to within 5 arc seconds of the nominal output after system power is applied.

Figure 9.1 shows the approximate variation in warm up time with the time the system has been off prior to test. Part of the warm up time is caused by differences in output of the pairs of LEDs until they reach thermal equilibrium where they were balanced. This is particularly important in roll as seen in Table 9.2. Warmup should not be a problem when an LED control loop is employed or where the system is left running all the time. This factor will have to be carefully considered in a system incorporating time sharing to eliminate interference between channels.

Also shown in Table 9.2 is the system recovery time after the beam has been blocked. The roll response reflects the output filter employed in that channel to improve signal to noise characteristics for testing purposes.

9.2.3 Interference Between Channels

The interference effect of the three channels on each other was determined by turning on the channels separately and in different combinations. The results are tabulated in Table 9.3. Data was taken of this effect with all angles set at 0 degrees and again at $.5^{o}$. Only the latter is shown in the figure since the effects on the sum signals were similar. As expected, the pitch channel (λ_c = 800 nm) has the most effect on the yaw channel (λ_c = 860 nm) and yaw has the most effect on the roll channel (λ_c = 950 nm). The reason is that the LED output trails off to longer wavelengths but cuts off sharply at the shorter wavelengths (pitch is least affected).

Because of the decrease in pitch and yaw LED outputs relative to the roll LEDs, the change in roll shown in the figure is only about half that expected with equal beam power in all channels.

The change observed in system output is a relatively constant effect. The change due to interference will change proportionally to the effect on the sum signal of that channel. For example, a 20% change in the effect of yaw on the roll channel will only change the output by 4 arc seconds at the nominal angle of .5 degrees. The AGC scale factor adjustment will be made with all channels operating in order to take this interference into account.

9.3 Calibration

9.3.1 General

The light level control calibration originally planned was reduced to a verification of the range switch function at a fixed range of 25 feet and a test of the AGC function by placing attenuators in the path of the LED beam. This is reported in section 9.4.3.

Angular sensitivity calibration of the system was performed in order to relate the system output voltages to the angular relation of a given coordinate system. This is discussed in more detail in section 9.10.

In order to test the system, an independent measuring system using turn tilt tables, mirrors and autocollimators is required. This means

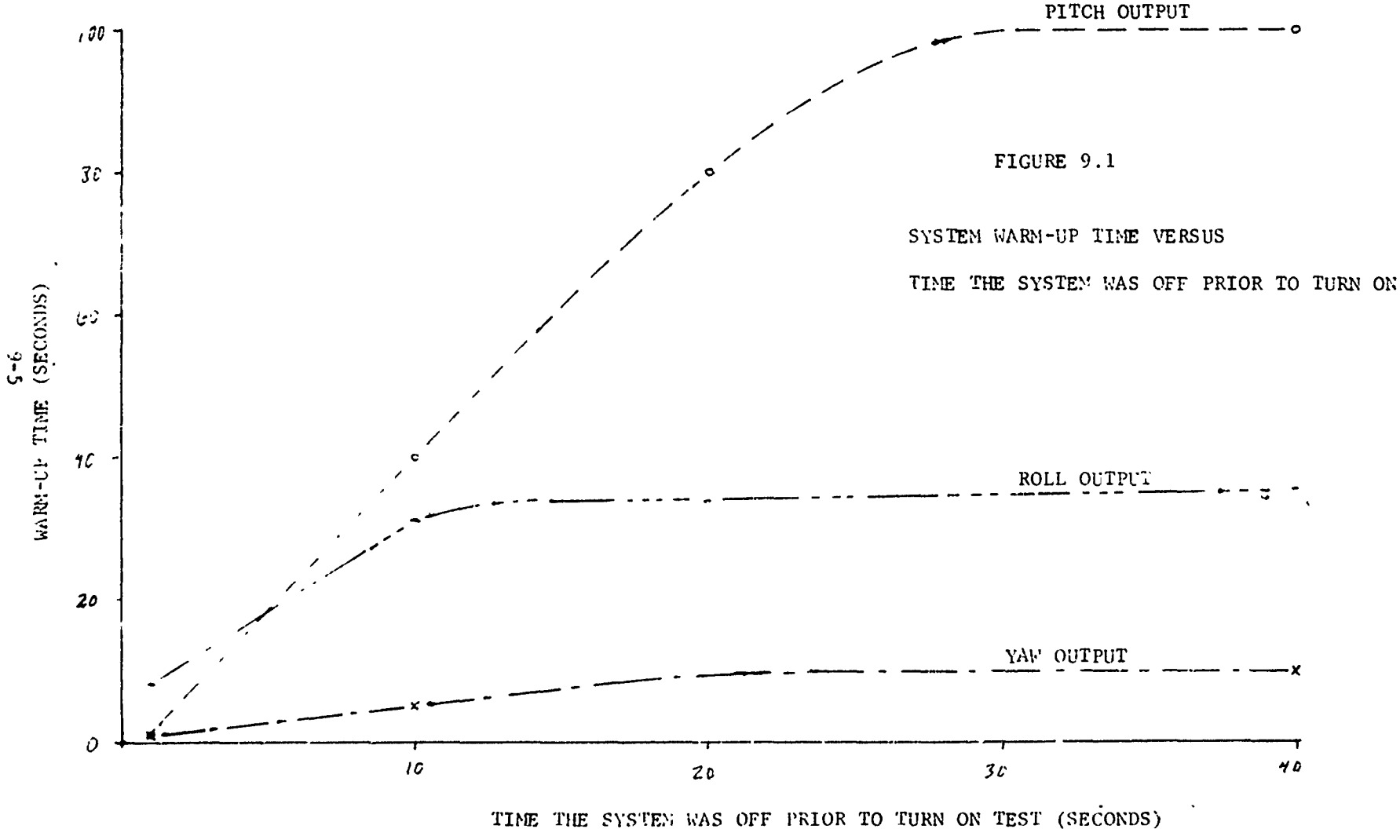

FIGURE 9.1

SYSTEM WARM-UP TIME VERSUS

TIME THE SYSTEM WAS OFF PRIOR TO TURN ON

Nominal Angle: Pitch = Yaw = Roll = 1800 arc seconds

CHANNELS ON	CHANGE IN ROLL OUTPUT(1)	PERCENT CHANGE(2) IN ROLL SUM
Roll On	-	-
Roll + Pitch On	10 MV	.204%
Roll + Yaw On	20 MV	1.020%
All Channels On	25 MV	1.224%
	CHANGE IN YAW OUTPUT(1)	PERCENT CHANGE(2) IN YAW SUM
Yaw On	-	-
Yaw + Roll On	15 MV	0.100%
Yaw + Pitch On	38 MV	2.233%
All Channels On	55 MV	2..33%
	CHANGE IN PITCH OUTPUT(1)	PERCENT CHANGE(2) IN PITCH SUM
Pitch On	-	-
Pitch + Yaw	3 MV	0.340%
Pitch + Roll	3 MV	0.780%
All Channels On	6 MV	0.975%

Table 9.3 Interference Between Channels

It should be noted that this acts as a relatively constant bias on the AGC and has only small effect on system output.

NOTE (1): These measurements are cross channel light leakage through their respective optical filters.

NOTE (2): Since all three channels operate together, the total light or sum, which controls the AGC must be considered in the calibration of each scale factor adjustment.

that another transformation is necessary and errors are developed in the monitoring system. The system output is related to the input angles (i_1, i_2 and i_3) by a simple angular coordinate transformation based on constraints within the two coordinate systems. The optic and electronic nonlinearities and misadjustments will be displayed when the output data is plotted and compared to predictions. These functions are determined theoretically and through test results. The relation between the desired angle and the system output voltage is the method of calibration of the system.

The relation is given in Table 9.4 along with the transformations (calibration curves) derived for the OAMS brassboard. This set of transformation equations will include all effects including the cross coupling in the coordinate transformation, optic and electronic nonlinearities and misadjustment, cross channel interference and any other effects except sensitivity to temperature and background radiation.

The data taken for calibration purposes havebeen plotted in Figures 9.2,9.3 and 9.4 together with the deviation from the associated transformation (calibration) equation. An indication of the predictability of the system is given in Table 9.5 which shows the deviation of the data from the calibration curve and the standard deviation for the set of data for each channel.

9.4 Accuracy Tests

9.4.1 Cross Coupling Accuracy

In order to evaluate system accuracy, 333 points were selected out of the three dimensional coordinate space defined by pitch, yaw and roll. The selection of these points and the deviation of the system output at these points compared to the calibration curves is given in Table 9.6. These are the results which determine the accuracy of the OAMS to measure angles and combines the effect of systematic and dynamic errors. For evaluation, the data for angles less than or equal to $\pm 1/2^{o}$ are treated separately from data for angles greater than $1/2^{o}$.

9.4.2 Extended Angular Range

The maximum useable range and the decrease in accuracy beyond the goal range of $\pm 1^{o}$ was determined out of $\pm 2^{o}$ in pitch and yaw and out to $\pm 3^{o}$ in roll. The data is shown in Figures 9.5, 9.6 and 9.7 together with the associated transformation equation. The change in the other channel outputs is also shown in these figures. Data was taken with the angles nominally set at 0^{o} and also at $1/2^{o}$. Only the nominal data at 0^{o} is shown because the data was similar out to 1.5^{o}. The change in all the DC sum signals with pitch shown in Figure 9.8 was typical of the effect in all channels.

9.4.3 Light Level Control

The range selection control evaluation was limited to changing the range switch to other positions while the system remained at the range of 25 feet. This verified that the range control resistors selected by calculation were approximately correct and maintained the scale factor at 1 mv/arc second $\pm 10\%$ for adjacent ranges. The extreme ranges could not be tested when the signals were either too low or saturated at the fixed range. The scale factor in the brassboard system will change with range. The selection of these resistors would normally be a calibration procedure performed at different values of range in order to keep a close tolerance on the scale factor.

	PITCH	YAW	ROLL
INPUT ANGLES IN TEST	i_1	i_2	i_3 (arc seconds)
SYSTEM OUTPUT VOLTAGE	V_1	V_2	V_3 (millivolts)

SYSTEM TRANSFER EQUATIONS (Calibration Curve)

$$V_1 = f_1(i_1) + g_1(i_2) + h_1(i_3) + R_1(i_2\, i_3)$$

$$V_2 = f_2(i_2) + g_2(i_1) + h_2(i_3) + R_2(i_1\, i_3)$$

$$V_3 = \underbrace{f_3(i_3)}_{\text{1st Order}} + \underbrace{g_3(i_1) + h_3(i_2) + R_3(i_1\, i_2)}_{\text{Caused by Crosscoupling, Nonlinearities, Misadjustment and Interference}}$$

f, g, h & k are functions determined through calibration procedure

BASIC COORDINATE TRANSFORMATION EXPECTED

$$V_1 = i_1 + i_2\, i_3$$

$$V_2 = -i_2 + i_1\, i_3$$

$$V_3 = -i_3 + \tfrac{1}{2}\, i_1\, i_2$$

Derived in paragraph 9.10 for present test setup

OAMS BRASSBOARD CALIBRATION CURVES

$$V_1 = (3397 + 5.7 \times 10^{-6} i_2^2) \sin(.01833\, i_1) - 1.5 \times 10^{-5} i_1^2 + 1.9 \times 10^{-6} i_2^2$$

$$V_2 = (3450 + 3.6 \times 10^{-6} i_1^2) \sin(.01705\, i_2) + 3.3 \times 10^{-3}\, i_1$$

$$V_3 = \left\{.991 + 1.5 \times 10^{-9} \left[(i_1 - 900)^2 + (i_2 + 900)^2\right]\right\} i_3 + 0.029\, i_1 - 2.3 \times 10^{-6}\, i_1^2$$

Table 9.4. Transformation Equations

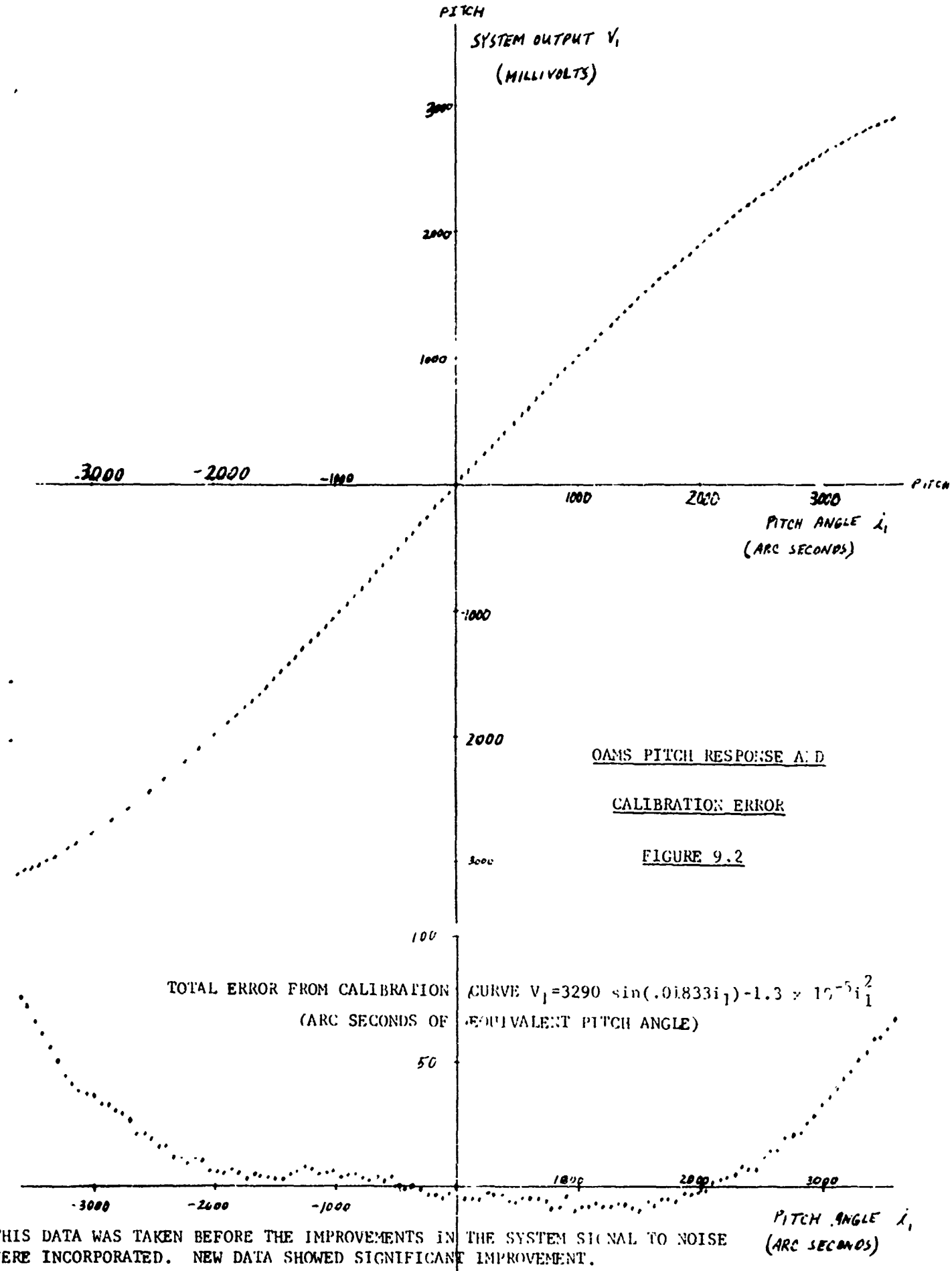

OAMS PITCH RESPONSE AND

CALIBRATION ERROR

FIGURE 9.2

THIS DATA WAS TAKEN BEFORE THE IMPROVEMENTS IN THE SYSTEM SIGNAL TO NOISE WERE INCORPORATED. NEW DATA SHOWED SIGNIFICANT IMPROVEMENT.

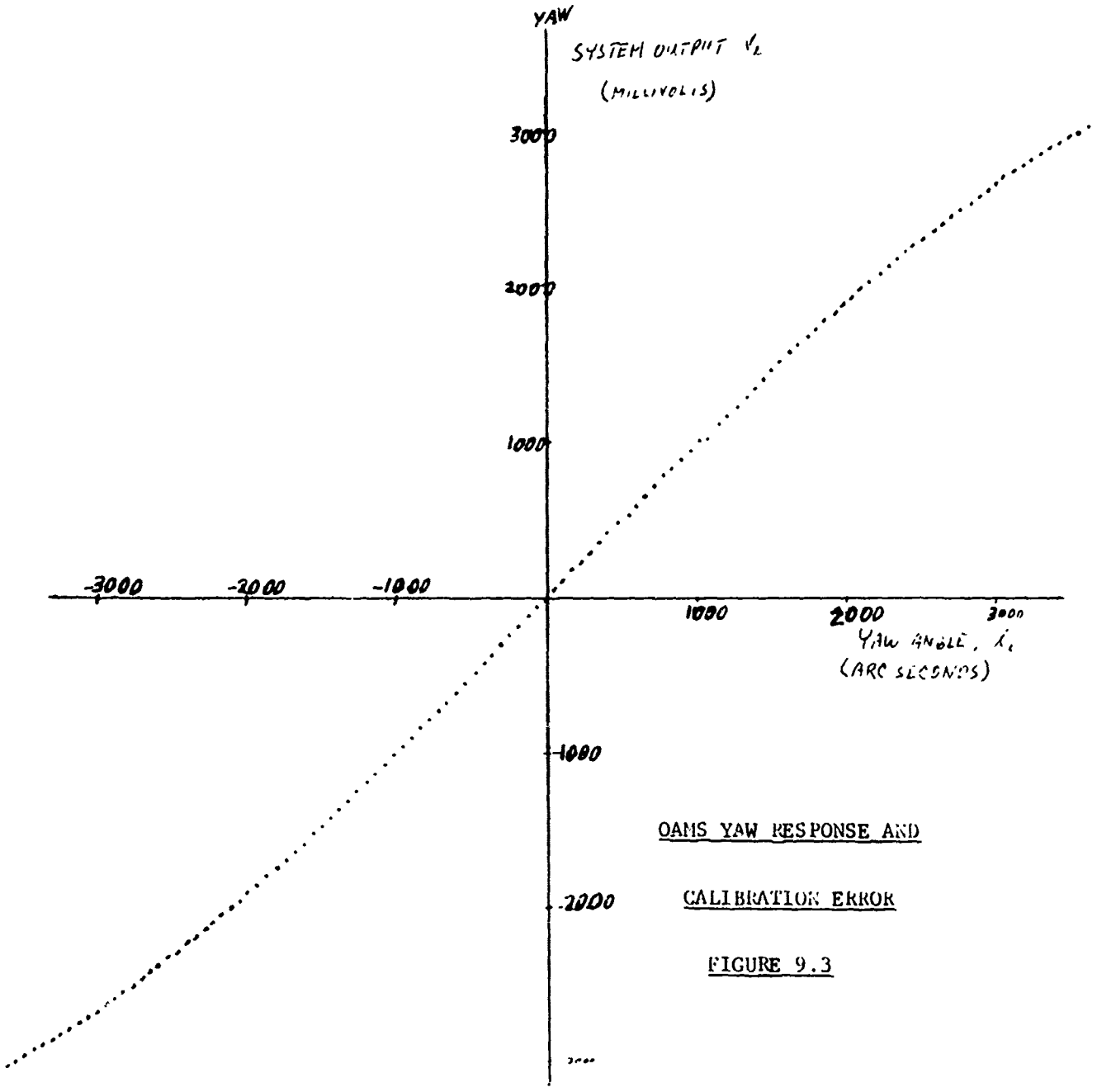

OAMS YAW RESPONSE AND

CALIBRATION ERROR

FIGURE 9.3

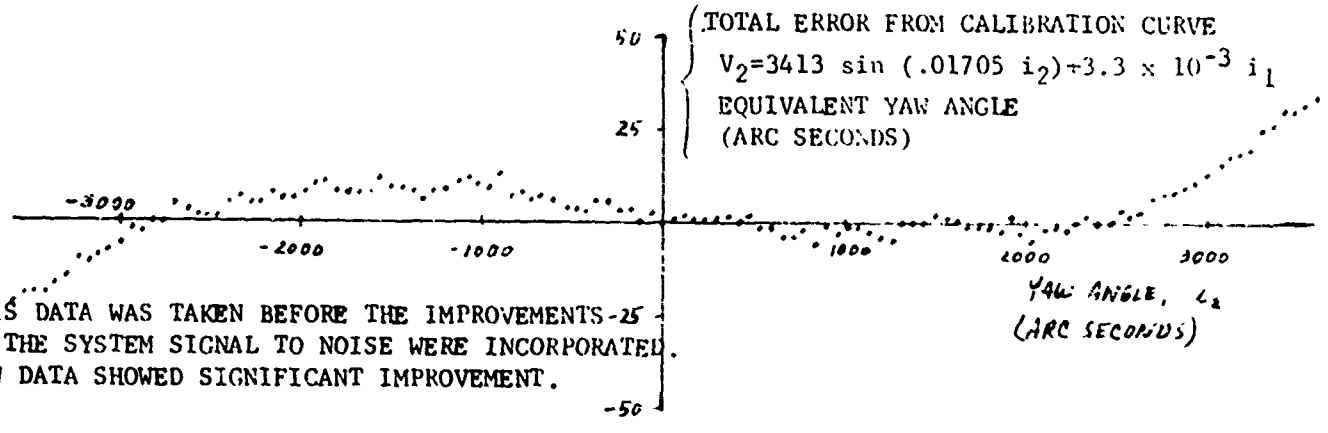

TOTAL ERROR FROM CALIBRATION CURVE

$V_2 = 3413 \sin(.01705\, i_2) + 3.3 \times 10^{-3}\, i_1$

EQUIVALENT YAW ANGLE
(ARC SECONDS)

THIS DATA WAS TAKEN BEFORE THE IMPROVEMENTS IN THE SYSTEM SIGNAL TO NOISE WERE INCORPORATED. NEW DATA SHOWED SIGNIFICANT IMPROVEMENT.

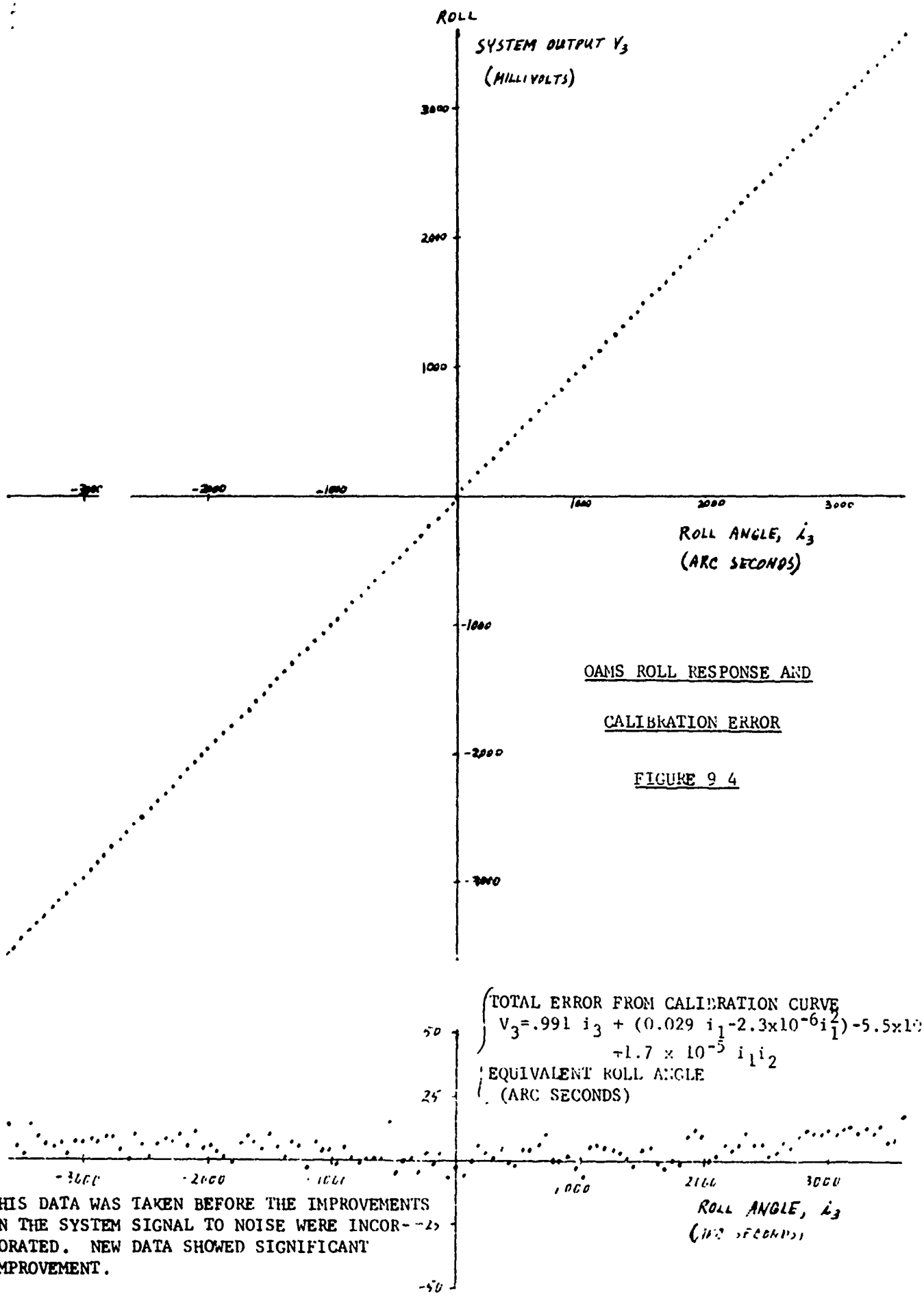

OAMS ROLL RESPONSE AND

CALIBRATION ERROR

FIGURE 9 4

THIS DATA WAS TAKEN BEFORE THE IMPROVEMENTS IN THE SYSTEM SIGNAL TO NOISE WERE INCORPORATED. NEW DATA SHOWED SIGNIFICANT IMPROVEMENT.

(SEE NOTE 4)	PITCH	YAW	ROLL
TOTAL ERROR (See Note 1)			
±1800 Second Range	5.6 sec.	5.7 sec.	4.7 sec.
±3600 Second Range	24 sec.	13.5 sec.	8.2 sec.
ESTIMATED DYNAMIC ERROR			
(See Note 2)	1.7 sec.	1.6 sec.	4.7 sec.
(See Note 3)	.8 sec.	1.5 sec.	6 sec.

NOTE 1: Standard Deviation of data from calibration curves without crosscoupling.

This error includes optic and electronic nonlinearities and misadjustments, short term instability, cross channel interference, noise and all testing errors including voltage and angle measurement.

NOTE 2: Standard deviation of data from calibration curves where systematic errors are minimum.

NOTE 3: 1σ value based on signal to noise measurements (see paragraph 9.8.2)

NOTE 4: Subsequent improvements have made substantial reduction in the signal to noise ratio of the system since these tests were made.

Table 9.5. Brassboard Calibration Error Without Crosscoupling

STANDARD DEVIATION (± ANGULAR RANGE) Note 1	PITCH	YAW	ROLL
σ(±30 Arc Minutes, All Angles) Note 2	8 sec	3.6 sec	16 sec
σ(±60 Arc Minutes, All Angles) Note 3	-	-	-

Table 9.6. Brassboard Calibration Error with Crosscoupling

Note 1: The pitch scale factor was increased 3% and the yaw scale factor was increased 1% above the values determined in the calibration test performed one week previously.

Note 2: 79 data points were taken in σ(±30'). They were not selected randomly. All extreme positions were included in the sampled positions.

Note 3: 333 total data points were taken for crosscoupling evaluation. The standard deviation σ(±60') was not determined because the calibration curves were derived for the ±30' range.

Note 4: The error shown in this table includes all system and test errors which have not been calibrated:

1. Optic nonlinearity and misadjustment
2. Electronic nonlinearity and misadjustment
3. Short term instability
4. Cross channel interference
5. Noise
6. Coordinate crosscoupling
7. Test errors in voltage and angle measurement
8. Accelerated LED aging, pitch and yaw channel.

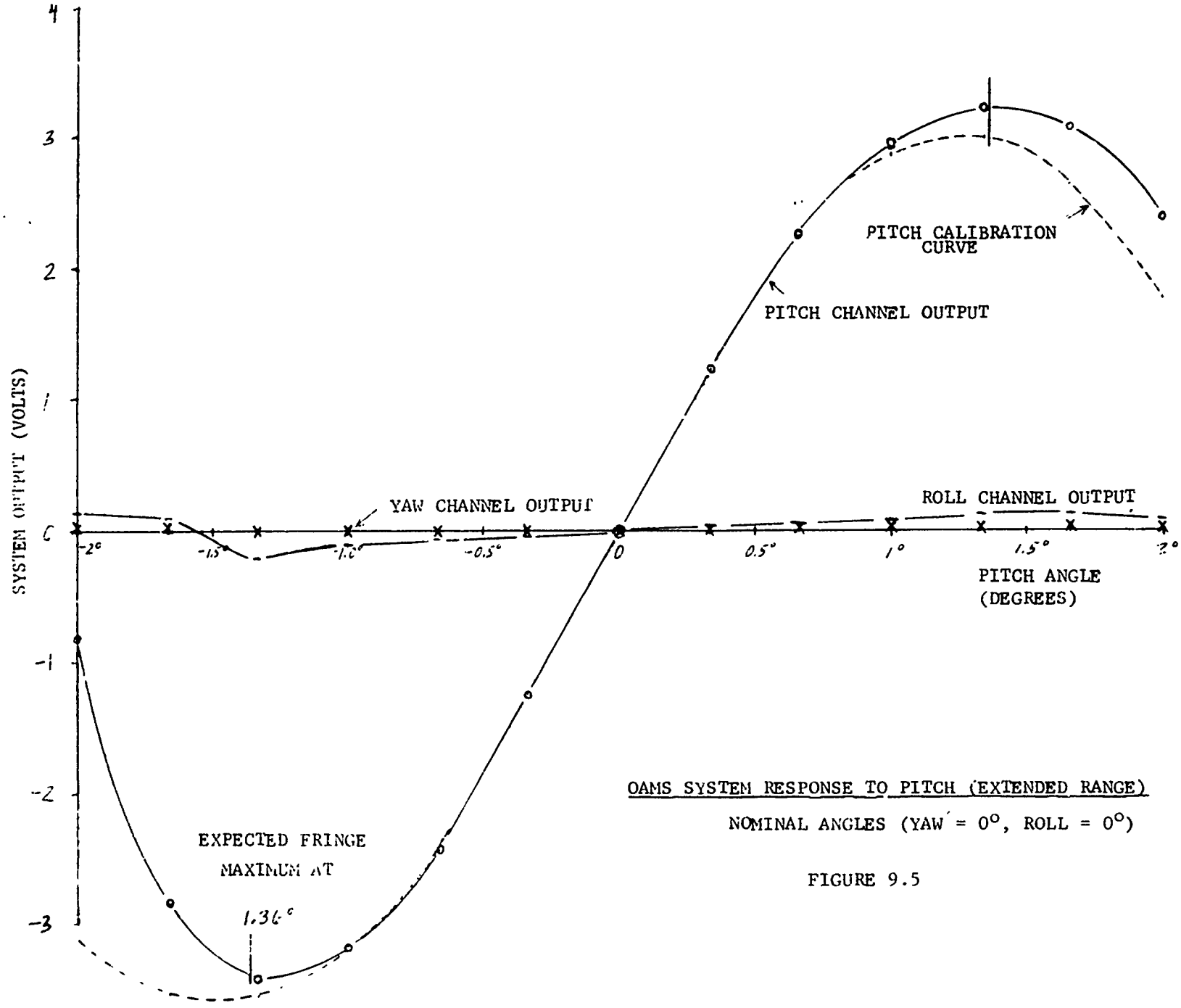

OAMS SYSTEM RESPONSE TO PITCH (EXTENDED RANGE)

NOMINAL ANGLES (YAW = 0°, ROLL = 0°)

FIGURE 9.5

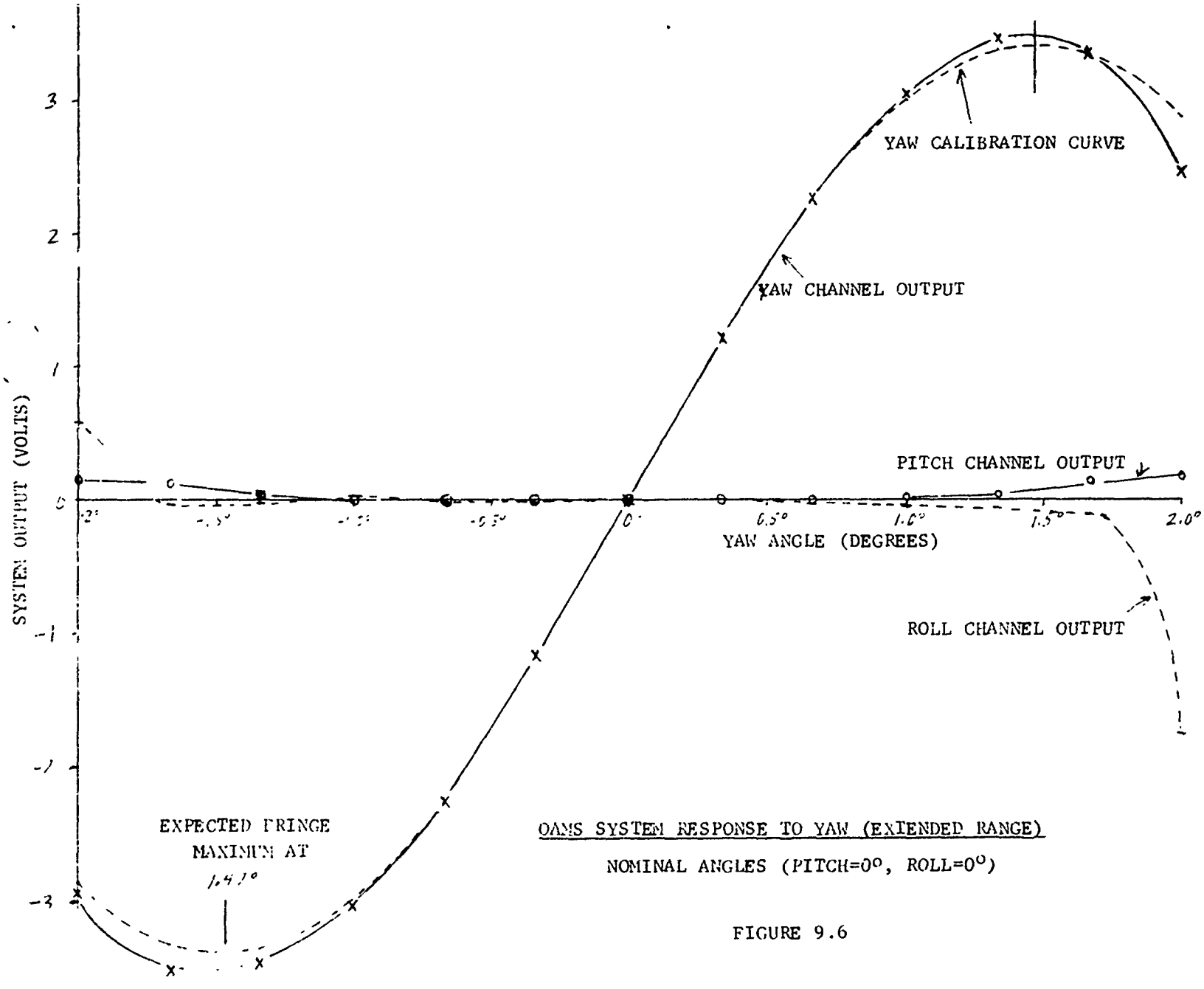

OAMS SYSTEM RESPONSE TO YAW (EXTENDED RANGE)

NOMINAL ANGLES (PITCH=0°, ROLL=0°)

FIGURE 9.6

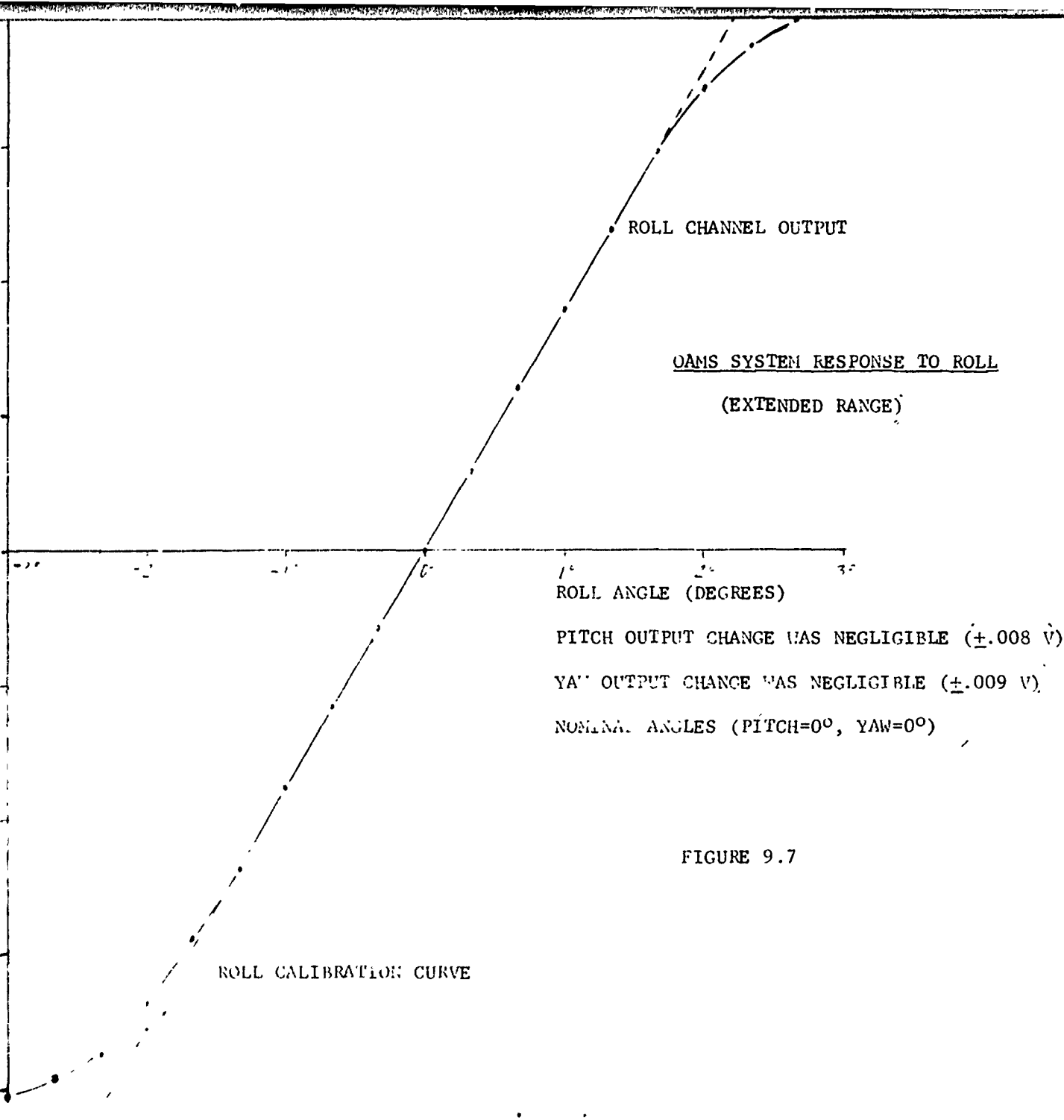

OAMS SYSTEM RESPONSE TO ROLL

(EXTENDED RANGE)

PITCH OUTPUT CHANGE WAS NEGLIGIBLE (±.008 V)

YAW OUTPUT CHANGE WAS NEGLIGIBLE (±.009 V)

NOMINAL ANGLES (PITCH=0°, YAW=0°)

FIGURE 9.7

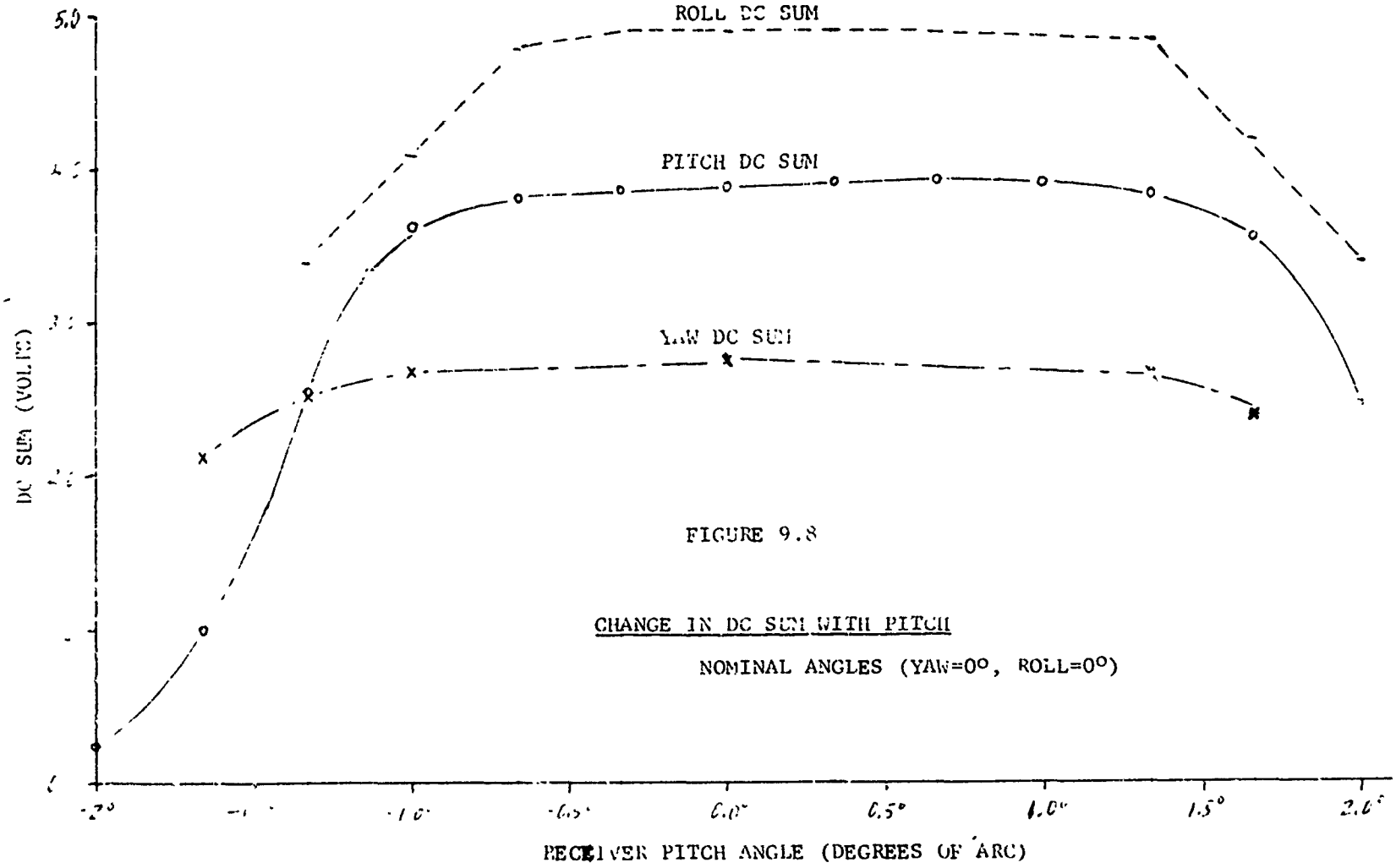

FIGURE 9.8

CHANGE IN DC SUM WITH PITCH

NOMINAL ANGLES (YAW=0°, ROLL=0°)

The AGC was functionally tested placing optical attenuators in the LED beam. Three attenuators were used to provide attenuation to 92%, 87.2% and 34%. The system was tested with a nominal angle at 0^{o} and again with $1/2^{o}$ in all channels. System output changed less than 200 millivolts in all cases, indicating that the AGC was functioning properly. The changes seen were attributed to wedge angles and birefringent effects in the attenuators.

9.4.4 Translation

The accuracy of the system for angle measuring is determined under the condition when the receiver and transmitter are translated relative to each other. It is important that the system be insensitive to this movement since there is no way to correct for it. Translation was performed ± 2.5 inches in the horizontal lateral direction and ± 3 inches in the direction of the system line of sight. Translation was performed to 82 different positions with nominal input angles of 1/2 degree and to 28 positions with nominal input angles of 0 degrees.

Typical deviations with translation are shown in Figures 9.9 and 9.10. The results of the test are summarized in Table 9.7.

9.5 Response Time

As discussed in the General Test Plan, the system response test was performed in two different ways.

9.5.1 Method 1

In this method the system remains at a constant angle (nominally $1/2^{o}$) while the AC modulation signal to the LEDs is interrupted. When the modulation signal is opened, the LEDs are driven only at their bias level which gives a system output of 0 volts. An angular step is simulated by suddenly applying the modulation to the LEDs. This is not a true system response because the LED drive may experience a delay but the receiver and signal processing electronics cannot tell the difference. Response and settling time is summarized in Table 9.8. Response measured in this way was within the specified 0.045 seconds. The roll channel response time was increased to reduce noise for testing and is not within the specified value.

9.5.2 Method 2

A counter-rotating wedge of 15 arc minutes total deflection was used to measure response in the lateral channels. This wedge can be set to vary only one channel at a time but was so massive that it could not be driven faster than 3 revolutions/second which was inadequate to test the required 10 Hz systems response. The data obtained is presented in Table 9.8.

9.6 Background Radiance

In order to uniformly fill the system field of view to determine response to background radiance , a sheet of white paper with three holes for the transmitter beam was placed in the optical path. The paper was irradiated by 2 tungsten bulbs at 500 watts power consumption and with a color temperature of 3200^{o}K. The system response to this background is shown as a function of the irradiance at the receiver from the background in Figures 9.11 and 9.12.

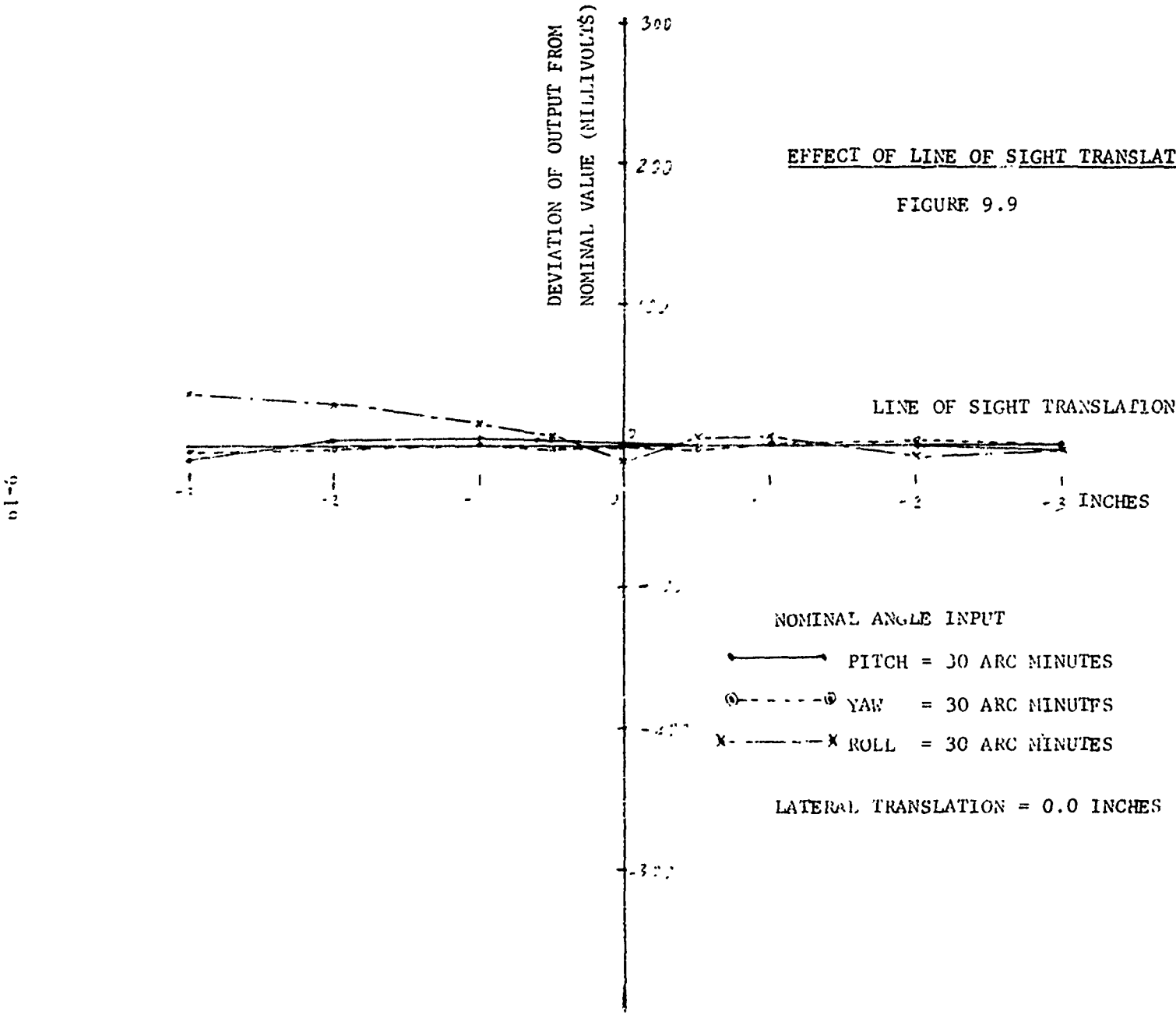

EFFECT OF LINE OF SIGHT TRANSLATION

FIGURE 9.9

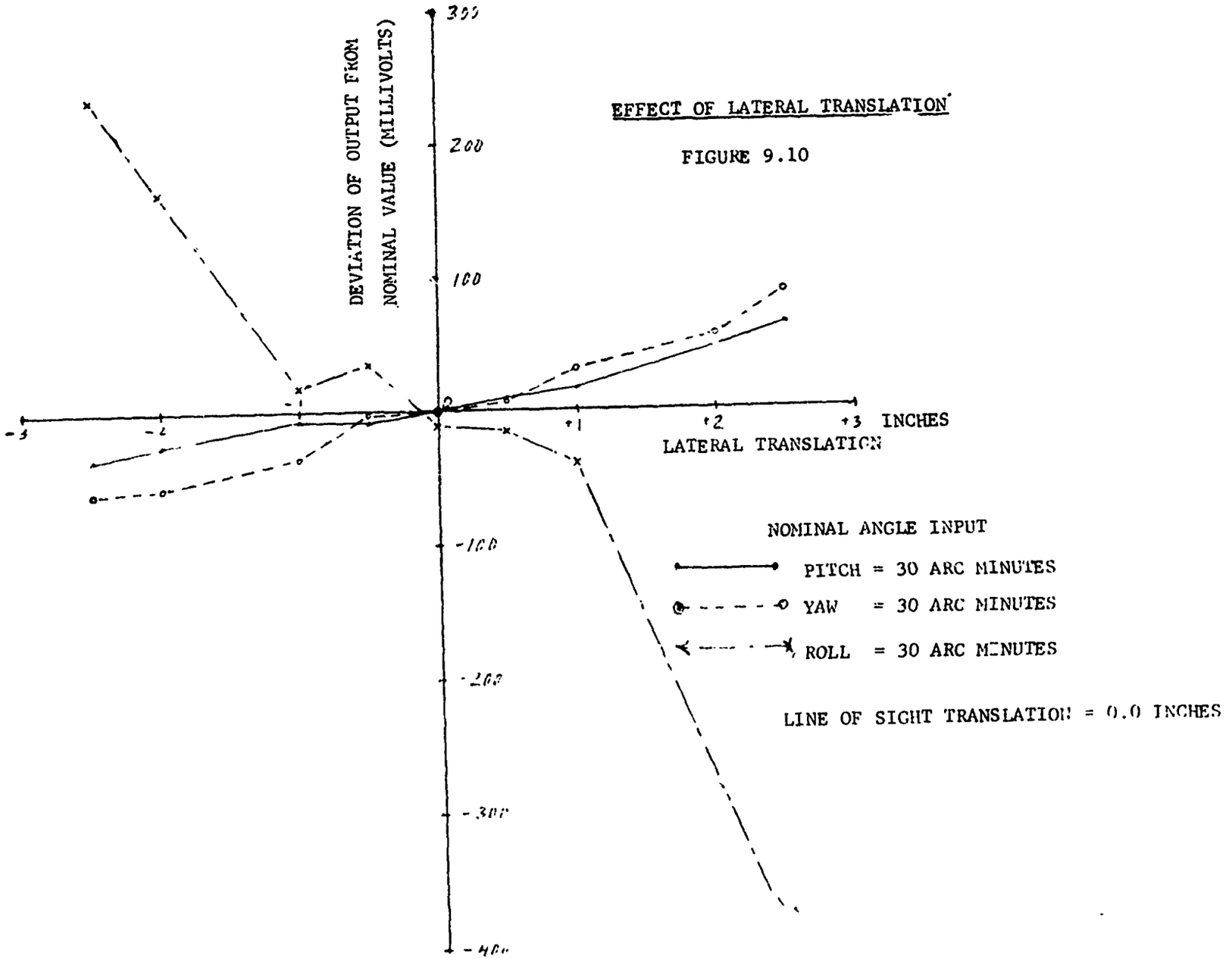

EFFECT OF LATERAL TRANSLATION

FIGURE 9.10

The standard deviation of readings taken during translation are shown. The nominal angles were pitch = 30', yaw = 30' and roll = 30'. The range of translation in inches (L.O.S. = Line of Sight, LAT = Lateral) is shown along with the number of readings in each group.

STANDARD DEVIATION (±LOS", ±LAT)	POSITIONS MEASURED	PITCH	YAW	ROLL
σ (±1", ±.5")	(15 positions)	11 sec	6 sec	23 sec
σ (±3", ±.5")	(27 positions)	10	6	25
σ (±3", ± 1")	(45 positions)	12	21	27
σ (±3", ±2.5")	(81 positions)	30	48	181

Table 9.7. Translation Effect

NOTE (1): The error shown in this table includes all system and test errors.

1. Noise
2. Short term instability (mostly noise)
3. Cross channel interference
4. LED imbalance without control loop for correction
5. Test errors in voltage measurement
6. Test errors in angle measurement (mirror flatness)
7. Autocollimator nonlinearity

NOTE (2): Subsequent improvements in the system improved the readings.

METHOD 1 - ANGULAR STEP FUNCTION SIMULATED ELECTRONICALLY

	RESPONSE TIME	SETTLING TIME
Applied Signal	.01 Second	.01 Second
Pitch Output	.04 (±.005) Sec.	.16 (±0.4) Sec.
Yaw Output	.035 (±.005) Sec.	.2 (±.01) Sec.
Roll Output	.7 (±.1) Sec.	3 (±.5) Sec.

METHOD 2 - ROTATING WEDGE ANGLE AT 3 HERZ

	RESPONSE	
Pitch Output	93%	down 0.63 db
Yaw Output	95%	down 0.45 db

Test is unable to determine response at 10 Herz

Table 9.8. OAMS Brassboard Response Time

FIGURE 9.11

OAMS SYSTEM RESPONSE TO BACKGROUND RADIATION

BACKGROUND PROVIDED BY WHITE PAPER PLACED SO AS TO FILL THE RECEIVER FIELD OF VIEW. THE BACKGROUND LEVEL WAS VARIED BY POSITIONING TUNGSTON LIGHTS (3200°K) AROUND PAPER.

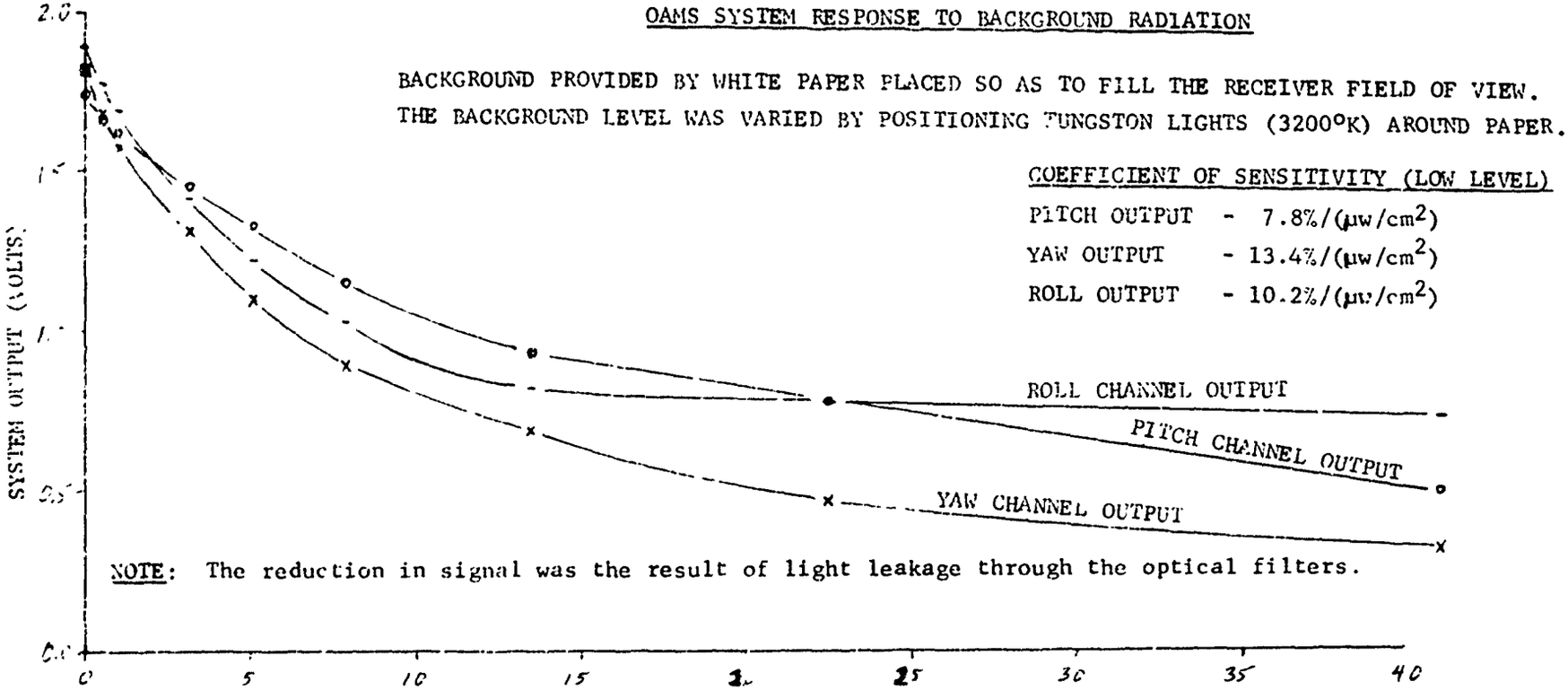

NOTE: The reduction in signal was the result of light leakage through the optical filters.

IRRADIANCE AT RECEIVER FROM BACKGROUND (μwatts/cm²)

(BACKGROUND LIMITED TO FIELD OF VIEW)

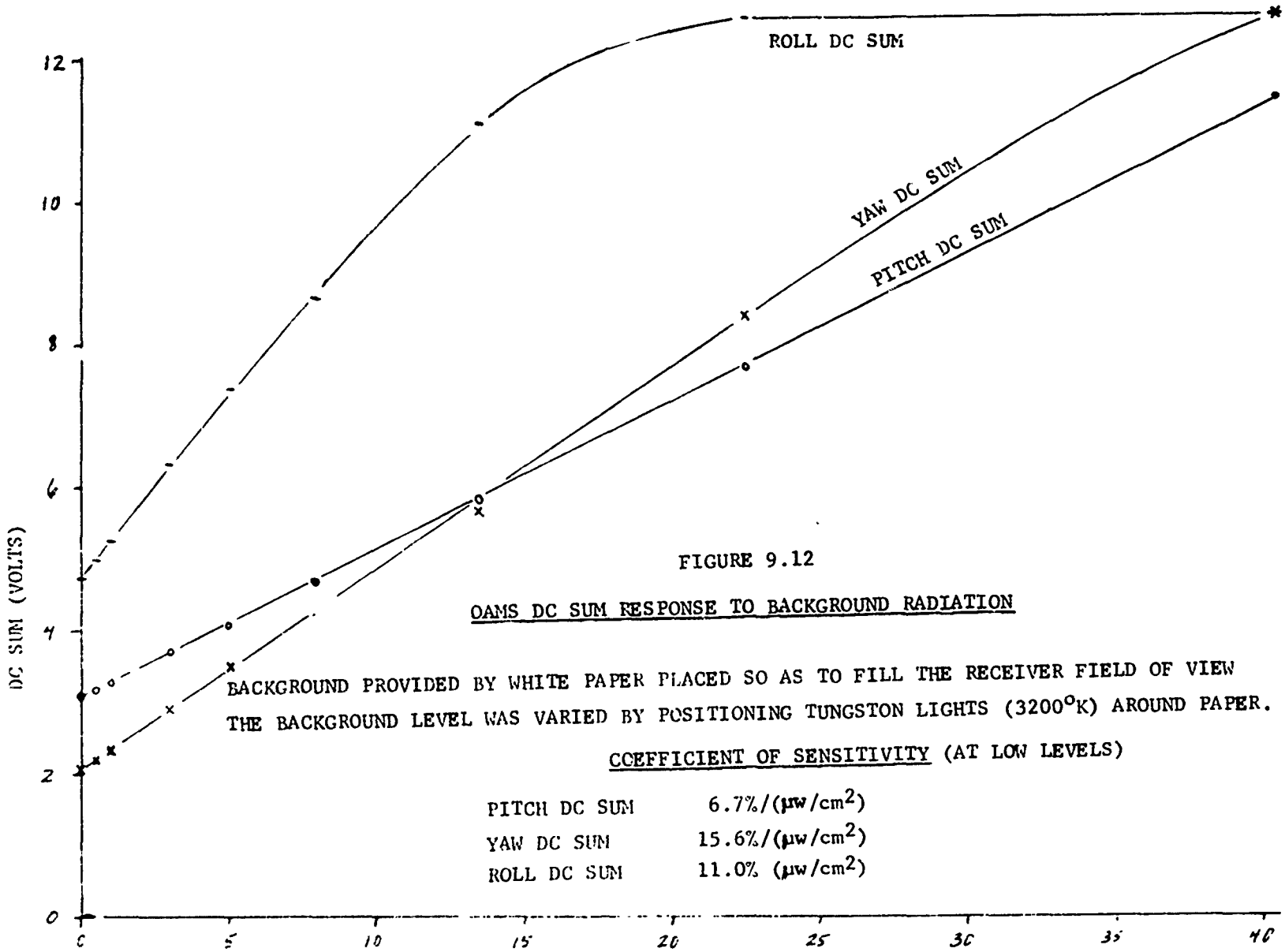

FIGURE 9.12

OAMS DC SUM RESPONSE TO BACKGROUND RADIATION

BACKGROUND PROVIDED BY WHITE PAPER PLACED SO AS TO FILL THE RECEIVER FIELD OF VIEW
THE BACKGROUND LEVEL WAS VARIED BY POSITIONING TUNGSTON LIGHTS (3200°K) AROUND PAPER.

COEFFICIENT OF SENSITIVITY (AT LOW LEVELS)

PITCH DC SUM	6.7%/(μw/cm²)
YAW DC SUM	15.6%/(μw/cm²)
ROLL DC SUM	11.0% (μw/cm²)

A single bare light bulb was then moved across and beyond the receiver field of view. The yaw channel Wollaston acceptance angle at $\pm 15^{\circ}$ can be seen in the system effects shown in Figures 9.13 and 9.14. Essentially all of the effect on the system is through the DC sum and the system AGC. For use in high background within the field of view, another method of AGC control would have to be employed.

9.7 Input Power Tests

The system response to applied voltage between 0 and 33 volts is shown in Figure 9.15. The response is presented in more detail in Figure 9.16 between 24 and 33 volts. The deviation of the system response is also given to indicate the effect on system accuracy. The +15 VDC changed ± 5 millivolts at the extremes of the 24 to 33 volt range.

The system operated for over 5 minutes at input voltages between 6 and 24 VDC without causing any damage to the system. The system accuracy decreased severely below 20-22 VDC input but the system continued to respond to angular input even at very low input power (4 volts) and signal levels. Supply current to the system and the DC sum signals dropped rapidly below a supply voltage of 20-22 volts.

9.8 General System Characteristics

9.8.1 Weight and Dimensions:

	Weight	Dimensions
Transmitter	10.8 lbs.	5.625" dia. x 6.759" = 167.96 cu. in.
Receiver	14.0 lbs.	5.625" dia. x 8.270" = 205.51 cu. in.
Electronics	110.0 lbs.	23" x 21" x 21"

9.8.2 Signal to Noise

The signal to noise data taken at 25 feet and 5 feet are given in Table 9.9. The increase in signal to noise at 5 feet is inversely proportional to the square of the distance as expected.

9.8.3 Power Consumption

The brassboard electronics takes 153 watts of power.

9.9 Temperature Effects

The effect of temperature on the transmitter is shown in Figure 9.17. The change in output indicates the need of an LED control loop to keep the LED output balanced over the large change seen in the DC sum signal. The response of the entire system over the 0° to 140°F temperature range is shown in Figure 9.18. Only the pitch channel was shown since it is typical of the other channels. Near 0°F, the system electronics became unstable. Data were taken for the complete system from 35°F to 140°F. Within the accuracy of the test, there was no temperature effects on the electronics other than what was observed for the transmitter and receiver. This means that further temperature compensation is not anticipated for the system electronics.

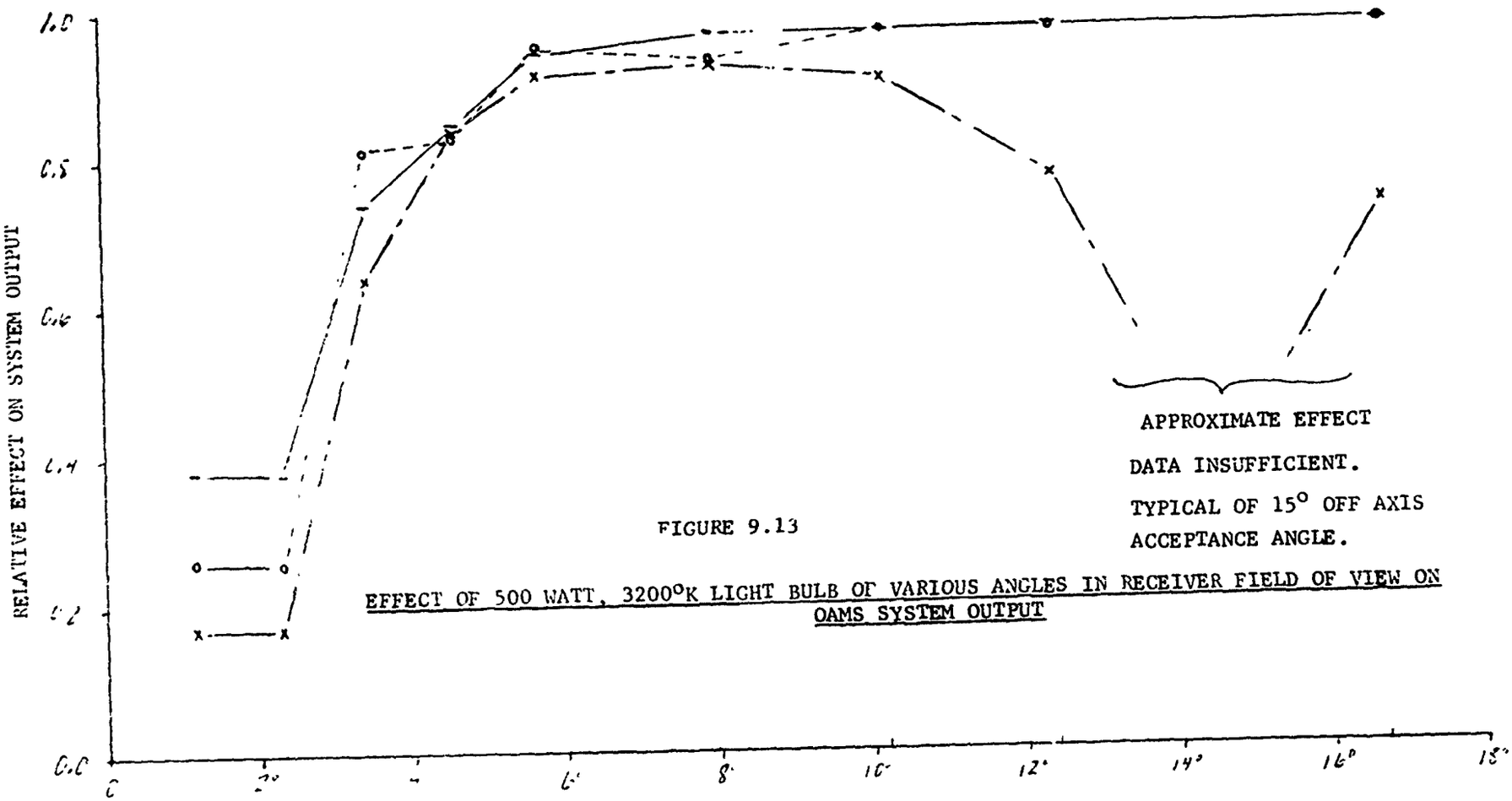

FIGURE 9.13

EFFECT OF 500 WATT, 3200°K LIGHT BULB OF VARIOUS ANGLES IN RECEIVER FIELD OF VIEW ON OAMS SYSTEM OUTPUT

FIGURE 9.14

EFFECT OF 500 WATT, 3200°K LIGHT BULB AT VARIOUS ANGLES IN RECEIVER FIELD OF VIEW ON OAMS SYSTEM DC SUM SIGNAL

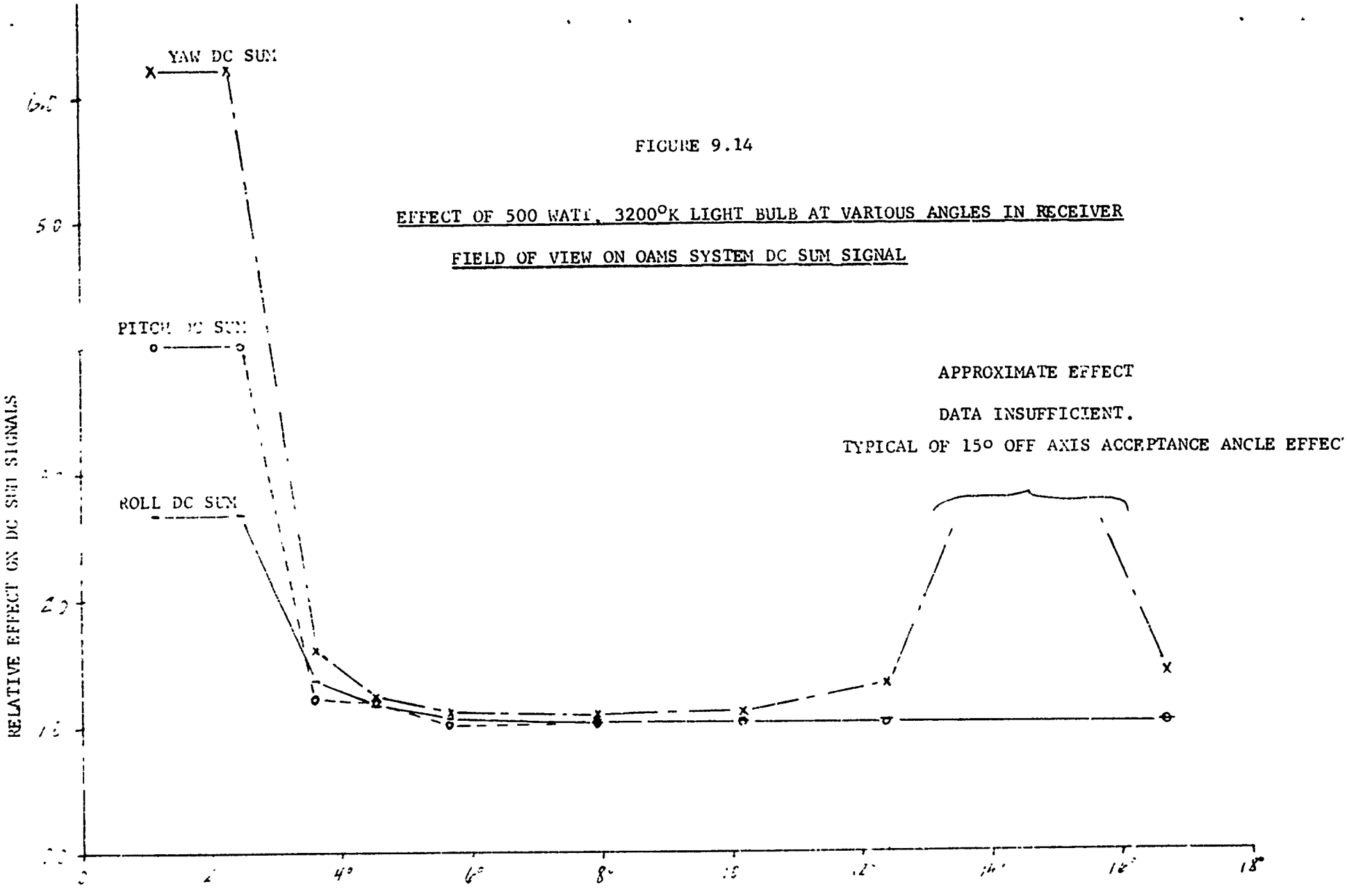

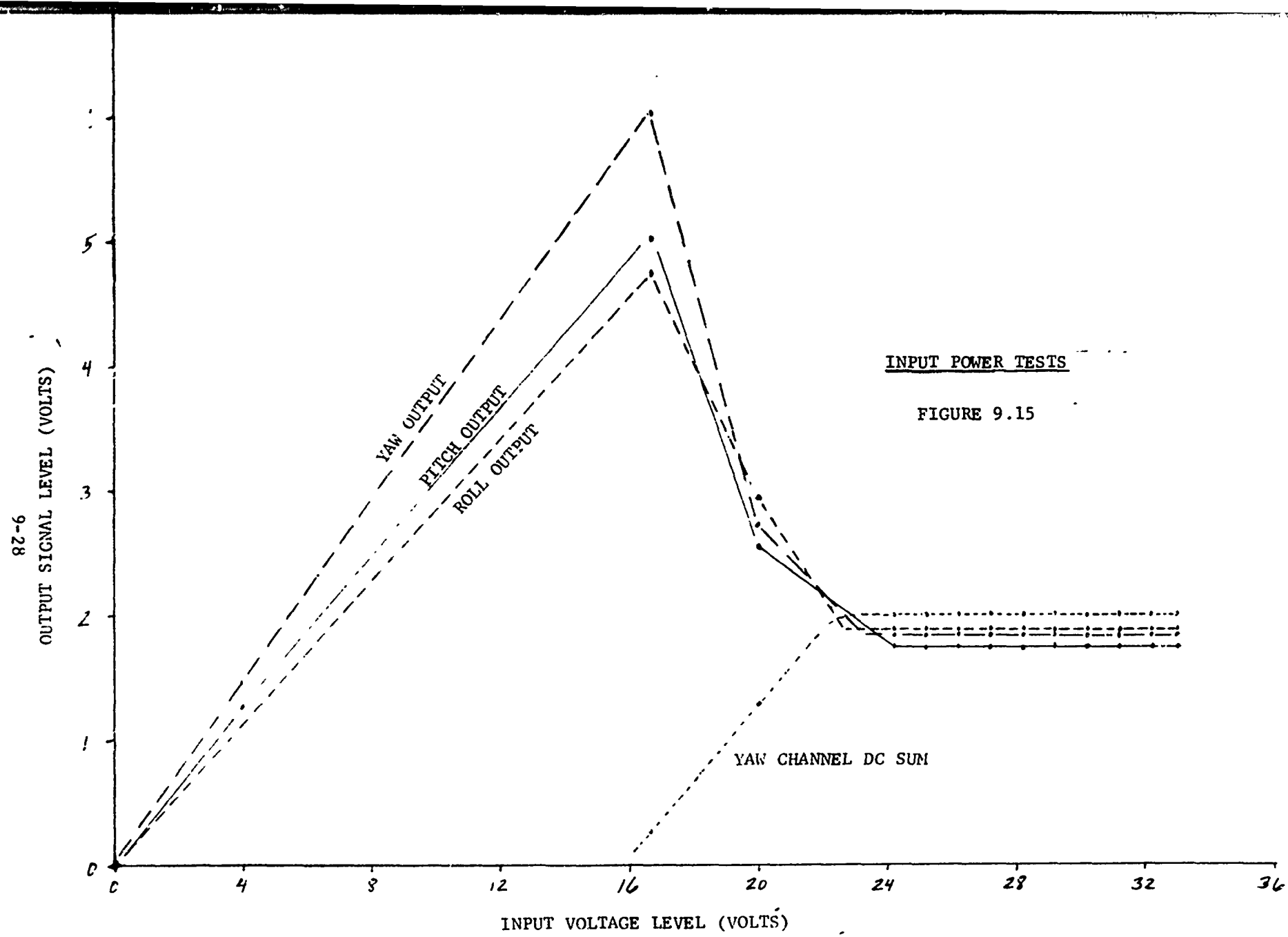

INPUT POWER TESTS

FIGURE 9.15

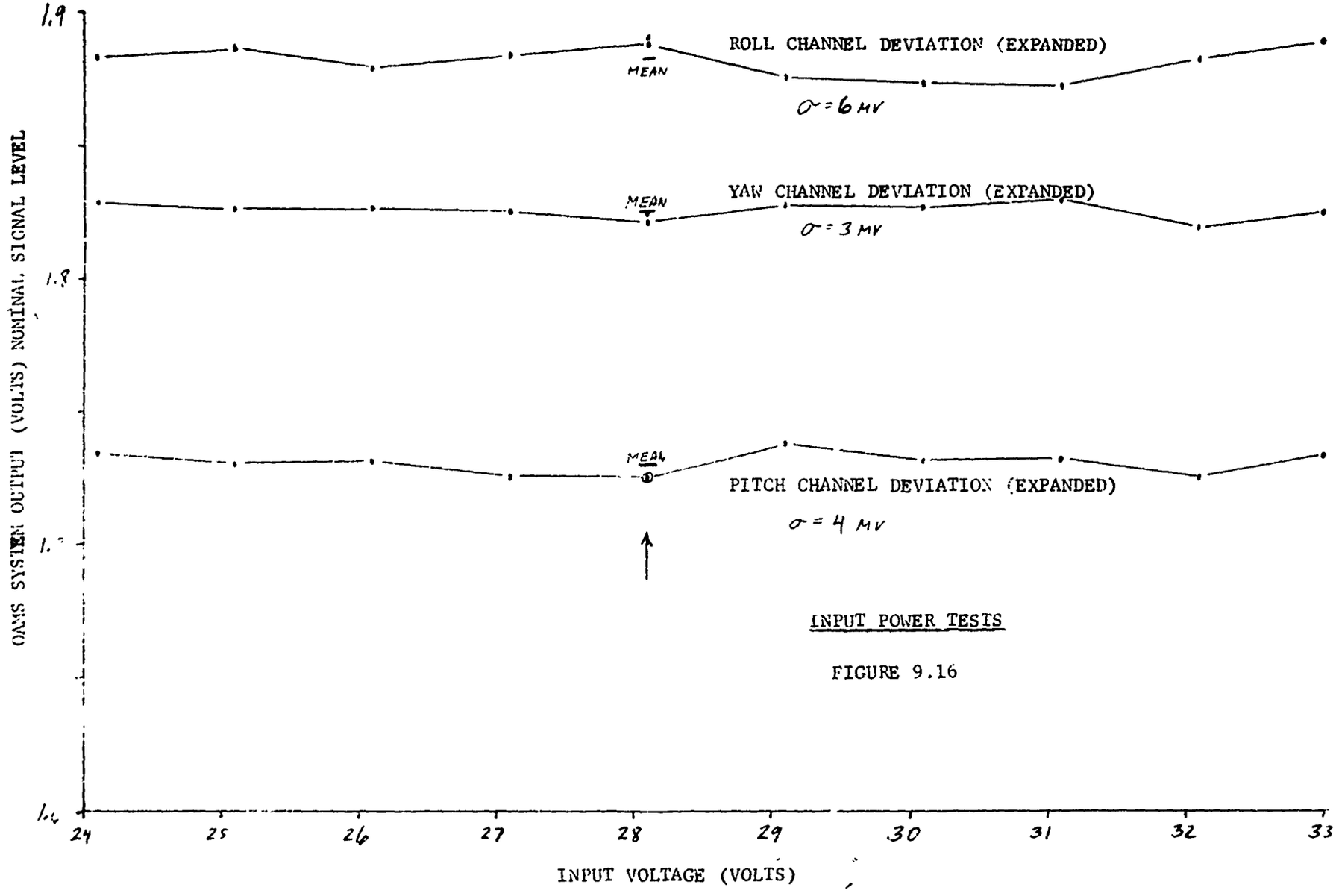

INPUT POWER TESTS

FIGURE 9.16

NOISE	LOW FREQUENCY SYSTEM BANDWIDTH	HIGH FREQUENCY SYSTEM BANDWIDTH
Pitch Output, 25 foot range	±1.5 Millivolt	.5 Millivolt p-p
Yaw Output	±3	1
Roll Output	*±12	.5
Pitch Output, 5 foot range	±1 Millivolt	.5 Millivolt p-p
Yaw Output	±0.5	.5
Roll Output		
Output Response = .045 Sec.	*±3	.5
Output Response = 0.63 Sec.	±0.5	.5

*Subsequent improvements in signal to noise ratio reduced the noise figure.

NOTE 1: Oscilloscope used for evaluation had .5 millivolts peak to peak high frequency noise on trace.

NOTE 2: The noise levels correspond to 2σ values where σ = Standard Deviation. A 2σ value represents a measurement maximum observed over a relatively long period.

Table 9.9. Noise on System Output Signals

FIGURE 9.17

EFFECT OF TEMPERATURE ON PITCH TRANSMITTER AND RECEIVER

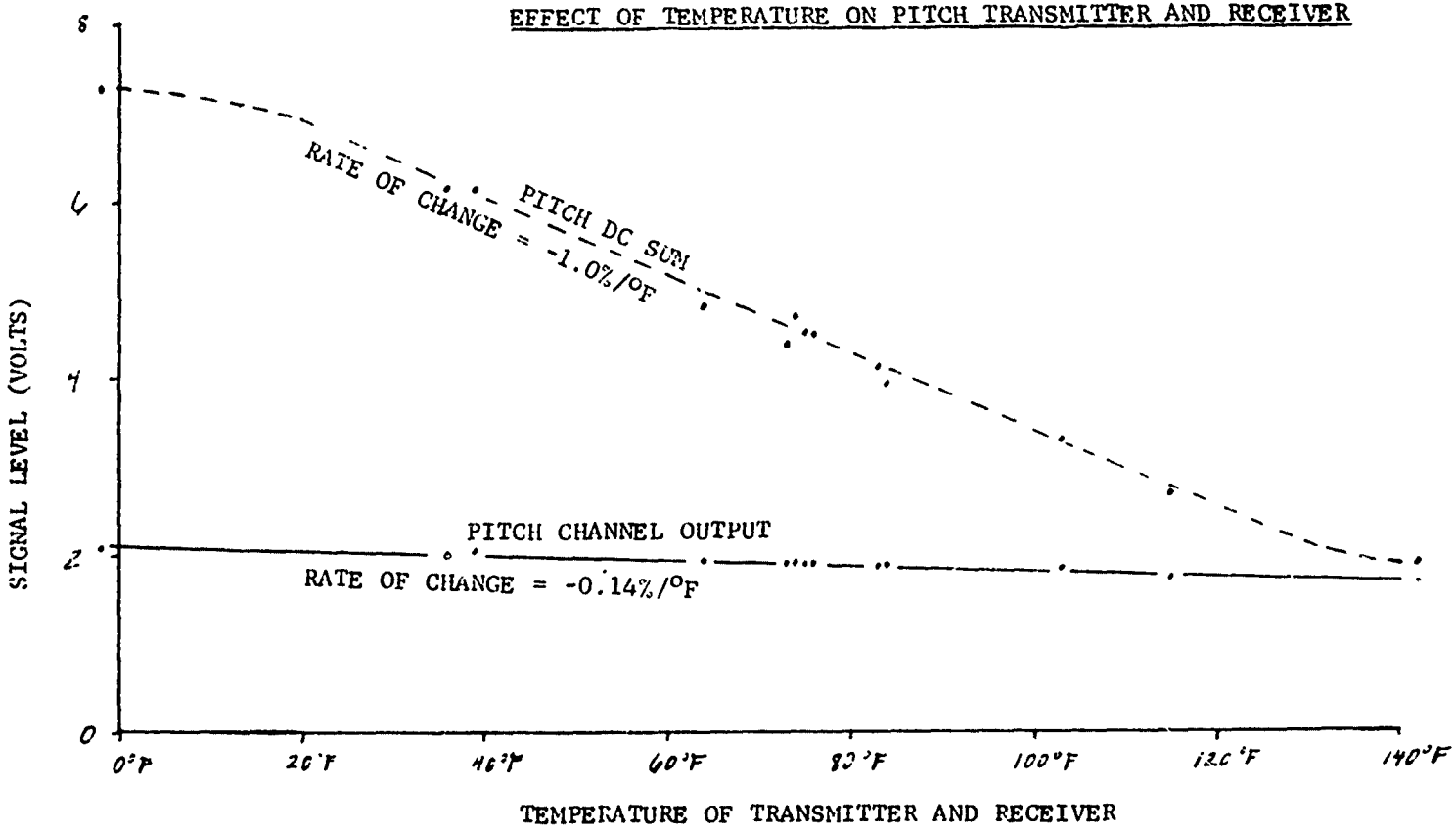

FIGURE 9.18

EFFECT OF TEMPERATURE ON PITCH SYSTEM

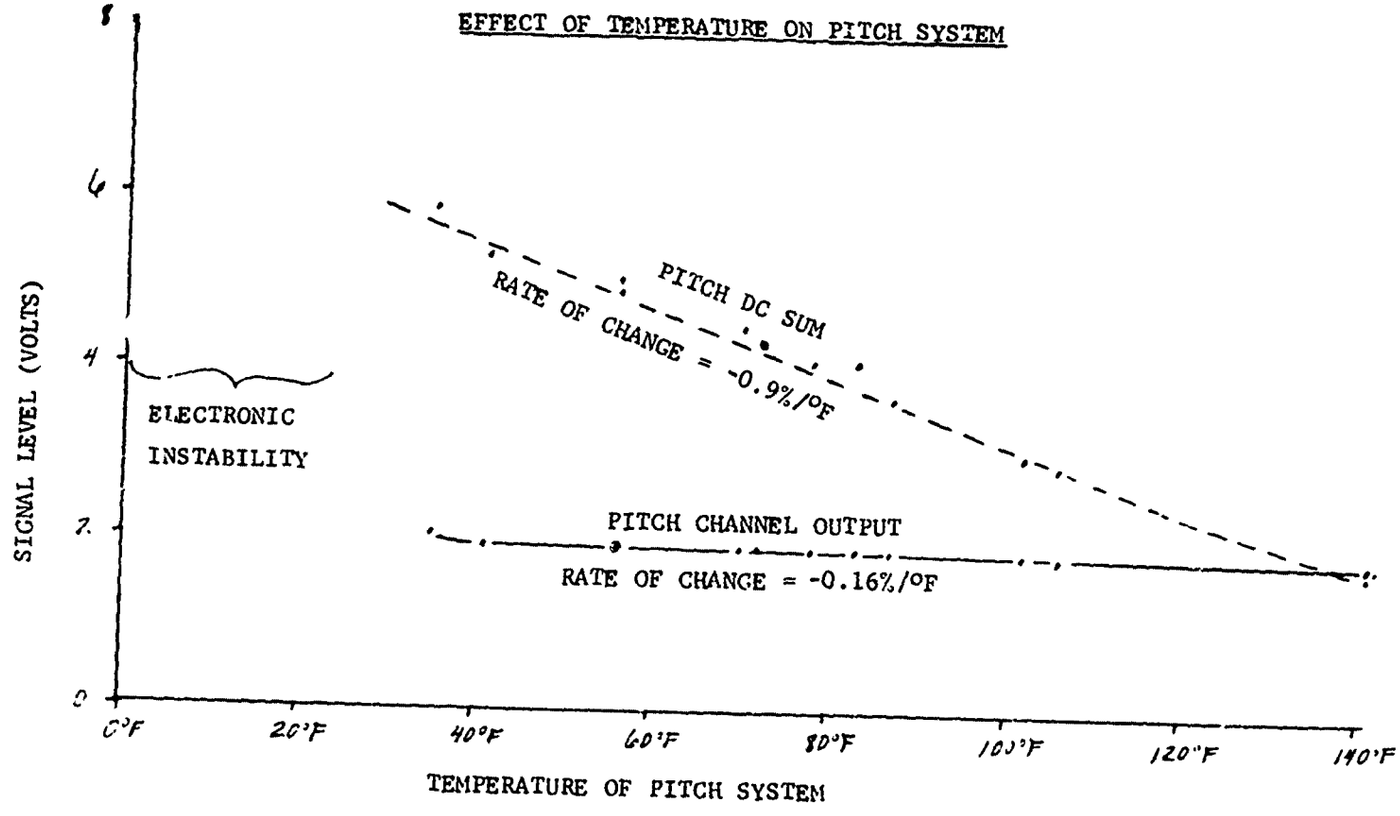

9.10 Coordinate Relationships for System Evaluation and Application

9.10.1 General Considerations

The purpose of the OAMS system is to relate the spatial coordinate system at one location (associated with the OAMS transmitter) to the spatial coordinate system at another location (associated with the OAMS target). The relationship between these points can be defined in general by 3 variables (i_1, i_2, and i_3) which are not uniquely determined until the spatial coordinate system of these points is defined. This is usually determined by system constraints in which movement can be applied through a series of gimbals or by external orientation such as established by a navigation system.

Figure 9.19 illustrates a reference coordinate system as defined by the OAMS statement of work and the coordinate system defined by the OAMS test set up. It can be seen that roll is the outer gimbal and yaw is the inner gimbal. The total transformation A_T is, therefore, made up of successive rotations in the following order: $A_T = A_y\ (i_2)\ A_p\ (i_1)\ A_R\ (i_3)$ where $A_R\ (i_3)$ is is the roll angle transformation, $A_p\ (i_1)$ is the pitch angle transformation and $A_y\ (i_2)$ is the yaw angle transformation.

When the coordinate axes are defined, they can be related to the OAMS coordinate system through the general coordinate transformation, A_T. The OAMS system output can be defined by the angular variables i_1, i_2 and i_3 corresponding to pitch, yaw and roll. This coordinate transformation will be derived below for the OAMS Phase I design and the available test set up.

9.10.2 Coordinate Transformation for System Evaluation

The coordinate transformation is defined by the following matrices:

$$A_R = \begin{vmatrix} \cos i_3 & \sin i_3 & 0 \\ -\sin i_3 & \cos i_3 & 0 \\ 0 & 0 & 1 \end{vmatrix} \quad A_P = \begin{vmatrix} \cos i_1 & 0 & -\sin i_1 \\ 0 & 1 & 0 \\ \sin i_1 & 0 & \cos i_1 \end{vmatrix} \quad A_Y = \begin{vmatrix} 1 & 0 & 0 \\ 0 & \cos i_2 & \sin i_2 \\ 0 & -\sin i_2 & \cos i_2 \end{vmatrix}$$

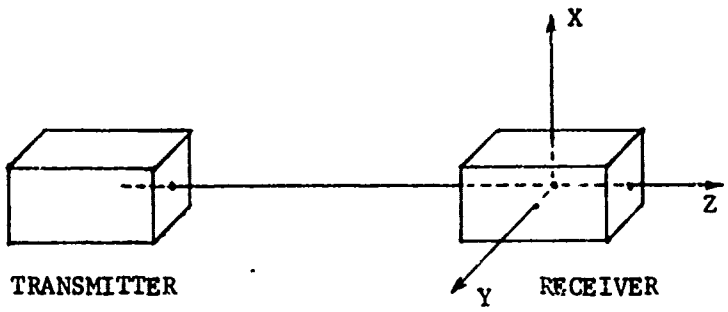

REFERENCE COORDINATE SYSTEM

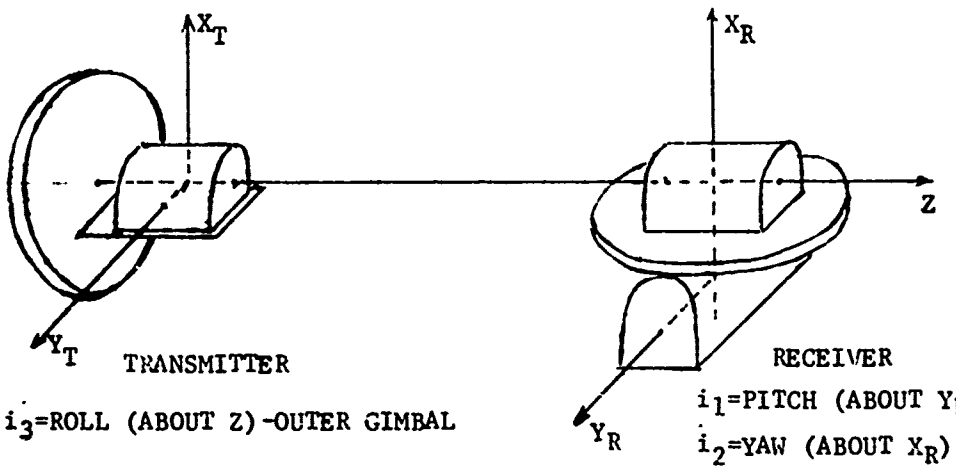

TEST SET-UP COORDINATE SYSTEM

FIGURE 9.19

DEFINITION OF COORDINATE SYSTEMS

$$A_T = A_Y A_P A_R = \begin{vmatrix} \cos i_3 \cos i_1 & \sin i_3 \cos i_1 & -\sin i_1 \\ -\sin i_3 \cos i_2 + \cos i_3 \sin i_1 \sin i_2 & \cos i_3 \cos i_2 + \sin i_3 \sin i_1 \sin i_2 & \cos i_1 \sin i_2 \\ \sin i_3 \sin i_2 + \cos i_3 \sin i_1 \cos i_2 & -\cos i_3 \sin i_2 + \sin i_3 \sin i_1 \cos i_2 & \cos i_1 \cos i_2 \end{vmatrix}$$

After angular movement, the moving and referenced coordinates are now related:

$$\begin{bmatrix} X' \\ Y' \\ Z' \end{bmatrix} = \begin{bmatrix} \quad \\ A_T \\ \quad \end{bmatrix} \begin{bmatrix} X \\ Y \\ Z \end{bmatrix}$$

MOVING REFERENCE

The general transformation is applied to the OAMS system in the following manner:

FOR PITCH: Consider now the coordinates referenced within the angle sensing crystal as shown in Figure 9.20. Take the projection of A' on the ZX plane to obtain the actual angle ψ between the plates relative to their sensitive axis.

$$\overrightarrow{P_{ZX}\,|\,Z'|} = (\sin i_3 \sin i_2 + \cos i_3 \sin i_1 \cos i_2)\,\hat{X} + (\cos i_1 \cos i_2)\,\hat{Z}$$

$$\psi = \tan^{-1}\left(\frac{\sin i_3 \tan i_2}{\cos i_1} + \cos i_3 \tan i_1\right) \approx i_1 + i_3 i_2 - \tfrac{1}{2} i_1 i_3^2$$

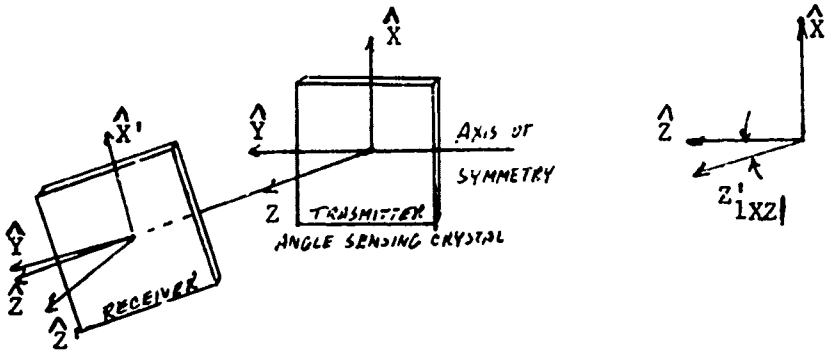

Figure 9.20 Pitch Coordinates

For Yaw: As for pitch, take the projection of Z' on the YZ plane as shown in Figure 9.21

$$\overline{P_{YZ} \mid Z'} = (-\cos i_3 \sin i_2 + \sin i_3 \sin i_1 \cos i_2)\,\hat{Y} - (\cos i_1 \cos i_2)\,\hat{Z}$$

$$W = \tan^{-1}\left(\frac{-\cos i_3 \tan i_2}{\cos i_1} + \sin i_3 \tan i_1\right) \cong - i_2 + i_1 i_3 - \tfrac{1}{2} i_2 \frac{i_1^2 - i_3^2}{2}$$

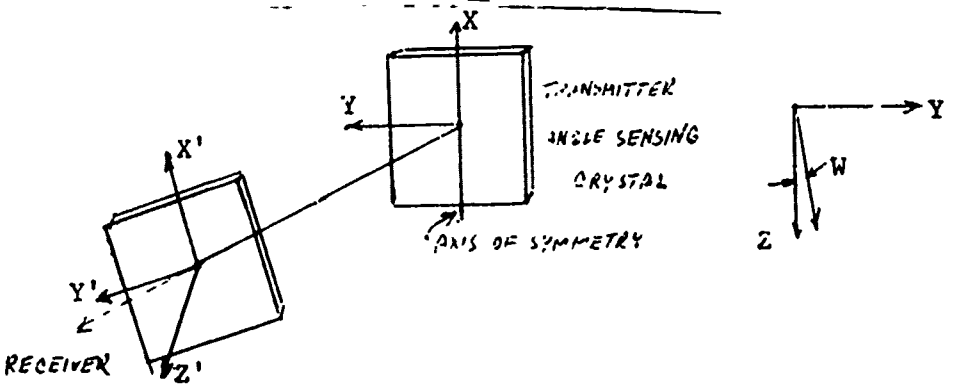

Figure 9.21 Yaw Coordinates

For Roll: Consider orthogonal vectors $\vec{A}_1$ and $\vec{A}_2$ related to the reference Wollaston and $\vec{A}_1'$ and $\vec{A}_2'$ related to the moving Wollaston as shown in Figure 9.22. The angle ρ_1 represents the angle between $P_{xy} |A_1'|$ (the projection of A_1' on the XY plane) and X. The angle ρ_2 represents the angle between $P_{xy} |A_2'|$ and Y.

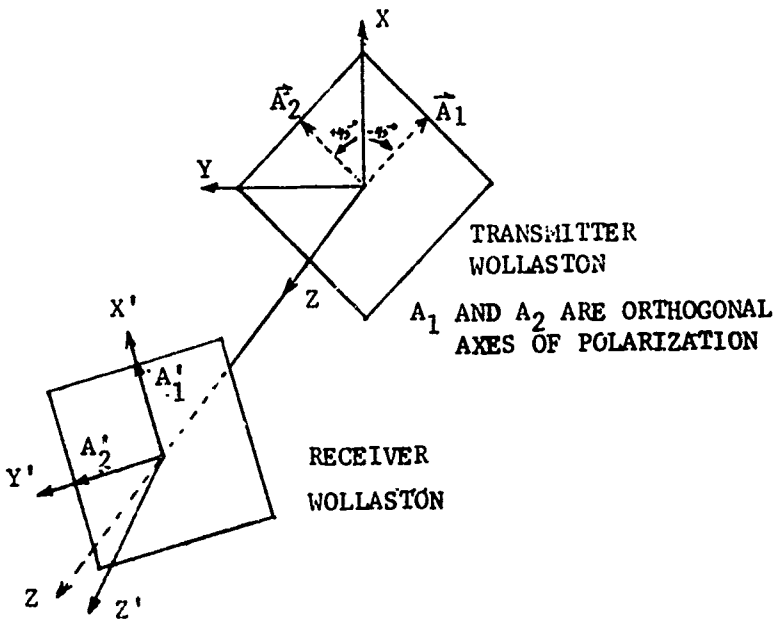

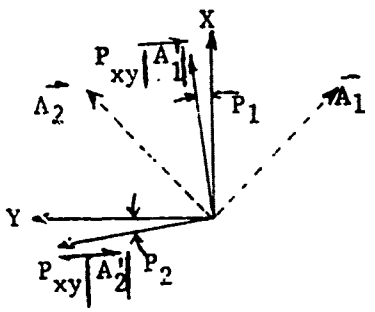

FIGURE 9.22 ROLL COORDINATES

$$\vec{A}_1 = \frac{\sqrt{2}}{2}\,\hat{X} - \frac{\sqrt{2}}{2}\,\hat{Y} \qquad \overrightarrow{P_{xy}\,|\,A_1'|} = (\cos i_3 \cos i_1)\,\hat{X} + (\sin i_3 \cos i_1)\,\hat{Y}$$

$$\vec{A}_2 = \frac{\sqrt{2}}{2}\,\hat{X} + \frac{\sqrt{2}}{2}\,\hat{Y} \qquad \overrightarrow{P_{xy}\,|\,A_2'|} = (-\sin i_3 \cos i_2 + \cos i_3 \sin i_1 \sin i_3)\,\hat{X}$$
$$+(\cos i_3 \cos i_2 + \sin i_3 \sin i_1 \sin i_2)\,\hat{Y}$$

$$P_1 = \tan^{-1}\left(\frac{-\sin i_3}{\cos i_3}\right) = -i_3$$

$$P_2 = \tan^{-1}\left(\frac{-\sin i_3 \cos i_2 + \cos i_3 \sin i_1 \sin i_3}{\cos i_3 \cos i_2 + \sin i_3 \sin i_1 \sin i_2}\right) \cong -i_3 + i_1 i_2 - \frac{i_3^3}{2}$$

The roll channel difference signal (angle dependent, AC term) as given in equation 28, Appendix D, is as follows

$$V_D = \frac{D}{4}\,(K_1A_1+K_2A_2)(R_1 i_{m1} + R_2 i_{m2})\,\sin\omega t \,\sin 2\theta_R$$

Deriving this equation using ρ_1 and ρ_2 gives the following:

$$V_D' = \frac{D}{4}\,(K_1A_1+K_2A_2)(R_1 i_{m1} \sin 2P_1 + R_2 i_{m2} \sin 2P_2)\,\sin\omega t$$

The difference in ρ_1 and ρ_2 is $(i_1 i_2 - \frac{i_3^3}{2})$ and when compared to the basic angle $2i_3$ has the total effect on the roll angle $\bar{\rho}_2$ as shown:

$$P = -i_3 + \tfrac{1}{2} i_1 i_2 - \frac{i_3^3}{4}$$

For calibration of the system, the following approximations are possible, neglecting effects of the signal processing electronics.

Pitch	$V_1 = \dot{\eta} \cong i_1 + i_3\, i_2$
Yaw	$V_2 = \omega \cong -i_2 + i_3\, i_1$
Roll	$V_3 = \dot{\rho} \cong -i_3 + \frac{1}{2}\, i_1\, i_2$

The sign convention in the analysis was that positive angle rotations correspond to the "right hand screw rule." This set of equations should relate OAMS system output voltage to the input angles during test under ideal optic and electronic linearity and adjustment.

9.11 Test Summary

The evaluation of the performance for a high accuracy system requires special consideration when the equipment used for evaluation is not significantly more accurate than the system in test. It is desirable that the combined test errors be 10 times less than the expected system errors. It is not possible to meet this error ratio in evaluation of the OAMS system. The major sources of system and measurement errors are listed in Table 9.10, together with the measured or estimated error magnitude associated with each source.

Uncertainties in system performance were primarily due to short term instability (including noise which was subsequently reduced by a factor of 20) and to LED imbalance during angle or translation movement which was improved by a redesigned LED balance control. Measurement uncertanties were primarily produced by the voltage and becomes the mirror flatness estimated at less than or equal to 20 arc seconds per inch of translation. The comparison of the performance to the calibration curves also included a small error since more terms could have been used in the calibration curve to express the function more accurately as shown in the error estimate.

It is expected that most of the error sources can be reduced to within the estimated values shown at the bottom of Table 9.10.

A summary of the test results on the OAMS brassboard model are given in Table 9.11A, B, C and D, together with a list of requirements from the OAMS Phase I statement of work. Most of this information has been described previously. Power consumption, weight and volume are shown in Table 9.11B and 9.11C. Table 9.11D summarizes the error evaluation for angular and translational movement described previously. Also shown in this table are the values of error which chould be expected from the system and measurement errors listed in Table 9.10. These expected values for error were obtained by combining the error sources which pertained to a particular test in an RMS manner. The error expected after the improvements listed in Table 9.10 have been implemented are significantly less in some cases as seen in the last column in Table 9.11D. All measured and estimated errors in Tables 9.10 and 9.11 are listed as a 2σ value in order to be compatible with the requirements as given in the statement of work for the contract. In this case σ represents the standard deviation of the data sample used to evaluate a particular performance characteristic.

SOURCE OF ERRORS IN BRASSBOARD EVALUATION

Error is stated as 2σ value equivalent angle (arc seconds) for evaluation at 25 feet.

	Pitch	Yaw	Roll
SYSTEM UNCERTAINTY			
*1. Short Term Instability (including noise)	**2 Sec.	**2 Sec.	**4 Sec.
*2. LED Imbalance with Angle and Translation, Calculated value for uncorrected system, Up to 1/2" angle or (±3" LOS, ±5" LAT) translation	1.3	1.3	14
Up to 1° angle or (±3" LOS, ±2.5 " LAT) translation	2.6	2.6	28
*3. Cross Channel Interference (±1°)	1	5	2
4. Optic and Electronic Nonlinearities	No Estimate Made -		
MEASUREMENT UNCERTAINTY			
*5. Error in Correcting Geometric Coordinate Crosscoupling Estimate	3	3	3
6. Voltage Measurement Errors	2	2	2
7. a. Angle Measuring Errors - Calibration	2	2	2
b. - Crosscoupling	4	4	4
* c. - Mirror Flatness Estimate	20 sec/in	20 sec/in	20 sec/in

	(Error with Improvement)		
* Expected Improvements in these areas:			
1. Signal to Noise Improvement	1	1	2
**This was accomplished in subsequent work			
2. Maintain LED Balance with Control Loop within ± 1.0%	1	1	1
3. More Polynomial Correction Terms	1	1	1
4. Improved Quality Mirrors and Mounts	5 sec/in	5 sec/in	5 sec/in

Table 9.10

	GOAL	REQUIREMENT	BRASSBOARD
MEASUREMENT RANGE			
Range	$\pm 1^{o}$	-	Pitch $\pm$ 1o Yaw $\pm$ 1° Roll $\pm 1^{o}$20 min
Calibrated Range	-	$\pm 1/2^{o}$	Pitch $\pm$40 min Yaw $\pm$50 min Roll $\pm 1^{o}$20 min
Calibration Curve	Polynomial function of angle only and less than 10 terms		Pitch 5 terms, angle only Yaw 5 terms, angle only Roll 3 terms, angle only
ACCURACY			
Systematic Error ($\pm 1/2^{o}$, 2σ)	-	5 sec	Refer to Figure 9-28D
Systematic Error ($\pm 1^{o}$, 2σ)	1 sec	-	UNDER EVALUATION
Dynamic Error	1 sec	5 sec	Pitch 1.30 Sec. Yaw .99 Sec. Roll 1.40 Sec.
TRANSLATION			
($\pm$ 1" LOS, $\pm$.5" LAT)	-	No Effect on System	Refer to Figure 9-28D
($\pm$3" LOS, $\pm$2.5" LAT)	No Effect on System	-	
SENSITIVITY		<16.7 mv/sec Bipolar output	Pitch 1.04 mv/sec max., bipolar Yaw 1.00 mv/sec max., bipolar Roll .991 mv/sec bipolar
SATURATION CHARACTERISTICS			
Full Scale	Hold full scale output for angles $\geq$ full scale deflection		Not done - brassboard designed to determine max. range.
Recovery Time		4 sec	Pitch Est. <1 sec Yaw <1 sec Roll 4 sec

Table 9.11A. Evaluation of OAMS Brassboard

	GOAL	REQUIREMENT	BRASSBOARD
SYSTEM RESPONSE			
Response Time , 0-90%	-	0.045 sec	Pitch 0.04 sec Yaw 0.035 sec Roll 0.04 sec
% Response	-	down 3 db at 10 hz	Pitch 93%, down .64db at 3 hz Yaw 95%, down .44db at 3 hz Roll not tested
OPERATING DISTANCE (Maintaining other Requirements)	0-50 ft.	0-25 ft.	Pitch 5-25 (5-50 est.) Yaw 5-25 (5-50 est.) Roll 5-25 (5-50 est.)
TEMPERATURE TEST			
Operating Range		0^{o}-140^{o}F	Trans/Rec. 0^{o}-140^{o}F System 35^{o}-140^{o}F
Performance		Performance Unaffected	Trans/Rec. (Change in output) Pitch -0.14%/^{o}F Yaw +0.1%/^{o}F Roll -0.36%/^{o}F System Pitch -0.16%/^{o}F Yaw +0.1%/^{o}F Roll -0.36%/^{o}F
Power Consumption		20 watts	150 watts
Input Power Test			
0-20 vdc input voltage		survive	survived
Polarity Reversal		survive	not tested
24-33 vdc Input Voltage		perform unaffected	perform unaffected
0.75 volt RMS Ripple 1 hz - 15khz		perform unaffected	not tested
±56 volt peak transients - 10 μsec duration 1 μsec rise time at 5pps		perform unaffected	not tested

Table 9.11B. Evaluation of OAMS Brassboard

	GOAL	REQUIREMENT	BRASSBOARD
WEIGHT			
Transmitter]	23 lbs.	54 lbs.	10.8 lbs.
Receiver]			14.0 lbs.
Electronics (exception made by agreement)	-	Included in Transmitter	110.0 lbs. (Weight not considered in brassboard).
VOLUME			
Transmitter	200 cu. in.	400 cu. in.	168 cu. in.
Receiver	200 cu. in.	375 cu. in.	206 cu. in.
Electronics (exception made by agreement)		Included in Transmitter	10,150 cu. in. Not considered in brassboard.
MISCELLANEOUS			
System Test Time			76 hours
Total System Time (2-17-75)			186 hours
Decrease in 7.3 LED output			Over 50% decrease during 76 hours of test.
Effect of Background Radiation (within $\pm$ 1.5° field of view) (effect seen through AGC control loop only)			Pitch - 7.8%/μw/cm^2) Yaw - 13.4%/μw/cm^2) Roll - 10.2%/μw/cm^2)

Table 9.11C. Evaluation of OAMS Brassboard

SEE NOTE 1	BRASSBOARD EVALUATION* Expected	Test	PROTOTYPE** Expected 2 σ Error
Calibration Data Compared to Calibration Curves:	2σ Error (arc seconds)		
Pitch	3.7 Sec.	11 Sec.	3.2 Sec.
Yaw	4.2	11	3.6
Roll	10.7	10	4.0
Data with Simultaneous Pitch, Yaw and Roll Compared to Calibration Curves:			
Pitch	5.9	16	5.7
Yaw	6.2	7	5.9
Roll	18	32	6.4
System Performance During Translation Compared to Nominal Value:			
Pitch ($\pm$1" LOS, $\pm$0.5" LAT)	21	22	5.7
($\pm$3" LOS, $\pm$0.5" LAT)	21	20	5.7
($\pm$3" LOS, $\pm$1" LAT)	21	24	5.7
Yaw ($\pm$1" , $\pm$0.5")	11	12	3.8
($\pm$3" , $\pm$0.5")	11	12	3.8
($\pm$3" , $\pm$1")	21	42	5.9
Roll ($\pm$1" , $\pm$0.5")	27	46	6.4
($\pm$3" , $\pm$0.5")	27	50	6.4
($\pm$3" , $\pm$1")	42	54	10.8
Predominant Error Sources	*Noise, LED Imbalance, Autocollimator & Mirror Flatness		- **Autocollimator & Mirror Flatness

NOTE: LOS = Line of Sight Translation
LAT - Lateral Translation

NOTE 1: Further test and evaluation is in process following subsequent improvements to the system.

Table 9.11D. Error Evaluation

10.0 CONCLUSIONS

The Optical Angular Motion Sensor was defined by SAMSO as a "sensor which will provide high resolution on angular deflection in Yaw, Pitch and Roll of a remote platform with reference to three axes determined at the sensor transmitter". It was primarily to be used in a large spacecraft to measure relative displacement between two points.

A concept was developed which utilized polarized light and birefringent crystals for angle sensing. The basic system was breadboarded and it verified the conceptual feasibility. A preliminary system design was made and an analysis performed which indicated that the system would meet the system requirements as stated in the Annex of this report.

Phase I

The phase I program included design, fabrication, test and evaluation of a brassboard model of a system which could be readily adapted to a flight model.

Section 2.1 lists the detail tasks required for the program and a brief summary of the results of the work on these tasks.

The overall system design was basically an optical transmitter, an optical receiver and the required electronics.

Transmitter

The transmitter was designed to produce three optical beams of modulated polarized light, one each for roll, pitch and yaw. The light sources selected were Light Emitting Diodes (LEDs) of three different wavelengths (colors) with two LEDs per channel. These sources were modulated at three discrete frequencies. The purpose of this design was to permit channel isolation by both optical and electronic means to prevent crosstalk between the channels.

The position of the transmitter is encoded onto the light beam by special birefringent crystals. The crystals develop a state of polarization which is a function of the angular position of the crystal surfaces. The crystals are designed to self compensate for temperature variations.

Receiver

The receiver senses the modulated coded light beams through crystals, identical to the transmitter except in opposite orientation. As long as the crystals are parallel the polarization state is unchanged. But when the angle of the transmitter is changed relative to the receiver, the phase of the polarization changes in relation to the sine of the angle between the axes of the crystals. The polarization states are separated by means of a Wollaston prism and two detectors. The signal on the two detectors is differenced to determine the phase relationship of the polarization states. The amplitude of the demodulated signal represents the angular relationship of the transmitter and receiver.

Electronics

The consist of a power supply, oscillators, LED drivers, preamplifiers, amplifiers, demodulators and control loops. The output is a DC voltage proportional to the angular relationship of the crystals.

System Performance

The system was set up in the laboratory on positioners and the positions were monitored by autocollimators. After calibration of the system tests were run on all three axes, calibration curves were run as described in this report, cross coupling between axes was plotted, long term drift was monitored and recorded, temperature cycling was performed from 0 to 140°F in an environmental chamber. The data from these tests are in this final report.

The transmitter and receiver performed as expected during the temperature tests. The AGC operated to hold the output constant within approximately $\pm 5\%$ even though the LED output varied approximately $\pm 30\%$ during the temperature cycle.

A dynamic angular displacement was introduced by a rotating optical wedge (Risley Prism) and the dynamic response was recorded. The system responded satisfactorily to these tests. Electronic response tests were also performed.

In both the transmitter and receiver a principle of duality was used for emitters and detectors. Both items are critical components. This design permitted the system to continue to operate with a failure of either an emitter or detector. This concept also improved the signal to noise ratio and improved the reliability factor substantially.

The system generally performed as predicted. The calibration curves were within the RMS requirement of the prime item specification. The effects of translation across the specified field of view within generally expected tolerances but improved techniques for monitoring these parameters are required.

Problem Areas

Some anomalies were experienced in the performance and during the test and evaluation. The LEDs used for the pitch and yaw showed a large drop in output energy with time. This makes these diodes unsatisfactory for use on the program.

A system for backup was designed for single color operation. It used a time division multiplex concept and was breadboarded for use with the brassboard. It has been partially evaluated at this date but the performance seemed to be comparable with the three color system except the response time was degraded. Appendix C.

The signal required for the roll channel is roughly 30 times the pitch and yaw, therefore, signal-to-noise ratio of the roll channel was high. To perform the evaluation tests, an integrating filter was added to the roll channel to reduce the effect of the noise.

Subsequent work resulting from the circuit analysis indicated that certain improvements could be made. These circuits were redesigned and tested. A reduction of the noise was over a factor of 20. The resulting performance of the roll channel is now well within the system requirements and does not require an integrating filter. The most recent improvements in the roll channel are not included in this final report. The pitch and yaw channel also were improved, but the improved performance is not recorded in this report.

A component delivery problem developed when the order for the parts were placed. Both operational amplifiers and precision resistors became a delivery problem because of the Military Specification. The final result was that some components were used that did not meet the full temperature requirements. This had no impact on the performance until the amplifier/demodulator section was cooled below 32°F and then the performance became erratic. It is expected that this will be satisfactory with temperature qualified military standard parts.

The LED control loop did not function properly in the system. It was removed and manual adjustments were installed. A design analysis determined that it was necessary to control the direct current level as well as the alternating current. The original design only controlled the AC level. The redesign is complete and the one channel of the system will be modified accordingly. The redesigned LED control loop now operated satisfactorily and is under test and evaluation.

Recommendations

A. Continue the basic three color system. This would require primarily:

1. Perform an in-depth, state-of-the-art survey of LED development with potential suppliers.

   NOTE: This was performed subsequent to this report

2. Procure test units for evaluation.

   NOTE: These are now on order.

3. Perform efficiency measurements.

4. Measure the geometrical energy profile.

5. Test the spectral distribution for optical design criteria.

6. Procure LEDs with favorable characteristics for reliability and life testing.

7. Redesign brassboard transmitter and receiver to accommodate the selected LEDs.

8. Modify transmitter and receiver and install the selected LEDs.

9. Modify LED driver circuits to match new LED's.

10. Improve signal-to-noise ratio.

11. Test electronic subassemblies in an environmental chamber and identify any components that change abnormally during temperature testing.

12. Install larger detectors in the receiver to improve light distribution during angular movements and translation.

13. Modify detector-preamplifier circuits for larger detectors.

14. Breadboard LED's and driver circuits, detectors and preamplifier circuits.

15. Perform complete temperature tests on new LED/driver system combined with new detector/preamplifier system.

16. Evaluate tests in 15.

17. Update electronic systems design based on brassboard tests, evaluation and performance analysis.

18. Update electronics system.

19. Perform system temperature tests.

20. Design, fabricate, assemble and calibrate special test fixtures for assembly, test and calibration of the OAMS system.

B. Suspend work on time division multiplex system at the present time.

11.0 REFERENCES

1. Polarized Light-Shurcliff, 1962
2. Electro-Optical Data Transmission, 1957 Gievers, Chrysler Missile Div. SP-Rl
3. Optical Synchro Transmission, 1958 Gievers, Chrysler Missile Division GY-RlJ
4. Twist Autocollimator Program (Mobile Minute Man) Contract AF01(6[illegible]10)-35620
5. 3 Axis Deck Flexure Measurement System Program Navy (Bu Ships) NOBs-78429 & NOBs-86472 and NOBs-90169
6. 3 Axis Synchro Transmission Techniques Program (AFAL-TR-64-280)
7. Laser Beam Tracking Instrument (Operation and Maintenance Manual) RADC (Contract F3-0635-71-C-0149)
8. Concepts of Classical Optics - Strong
9. Optical Crystallography - Wahlstrom
10. Analysis of Silicon Photo Detector/Amplifier Combinations Aerospace Corp. TOR-0073(3111)-4, S. I. Marcus
11. Polarized Stellar Optical Spacecraft Attitude Sensor - Chrysler Space

BIBLIOGRAPHY

Final Report - SAMSO TR-73-6
Performance Evaluation Test Plan - CEI No. 73-6-TP
Prime Item Development Specification - CEI No. 73-6
Critical Component Specifications
Silicon Photodetector - CEI No. 73-6-A
Emitting Source - Pitch Channel - CEI No. 73-6-B
Emitting Source - Yaw Channel - CEI No. 73-6-C
Emitting Source - Roll Channel - CEI No. 73-6-D
Angle Sensing Crystal - CEI No. 73-6-E

APPENDIX A

MUELLER MATRICES

This appendix presents a listing of the Mueller matrices used in this report. The basic Mueller matrices for polarization were obtained from Reference 11.

Light Sources: All sources are described by their Stokes vectors.

a) Unpolarized Source - $S = (1, 0, 0, 0)I_1$

b) Polarization Modulated LED source (defined in Appendix E)

$SL\ (0^o, 90^o) = \frac{1}{2}(I_1+I_2, I_1-I_2, 0, 0)$

$SL\ (45^o, -45^o) = \frac{1}{2}(I_1+I_2, 0, I_1-I_2, 0)$

where: I_1 and I_2 = Intensity of LED's 1 and 2

Polarizers: Polarizers resulting in a plane of polarization at an angle of θ degrees from the horizontal is written as $P(\theta^o)$.

$$P(-45^o) = \frac{1}{2}\begin{bmatrix} 1 & 0 & -1 & 0 \\ 0 & 0 & 0 & 0 \\ -1 & 0 & 1 & 0 \\ 0 & 0 & 0 & 0 \end{bmatrix}$$

$$P(+45^o) = \frac{1}{2}\begin{bmatrix} 1 & 0 & 1 & 0 \\ 0 & 0 & 0 & 0 \\ 1 & 0 & 1 & 0 \\ 0 & 0 & 0 & 0 \end{bmatrix}$$

Quarter Wave Plates: A quarter wave plate with its fast axis at θ degrees to the horizontal is written as $Q(\theta)$.

$$Q(0^o) = \begin{bmatrix} 1 & 0 & 0 & 0 \\ 0 & 1 & 0 & 0 \\ 0 & 0 & 0 & 1 \\ 0 & 0 & -1 & 0 \end{bmatrix}$$

$$Q(-45^o) = \begin{bmatrix} 1 & 0 & 0 & 0 \\ 0 & 0 & 0 & 1 \\ 0 & 0 & 1 & 0 \\ 0 & -1 & 0 & 0 \end{bmatrix}$$

Angle Sensing Crystals: An angle sensing crystal with sensitive axis at θ degrees from the horizontal is written as $ASC(\alpha, \theta)$, where α is the angle of incidence of light about the sensitive axis.

a) Regular ASC

$$ASC(\alpha, 0^o) = ASC(\alpha, 270^o) = \begin{bmatrix} 1 & 0 & 0 & 0 \\ 0 & \text{Cos } k\alpha & 0 & -\text{Sin } k\alpha \\ 0 & 0 & 1 & 0 \\ 0 & \text{Sin } k\alpha & 0 & \text{Cos } k\alpha \end{bmatrix}$$

$$ASC(\alpha, 90^o) = ASC(\alpha, 180^o) = \widetilde{ASC(\alpha, 0^o)} \quad \text{(transposed matrix)}$$

where k = Angle sensing crystal transfer function optical phase shift (radians or degrees) per angle of incidence (radians or degrees) .

Roll Matrix: The matrix used to rotate the transmitter through an angle θ_R relative to the receiver is given by

$$T^{-1} = \begin{bmatrix} 1 & 0 & 0 & 0 \\ 0 & \text{Cos } 2\theta_R & -\text{Sin } 2\theta_R & 0 \\ 0 & \text{Sin } 2\theta_R & \text{Cos } 2\theta_R & 0 \\ 0 & 0 & 0 & 1 \end{bmatrix}$$

Wollaston Prism: A wollaston prism resolving incomming radiation onto two orthogonal axes oriented at θ_1, degrees and θ_2 degrees is written as $W(\theta_1, \theta_2)$. The two spatially separated beams are distinguished by the ± 1 terms; a plus value for one beam and a minus one value for the other.

$$W(0^\circ, 90^\circ) = \tfrac{1}{2}\begin{bmatrix} 1 & \pm 1 & 0 & 0 \\ \pm 1 & 1 & 0 & 0 \\ 0 & 0 & 0 & 0 \\ 0 & 0 & 0 & 0 \end{bmatrix}$$

$$W(+45^\circ, -45^\circ) = \tfrac{1}{2}\begin{bmatrix} 1 & 0 & \pm 1 & 0 \\ 0 & 0 & 0 & 0 \\ \pm 1 & 0 & 1 & 0 \\ 0 & 0 & 0 & 0 \end{bmatrix}$$

Reference 11 - "Polarized Stellar Optical Spacecraft Attitude Sensor", Spicer, J.A. and Loebs, W.F., Chrysler Corporation Space Division IR&D Program CWO-890321/920332, March, 1968 (Unclassified).

APPENDIX B

FAR FIELD IRRADIANCE OF A LIGHT EMITTING DIODE AND LENS COMBINATION

1.0 THEORY

Referring to figure B-1( ), consider an extended luminous source at 0 placed behind the lens. The entrance pupil of the optical system will be considered to coincide with the lens. The flux passing through an arbitrary axial point, P, is the same as that flux passing through the image of P, denoted by P', considering only the radiation from the source which can pass through the entrance pupil, i.e., the flux at P is the same as the flux through P' created by an effective source area, Q, as shown in the figure, and considering only the flux which falls within the angular cone, $\pm 2\alpha$.

An incremental area, dS, at P will be imaged at P' as an area dS', where

$$dS = m^2 dS'$$

where m is the magnification experienced by a transverse line segment at P' as imaged at P. Therefore, the irradiance, E, or flux per unit area at the point P is obtained by dividing the irradiance at P' (considering only the effective source area) by the area magnification, m^2.

$$E = \frac{E^1}{m^2}$$

For an aplanatic system

$$m = \frac{\sin\alpha}{\sin\beta}$$

Therefore

$$E = E^1 \frac{\sin^2\alpha}{\sin^2\beta}$$

Where E^1 can be found by the usual integration

$$E^1 = \int_Q \frac{B dA \cos^4\theta}{r_o^2} = \iint \frac{B(\theta, X', Y') \cos^4\theta \, dx' \, dy'}{r_o^2}$$

X^1, Y^1 = coordinates on the source

$B(\theta, X^1, Y^1)$ = source brightness at X^1, Y^1 in the direction of the point P'

$\cos\theta = \hat{r} \cdot \hat{r}_o$ as shown in figure one (b)

r_o = distance of point P' from the source

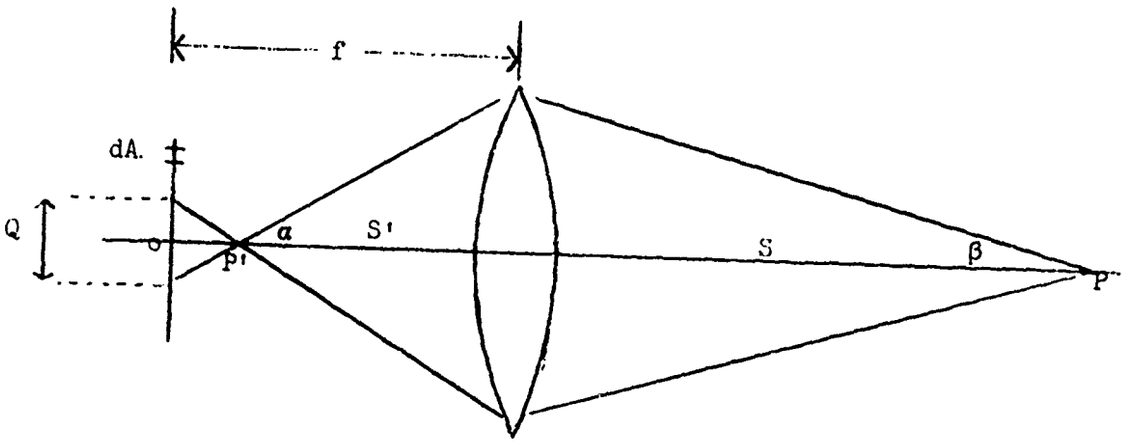

Figure B-1a, LED Collimator Parameters

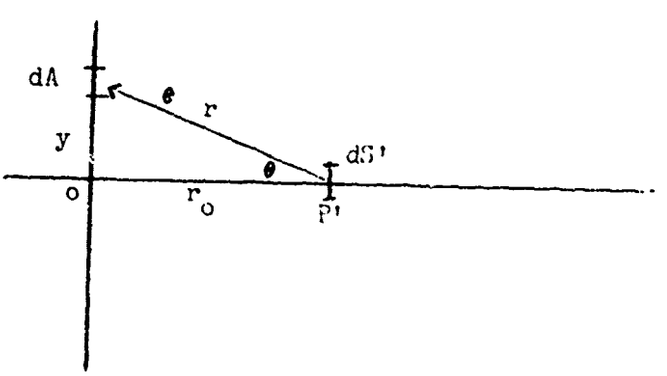

Figure B-1b, Coordinate System on LED side of Lens

2.0 Lambertian Sources

For a Lambertian source, for which the brightness is a constant and the radiant intensity $I(\theta)$ varies as the $\cos\theta$, the calculation for E^1 is greatly simplified.

$$B(\theta) = B_o = \text{constant} = \text{watts/cm}^2 \text{ sterad}$$

$$I(\theta) = I_o \cos\theta = \text{watts/sterad}$$

$$I_o = B_o A, \quad A = \text{total area of source}$$

$$E^1 = B_o \sin^2\alpha$$

and the irradiance at the point P becomes

$$E = B \sin^2\alpha \frac{\sin^2\beta}{\sin^2\alpha} = B_o \sin^2\beta$$

For the far field

$$\sin\beta \approx \tan\beta = \frac{D}{2S}$$

where D is the diameter of the lens and S is the range, the illumination becomes

$$E = B_o \frac{D^2}{4S^2}$$

For a Lambertian Source

$$B = \frac{I}{\pi A} = \frac{P_T}{\pi A}$$

where P_T is the total power radiated in a hemisphere, therefore, the axial irradiance becomes

$$E = \frac{P_T}{A} \frac{D^2}{4S^2}$$

The axial irradiance is a function only of the collimating lens diameter and is independent of focal length.

3.0 Non-Lambertian Sources

Non-Lambertian sources are treated as in section 1.0 except that the integration over the source must be performed. This requires detailed knowledge of the source brightness as a function of direction and position on the source emitting surface. In almost all cases the integral will have to be evaluated numerically.

A slight simplification can be obtained if it is assumed that the source is uniform and that the source brightness is constant over the source emitting area, i.e., the brightness is a function of direction only. It is now possible to define a function $\psi(\theta)$ which is the average radiance of the emitting surface.

$$\psi(\theta) = \frac{I(\theta)}{A}$$

which is related to the source brightness by

$$B(\theta) = \frac{I(\theta)}{A\cos\theta} = \frac{\psi(\theta)}{\cos\theta}$$

The radiance at the image point now becomes

$$E^1 = \int_Q \frac{B\,dA\cos^4\theta}{r_o^2}$$

$$= \int \frac{\psi(\theta)}{\cos\theta}\, 2\pi \frac{r_o^2 \tan\theta \sec^2\theta\, d\theta \cos^4\theta}{r_o^2}$$

$$= 2\pi \int_{Q=0}^{\alpha} (\theta) \sin\theta\, d\theta$$

$$= \frac{2\pi I_o}{A} \int_o N(\theta) \sin\theta\, d\theta$$

$$= \frac{2\pi I_o}{A} G(\alpha)$$

where $G(\alpha) = \int_o^{\alpha} N(\theta) \sin\theta\, d\theta$

and $N(\theta)$ is the normalized radiant intensity function. $I(0) = I_o N(\theta)$

This function, $N(\theta)$, must be obtained experimentally for non-Lambertian sources. For Lambertian sources $N(\theta) = \cos\theta$. The integration for $G(\alpha)$ must be numerically evaluated.

It is necessary to use the above approach because in many cases, i.e., LED's, one does not possess sufficient knowledge of the brightness, $B(\theta, x^1, y^1)$ of the light emitting area; and it becomes necessary to deduce an approximation to this function from the relatively far field intensity pattern. This approach essentially assumes that the source brightness is constant across the emitting surface or for that matter any beam cross-section near the emitting surface.

For example, in the case of a commercial LED with a small lens cap (approximately 5 - 10 mm focal length) placed above the emitting area, and usually a reflecting surface behind the emitter it is very difficult to determine the brightness function without the use of highly specialized equipment. A further complication arises from the fact that the brightness is non-uniform across the emitting area. A number of dark spots can usually be observed which are probably due to electrical contacts to the material, material property variations, and non-uniform heat sinking.

In such a case the only resource is to treat the device as a unit. The illuminated portion of the lens cap is considered to be the source area. This source area is then assumed to be of uniform brightness. This assumption is justified in that the lens focal length is usually large in comparison to the size of the emitting area (approximately .5 mm) and that multiple reflections occurring within the LED case tend to evenly distribute the light over the lens cap. Each element, dA', of the lens cap is then assumed to possess the same radiance function, $I(\theta)$, as the entire device. From this the function $G(\alpha)$ is obtained as shown above.

The irradiance at the point of interest, P, is obtained by dividing E^1 by the transverse magnification, i.e.,

$$E = \frac{2\pi I_o}{A} \quad G(\alpha) \frac{\sin^2\beta}{\sin^2\alpha}$$

If the axial intensity, I_o, is not known it can be calculated from the total power output of the source. The total energy radiated within a cone of half angle α is given by

$$P(\alpha) = 2\pi \int_o^\alpha I(\theta) \sin\theta \, d\theta \qquad I(\theta) = I_o N(\theta)$$

$$= 2\pi I_o G(\alpha)$$

The total energy emitted in a hemisphere is

$$P_T = 2\pi I_o G(\tfrac{\pi}{2})$$

$$\text{or} \quad I_o = \frac{P_T}{2\pi G(\pi/2)}$$

Therefore, the axial irradiance at point P is

$$E = \frac{P_T}{A} \frac{G(\alpha)}{G(\frac{\pi}{2})} \frac{\sin^2\beta}{\sin^2\alpha}$$

$$= \frac{P_T}{A} \frac{D^2}{4S^2} \frac{G(\alpha)}{G(\frac{\pi}{2})} \frac{1}{\sin^2\alpha}$$

The quantity in parentheses is the same as that for a Lambertian emitter. Referring to figure B-1(a) the angle α is inversely proportional to the lens focal length.

$$\sin\alpha \approx \tan\alpha = \frac{D}{2f}$$

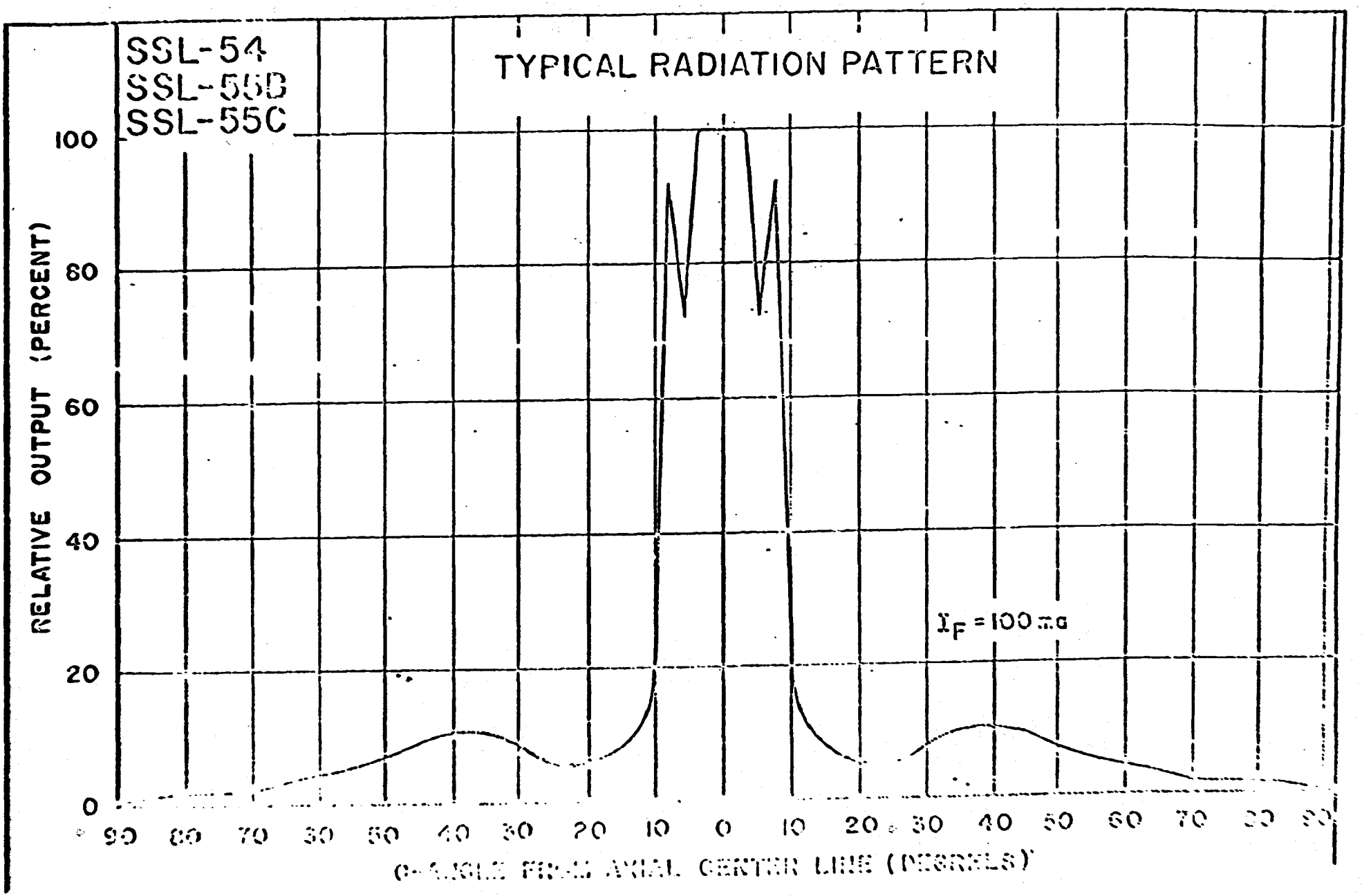

Figure B-2, Manufacturer's Data on LED Radiation Pattern

FLV 104

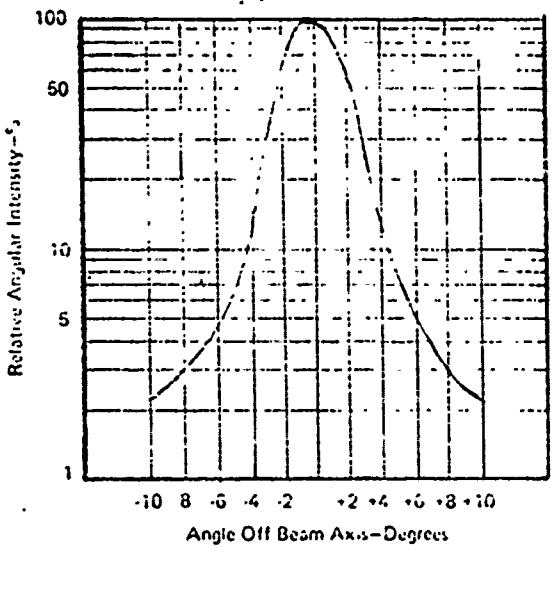

Figure B-3, Manufacturer's Data on LED Radiation Pattern

The term $G(\alpha)/G(\frac{\pi}{2})$ is the fraction of the total energy collected by the lens. This is an increasing function of α, and illustrates the obvious fact that for the same diameter lens, the collection efficiency is inversely proportional to focal length. The last term, $1/\sin^2\alpha$, represents a loss in energy flux density due to the magnification of the optics. As the focal length of the lens becomes shorter, the magnification increases and the energy from the source is spread over a larger area. In other words, referring to figure B-1(a), the same energy that passes through incremental area dS^1 also passes through incremental area dS. However, as the focal length becomes shorter (α becomes larger), the incremental area dS becomes larger. The same energy is spread over a larger area and the energy density is therefore reduced.

These last two contributions to the far field irradiance are counter acting, one causing an increase in intensity and othe other a decrease. In the case of a Lambertian emitter, these two terms exactly cancel, and the resulting far field irradiance is independent of focal length. For non-Lambertian sources, the value of α and hence focal length must be found for which the function

$$\frac{G(\alpha)}{\sin^2\alpha}$$

is a maximum. The optimum focal length is that corresponding to this value of

$$\tan\alpha = \frac{D}{2f}$$

NOTE: In many cases the optimum value of α and therefore the optimum focal length is not physically practical. For instance in most cases the function

$$\frac{G(\alpha)}{\sin^2\alpha}$$

reaches a maximum for very small values of α usually less than 1.0 degrees. This implies a very large focal length. In such cases a design should utilize the longest focal length consistent with the field of view requirements. For example, if the minimum half field of view is Φ, then the optimum focal should be chosen such that

$$f = \frac{d}{2\tan\Phi}$$

where d is the diameter of the source. Then the angle α is calculated by

$$\tan\alpha = \frac{D}{2f}$$

and this value of α used to determine $G(\alpha)$ and the far field irradiance.

TABLE B.1

INTEGRATED FLUX G(α) VS. ANGLE

G (α)

	GE SSL 55C	FLV 104 (FAIRCHILD)
0 degrees	0.00 X 10^{-3} mw	0.00 X 10^{-3} mw
.5	0.04	.08
1.0	0.15	.16
1.5	0.33	.32
2.0	0.60	.49
2.5	0.94	.67
3.0	1.36	.86
3.5	1.85	.99
4.0	2.38	1.11
4.5	2.94	1.18
5.0	3.53	1.25
5.5	4.15	1.30
6.0	4.77	1.34
6.5	5.56	1.38
7.0	6.41	1.42
7.5	7.33	1.45
8.0	8.42	1.49
8.5	9.58	1.52
9.0	10.4	1.56
9.5	11.1	1.59
10.0	11.8	1.62
15.0	13.9	1.95
20.0	15.7	1.95
40.0	30.0	
60.0	49.9	
80.0	59.2	
90.0	61.5	

4.0 Particular LED's and Their Application to OAMS

Two LED's with built in lens caps were investigated for their use in the transmitter. These units contain a light emitting area placed at the focus of a very small short focal length lens. The present application requires the LED to be placed at the focus of an external collimating lens. Maximum lens aperture is 1.5 cm. In this application the LED lens cap is considered to be the emitting area. The radiant intensity, $I(\theta)$, and power P_T is provided by the manufacturer. From these specifications it is necessary to calculate the function $G(\alpha)$ in order to obtain the far field intensity pattern.

The normalized radiant intensity patterns, $N(\theta)$, for two LED's are shown in figures B-2 and B-3, the Fairchild FLV104 emits in the red region of the visible spectrum and the GE SSL-55C is a near I.R. emitter. The function $N(\theta)$ $\sin\theta$ is calculated and tabulated as a function of θ. The function $G(\theta)$ is then calculated by means of a graphical integration of this tabulation, i.e.,

$$G(\alpha) = G(n\Delta\theta) = \sum_{i=1}^{n} N_i(\theta) \sin\theta_i \Delta\theta$$

The values of $G(\alpha)$ are shown in table B-1 for the ranges over which manufacturer data is available. The optimum value of α and hence focal length is that for which the function $G(\alpha)/\sin^2\alpha$ is a maximum. This occurs at about $\alpha = 1.0$ degree for the GE unit and less than 1.0 degree for the Fairchild unit. This represents an unreasonably large focal length. However, the next requirement of the system is that the total field of view of the system be at least 3.0 degrees. The maximum focal length then becomes

$$f = \frac{d}{2 \tan\Phi}$$

where d is the diameter of the lens cap, Φ is the half field of view. Also

$$\tan\alpha = \frac{D}{2f} = \frac{D}{d} \tan\Phi$$

The following illustrates the calculations for each LED.

<u>FLV104</u>

The manufacturer specifications are:

I_o = 4.0 mw/sterad

P_T = not specified

d = .188 cm

A = 1/4 d^2 = .028 cm^2

Φ = 1.50^o = .0263 rad

D = 1.5 cm

The required focal length is

$$f = \frac{d}{2 \tan\Phi} = \frac{0.188}{2 \times .0263} = 3.57 \text{ cm}$$

$$\tan\Phi = \frac{D}{2f} = \frac{1.5}{2 \times 3.57} = 0.210$$

$$\alpha = 11^{o}50' \quad \sin\alpha = .205$$

From the graph, the value of $G(\alpha)$ is found

$$G(11^{o}50') = 1.74 \times 10^{-3} \text{ mw}$$

The axial irradiance can then be found from

$$E = \frac{2\pi I_o}{A} \frac{G(\alpha)}{\sin^2\alpha} \frac{D^2}{45^2}$$

$$E = (8.95 \times 10^{2}) \frac{1.74 \times 10^{-3}}{0.042} \frac{1.5^2}{45^2}$$

$$= (8.95 \times 10^{2}) (4.15 \times 10^{-2}) (0.563) \frac{1}{S^2}$$

$$= 20.9 \times \frac{1}{S^2} \text{ mw/cm}^2$$

At S = 50 ft = 1.524×10^{3} cm

$$E = 9.0 \times 10^{-6} \text{ mw/cm}^2 \text{ @ 50 ft}$$

GE-SSL 55C

The manufacturer's specifications for this unit are as follows:

I_o = not specified

P_T = 19 mw @ 50 ft.

d = 0.396 cm

A = 0.0126 cm^2

Φ = 1.5^{o} = .0263 rad

D = 1.5 cm

$G(\frac{\pi}{2}) = 6.15 \times 10^{-2}$ mw

Since I_o is not specified the following equation is used

$$E = \frac{P_T}{A} \frac{G(\sigma)}{G(\frac{\pi}{2})} \frac{1}{\sin^2\alpha} \frac{D^2}{4S^2}$$

As in the previous example the focal length is found

$$f = \frac{d}{2 \tan\Phi} = 7.53 \text{ cm}$$

$$\tan\alpha = \frac{D}{2f} = 0.096$$

$$\sin\alpha = 0.096$$

$$= 5^{o}29'$$

From the graph, the function $G(\alpha)$ is found:

$$G(\alpha) = G(5^{o}29') = 4.15 \times 10^{-3} \text{ mw}$$

The axial radiant intensity is then

$$E = \frac{19}{0.126} \quad \frac{4.15 \times 10^{-3}}{6.15 \times 10^{-2}} \quad \frac{1}{0.0092} \quad \frac{2.25}{45^2}$$

$$= 626 \times \frac{1}{S^2}$$

$$= 2.69 \times 10^{-4} \text{ mw/cm}^2 \text{ @ 50 ft}$$

$$0.269 \text{ mw/cm}^2$$

GE SSL-55C (Modified) - Lambertian Source

This unit consisted of an SSL55C with the lens cap removed. In this case the LED behaves as a simple Lambertian emitter. The following are the manufacturer's specifications

$P_T = 19$ mw

$d = .025'' = .0635$ cm

$A = 40.3 \times 10^{-2}$ cm^2

$d_2 = .050'' = .127$ cm

$A_2 = 1.61 \times 10^{-2}$ cm^2

These units consist of an emitting area .025 in square placed within a small reflector of .050 in diameter. This reflector redirects toward the front the light which would normally be emitted and absorbed in the rear of the emitting surface. However, from the equation for axial radiant intensity in section 2.0, the pertinent parameter determining the far field radiation density is the radiation density at the emitting surface, i.e.,

$$\frac{P_T}{A}$$

One had the option of using the total reflector area as the source or just the center emitting area. In the first case the average energy density across the source will be less than that of just the emitting area since the energy is spread over a larger area. The energy density will have a relatively constant value across the reflector and then peak sharply in the center where the emitting area is located. This profile will also be projected into the far field of view. The angular spread of the more intense center portion will be inversely proportional to the focal length of the collimating lens. In the SAMSO application it is desired that the radiation density be as uniform as possible within the 3.0 degree field of view. Thus, only the emitting area is considered in calculating the far field radiant intensity. Also, the total power output should be derated since the light ordinarily emitted from the rear of the LED is not used.(This is probably a worst case consideration, since the inclusion (of) a reflector behind the LED emitting area will not be 100% efficient and double the forward power output). The far field radiant intensity will be given by

$$E = \frac{\frac{1}{2}P_T}{A_1} \quad \frac{D^2}{4S^2}$$

and the focal length by

$$F = \frac{d_1}{2 \tan\Phi} \quad , \quad \Phi = \tfrac{1}{2}FOV$$

For the modified GE SSL 55C, these values are: ($D = 1.5$ cm, $= 1.5^o$)

$$E = 1325 \times \frac{1}{S^2}$$

$$= 0.57 \times 10^{-3} \text{ mw/cm}^2$$

$$= 0.57 \text{ mw/cm}^2$$

$$f = 1.2 \text{ cm}$$

The required focal length is probably too small for a 1.5 cm diameter lens. This can be increased with the result that the axial intensity will remain the same but the intensity at the edge of the field of view will decrease to about 50%.

Appendix C

ELECTRONIC TIME SHARING SYSTEM

In the Optical Angular Motion Sensor program the initial concept was to utilize three colors, one for each channel. The design was predicated on GaAs LEDs for one wavelength and GaAlAs LEDs for the other two wavelengths. These LEDs were selected as a result of a development program by AFAL in which these diodes were developed and indicated an extremely long projected lifetime.

During the OAMS development program the vendor (TI) substituted GaAs Phosphide at these wavelengths with the promise that these were comparable in life and wavelength. Since they discontinued manufacture of GaAlAs LEDs the GaAsP was accepted for the OAMS program and were placed under test.

The test results showed that these LEDs dropped in output power by approximately 50% after 200 hours of operation. The same general pattern was again experienced during further testing.

This made the GaAsP LEDs unsuitable for use in a spacecraft which requires an expected lifetime of over three years for all components.

A study showed that it was possible to utilize one type source such as the GaAs LEDs for all three channels. But since they must be separated, this could be accomplished by time division multiplexing of both the transmitter channels and the respective receiver channels. This technique would permit using one type source and basically the same mechanical configuration as applied in the brassboard design.

The time division multiplexing was implemented in the brassboard as described in the following paragraphs.

Time Sharing Network Operation

The time sharing network operates from either a square wave or a sine wave input and provides self correcting timing for the three channel transmitters and for the channel output memory for sequential channel operation. (For electronic diagram, see figure C1).

First to be described will be the binary counter. An input signal is applied through capacitor C1 to a pulse shaping network consisting of amplifier A1 and the common emitter transistor stage containing transistor Q1. The output of the transistor stage provides a TTL logic compatible clock pulse to the first stage of the logic counter. The counter is arranged in the following manner. Binary elements FF-A through FF-E count in a straight binary with elements FF-B, C, D and E being synchronous and triggered from FF-A. Nand gates G1 through G8 provide the synchronous action.

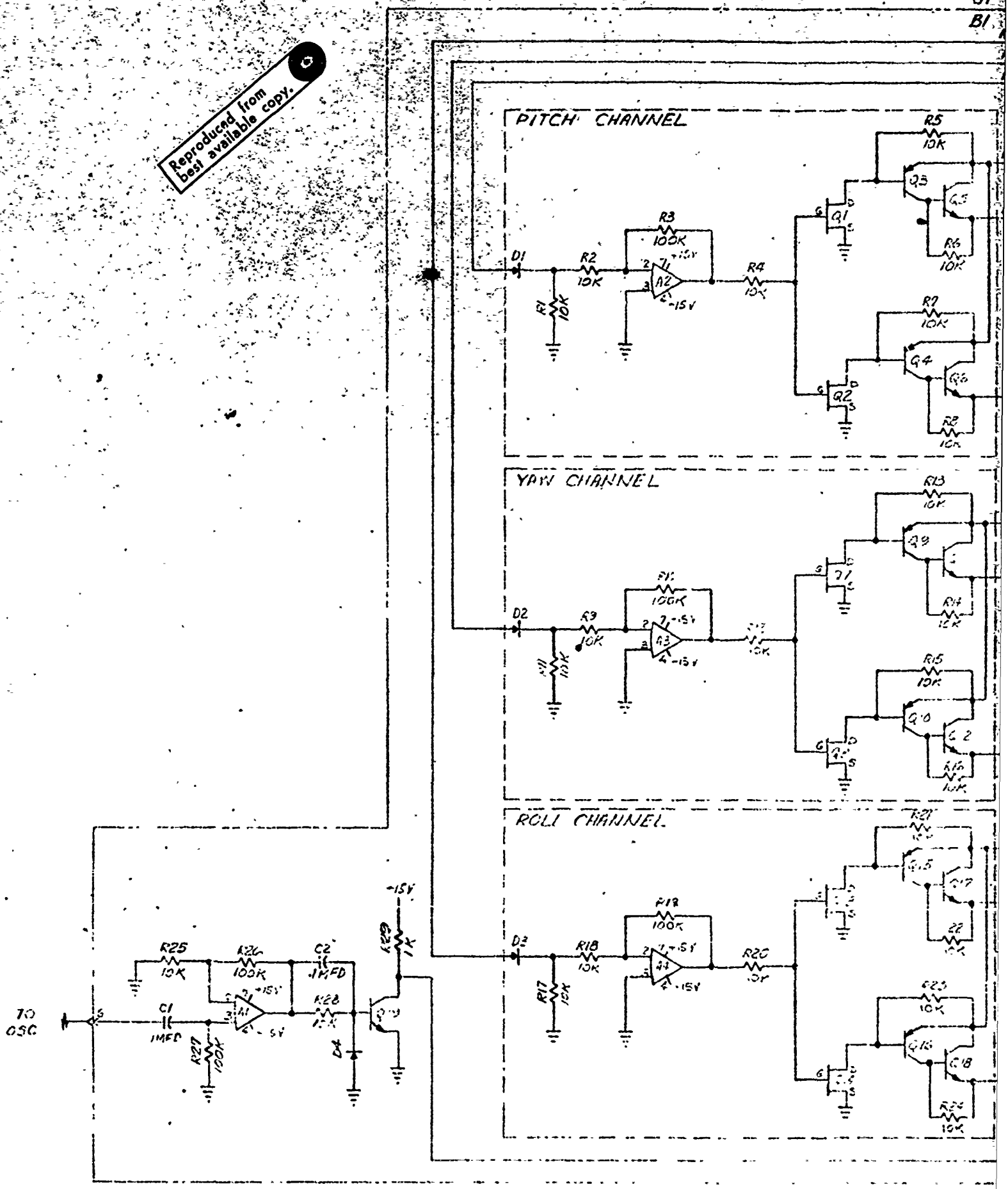

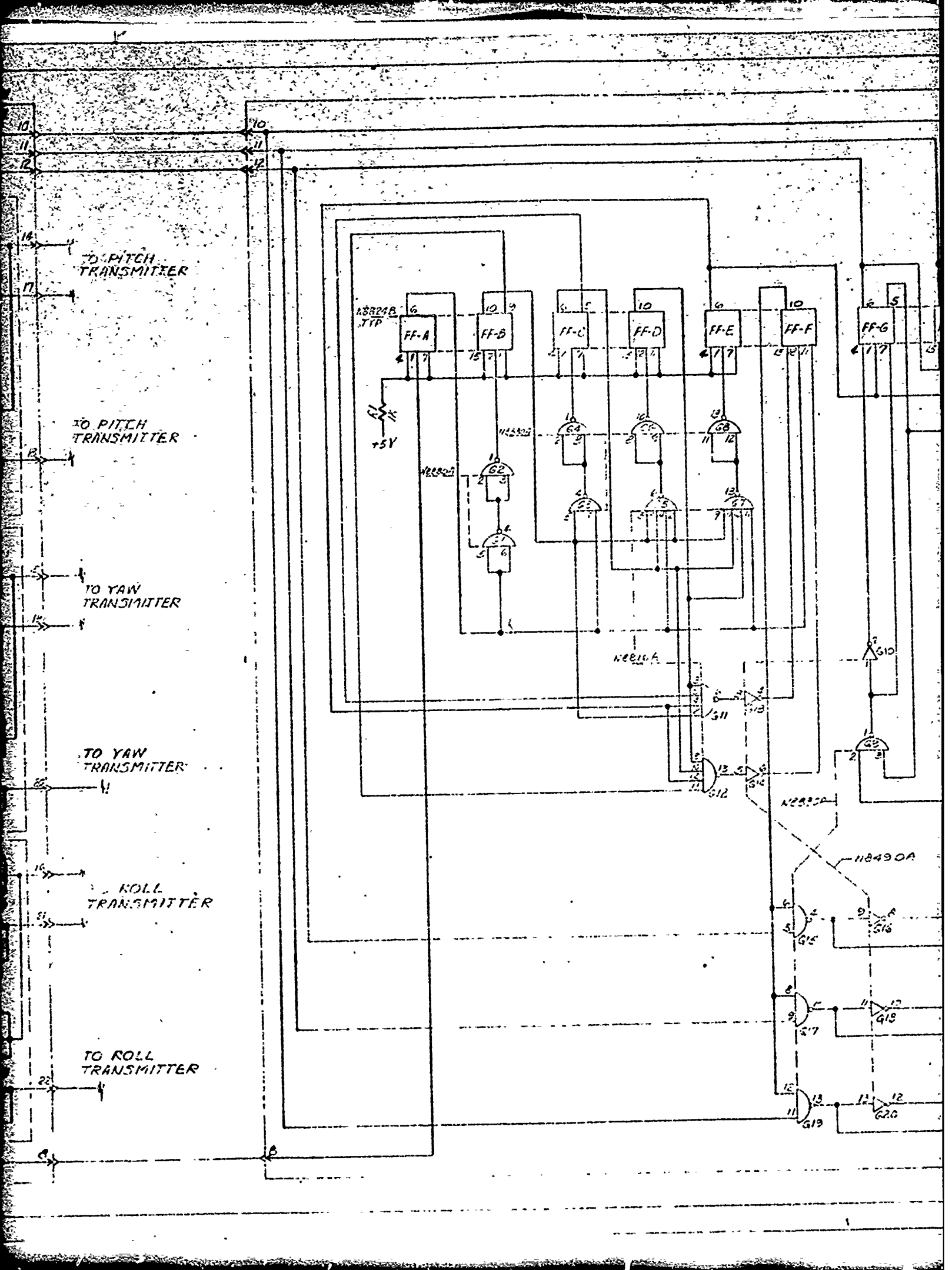
TO PITCH TRANSMITTER
TO PITCH TRANSMITTER
TO YAW TRANSMITTER
TO YAW TRANSMITTER
ROLL TRANSMITTER
TO ROLL TRANSMITTER
FF-A
FF-B
FF-C
FF-D
FF-E
FF-F
FF-G
+5V
G1
G2
G3
G4
G5
G6
G7
G8
G9
G10
G11
G12
G13
G14
G15
G16
G17
G18
G19
G20

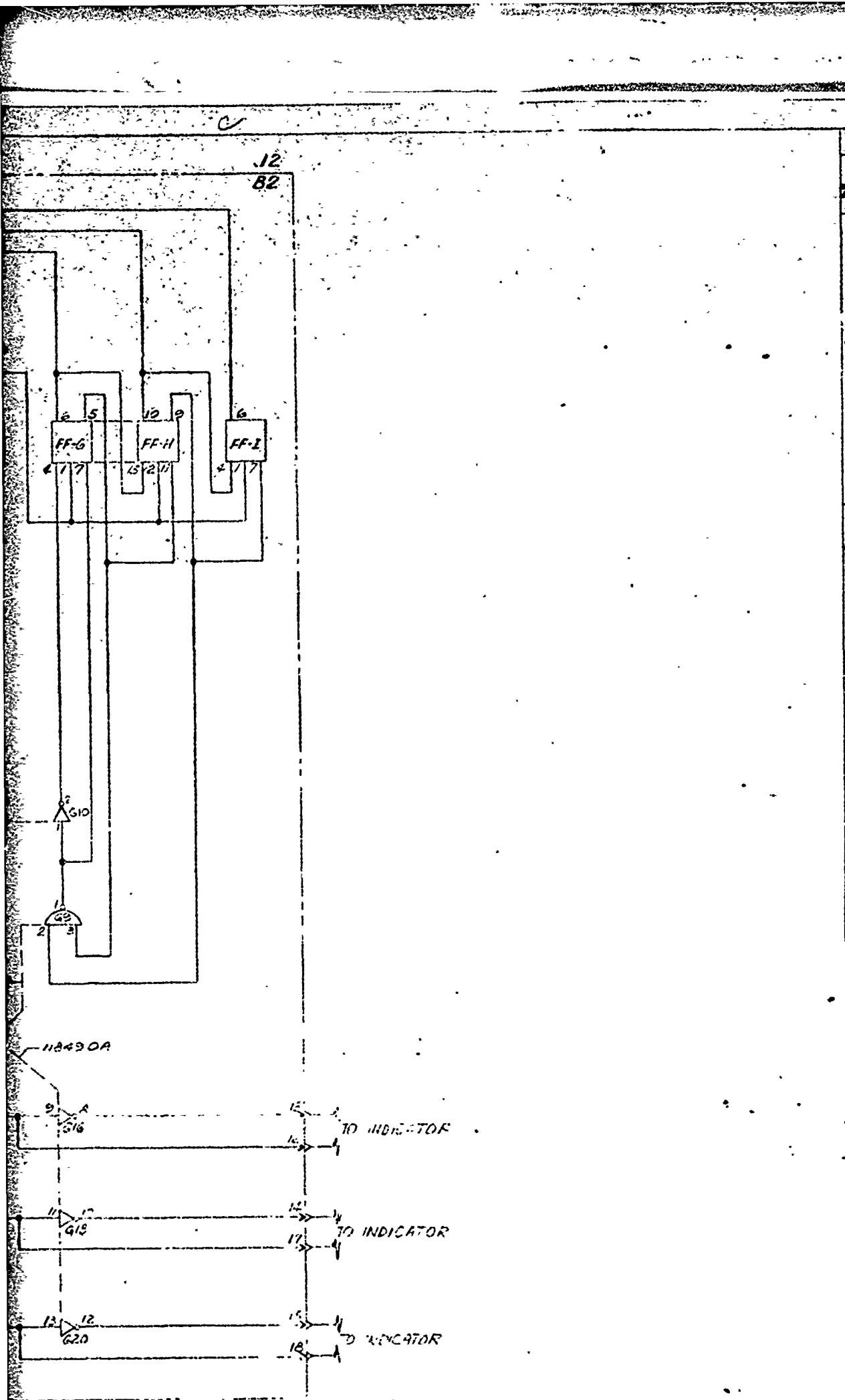
C
12
B2
FF-G
FF-H
FF-I
G10
G9
11A43OA
G16
TO INDICATOR
G19
TO INDICATOR
G20
TO INDICATOR
PAR
ITEM NO.
UNIT REQ'D
PART NUM
B1
B2
NOTES:
1
2

FIGURE C-1

NEXT ASSY NUMBER
SKC 899

PARTS LIST

BOARD NO.	ITEM NO.	QUANTITY REQD	PART NUMBER	DESCRIPTION	REMARKS
B1	R1,R2,R5,R6,R11,R13,R15,R16,R17,R18,R21,R22,R23,R24,R25,R26,R27,R28,R29,R30,R31,R32,R33,R34,R35,R36,R37,R38,R39,R40,R41,R42,R43,R44,R45,R46,R47,R48,R49,R50,R51,R52,R53,R54,R55,R56,R57,R58,R59,R60,R61,R62,R63,R64,R65,R66,R67,R68,R69,R70,R71,R72,R73,R74,R75,R76,R77,R78,R79,R80,R81,R82,R83,R84,R85,R86,R87,R88,R89,R90,R91,R92,R93,R94,R95,R96,R97,R98,R99,R100,R101,R102,R103,R104,R105,R106,R107,R108,R109,R110,R111,R112,R113,R114,R115,R116,R117,R118,R119,R120,R121,R122,R123,R124,R125,R126,R127,R128,R129,R130,R131,R132,R133,R134,R135,R136,R137,R138,R139,R140,R141,R142,R143,R144,R145,R146,R147,R148,R149,R150,R151,R152,R153,R154,R155,R156,R157,R158,R159,R160,R161,R162,R163,R164,R165,R166,R167,R168,R169,R170,R171,R172,R173,R174,R175,R176,R177,R178,R179,R180,R181,R182,R183,R184,R185,R186,R187,R188,R189,R190,R191,R192,R193,R194,R195,R196,R197,R198,R199,R200,R201,R202,R203,R204,R205,R206,R207,R208,R209,R210,R211,R212,R213,R214,R215,R216,R217,R218,R219,R220,R221,R222,R223,R224,R225,R226	23	10K	RESISTOR	
	R3	1	100K	RESISTOR	
	R4	1	1K	"	
	Q1,Q2,Q3,Q4,Q5,Q6	6	2N1684	TRANSISTOR	
	Q7	1	2N2222	"	
	Q8,Q9,Q10,Q11,Q12,Q13	6	2N1613	"	
	Q14	1	2N2907	"	
	C1	1	1MFD	CAPACITOR	
	C2	1	1MFD	"	
	U1,U2,U3,U4	4	741	AMPLIFIER	
	D1,D2,D3,D4	4	IN4154	DIODE	
B2	FF1,FF2,FF3,FF4,FF5	5	N8822B	BINARY	
	G1,G2,G3,G4,G5,G6,G7,G8,G9,G10,G11,G12	12	N8832A	GATE	
	G13,G14	2	N8832A	GATE	
	G15,G16	2	N8832A	GATE	
	R1	1	1K	RESISTOR	

NOTES:

1 BINARY; POWER DRIVE IS CONNECTED TO PIN 12
GROUND IS CONNECTED TO PIN 5

2 GATES; POWER DRIVE IS CONNECTED TO PIN 14
GROUND IS CONNECTED TO PIN 7

FIGURE C-1

Element FF-F provides a glitch-free trigger pulse at the proper time as required for each channel output memory. Nand gates G11, 12, 13 and 14 determine the time and length of the pulse. Binary elements FF-G, H and I sequentially provide a gate output for use in sequentially gating on the channel transmitters with binary element FF-E providing the trigger pulse.

Transmitter gating is the same for each channel and will be described in detail for the pitch channel. The inputs to diodes D1, D2 and D3 are either zero or plus five volts with only one of the three being high at a time. When the input to D1 is high, the pitch channel transmitter is gated on in the following manner. With plus five volts applied to diode D1, the output from inverting amplifier A2 will be in negative saturation with a voltage level approaching negative fifteen volts. This negative level will turn off FET transistors Q1 and Q2. In this condition, transistors Q3, Q4, Q5 and Q6 will also be turned off and current flow through the light emitting diodes will not be interrupted and the transmitter will operate in a normal manner.

When the positive gating voltage is removed from diode D1 and zero volts is applied, the output from amplifier A2 will be near zero. With this voltage applied to the gate of transistors Q1 and Q2, they will turn on transistors Q3, Q4, Q5 and Q6. Q3 and Q4 will be saturated and Q5 and Q6 will be on the verge of saturation. Since the collector to emitter voltage of transistors Q5 and Q6 is then less than the forward conduction voltage of the light emitting diodes, the driver currents will flow through the transistors and not through the diodes. Thus, the transmitter is turned off with no transient effect on the power supply. The yaw and roll channels operate in the same manner as each is gated on and off.

Signal output from each channel is converted in its corresponding panel meter to digital form and stored by the digital memory following an update command. Nand gates G15 and G20 update the panel meters with the display and corresponding digital output from each panel meter being the time shared outputs.

Time Sharing System Response Analysis

The time sharing system operates as a sample data system by alternately illuminating the individual axis LEDs for a duration of t seconds to allow the electronics to stabilize for a measurement. Since three axes are to be sampled in sequence, each channel is sampled every 3t seconds. The readout electronics to be analyzed is illustrated in figure C.2. It consists of a second order presample low pass filter, sample/hold circuit, and interpolation low pass filter.

FIGURE C.2 - READOUT ELECTRONICS

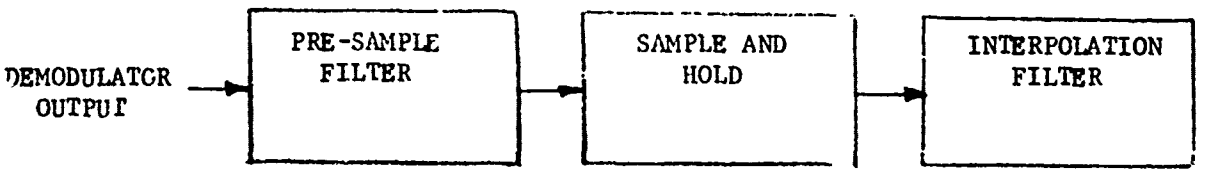

The output of the demodulator is a full wave rectified sine wave t seconds long occurring at a repetition rate of 1/3t pulses/second. The objective of the presample filter is to develop for each sample a voltage proportional to the sensor error signal. It is a second order filter with the following transform function:

$$(1)\quad \frac{C(s)}{R(s)} = \frac{\omega_n^2}{S^2+2\delta\,\omega_n S+\omega_n^2}$$

For $\delta<1$, the response of this filter to a step input is given by:

$$(2)\quad C(t) = 1 - \frac{e^{-\delta\omega_n t}}{(1-\delta^2)^{\frac{1}{2}}} \operatorname{Sin}\left[\omega_n t\,(1-\delta^2)^{\frac{1}{2}} + \tan^{-1}\frac{(1-\delta^2)^{\frac{1}{2}}}{\delta}\right],$$

which is a damped oscillatory response as illustrated in figure C.3.

FIGURE C.3 - DAMPED OSCILLATORY RESPONSE

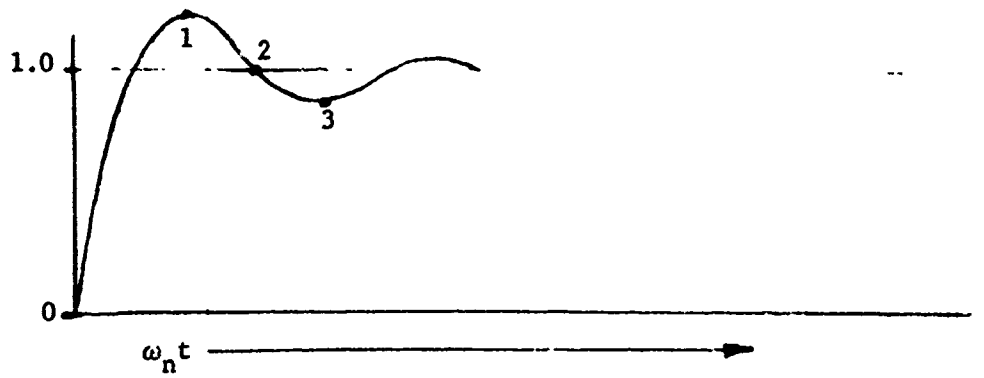

Values of $\omega_n t$ and % error for (1) first overshoot, (2) second crossover, and (3) first undershoot are listed in table C.1 for various values of damping factors .

TABLE C.1

DAMPING FACTOR δ	$\omega_n t$			% ERROR		
	1	2	3	1	2	3
0.6	3.9	6.7	7.8	9.5	0	.899
0.7	4.4	7.7	8.8	4.6	0	.211
0.8	5.2	9.4	10.4	1.5	0	.023
0.9	7.2	13.4	14.4	0.15	0	.300

The time required to reach the final value within a fixed tolerance and a given value of δ is an inverse function of the presample filter bandwidth as established by its break frequency $f_o = \omega_n/2\pi$.

The highest value of t is also limited by the required sample rate since $f_s = 1/3t$. Therefore, for a given filter, the lowest value of $\omega_n t$ consistent with desired accuracy is required. Candidates in table 1 most closely meeting the above criteria are $\omega_n t = 7.7$ ($\delta = .7$, point 2) and $\omega_n t = 7.2$ ($\delta = .9$, point 1). For the purpose of this analysis $\omega_n t = 7.7$ will be used in the following computations.

For $\omega_n t = 7.7$:

(3) $$f_s = \frac{2\pi f_o}{3(7.7)} = 0.272\ f_o$$

The value of f_s; and, therefore, f_o is dependent upon:

a) required response - 10 hz

b) rate of signal spectrum cutoff from 10 hz

c) allowable aliasing error

Sampling rates required for a signal aliasing error < 1% and 10 hz response are illustrated below for various assumed signal spectrum cutoff rates. The sampling rate (f_s) and related presample filter break frequency (f_o) for different rates of signal spectrum cutoff from 10 Hz are shown in table C.2.

TABLE C.2

RATE OF CUTOFF	f_s	f_o
12 db/octave	300 hz	1103 hz
18 db/octave	100 hz	368 hz
30 db/octave	50 hz	184 hz

Increasing the value of f_o increases the input noise spectrum to the sample/hold circuit. In addition to increased noise within the sampling bandwidth an aliasing power error is also introduced by the noise which is given by:

(4) $$V_a^2 = \int_{f_{s/2}}^{f_o} N^2(f)\ df = N^2(f)\ \left| f_o - f_{s/2} \right| ,$$

$N^2(f)$ = Constant noise power spectrum

and evaluated in table C.3

TABLE C.3

RATE OF CUTOFF	V_a^2
12 db/octave	954 $N^2(f)$
18 db/octave	318 $N^2(f)$
30 db/octave	159 $N^2(f)$

The need for rapid rate of signal spectrum cutoff is evident to minimize the level of noise in the time sharing system.

In summary, the time sharing system using the approach outlined in figure C.1 will experience an increased noise level over the continuous system. The magnitude of this increase is dependent upon the rate of signal spectrum cutoff and the bandpass of the low pass interpolation filter. If the signal spectrum can not be constrained within the 10 hz bandwidth and the illustrated rates of cutoff, signal aliasing error will increase beyond 1%. A corresponding increase in the sampling rate will then be required to maintain the 1% aliasing error. The higher sampling rate will also cause a further increase in the input noise spectrum to the sample/hold circuit.

APPENDIX D

MODULATED LED SYSTEMS

To overcome the disadvantages of an EOLM such as high voltage and fragile crystals(KD*P), a new concept for polarization modulation was developed. In the selection of sources the recent developments in the Light Emitting Diode field have made them the best available sources for OAMS application. Since they can be readily modulated, 2 systems of modulation are considered.

1. Intensity modulated LED's which employ polarization modulation to simulate EOLM operation was selected for the system and is described in Appendix E.

2. Intensity modulated LED's which employ no polarization modulation.

The modulated LED systems are systems with three separate axes for pitch, roll and yaw. Each axis will have its own light source/sources. The LED's are of small size and high efficiency and have ability to operate at high modulation frequencies.

Intensity Modulated LED's Which Employ No Polarization Modulation

A schematic diagram of a system employing intensity modulation with no polarization modulation is presented in figure D-1. In this system a single LED source in each axis is intensity modulated. Since each LED is driven at a different frequency, the angular information of the three axes is discriminated by narrow bandpass filtering. The optical design of the pitch and yaw axes are identical; one is simply twisted 90° relative to the other. The optical elements and their orientations are the same as those used in the pitch axis of the LED modulated system. The roll axis transmitter consists of a LED and plane polarizer. Its receiver consists of a plane polarization analyzer oriented at 45° to the polarization of the transmitter. The signal processing for this system is different from previously discussed systems and is presented in figure D-2.

Pitch Axis Transmitter

The pitch axis transmitter optics consists of a single LED light source, a plane polarizer, a quarter wave plate, and an angle sensing crystal.

The transmitter characteristics are obtained from the Meuller matrix expression

$$(1)\quad \text{PITCH SOURCE} = \left[AC(\alpha_1,\ 0^\circ)\right]\left[Q(0^\circ)\right]\left[P(45^\circ)\right]\left[S\right]$$

$$(2)\quad \text{PITCH SOURCE} = \begin{vmatrix} 1 \\ \text{Sin } k\alpha_1 \\ 0 \\ -\text{Cos } k\alpha_1 \end{vmatrix} \begin{vmatrix} \\ \frac{1}{2}I_p \text{Sin } W_p t \\ \\ \end{vmatrix},$$

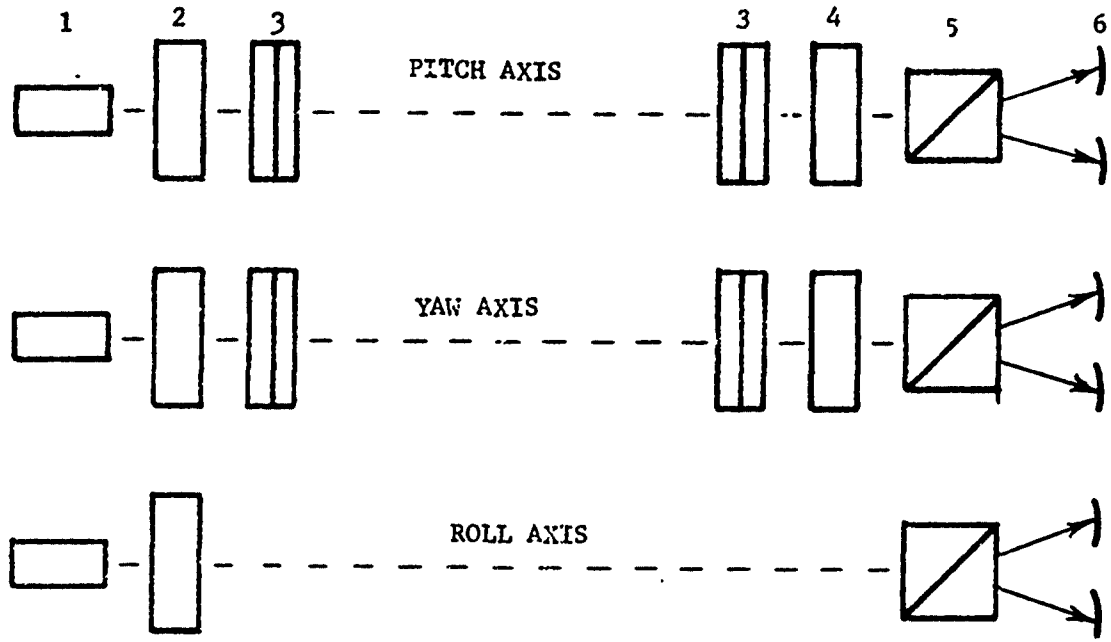

ITEM NUMBER	COMPONENT
1	LED LIGHT SOURCE
2	PLANE POLARIZER
3	REGULAR ANGLE SENSING CRYSTAL
4	QUARTER WAVE PLATE
5	WOLLASTON PRISM
6	DETECTORS

FIGURE D-1. INTENSITY MODULATED LED SYSTEM OPTICS

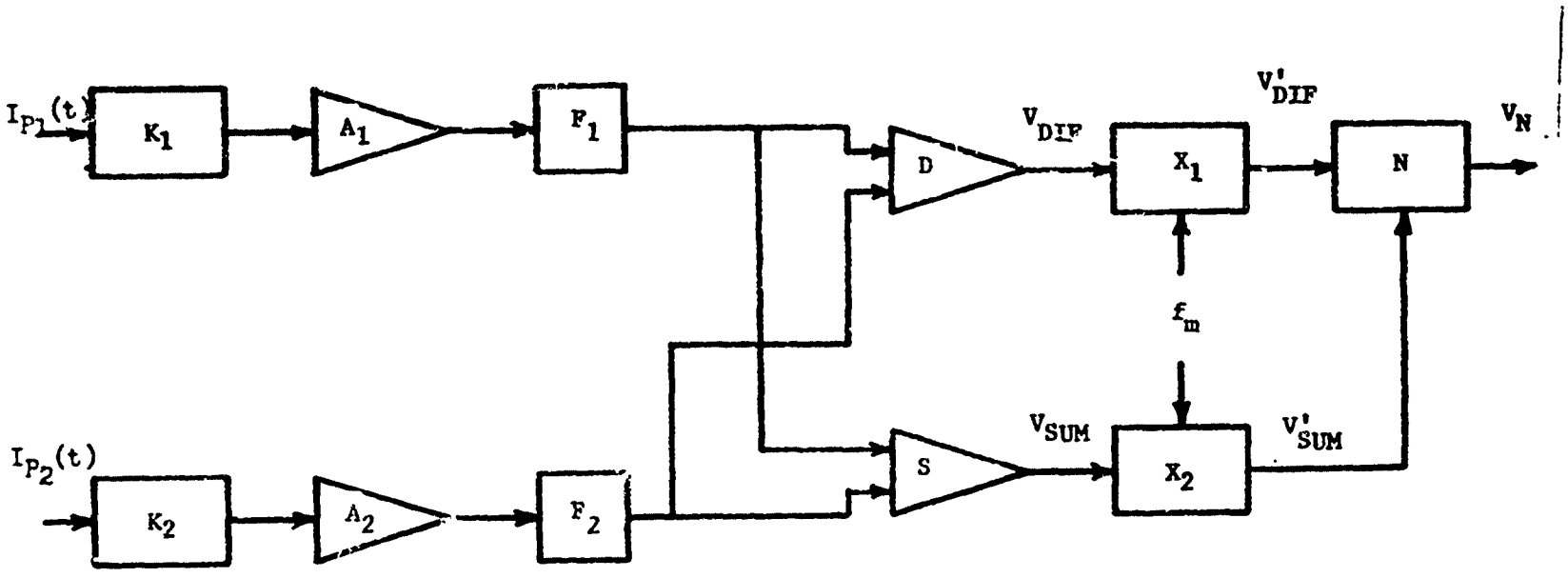

K_1 & K_2 - DETECTOR RESPONSIVITY
A_1 & A_2 - PREAMPLIFIER GAIN
S - SUMMING AMPLIFIER GAIN
D - DIFFERENTIAL AMPLIFIER GAIN
F_1 & F_2 - BAND PASS FILTER GAIN
N - AGC DIVIDER NETWORK GAIN
X_1 & X_2 - DEMODULATOR GAIN
f_m - MODULATION FREQUENCY

FIGURE 2 INTENSITY MODULATED LED SYSTEMS

where α_1 = pitch angle of the light beam relative to the transmitter angle sensing crystal

I_P = intensity of pitch axis source

W_P = angular frequency of pitch axis source

The roll angle, θ_R, of the transmitter relative to the target is introduced by use of the twist matrix T^{-1} which results in

$$(3) \quad \text{PITCH SOURCE} = \begin{vmatrix} 1 \\ \text{Sin } k\alpha_1 \text{ Cos } 2\theta_R \\ \text{Sin } k\alpha_1 \text{ Sin } 2\theta_R \\ -\text{Cos}k\alpha_1 \end{vmatrix} \frac{1}{2} I_P \text{Sin } W_P t$$

Yaw Axis Transmitter

The yaw axis transmitter optics are identical to the pitch axis except for the orientation of the angle sensing crystal sensitive axis. The yaw source output is given by

$$(4) \quad \text{YAW SOURCE} = \left[T^{-1}\right]\left[AC(B_1, 90^\circ)\right]\left[Q(0^\circ)\right]\left[P(45^\circ)\right]\left[S\right]$$

$$(5) \quad \text{YAW SOURCE} = \begin{vmatrix} 1 \\ -\text{Sin } k_{B1} \text{ Cos } 2\theta_R \\ -\text{Sin } k_{B1} \text{ Sin } 2\theta_R \\ \text{Cos } k_{B1} \end{vmatrix}$$

where B_1 = yaw angle of the light beam relative to the transmitter angle sensing crystal

I_Y = intensity of yaw axis LED

W_Y = angular frequency of yaw axis source

Roll Axis Transmitter

The roll axis transmitter optics consist of a LED light source and a plane polarizer. The foll axis output is given by

$$(6) \quad \text{ROLL SOURCE} = \left[T^{-1}\right]\left[P(45^\circ)\right]\left[S\right]$$

$$(7) \quad \text{ROLL SOURCE} = \begin{vmatrix} 1 \\ -\text{Sin } 2\theta_R \\ \text{Cos } 2\theta_R \\ 0 \end{vmatrix} \frac{1}{2} I_R \text{Sin } W_p t$$

where I_R = intensity of roll axis LED

W_R = angular frequency of roll axis source

Total Source

Each receiver axis sees an intensity which is the sum of the three transmitters and the unpolarized background. The effective total source is

$$(8) \quad \text{TOTAL SOURCE} = \left[\text{PITCH SOURCE}\right] + \left[\text{YAW SOURCE}\right] + \left[\text{ROLL SOURCE}\right] + \left[\text{BG}\right]$$

where BG = $(1, 0, 0, 0)I_{BG}$ is the unpolarized background matrix.

Pitch Axis Receiver

The pitch axis receiver optics consist of an angle sensing crystal and a Wollaston prism following by optics to focus the light onto the two detectors. The intensities of the two beams emerging from the Wollaston analyzer are given by the matrix expression.

$$(9) \quad \text{PITCH OUTPUT} = \left[W(0^\circ)\right]\left[AC(\alpha_2, 180^\circ)\right]\left[\text{TOTAL SOURCE}\right]$$

which results in

$$(10) \quad I_{P1} = \tfrac{1}{2}I_{BG} + \tfrac{1}{2}I_P\left[1+\text{Sin } k(\alpha_1 - \alpha_2)-ER1\right]\text{Sin } W_p t + (I_Y \text{ Sin } W_Y t \text{ term}) + (I_R \text{ Sin } W_R t \text{ term})$$

$$(11) \quad I_{P2} = \tfrac{1}{2}I_{BG} + \tfrac{1}{2}I_P\left[1-\text{Sin } k(\alpha_1 - \alpha_2)+ER1\right]\text{Sin } W_p t + (I_Y \text{ Sin } W_Y t \text{ term}) + (I_R \text{ Sin } W_R t \text{ term})$$

where I_{P1} and I_{P2} = intensities on detectors 1 and 2 respectively

$ER1 = \text{Sin } k\alpha_1 \text{ Cos } k\alpha_2 (1-\text{Cos } 2\theta_R)$

Pitch Axis Electronic Processing

The pitch output intensities are detected and preamplified to yield the outputs V_{P1} and V_{P2}.

$$(12) \quad V_{P1} = K_1A_1I_{P1} \text{ and } V_{P2} = K_2A_2I_{P2}$$

These signals are passed through bandpass filters F_1 and F_2 centered at W_P to yield V'_{P1} and V'_{P2}.

$$(13) \quad V'_{P1} = \tfrac{1}{2}F_1K_1A_1\ I_{BG}+\tfrac{1}{2}I_P\left[1+\text{Sin } k\theta_P-ER1\right]\text{Sin } W_p t$$

$$(14) \quad V'_{P2} = \tfrac{1}{2}F_2K_2A_2\ I_{BG}+\tfrac{1}{2}I_P\left[1-\text{Sin } k\theta_P+ER1\right]\text{Sin } W_p t$$

where F_1 and F_2 are the bandpass filter gains

The sum, V_{SUM}, and difference, V_{DIF}, outputs are given by

(15) $V_{SUM} = S\left\{V'_{P1}+V'_{P2}\right\} \qquad V_{DIF} = D\left\{V'_{P1}-V'_{P2}\right\}$

where S and D are the gains of the sum and difference amplifiers. These are then demodulated by networks X_1 and X_2 to yield

(16) $V'_{SUM} = \frac{1}{2}X_2\, S(F_1K_1A_1+F_2K_2A_2)I_P\left[1+2I_{BG}/I_P(t)+FK(\text{Sin } k\theta_P-ER1)\right]$

(17) $V'_{DIF} = \frac{1}{2}X_1\, D(F_1K_1A_1+F_2K_2A_2)I_P\left[\text{Sin } k\theta_P-ER1+FK(1+2I_{BG}/I_P(t)\right]$

where $FK = (F_1K_1A_1-F_2K_2A_2)/(F_1K_1A_1+F_2K_2A_2)$

The output of the AGC network is

(18) $V_N = N\,\dfrac{V'_{DIF}}{V'_{SUM}} = N\,\dfrac{X_1D}{X_2S}\left[\dfrac{\text{Sin } k\theta_P -ER1+ER2}{1+ER3+ER4}\right]$

where $ER1 = \text{Sin } k_1 \text{ Cos } k_2(1-\text{Cos } 2\theta_R)$

$ER2 = FK(1+2I_{BG}/I_P(t))$

$ER3 = 2I_{BG}/I_P(t)$

$ER4 = FK(\text{Sin } k\theta_R-ER1)$

The term ER1 contributes a negligible zero shift error of about 0.1 arc seconds. By optically filtering the input, the ER3 term also becomes negligible. The ER2 term is more serious. If the detector responsivity and detector preamplifier combination for both legs can be held constant so that $FK = 10^{-3}$, then the ER2 term can contribute an error as large as 2 arc seconds. The ER4 term contributes a negligible scale factor error.

Yaw Axis Receiver

The yaw axis receiver is identical to the pitch angle receiver except that its angle sensing crystal matrix is $AC(B_2,270^o)$ instead of $AC(\alpha_2, 180^o)$

Roll Axis Receiver

The roll axis receiver optics consist of a Wollaston prism followed by optics to focus the light onto the two detectors. The intensities of the two beams emerging from the Wollaston analyzer are given by the maxtrix expression

(19) ROLL OUTPUT $= \left[W(0^o)\right]\left[\text{TOTAL SOURCE}\right]$

which results in

(20) $I_{R1} = \frac{1}{2}I_R(1-\text{Sin } 2\theta_R)\text{ Sin } W_Tt+\frac{1}{2}I_P(1+\text{Sin } k\alpha_1 \text{ Cos } 2\theta_R)\text{ Sin } W_Pt$

$+\frac{1}{2}I_Y(1-\text{Sin } kB_1 \text{ Cos } 2\theta_R)\text{ Sin } W_Yt + \frac{1}{2}I_{BG}$

(21) $I_{R2} = \frac{1}{2}I_R(1+\sin 2\theta_R)\sin W_T t + \frac{1}{2}I_P(1-\sin k\alpha_1 \cos 2\theta_R)\sin W_P t$

$+\frac{1}{2}I_Y(1+\sin kB_1 \cos 2\theta_R)\sin W_Y t + \frac{1}{2}I_{BG}$

These intensities are detected and processed electronically exactly as they were for the pitch axis. The roll angle output is given by

(22) $V_N = N\frac{X_1 D}{X_2 S}\frac{\sin 2\theta_R - ER5}{1+ER6}$

where $ER5 = FK(1+2I_{BG}/I_R)$

$ER6 = FK \sin 2\theta_R + 2I_{BG}/I_R$

$FK = (F_1K_1A_1 - F_2K_2A_2)/(F_1K_1A_1 + F_2K_2A_2)$

Here, as in the case of the pitch and yaw axes, the FK term in the numerator of Equator 22 is the dominant error term. If $FK \approx 2 \times 10^{-5}$ then an error of 2 arc seconds can occur. The weakness of this intensity modulated system is the accuracy to which the detector responsivity, preamp balance, FK, must be held.

APPENDIX E

OAMS ERROR ANALYSIS

The intent of this analysis is to develop a mathematical model of the OAMS system concept to permit identification and evaluation of potential sensor error sources. The OAMS optical model development contained herein uses Mueller matrices to determine the first order optical signal characteristics of the radiation sensed by each detector contained in the sensor. With this information an analysis of the sensor, including its electronics, can be made to illustrate the sensor performance capabilities and limitations.

1.0 OPTICAL MODEL DEVELOPMENT

The OAMS system concept utilizes three independent optical systems to measure relative angle about three (3) orthogonal axes between the transmitter and receiver assemblies. To eliminate cross coupling the light sources for each axis operate at different wavelengths and modulation frequencies. The sensor consists of two identical and orthogonal lateral sensing systems (one for pitch and one for yaw) and one roll sensing system.

The following is a mathematical model development for the OAMS transmitter and sensing systems to define the optical signal characteristics of the radiation sensed by each detector.

1.1 LED Polarization Modulated Source

The light source in this concept is designed to give a sinusoidally varying polarization output while yielding a constant total intensity output. It consists of two sinusoidally driven LED's and a Wollaston prism as shown in Figure E-1. Unpolarized light from LED #1 is divided by the Wollaston prism into two beams, one vertically polarized and one horizontally polarized. Unpolarized light from LED #2 is also divided by the Wollaston prism into a horizontally and a vertically polarized beam. These beams are directed in such a way that two of the four resulting beams combine to form a central beam which is the net transmitter output. The other two divergent beams are masked off and are not allowed to combine in the transmitter output.

If each LED is driven by a sinusoidally varying current of $i_1(t) = i_{b1}+i_{m1}\text{Sin}\,\omega t$ and $i_2(t) = i_{b2}- i_{m2}\text{Sin}\,\omega t$, the polarized illumination output of the two beams may be expressed as:

(1) $I_H = \frac{1}{2}I_1=\frac{1}{2}R_1 \left[i_{b1}+i_{m1}\text{Sin}\,\omega t\right]$

(2) $I_V = \frac{1}{2}I_2=\frac{1}{2}R_2 \left[i_{b2}-i_{m2}\text{Sin}\,\omega t\right]$

where I_H and I_V refer to the intensities polarized horizontally and vertically respectively, R is the LED responsivity, and I is the unpolarized LED output, i_b is the LED DC bias current level, i_m is the modulation peak current level, and subscripts are for LED's 1 and 2.

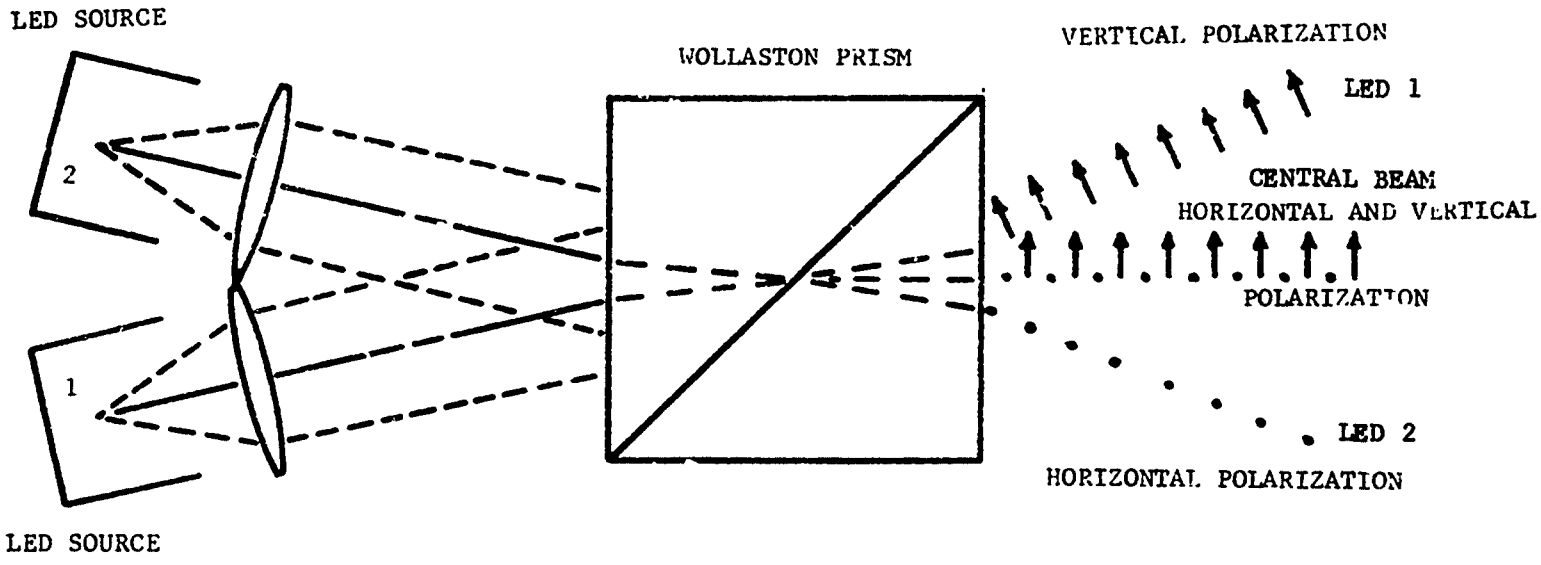

LED UNPOLARIZED OUTPUTS

$$I_1(t) = R_1 \ (i_{b1}+i_{m1} \ \mathrm{Sin}\omega t)$$

$$I_2(t) = R_2 \ (i_{b2}-i_{m2} \ \mathrm{Sin}\omega t)$$

STOKES VECTOR OF CENTRAL BEAM
FOR $R_1=R_2=R$ and $i_{b1}=i_{b2}=i_{m1}=i_{m2}=i$

$$\begin{pmatrix} I_H + I_V \\ I_H - I_V \\ 0 \\ 0 \end{pmatrix} = Ri \begin{pmatrix} 1 \\ \mathrm{Sin}\ wt \\ 0 \\ 0 \end{pmatrix}$$

POLARIZATION MODULATED TWIN LED SOURCE
FIGURE E-1

We can now construct the Stokes vector describing this source. Assume that $R_1=R_2=R$ and $i_{b1}=i_{b2}=i_{m1}=i_{m2}=i$, then the total source output is:

(3) $$I_H+I_V = \tfrac{1}{2}Ri(1+\sin\omega t) + \tfrac{1}{2}Ri(1-\sin\omega t) = Ri$$

The total source output is constant.

The horizontal-vertical polarization preference is given by:

(4) $$I_H-I_V = \tfrac{1}{2}Ri(1+\sin\omega t) - \tfrac{1}{2}Ri(1-\sin\omega t) = Ri\sin\omega t$$

which means that the polarization is sinusoidally modulated.

Since the $\pm 45^\circ$ components and the right and left hand circular components are zero, then the Stokes vector is given by:

(5) $$\left[SL(0^\circ, 90^\circ)\right] = \begin{bmatrix} I_H + I_V \\ I_H - I_V \\ 0 \\ 0 \end{bmatrix} = \begin{bmatrix} I_1 + I_2 \\ I_1 - I_2 \\ 0 \\ 0 \end{bmatrix} = \begin{bmatrix} Ri \\ Ri\sin\omega t \\ 0 \\ 0 \end{bmatrix}$$

1.2 Lateral Axis

An optical schematic diagram of the lateral axis sensing system is illustrated in Figure E-2. The transmitter consists of a Wollaston prism (W_T) whose planes of polarization are oriented at $\pm 45^\circ$ to combine the light from two (2) amplitude modulated light emitting diode (LED) sources such that the light from one source is polarized in a plane at $+45^\circ$ while that from the other source is polarized in a plane at -45°. A quarter ($\lambda/4$) waveplate is subsequently used to convert the linear polarized light to circular polarized light. The light is then passed through the first of two matched angle sensing crystals (ASC_T). The second matched crystal (ASC_R) is contained in the receiver followed by a Wollaston prism (W_R) The stokes vector of the central beam in this case is given by:

(6) $$\left[SL(45^\circ, -45^\circ)\right] = \tfrac{1}{2}\begin{bmatrix} I_1 + I_2 \\ 0 \\ I_1 - I_2 \\ 0 \end{bmatrix}$$

where

(7) $$I_1 = R_1(i_{b1}+i_{m1}\sin\omega t)$$

(8) $$I_2 = R_2(i_{b2}-i_{m2}\sin\omega t)$$

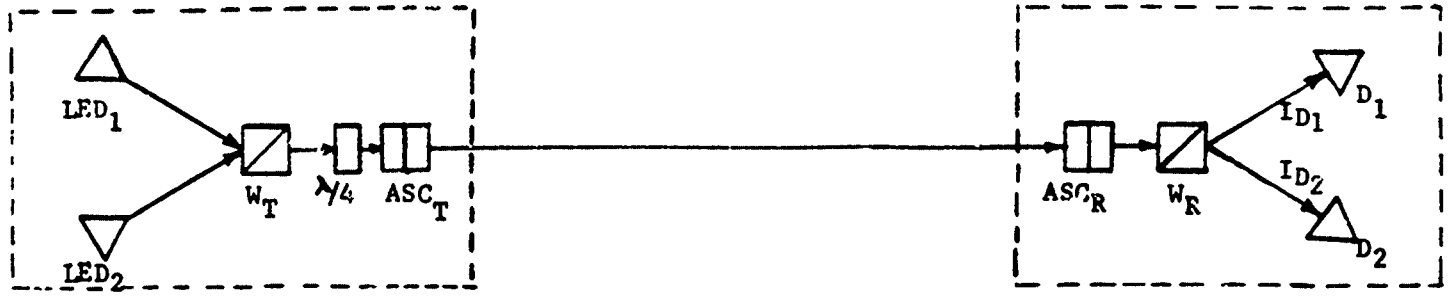

LED - LIGHT EMITTING DIODE
W_T - WOLLASTON PRISM - TRANSMITTER
W_R - WOLLASTON PRISM - RECEIVER
$\lambda/4$ - QUARTER WAVEPLATE
ASC_T - ANGLE SENSING CRYSTALS - TRANSMITTER
ASC_R - ANGLE SENSING CRYSTALS - RECEIVER
D - DETECTORS

FIGURE E-2

LATERAL AXIS OPTICAL SCHEMATIC

and I = LED output intensity
i_b = LED D.C. bias current
i_m = LED peak modulation current
R = LED responsivity
ω = modulation frequency
1 and 2 = subscripts for LED #1 and LED #2.

Expressions 7 and 8 reflect the fact that the d.c. bias current and the a.c. modulation current are set independently. We cannot set $i_m=i_b$ since LED operation is not linear at very low current levels. Thus i_b must be greater than i_m.

The light leaving the transmitter after passing through the $\lambda/4$ waveplate and first angle sensing crystal (ASC_T), may be found by the following matrix equation:

(9) $$\text{LATERAL OUTPUT} = \left[\text{ASC}(\alpha,\ 0^\circ)\right]\ \left[Q(90^\circ)\right]\ \left[\text{SL}(+45^\circ,\ -45^\circ)\right]$$

(10) $$\text{LATERAL OUTPUT} = \tfrac{1}{2}\begin{bmatrix} I_1 + I_2 \\ 0 \\ (I_1 - I_2)\text{Sin } k\alpha \\ (I_1 - I_2)\text{Cos } k\alpha \end{bmatrix}$$

where: α - Angle of incidence of light about the sensitive axis of the transmitter angle sensing crystal.

κ - Optical gain of angle sensing crystal-optical phase shift (radians or degrees) per angle of incidence (radians or degrees).

To define the light arriving at the receiver the expression for the light leaving the transmitter must be modified to include unpolarized background light and relative rotation about the roll axis.

Light arriving at the receiver may be found by the following matrix equation

(11) $$\text{LATERAL INTENSITY} = \left[T^{-1}\right]\left[\text{LATERAL OUTPUT}\right] + \left[I_{BG}\right]$$

(12) $$\text{LATERAL INTENSITY} = \tfrac{1}{2}\begin{bmatrix} I_1 + I_2 + 2I_{BG} \\ (I_1 - I_2)\text{Sin } k\alpha\text{Sin } 2\theta_R \\ (I_1 - I_2)\text{Sin } k\alpha\text{Cos } 2\theta_R \\ (I_1 - I_2)\text{Cos } k\alpha \end{bmatrix}$$

where: I_{BG} = unpolarized background radiation

θ_R = roll axis relative attitude error about line of sight between transmitter and receiver

The lateral axis receiver consists of an angle sensing crystal (matched to the transmitter angle sensing crystal) and a Wollaston prism. An optical filter is also included to filter out radiation of the other two axes and background radiation. The light impinging on each detector (I_{D1} and I_{D2}) is determined by:

(13) $$\left|\text{LATERAL OUTPUT}\right| = \left|W(\pm 45^{o})\right| \left|\text{ASC}(\beta, 90^{o})\right| \left|\text{LATERAL INTENSITY}\right|$$

(14) $$I_{D1} = \tfrac{1}{2}(I_1+I_2+2I'_{BG}) + \tfrac{1}{2}(I_1-I_2) \left|\text{Sin } k\theta\text{-Sin } k\alpha\text{Cos } k\beta(1\text{-Cos } 2\theta_R)\right|$$

(15) $$I_{D2} = \tfrac{1}{2}(I_1+I_2+2I'_{BG}) - \tfrac{1}{2}(I_1-I_2) \left|\text{Sin } k\theta\text{-Sin } k\alpha\text{Cos } k\beta(1\text{-Cos } 2\theta_R)\right|$$

where: β = angle of incidence of light about the sensitive axis of the receiver angle sensing crystal

$\theta = \alpha-\beta$ = lateral axis - relative attitude error

I'_{BG} = background radiation within the spectral bandpass of the optical filter

It is assumed in expression 13 that only a negligible amount of radiation from the other two axes is transmitted by the optical filter. Any radiation that is transmitted will be attenuated further by electronic filtering and will not affect the output.

1.3 Roll Axis

An optical schematic diagram of the roll axis sensing system is illustrated in Figure E-3. As previously discussed for the lateral axis a Wollaston prism (W_T) is also used for the roll axis to combine the amplitude modulated light from the two LED sources. Another Wollaston prism (W_R), is used in the receiver to analyze the incoming light to determine the relative misalignment about the roll axis.

As previously shown for the lateral axis, the light from the LED combiner Wollaston prism (W_T) may be defined by the following column matrix.

(16) $$SL(45^{o}, -45^{o}) = \tfrac{1}{2}\begin{bmatrix} I_1 + I_2 \\ 0 \\ I_1 - I_2 \\ 0 \end{bmatrix}$$

where: $I_1 = R_1(i_{b1} + i_{m1}\,\text{Sin}\omega t)$

$I_2 = R_2(i_{b2} - i_{m2}\,\text{Sin}\omega t)$

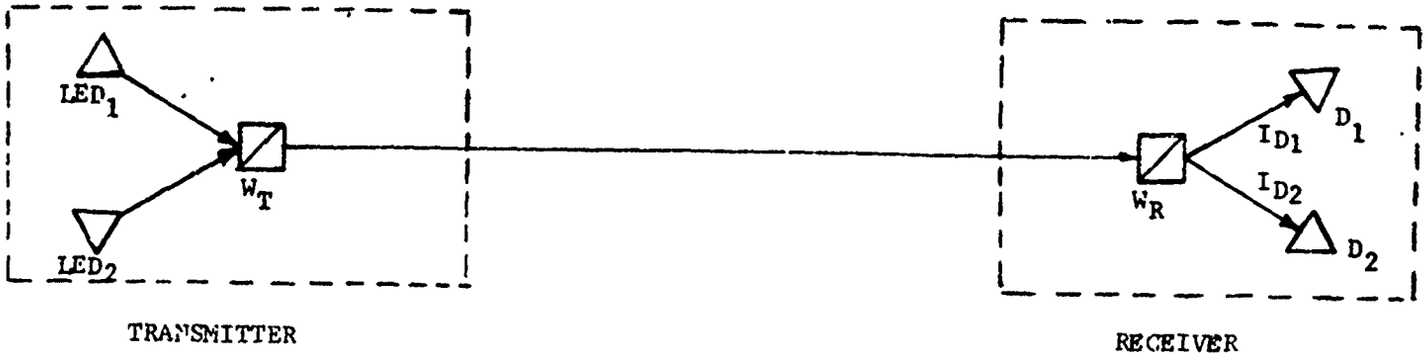

LED - LIGHT EMITTING DIODE
W_T - WOLLASTON PRISM - TRANSMITTER
W_R - WOLLASTON PRISM - RECEIVER
D - DETECTORS

FIGURE E-3

ROLL AXIS OPTICAL SCHEMATIC

The light impinging on each detector after passing through the receiver Wollaston prism (W_R), considering unpolarized background and relative rotation about the roll axis, may be found by the following matrix equation.

$$(17) \quad \left[\text{ROLL OUTPUT}\right] = \left[W(0^o, 90^o)\right] \left[T^{-1}\right] \left[SL(-45^o, +45^o)\right] + \left[I_{BG}\right]$$

$$(18) \quad I_{D1} = \tfrac{1}{2} \left[(I_1+I_2+2I'_{BG}) + (I_1-I_2)\text{Sin } 2\theta_R\right]$$

$$I_{D2} = \tfrac{1}{2} \left[(I_1+I_2+2I'_{BG}) - (I_1-I_2)\text{Sin } 2\theta_R\right]$$

2.0 CAMS ELECTRONIC MODEL DEVELOPMENT

A schematic diagram of the electronic signal processing system for one axis is illustrated in figure E-4. The same system is used for each axis of the sensor. The electronic signal processing techniques utilized by Chrysler obtain a sum and difference of the detector outputs to extract a unique error signal representing the relative attitude error. Assuming linear gain transform functions the sum and difference output voltages may be expressed as:

$$(19) \quad V_D = D \left[I_{D1} K_1 A_1 - I_{D2} K_2 A_2\right]$$

$$(20) \quad V_S = S \left[I_{D1} K_1 A_1 + I_{D2} K_2 A_2\right]$$

The difference output is used to obtain the relative difference in angle between the transmitter and receiver. The sum output provides a measure of the total light received by the two detectors and is generally used to provide an automatic gain control (AGC) to compensate for light level and detector responsivity changes.

At this point, consider the basic wave forms appearing in the system. This discussion applies equally to the lateral or roll axes, but for the sake of clarity only the roll will be discussed. Figure E-5 presents the LED outputs described by expressions 1 and 2. These are simply LED intensities sinusoidally driven 180° out of phase. Feedback loops are employed to insure that the amplitudes as measured by the receiver are equal. The sum of these intensities will then be a D.C. level as shown.

FIGURE E-4

. OAMS ELECTRONIC FUNCTIONAL BLOCK DIAGRAM

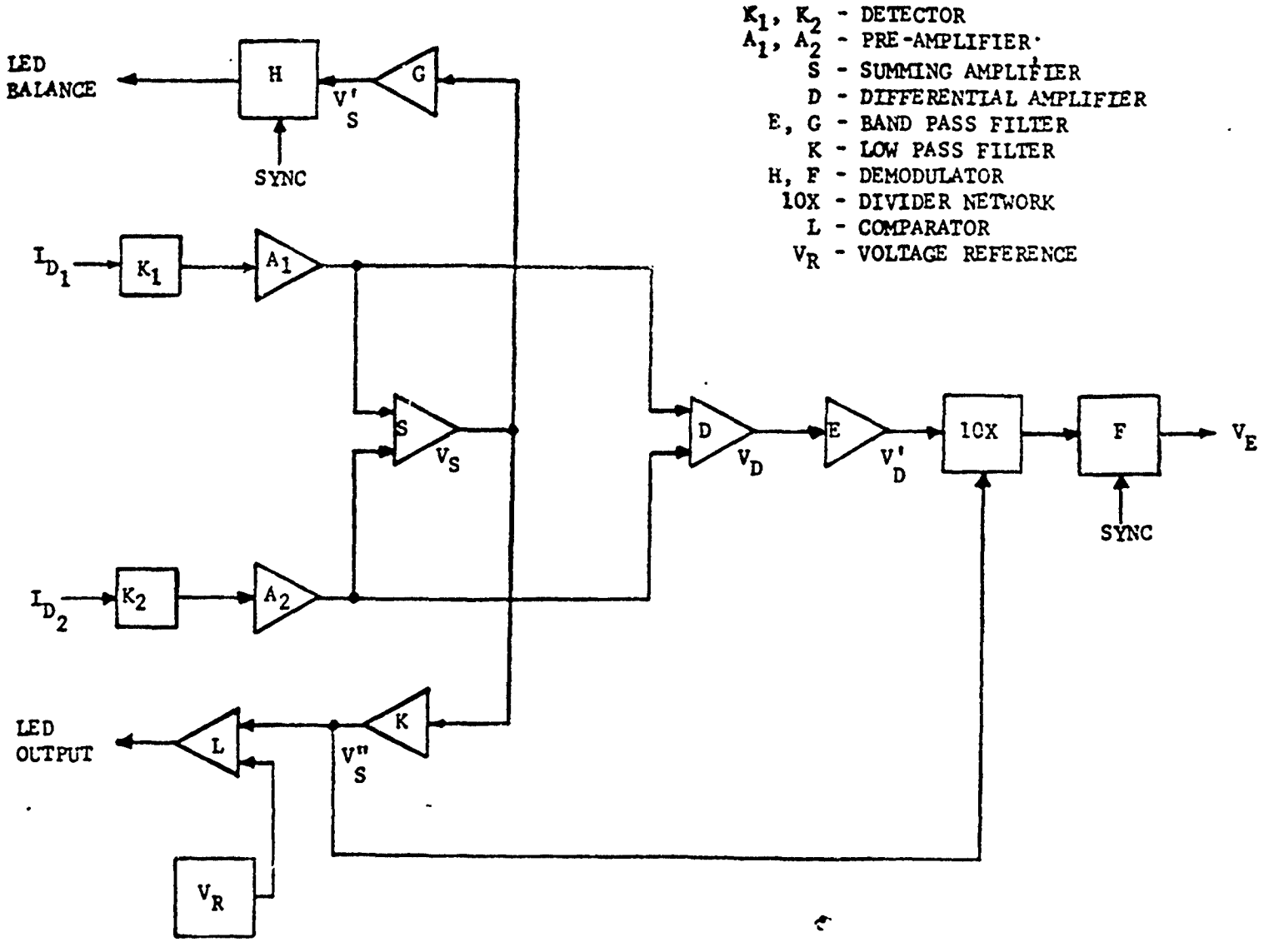

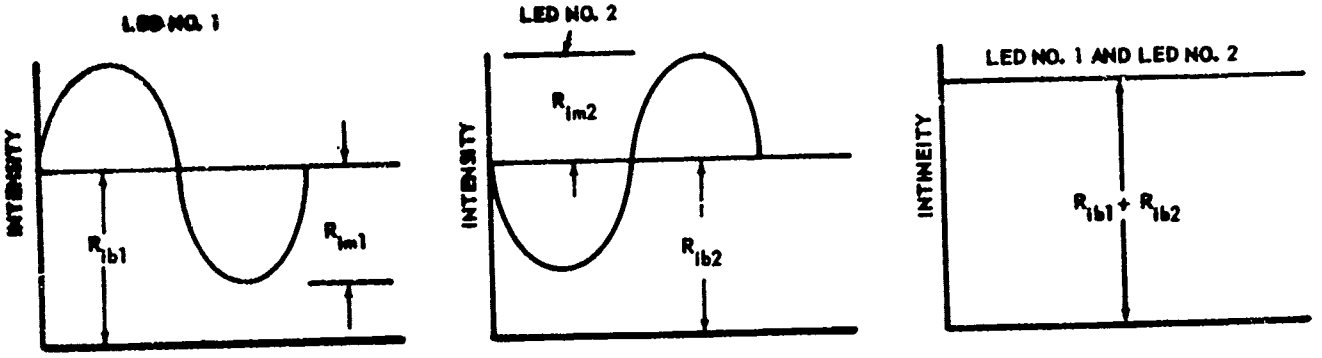

Figure E-5. TRANSMITTER WAVEFORMS

Figure E-6 presents the illumination (I_{D1} and I_{D2}) on the two detectors of the receiver when $\theta_R=0$. Light from LED's 1 and 2 are split evenly by the receiver Wollaston prism so that each detector sees only a D.C. level. The sum and difference outputs defined in expressions 20 and 19 are also d.c. levels.

Figure E-7 presents the illumination (I_{D1} and I_{D2}) on the two detectors of the receiver when $\theta_R \neq 0$. Light from LED's 1 and 2 are no longer evenly split by the Wollaston such that detector #1 receives a greater amplitude while the amplitude on detector #2 is diminished. Light from LED #2 is split by the Wollaston such that detector #1 receives a lesser amplitude while detector #2 receives a greater amplitude. The total intensity on each detector is no longer d.c. Detector #1 sees an a.c. signal in phase with LED #1 while detector #2 sees an a.c. signal of the same amplitude but 180° out of phase. In each case, the amplitude is proportional to the sine of the roll angle. Figure E-8 presents the sum and difference signals resulting from the detector illuminations of Figure E-7 The sum signal is a d.c. signal which is used to monitor the overall system illumination for AGC. The difference from expression 16 is in the phase with LED #1 and detector #1 and has twice the amplitude of the detector #1 signal. Again the amplitude of the difference signal is proportional to the sine of the roll angle. If a difference signal in phase with LED #1 signifies a positive angle, then a negative angle corresponds to the difference signal being out of phase with LED #1.

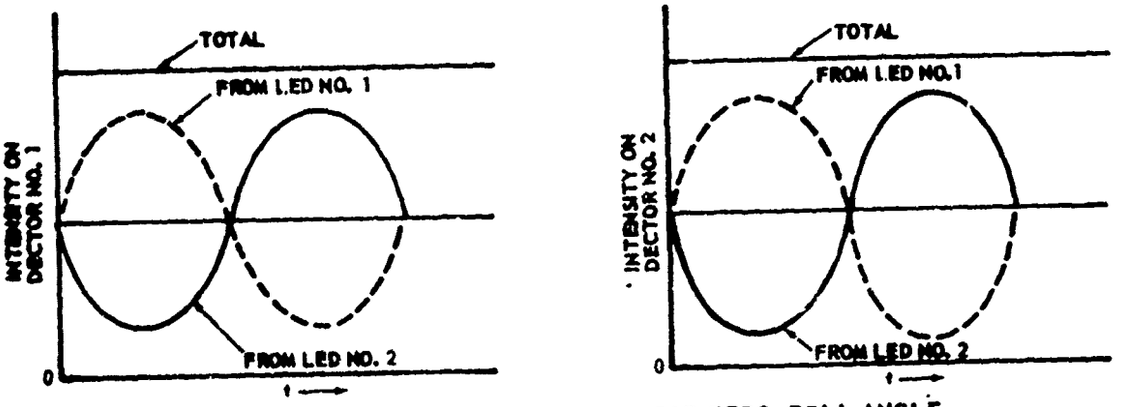

Figure E-6 DETECTOR ILLUMINATION FOR ZERO ROLL ANGLE

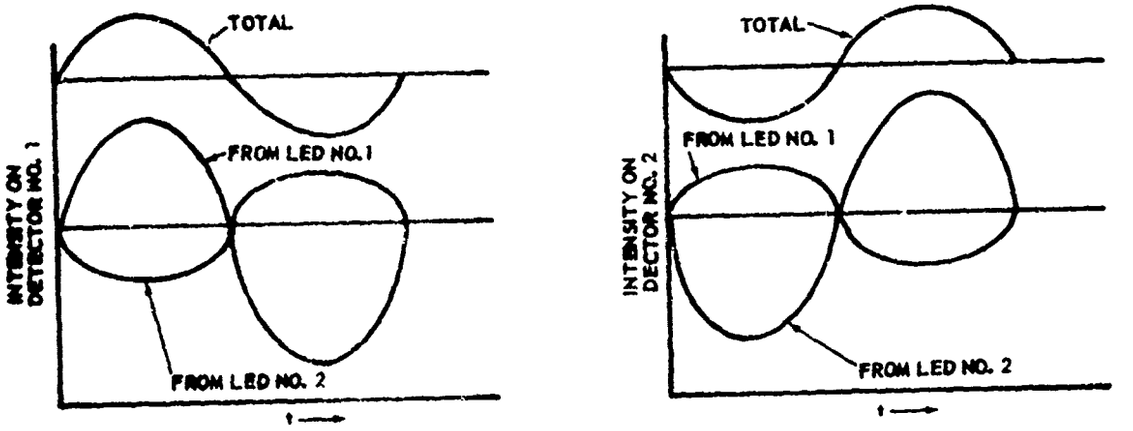

Figure E-7 DETECTOR ILLUMINATION FOR NON-ZERO ROLL ANGLE

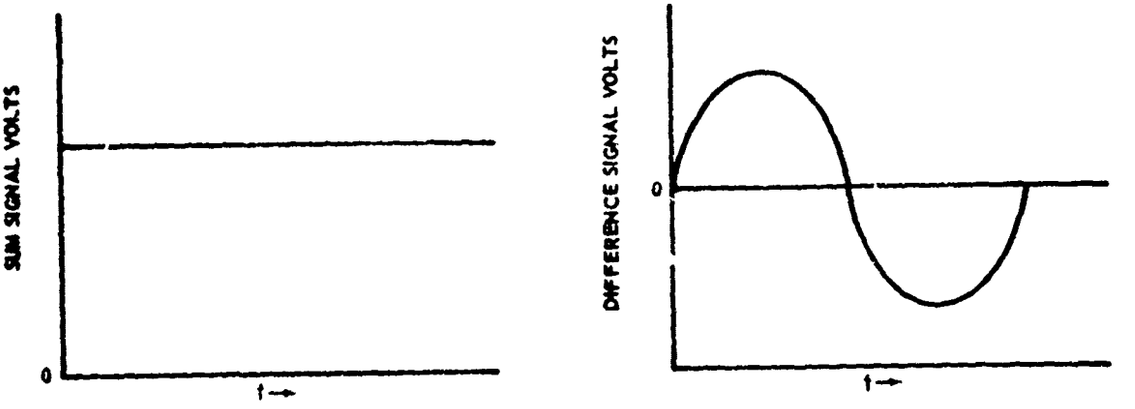

Figure E-8 SUM AND DIFFERENCE SIGNALS

2.1 Lateral Axis

Upon substituting expressions for I_{D1} and I_{D2} (equations 14 and 15) and expressions for I_1 and I_2 into equations 19 and 20, the following expressions are obtained for the difference and sum of the lateral axis detector outputs.

(21) $$V_D = \frac{D}{4}\Big\{\Big[(R_1 i_{b1} + R_2 i_{b2} + 2I'_{BG}) + (R_1 i_{m1} - R_2 i_{m2})\sin\omega t\Big]\Big[K_1A_1 - K_2A_2\Big] + \Big[(R_1 i_{b1} - R_2 i_{b2}) + (R_1 i_{m1} + R_2 i_{m2})\sin\omega t\Big]\Big[K_1A_1 + K_2A_2\Big]\Big[\sin k\theta - \cos k\beta \sin k\alpha(1 - \cos 2\theta_R)\Big]\Big\}$$

(22) $$V_S = \frac{S}{4}\Big\{\Big[(R_1 i_{b1} + R_2 i_{b2} + 2I'_{BG}) + (R_1 i_{m1} - R_2 i_{m2})\sin\omega t\Big]\Big[K_1A_1 + K_2A_2\Big] + \Big[(R_1 i_{b1} - R_2 i_{b2}) + (R_1 i_{m1} + R_2 i_{m2})\sin\omega t\Big]\Big[K_1A_1 - K_2A_2\Big]\Big[\sin k\theta - \cos k\beta \sin k\alpha(1 - \cos 2\theta_R)\Big]\Big\}$$

where: K - detector responsivity

A - Preamplifier gain

D - Differential amplifier gain

S - Summation amplifier gain

θ - $(\alpha-\beta)$ = lateral axis angle to be measured

The above equations may be reduced to ideal system model equations by assuming that the following conditions are true. The errors introduced when these conditions are not true will be discussed later in the appendix.

- o PERFECT LED OUTPUT BALANCE ($R_1 i_{m1} = R_2 i_{m2}$)
- o PERFECT DETECTOR/PRE-AMPLIFIER GAIN BALANCE ($K_1A_1 = K_2A_2$)
- o ZERO ROLL CROSS COUPLING ($\theta_R = 0°$)
- o ZERO UNPOLARIZED BACKGROUND ($I'_{BG} = 0$)
- o PERFECT MODULATION ($i_{b1} = i_{m1}$ & $i_{b2} = i_{m2}$)

The ideal equations for the difference and sum expressions are:

(23) $$V_D = \frac{D}{4}(K_1A_1 + K_2A_2)(R_1 i_{m1} + R_2 i_{m2})\sin\omega t \sin k\theta$$

(24) $$V_S = \frac{S}{4}(K_1A_1 + K_2A_2)(R_1 i_{m1} + R_2 i_{m2})$$

The difference signal (V_D), which is an AC signal, is processed through a narrow band filter centered at a frequency of $\omega/2\pi$. The summation signal (V_S), is used to normalize the difference signal for variations in detector/preamplifier gain changes and LED responsivity/peak modulation current changes. After normalization by the divider network and demodulation the resultant output signal may be expressed as:

(25) $$V_E = \frac{XEFV_D}{KV_S} = \frac{X\ FED}{KS} \sin k\theta$$

where: X - divider network gain

E - bandpass filter gain

F - demodulation gain

K - low pass filter gain

The significant advantage of this approach in the ideal case is illustrated by Equation 25 which does not contain expressions for LED responsivities, detector responsivities and preamplifier gains. Normalization of these parameters will greatly assist accuracy and long term stability of the sensor.

2.2 ROLL AXIS

When substituting expressions for I_{D1} and I_{D2} (equation 18) and expressions of I_1 and I_2 into equations 19 and 20, the following expressions are obtained for the difference and sum of the roll axis detection outputs.

(26) $$V_D = \frac{D}{4}\Big\{ \Big|(R_1 i_{b1}+R_2 i_{b2}+2I'_{BG})+ (R_1 i_{m1}-R_2 i_{m2}) \sin\omega t\Big| \Big|K_1A_1-K_2A_2\Big| + \Big|(R_1 i_{b1}-R_2 i_{b2}) + (R_1 i_{m1}+R_2 i_{m2}) \sin\omega t\Big| \Big|K_1A_1+K_2A_2\Big| \Big|\sin 2\theta_R\Big|\Big\}$$

(27) $$V_S = \frac{S}{4}\Big\{ \Big|(R_1 i_{b1}+R_2 i_{b2}+2I'_{BG})+ (R_1 i_{m1}-R_2 i_{m2}) \sin\omega t\Big| \Big|K_1A_1+K_2A_2\Big| + \Big|K_1A_1-K_2A_2\Big| \Big|(R_1 i_{b1}-R_2 i_{b2})+(R_1 i_{m1}+R_2 i_{m2}) \sin\omega t\Big| \Big|\sin 2\theta_R\Big|\Big\}$$

The ideal equations for the difference and sum expressions and output signal may be formed using the same procedure as outlined for the lateral axis. These equations are:

(28) $$V_D = \frac{D}{4} (K_1A_1+K_2A_2) (R_1 i_{m1}+R_2 i_{m2}) \sin\omega t \sin 2\theta_R$$

(29) $$V_S = \frac{S}{4} (K_1A_1+K_2A_2) (R_1 i_{m1}+R_2 i_{m2})$$

(30) $$V_E = \frac{XEFV_D}{KV_S} = \frac{X\ FED}{KS} \left[\sin 2\theta_R\right]$$

The normalization features outlined for the lateral axis are also true for the roll axis.

3.0 SYSTEM ERROR ANALYSIS

The previous paragraphs discussed the ideal system equations to illustrate some of the features of the approach being utilized by Chrysler. These ideal equations assumed the following conditions.

- o PERFECT LED MODULATION BALANCE ($R_1 i_{m1} = R_2 i_{m2}$)
- o PERFECT DETECTOR/PRE-AMPLIFIER GAIN BALANCE ($K_1 A_1 = K_2 A_2$)
- o ZERO ROLL CROSS COUPLING ($\theta = 0^o$)
- o ZERO UNPOLARIZED BACKGROUND ($I_{BG} = 0$)
- o PERFECT MODULATION ($i_{b1} = i_{m1}$ & $i_{b2} = i_{m2}$)

The following paragraphs will evaluate the effect when these conditions are not true.

3.1 Differential Output

Errors introduced by non-ideal conditions can be best evaluated by an analysis of the differential output signal after passing through the bandpass filter (E). The output of the filter (V_D') for the lateral and roll axes may be expressed as:

Lateral Axis:

$$(31)\quad V_D' = \frac{ED}{4}\Big\{ \underbrace{\Big|(R_1 i_{m1} + R_2 i_{m2})\ (K_1 A_1 + K_2 A_2)\ \mathrm{Sin}\ k\theta\Big|}_{(1)}\ \mathrm{Sin}\omega t + \underbrace{\Big|(R_1 i_{m1} - R_2 i_{m2})\ (K_1 A_1 - K_2 A_2)\Big|}_{(2)}\ \mathrm{Sin}\omega t + \underbrace{\Big|(R_1 i_{m1} + R_2 i_{m2})\ (K_1 A_1 + K_2 A_2)\ (\mathrm{Cos}\ k\beta\ \mathrm{Sin}\ k\alpha)\ (1-\mathrm{Cos}2\theta_R)\Big|}_{(3)}\ \mathrm{Sin}\omega t \Big\}$$

Roll Axis:

$$(32)\quad V_D' = \frac{ED}{4}\Big\{ \underbrace{\Big|(R_1 i_{m1} + R_2 i_{m2})\ (K_1 A_1 + K_2 A_2)\ \mathrm{Sin}\ 2\theta_R\Big|}_{(1)}\ \mathrm{Sin}\omega t + \underbrace{\Big|(R_1 i_{m1} - R_2 i_{m2})\ (K_1 A_1 - K_2 A_2)\Big|}_{(2)}\ \mathrm{Sin}\omega t \Big\}$$

Term 1 - Ideal equation for difference signal

Term 2 - The magnitude of this error is dependent upon the degree of LED output modulation unbalance as diminished by the degree of detector/pre-amplifier unbalance. Balance of both factors must be controlled to maintain this error to an acceptable level. This term represents an offset error which may be found at null by:

Lateral Axis:

(33) $\theta_e = \frac{1}{k}$ Arc Sin (η_{Ri}) (η_{KA})

Roll Axis:

(34) $\theta_{Re} = \frac{1}{2}$ Arc Sin (η_{Ri}) (η_{KA})

where:

$$\eta_{Ri} = \frac{(R_1 i_{m1} - R_2 i_{m2})}{(R_1 i_{m2} + R_2 i_{m2})} \qquad \eta_{KA} = \frac{(K_1 A_1 - K_2 A_2)}{(K_1 A_1 + K_2 A_2)}$$

The magnitude of the offset error at null is illustrated in table E-1 for various values of η_{Ri} and η_{KA} and for a nominal value of k=60.

TABLE E-1

$\eta_{Ri} = \eta_{KA}$	θ_e	θ_{Re}
0.01	0.34"	10.31"
0.02	1.38"	41.25"
0.03	3.09"	92.82"
0.04	5.50"	165.01"
0.05	8.59"	257.83"

Substantial errors are introduced by this term, particularly in the roll axis. However, by controlling LED modulation balance as discussed in paragraph 3.4, the error cause by this term is converted to a scale factor error much less sensitive to values of η_{Ri} and η_{KA}.

Term 3- The magnitude of this term is dependent upon the amount of misalignment of the matched crystals about the roll axis (θ_R) and the angle of incidence of light passing through each of the matched crystals (α and β). When the receiver assembly is on the longitudinal axis of the transmitter (i.e., no translation), $\alpha = 0$ and therefore the error is zero. When translated off axis the error is essentially proportional to α.

The error introduced by this term is an offset-error which may be found by:

(35) $\theta_e = \frac{1}{k}$ Arc Sin $\left| \text{Cos } k\beta \text{ Sin } k\alpha \ (1 - \text{Cos} 2\theta_R) \right|$

The magnitude of the offset error introduced by this term is illustrated in figure E-9. The roll axis design goal for OAMS is $\theta_R = \pm 1^o$. For this range the worst case error is in the order of ± 1". Term 3 is considered negligible.

Figure E-9
ROLL AXIS CROSS COUPLING ERROR

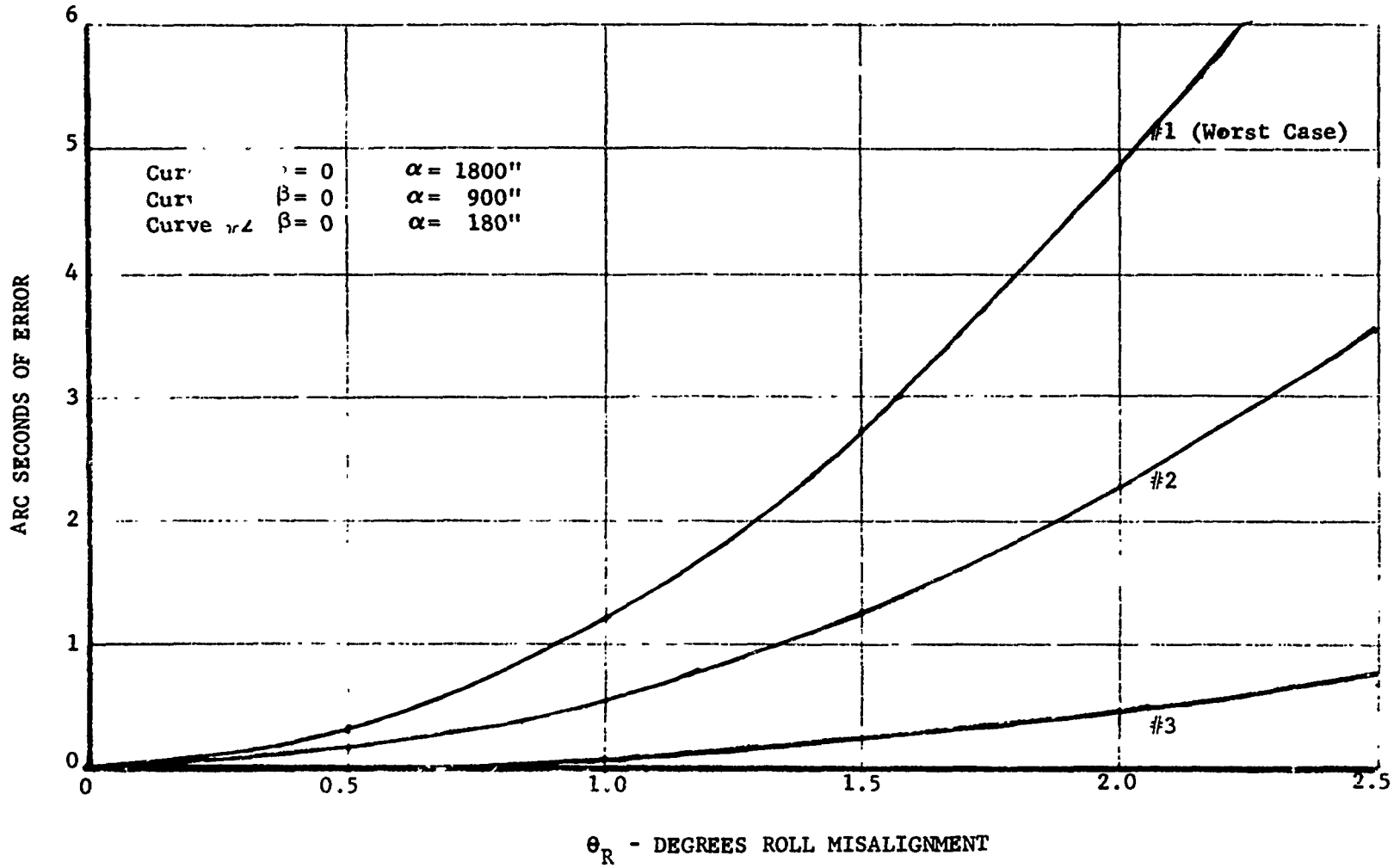

3.2 SUMMATION OUTPUT

The summation output is used to control the overall LED output, LED modulation balance and for AGC.

The summation output (V_S'') after processing through a low pass filter (K) is compared with a reference voltage to provide an error signal to control the LED output. This approach will maintain reasonably constant detector light levels for optimum detector/preamplifier operation and provide the maximum voltage level for best divider network operation.

The output for the low pass filter for a lateral axis system (or ROLL AXIS by replacing sin (kθ) with sin $2\theta_R$) may be expressed as:

$$(36) \quad V_S'' = \frac{KS}{4}\left|(R_1 i_{b1}+R_2 i_{b2}+2I'_{BG})\ (K_1A_1+K_2A_2) + (R_1 i_{b1}-R_2 i_{b2})\ (K_1A_1-K_2A_2)\ \text{Sin}\ k\theta\right|$$

(1) (2)

Term 1 - This term is used to normalize the $(R_1 i_{m1}+R_2 i_{m2})$ coefficient in the ideal equation for the difference signal. Due to
$(R_1 i_{b1}+R_2 i_{b2}+2I'_{BG}) > (R_1 i_{m1}+R_2 i_{m2})$
a scale factor error will be introduced which can only be accommodated by calibration since in all cases $i_{b1} > i_{m1}$, $i_{b2} > i_{m2}$, and $I'_{BG} > 0$.

Term 2 - The magnitude of this term is dependent upon the difference of LED bias currents as diminished by the detector/preamplifier unbalance and Sin kθ for lateral axis or Sin $2\theta_R$ for roll axis.

The error contributions for these terms are evaluated in paragraph 3.4.

The summation output (V_S') after processing through a bandpass filter (G) centered at the modulation frequency provides an AC signal which is a measure of the unbalance between the LED modulation amplitudes $R_1 i_{m1}$ and $R_2 i_{m2}$. Under ideal conditions this signal can be expressed as:

$$(37) \quad V_S' = \frac{GS}{4}\left|(K_1A_1+K_2A_2)\ (R_1 i_{m1}-R_2 i_{m2})\right| \text{Sin}\omega t$$

Under non-ideal conditions this signal is expressed for the lateral axis by:

$$(38) \quad V_S' = \frac{GS}{4}\Bigg\{\left|(R_1 i_{m1}-R_2 i_{m2})\ (K_1A_1+K_2A_2)\right|\ \text{Sin}\omega t$$

(1)

$$+\left|(R_1 i_{m1}+R_2 i_{m2})\ (K_1A_1-K_2A_2)\ \text{Sin}\ k\theta\right|\ \text{Sin}\omega t$$

(2)

$$+\left|(R_1 i_{m1}+R_2 i_{m2})\ (K_1A_1-K_2A_2)\ (\text{Cos}\ k\beta\ \text{Sin}\ k\alpha)\ (1-\text{Cos}\ 2\theta_R)\right|\ \text{Sin}\omega t\Bigg\}$$

(3)

and for the roll axis by:

$$(39)\quad V_S' = \frac{GS}{4}\Bigg\{ \underbrace{\left|(R_1 i_{m1} - R_2 i_{m2})\ (K_1A_1 + K_2A_2)\right| \mathrm{Sin}\omega t}_{(1)} + \underbrace{\left|(R_1 i_{m1} + R_2 i_{m2})\ (K_1A_1 - K_2A_2)\ \mathrm{Sin}\ 2\theta_R\right| \mathrm{Sin}\omega t}_{(2)} \Bigg\}$$

Term 1 - Ideal equation for AC signal portion of V_S'

Term 2 - The feedback control loop will adjust the current gain thru one LED until $V_S' = 0$. Under ideal conditions $V_S' = 0$ when $R_1 i_{m1} = R_2 i_{m2}$. Under non-ideal conditions for the lateral axis, assuming Term 3 in equation 38 is negligible, $V_S' = 0$ when:

$$(40)\quad R_1 i_{m1} - R_2 i_{m2} = -\left[(R_1 i_{m1} + R_2 i_{m2}) \frac{(K_1A_1 - K_2A_2)}{(K_1A_1 + K_2A_2)}\right] \mathrm{Sin}\ k\theta$$

and for the roll axis:

$$(41)\quad R_1 i_{m1} - R_2 i_{m2} = -\left[(R_1 i_{m1} + R_2 i_{m2}) \frac{(K_1A_1 - K_2A_2)}{(K_1A_1 + K_2A_2)}\right] \mathrm{Sin}\ 2\theta_R$$

The error contribution of this term is further evaluated in paragraph 3.4.

Term 3 - The magnitude of this error is negligible since the worst case value of $\mathrm{Cos}\ k\beta\ \mathrm{Sin}\ k\alpha\ (1 - \mathrm{Cos}\ 2\theta_R) = \mathrm{Sin}\ k\theta$ when θ is approximately 1".

3.3 System Output

The system output equation (V_E) may be expressed as:

$$(42) \qquad V_E = \frac{10\ XF\ V_D'}{V_S''}$$

Substituting equations 31 (less Term 3) and 36 for V_D' and V_S'' results in the following equation for the lateral axis.

$$(43) \qquad V_E = K_3 \left\{ \frac{(R_1 i_{m1} + R_2 i_{m2})\ \text{Sin}\ k\theta + (R_1 i_{m1} - R_2 i_{m2})\ (\eta_{KA})}{(R_1 i_{b1} + R_2 i_{b2} + 2I'_{BG}) + (R_1 i_{b1} - R_2 i_{b2})(\eta_{KA})\ \text{Sin}\ k\theta} \right\}$$

where $K_3 = \frac{10\ EDXF}{KS}$ $\qquad$ $\eta_{KA} = \frac{K_1 A_1 - K_2 A_2}{K_1 A_1 + K_2 A_2}$

Substituting equation 40 for $(R_1 i_{m1} - R_2 i_{m2})$ and re-arranging terms yields;

$$(44) \qquad V_E = K_3 \left\{ \left[\frac{(R_1 i_{m1} + R_2 i_{m2})}{(R_1 i_{b1} + R_2 i_{b2})} \right] \left[\frac{1}{1+H} \right] \left[\frac{1}{1+G} \right] \left[1 - (\eta_{KA})^2 \right] \text{Sin}\ k\theta \right\}$$

where $G = (\eta_{Ri_b})\ (\eta_{KA})\ \text{Sin}\ k\theta$

$$\eta_{Ri_b} = \frac{R_1 i_{b1} - R_2 i_{b2}}{R_1 i_{b1} + R_2 i_{b2} 2I'_{BG}}$$

$$H = \frac{2I'_{BG}}{(R_1 i_{b1} + R_2 i_{b2})}$$

$$(45) \qquad V_E = K_3 K_4 K_5 K_6 K_7\ \text{Sin}\ k\theta$$

Roll axis equations are the same, except Sin $k\theta$ is replaced by Sin $2\theta_R$.

Variations in each of the K terms will introduce scale factor errors once the system is calibrated. The following is a discussion of the error sources for each term.

$$(46) \qquad K_3 = \frac{10\ EDXF}{KS}$$

The value of K_3 is a function of the linear scale factors of the electronic elements identified in the above equation. The % scale factor error = f(% dK_3).

$$(47) \qquad K_4 = \frac{(R_1 i_{m1} + R_2 i_{m2})}{(R_1 i_{b1} + R_2 i_{b2})}$$

The equation for K_4 may be modified by the following relationships introducing the modulation index m.

$$m_1 = \frac{i_{m1}}{i_{b1}} \qquad m_2 = \frac{i_{m2}}{i_{b2}}$$

let $R_1 i_{b1} = Ri_b$ let $m_1 = m$

$R_2 i_{b2} = Ri_b + \Delta Ri_b$ $m_2 = m + \Delta m$

$$(48) \qquad K_4 = \frac{Ri_b m + (Ri_b + \Delta Ri_b)(m+\Delta m)}{2Ri_b + \Delta Ri_b}$$

Expanding and re-arranging terms

$$(49) \qquad K_4 = m + \frac{Ri_b \Delta m + \Delta Ri_b \Delta m}{2Ri_b + \Delta Ri_b}$$

Since $2Ri_b \gg \Delta Ri_b$

$$(50) \qquad K_4 = m + \frac{\Delta m}{2} = m\left[1 + \frac{\Delta m}{2m}\right]$$

Therefore, the value of K_4 is a function of the modulation index m and unbalance in modulation indices $\Delta m = m_2 - m_1$. The % scale factor error = f (% dm, % $d\Delta m/2$)

$$(51) \qquad K_5 = \frac{1}{1+H}$$

If $H \ll 1$ $K_5 = 1-H$

$$(52) \qquad K_5 = \left[1 - \frac{2i'_{BG}}{(R_1 i_{b1} + R_2 i_{b2})}\right]$$

The value of K_5 is a function of H which is the ratio of the background radiation level to the total average LED output. The % scale factor error = f (% dH)

$$(53) \qquad K_6 = \frac{1}{1+G}$$

Since $G \ll 1$ $K_6 = 1-G$

$$(54) \qquad K_6 = \left|1 - (\eta_{Ri_b})\ (\eta_{KA})\ \text{Sin}\ k\theta\right|$$

The value of K_6 is a function of the difference in the LED DC light levels (ΔRi_b) diminished by the detector/pre-amplifier unbalance and value of Sin $k\theta$ for lateral axes and Sin $2\theta_R$ for roll axis.

The magnitude of K_6 and % scale factor error for various values of η_{Ri_b} and η_{KA} are illustrated in Table E-2.

Table E-2

$\eta_{Ri_b}=\eta_{KA}$	LATERAL θ=1800"		ROLL θ_R=1800"	
	K_6	% Error	K_6	% Error
0.01	0.99995	0.005%	1	0.001%
0.02	0.99980	0.020%	0.99999	0.001%
0.03	0.99955	0.045%	0.99998	0.002%
0.04	0.99920	0.080%	0.99997	0.003%
0.05	0.99875	0.125%	0.99996	0.004%

(55) $$K_7 = \left[1-(\eta_{KA})^2\right]$$

The value of K_7 is a square function of the difference in detector/pre-amplifier unbalance. The magnitude of K_7 and % scale factor error for various values of η_{KA} are illustrated in Table E-3.

Table E-3

η_{KA}	K_7	% Error
0.01	0.9999	0.01%
0.02	0.9996	0.04%
0.03	0.9991	0.09%
0.04	0.9984	0.16%
0.05	0.9975	0.25%

3.4 System Error Analysis Summary

Error sources resulting in dynamic errors were evaluated for the OAMS concept described in figures E-2, E-3 and E-4, with the following results.

a) First order scale factor errors would be introduced by changes in the following parameters:

- m - modulation index
- Δm - unbalance in modulation indices
- D - differential amplifier gain
- E - bandpass filter gain
- F - demodulator gain
- 10X - divider network gain
- K - low pass filter gain
- S - summation amplifier gain
- H - ratio of background radiation to total average LED output.

Stable electronic circuits are required for these functions.

b) No null offset errors would exist if the LED modulation balance feedback control is used. Without this control, significant offset errors would be experienced in the roll axis.

c) LED modulation balance feedback control would have to equally adjust both the i_b and i_m current levels of the controlled LED to preclude a first order error due to a change in the modulation index.

d) The K_6 and K_7 terms will be reduced to negligible levels if unbalances in LED output and detector/pre-amplifier gains are maintained within 2% to 3%.

4.0 POLARIZED OPTICAL MISALIGNMENT ANALYSIS

In the previous lateral axis system error analysis, the alignment of the crystalline axis of the polarized optical elements about the planes of polarization was assumed to be perfect. The intent of this analysis is to evaluate the sensitivity of element misalignment to determine the degree of departure from the ideal case.

The optical references for this analysis are the transmitter wollaston planes of polarization aligned at azimuth angles of $\pm 45^{\circ}$. The analysis approach modifies the ideal lateral axis math model by rotating the various elements, one at a time, ϕ degrees from the ideal azimuth. The resulting effect is evaluated for each element over a range of $\theta = (\alpha - \beta) = \pm 1800''$ under the following conditions:

1. No translation (α=0) and no roll misalignment ($\theta_R = 0$).
2. No translation (α=0) and $\pm 1^{\circ}$ roll misalignment ($\theta_R = \pm 1^{\circ}$).
3. 2.5 inch translation at 25 feet ($\alpha \approx \pm 1800''$) and $\pm 1^{\circ}$ roll misalignment ($\theta_R = \pm 1^{\circ}$).

Element misalignment to be evaluated include:

- o Transmitter/Target Roll Axis ($R_{2\theta}$)
- o Transmitter $\lambda/4$ waveplate (Q)
- o Transmitter Angle Sensing Crystal (ASC_{α})
- o Receiver Angle Sensing Crystal (ASC)
- o Receiver Wollaston (W)

4.1 Ideal Math Model

The ideal math model for the polarized optical elements may be formed by the following matrix equation.

$$(56) \quad \left[I_{D1} \; ; \; I_{D2}\right] = \left[W_T\right]\left[ASC_{\beta}\right]\left[R_{2\theta}\right]\left[ASC_{\alpha}\right]\left[Q\right]\left[I\right]$$

$$(57) \quad \left[I_{D1} \; ; \; I_{D2}\right] =$$

$$\frac{1}{2}\begin{bmatrix} 1 & 0 & \pm 1 & 0 \\ 0 & 0 & 0 & 0 \\ \pm 1 & 0 & 1 & 0 \\ 0 & 0 & 0 & 0 \end{bmatrix}\begin{bmatrix} 1 & 0 & 0 & 0 \\ 0 & 1 & 0 & 0 \\ 0 & 0 & C_{\beta} & -S_{\beta} \\ 0 & 0 & S_{\beta} & C_{\beta} \end{bmatrix}\begin{bmatrix} 1 & 0 & 0 & 0 \\ 0 & C_{2\theta} & S_{2\theta} & 0 \\ 0 & -S_{2\theta} & C_{2\theta} & 0 \\ 0 & 0 & 0 & 1 \end{bmatrix}\begin{bmatrix} 1 & 0 & 0 & 0 \\ 0 & 1 & 0 & 0 \\ 0 & 0 & C_{\alpha} & S_{\alpha} \\ 0 & 0 & -S_{\alpha} & C_{\alpha} \end{bmatrix}\begin{bmatrix} 1 & 0 & 0 & 0 \\ 0 & 1 & 0 & 0 \\ 0 & 0 & 0 & -1 \\ 0 & 0 & 1 & 0 \end{bmatrix}\begin{bmatrix} Ri \\ 0 \\ RiSin\omega t \\ 0 \end{bmatrix}$$

where: $C_{\alpha} = \text{Cos } k\alpha$ $\quad C_{\beta} = \text{Cos } k\beta$ $\quad C_{2\theta} = \text{Cos } 2\theta_R$

$S_{\alpha} = \text{Sin } k\alpha$ $\quad S_{\beta} = \text{Sin } k\beta$ $\quad S_{2\theta} = \text{Sin } 2\theta_R$

k = ASC Optical gain ($k=60$)

α = ASC_α Incident angle from crystal surface perpendicular

β = ASC_β Incident angle from crystal surface perpendicular

θ_R = Roll axis relative attitude error about line of sight between transmitter and target ($\theta_R = \pm 1^\circ$)

R = LED responsivity

i = LED current

ω = Modulation frequency

I_{D1} = Detector #1 light intensity

I_{D2} = Detector #2 light intensity

The matrix equation solution yields the following expression for detector light intensity

$$(58) \quad I_{D1} = \frac{Ri}{2}\left\{ 1 + \left|\text{Sin } k(\alpha-\beta) - \text{Cos } k\beta \text{ Sin } k\alpha \,(1-\text{Cos } 2\theta_R)\right| \text{Sin}\omega t \right\}$$

$$(59) \quad I_{D2} = \frac{Ri}{2}\left\{ 1 - \left|\text{Sin } k(\alpha-\beta) - \text{Cos } k\beta \text{ Sin } k\alpha \,(1-\text{Cos } 2\theta_R)\right| \text{Sin}\omega t \right\}$$

The output of the differential amplifier may be found by:

$$(60) \quad V_D = DKA\,(I_{D1} - I_{D2})$$

$$= DKARi \left|\text{Sin } k\,(\alpha-\beta) - \text{Cos } k\beta \text{ Sin } k\alpha \,(1-\text{Cos } 2\theta_R)\right| \sin\omega t$$

where: D = differential amplifier gain

K = detector responsivity

A = preamplifier gain

4.2 Misalignment Analysis

The element misalignment under conditions specified in paragraph 4.0 are evaluated in the following paragraphs. The error introduced for misalignment angle (ϕ) is found by:

$$E_\phi = \frac{3600}{k}\left|\text{Arc Sin } k\,(\alpha-\beta)' - \text{Arc Sin } k\,(\alpha-\beta)\right| \text{ arcseconds}$$

where: $\text{Sin } k\,(\alpha-\beta)' = \text{Sin } k\,(\alpha-\beta)$ + error terms

and $k = 60$

4.2.1 Transmitter/Receiver Roll Axis Misalignment

Equation 60 is modified by substituting $\theta_R = \theta_R + \phi_R$; where ϕ equals the roll misalignment over and above the roll axis operating range θ_R. In this case;

$$\text{Sin } k(\alpha-\beta)' = \text{Sin } k(\alpha-\beta) - \text{Cos } k\beta \text{ Sin } k\alpha \left[1-\text{Cos } 2(\theta_R+\phi_R)\right]$$

For values of $\phi_R = 0.5^o$ and 5.0^o;

Condition 1 $\alpha = 0$ $\theta_R = 0^o$

$E\phi_R = 0$ Since Sin $k\alpha = 0$

The lateral axis readout will not indicate errors due to roll axis misalignment. However, the readout will be referenced to the receiver coordinates rather than the transmitter coordinates. When $\alpha = 0$, the transmitter emits only circular polarized light and as such does not provide a roll azimuth reference for the receiver. When referenced to the transmitter, the cross coupling error introduced in one lateral axis is proportional to Sin θ_R of the orthogonal lateral axis angular deviation. At $\theta_R = 1^o$, the error is in the order of 1.75%. If desired, this error can be corrected mathematically over the θ_R operating range of $\pm 1^o$ using the roll axis readout data.

Condition 2 $\alpha = 0$ $\theta_R = \pm 1^o$

Same as Condition 1.

Condition 3 $\alpha = \pm 1800"$ $\theta_R = \pm 1^o$

Considering the target coordinates, the indicated error due to roll axis misalignment over the range of $(\alpha-\beta) = \pm 1800"$ is illustrated in figure J-10 for values of $\phi_R = 0.5^o$ and 5.0^o. The worst case errors with translation over the $\alpha = \pm 1800"$ range occurs when $\theta_R = +1^o$. If $\phi_R = -\phi_R$ then the worst case error would be comparable and occur when $\theta_R = -1^o$. The data illustrated in figure E-10 include the roll axis cross coupling error which is a maximum of $\pm 1.21"$ at $\phi_R = 0^o$ and $\alpha = \pm 1800"$ over the θ_R operating range of $\pm 1.0^o$.

The roll axis cross coupling error over the θ_R operating range, as discussed under Condition 3, is inherent in the sensor design and cannot be readily corrected. Fortunately the maximum value of this error is $\pm 1.21"$. Additional errors introduced by ϕ_R can be substantial and can only be controlled by minimizing the value of ϕ_R during sensor alignment.

4.2.2 Transmitter $\lambda/4$ Waveplate Misalignment

Equation 57 is modified by substituting $[Q] = [Q]_\phi$ representing a $\lambda/4$ waveplate rotation of ϕ degrees.

E-10 ROLL AXIS CROSS COUPLING ERROR

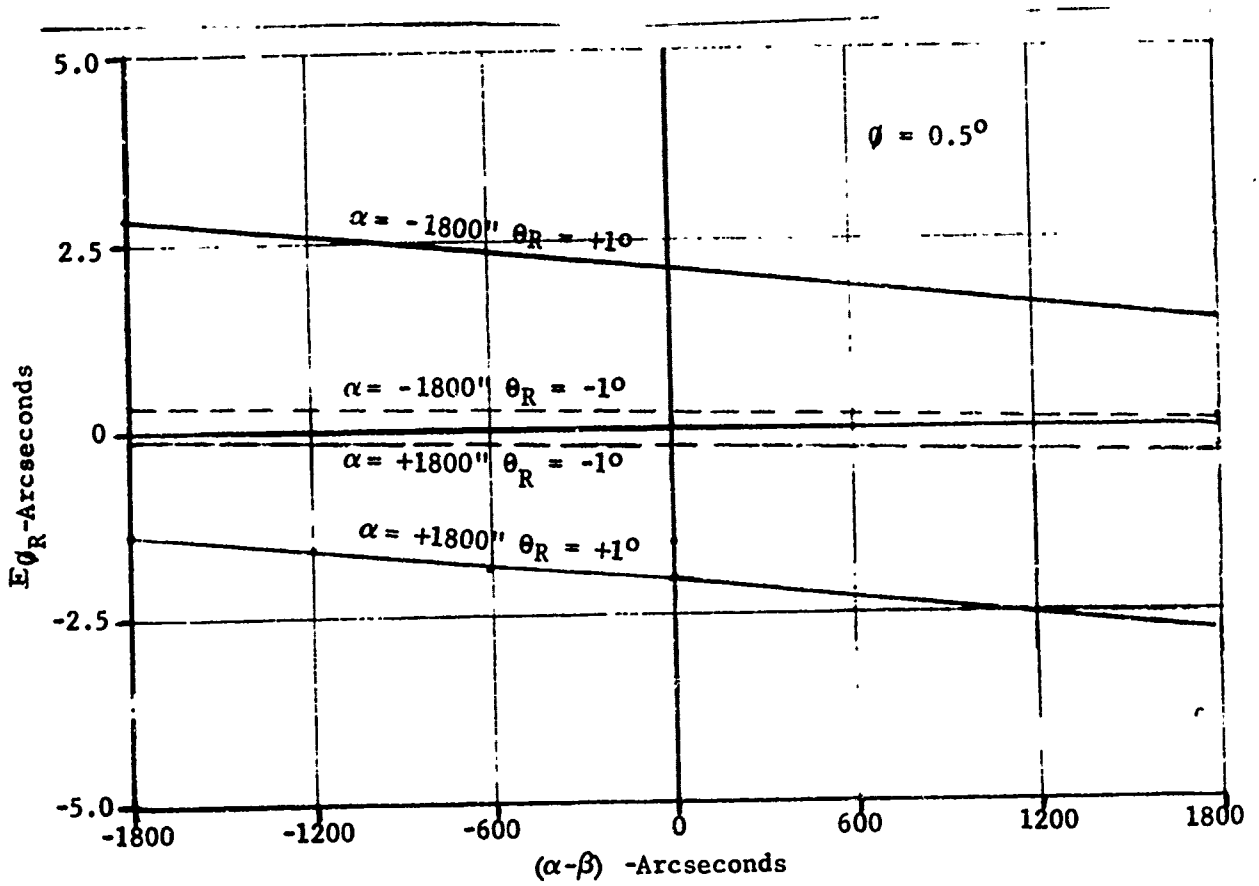

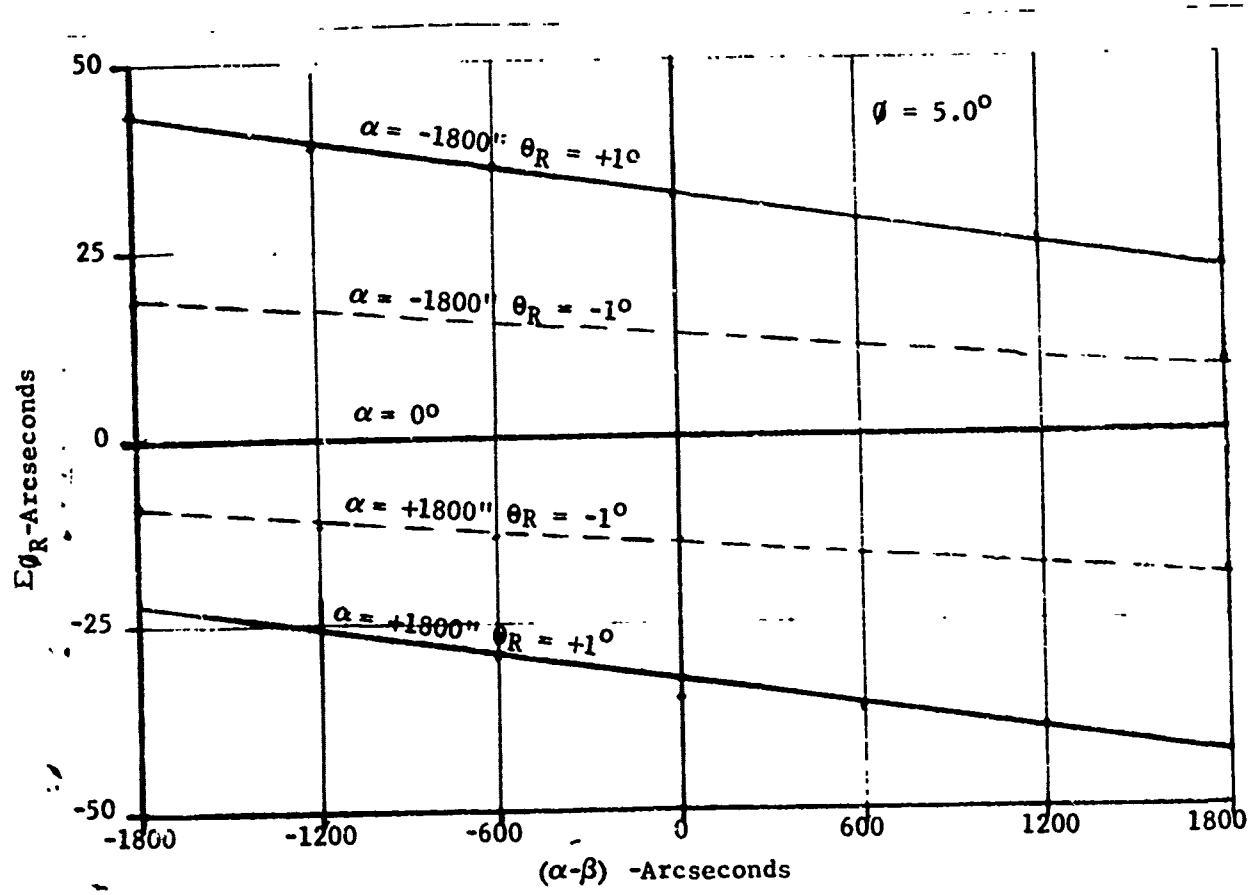

(64) $$\left[Q\right] = \left[Q\right]_{\phi} = \left[T(-2\phi)\right]\left[Q\right]\left[T(2\phi)\right]$$

where

$$\left[T(2\phi)\right] = \begin{bmatrix} 1 & 0 & 0 & 0 \\ 0 & C_{2\phi} & S_{2\phi} & 0 \\ 0 & -S_{2\phi} & C_{2\phi} & 0 \\ 0 & 0 & 0 & 1 \end{bmatrix}$$

and $C_{2\phi} = \text{Cos } 2\phi_R$

$S_{2\phi} = \text{Sin } 2\phi_R$

(65) $$\left[Q\right]_{\phi} = \begin{bmatrix} 1 & 0 & 0 & 0 \\ 0 & C_{2\phi}^2 & C_{2\phi}S_{2\phi} & S_{2\phi} \\ 0 & C_{2\phi}S_{2\phi} & S_{2\phi}^2 & -C_{2\phi} \\ 0 & -S_{2\phi} & C_{2\phi} & 0 \end{bmatrix}$$

The error related to this term is;

(66) $$E\phi_Q = 60 \left|\text{Arc Sin } k(\alpha-\beta)' - \text{Arc Sin } k(\alpha-\beta)\right| \text{ Arc seconds}$$

where: $\text{Sin } k(\alpha-\beta)' = -\text{Cos } 2\phi_R \text{ Sin } 2\phi_R \text{ Sin } 2\theta_R \text{ Cos } k\beta$

$+(\text{Sin } 2\phi_R)^2(\text{Cos } 2\theta_R \text{ Cos } k\alpha \text{ Cos } k\beta + \text{Sin } k\alpha \text{ Sin } k\beta)$

$+\text{Cos } 2\phi_R (\text{Cos } 2\theta_R \text{ Sin } k\alpha \text{ Cos } k\beta - \text{Cos } k\alpha \text{ Sin } k\beta)$

For values of $\phi_R = 0.5^o$ and 5.0^o;

<u>Condition 1</u> $\alpha = 0$ $\theta_R = 0^o$

$\text{Sin } k(\alpha-\beta) = (\text{Sin } 2\phi_R)^2 \text{ Cos } k\beta - \text{Cos } 2\phi_R \text{ Sin } k\beta$

The indicated error over the range of $(\alpha-\beta) = \pm 1800"$ is illustrated in figure E-11 for values of $\phi_R = 0.5^o$ and 5.0^o.

<u>Condition 2</u> $\alpha = 0$ $\theta_R = \pm 1^o$

$\text{Sin } k(\alpha-\beta)' =$

$\left[(\text{Sin } 2\phi_R)^2 \text{ Cos } 2\theta_R - \text{Cos } 2\phi_R \text{ Sin } 2\phi_R \text{ Sin } 2\theta_R\right] \text{Cos } k\beta - \text{Cos } 2\phi_R \text{ Sin } k\beta$

E-11 QUARTER WAVEPLATE MISALIGNMENT ERROR

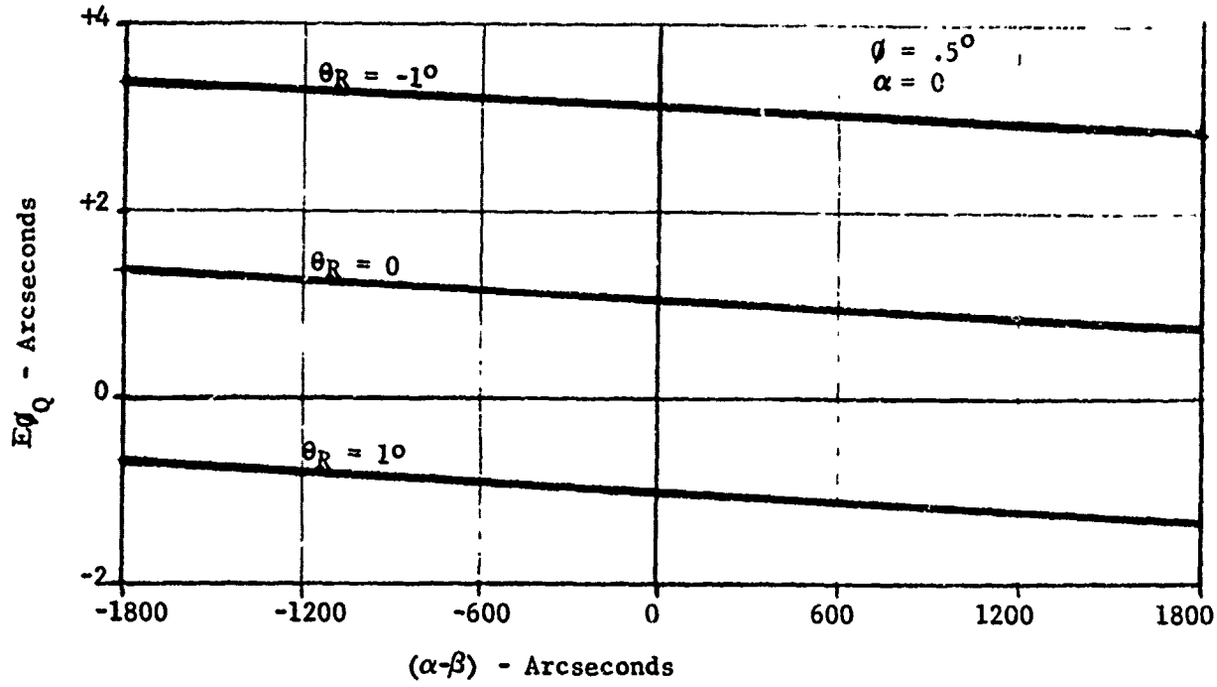

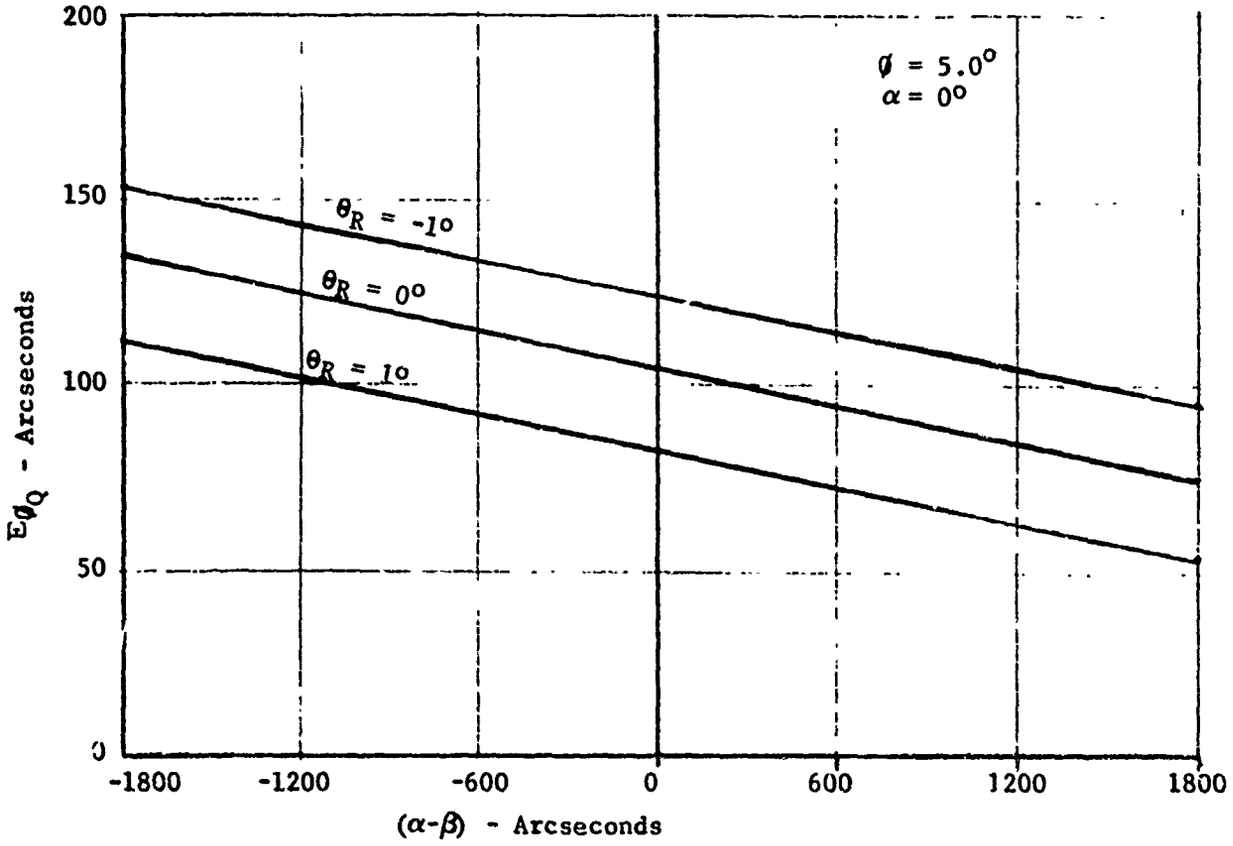

The indicated error over the range of $(\alpha-\beta) = \pm 1800"$ is illustrated and compared with Condition 1 in figure E-11 for values of $\phi_R = 0.5^o$ and 5.0^o. θ_R varying over the range of $\pm 1^o$ creates an error band about the $\theta_R = 0$ curve which is approximately $\pm 2"$ wide for $\phi_R = 0.5^o$ and $\pm 20"$ wide for $\phi_R = 5.0^o$.

Condition 3 $\alpha = \pm 1800"$ $\theta_R = \pm 1^o$

The indicated error over the range of $(\alpha-\beta) = \pm 1800"$ is illustrated in figure J-12 for values of $\phi_R = 0.5^o$ and 5.0^o. Translation over a range of $\alpha = \pm 1800"$ increases the error band a slight amount over Condition 2. At the widest point the error band is 5.4" for $\phi = 0.5^o$ and 48" for $\phi = 5.0^o$. When $\theta_R = 0^o$ the error is independent of α and equal to the Condition 1 values.

4.2.3 Transmitter Angle Sensing Crystal Misalignment

Equation 57 is modified by substituting $\left[ASC_\alpha\right] = \left[ASC_\alpha\right]_\phi$ representing an angle Sensing Crystal (ASC) rotation of ϕ degrees.

(67) $$\left[ASC_\alpha\right]_\phi = \left[T(-2\phi)\right] \left[ASC_\alpha\right] \left[T(2\phi)\right]$$

(68) $$\left[ASC_\alpha\right]_\phi = \begin{bmatrix} 1 & 0 & 0 & 0 \\ 0 & C_{2\phi}^2+S_{2\phi}^2 C_\alpha & C_{2\phi}S_{2\phi}(1-C_\alpha) & -S_{2\phi}S_\alpha \\ 0 & C_{2\phi}S_{2\phi}(1-C_\alpha) & S_{2\phi}^2+C_{2\phi}^2 C_\alpha & C_{2\phi}S_\alpha \\ 0 & +S_{2\phi}S_\alpha & -C_{2\phi}S_\alpha & C_\alpha \end{bmatrix}$$

The error related to this term is;

(69) $$E_{\phi_\alpha} = 60 \left|\text{Arc Sin } (\alpha-\beta)' - \text{Arc Sin } (\alpha-\beta)\right| \text{ Arcseconds}$$

where: $\text{Sin } k(\alpha-\beta)' = \text{Sin } k(\alpha-\beta) - \text{Cos } k\beta \text{ Sin } k\alpha\left[1-\text{Cos } 2(\phi_R-\theta_R)\right]$

For values of $\phi_R = 0.5^o$ and 5.0^o;

Condition 1 $\alpha = 0$ $\theta_R = 0^o$

$E_{\phi_\alpha} = 0$ Since Sin k = 0

When $\alpha = 0$ the circular polarized light from the transmitter is not affected by the azimuth orientation of the transmitter ASC.

Condition 2 $\alpha = 0$ $\theta_R = \pm 1^o$

Same as Condition 1

Condition 3

Data illustrated in figure E-10 and related comments apply to this case when $-\theta_R$ is substituted for θ_R.

E-12 QUARTER WAVEPLATE MISALIGNMENT ERROR

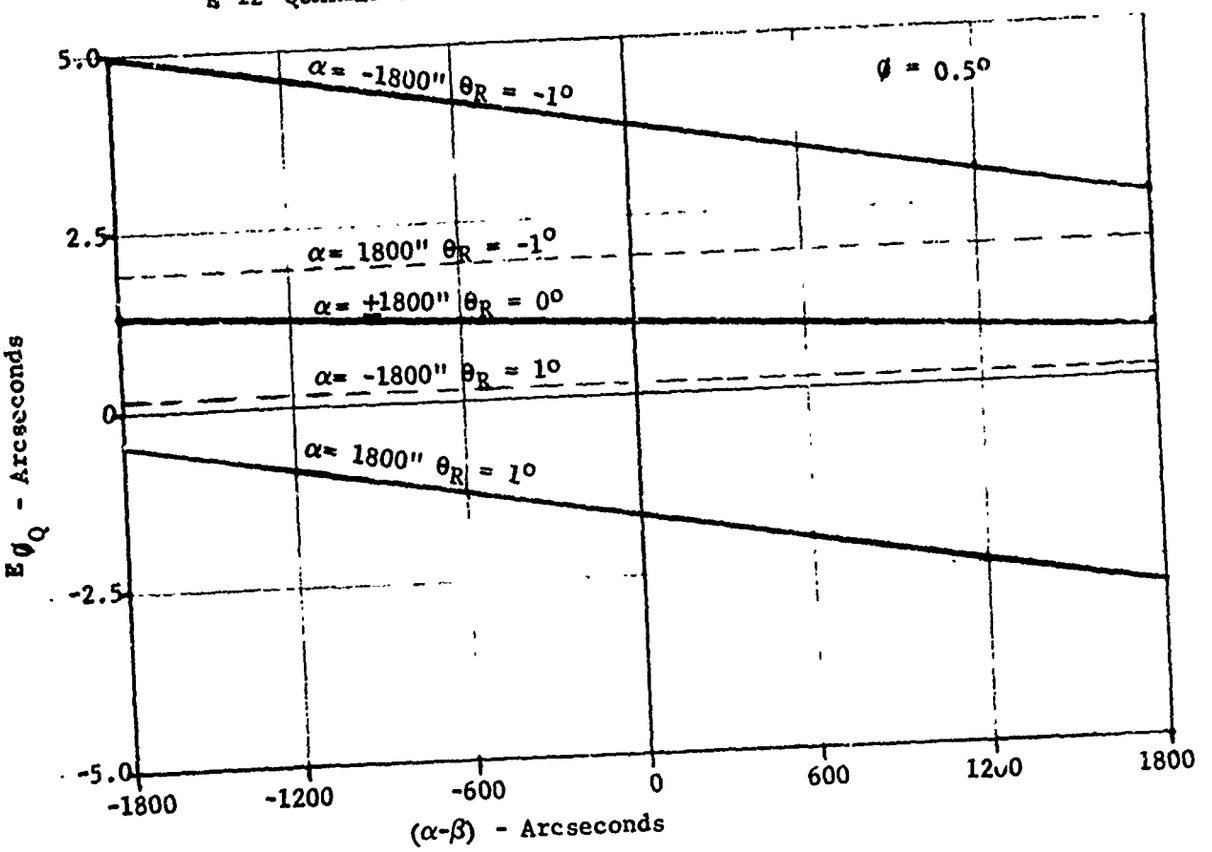

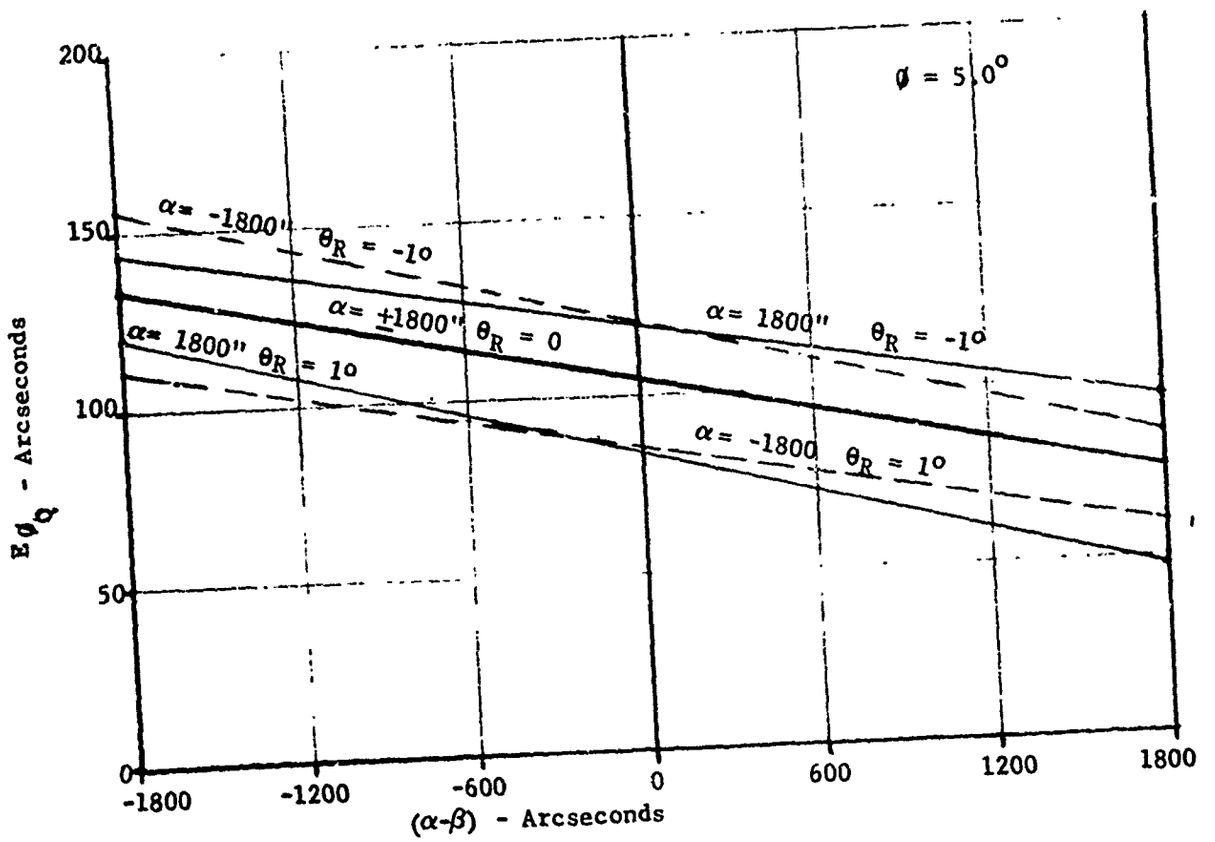

4.2.4 Receiver Angle Sensing Crystal Misalignment

Equation 57 is modified by substituting $\left|ASC_\beta\right| = \left|ASC_\beta\right|_\phi$ representing an angle sensing crystal (ASC) rotation of ϕ degrees.

(70) $$\left|ASC_\beta\right|_\phi = \left|T(-2\phi)\right| \left|ASC_\beta\right| \left|T(2\phi)\right|$$

(71) $$\left|ASC_\beta\right|_\phi = \begin{bmatrix} 1 & 0 & 0 & 0 \\ 0 & C_{2\phi}^2+S_{2\phi}^2C_\beta & C_{2\phi}S_{2\phi}(1-C_\beta) & S_{2\phi}S_\beta \\ 0 & C_{2\phi}S_{2\phi}(1-C_\beta) & S_{2\phi}^2+C_{2\phi}^2C_\beta & -C_{2\phi}S_\beta \\ 0 & -S_{2\phi}S_\beta & C_{2\phi}S_\beta & C_\beta \end{bmatrix}$$

The error related to this term is;

(72) $$E_{\phi\beta} = 60 \left| \text{Arc Sin } k(\alpha-\beta)' - \text{Arc Sin } k(\alpha-\beta) \right| \text{ Arcseconds}$$

where: $\text{Sin } k(\alpha-\beta)' =$

$$\text{Sin } k\alpha \,(\text{Cos } 2\phi_R \text{ Sin } 2\phi_R \text{ Sin } 2\theta_R - \text{Cos } 2\theta_R \text{ Cos}^2 2\phi_R)\,(1-\text{Cos } k\beta) +$$

$$\text{Cos } 2\theta_R \text{ Sin } k\alpha - \text{Cos } 2\phi_R \text{ Cos } k\alpha \text{ Sin } k\beta$$

For values of $\phi_R = 0.5^\circ$ and 5.0°;

Condition 1 $\alpha = 0$ $\theta_R = 0$

$$\text{Sin } k(\alpha-\beta)' = -\text{Cos } 2\phi_R \text{ Sin } k\beta$$

The indicated error over the range of $(\alpha-\beta) = \pm 1800''$ is illustrated in figure E-13 for values of $\phi_R = 0.5^\circ$ and 5.0°.

Condition 2 $\alpha = 0$ $\theta_R = \pm 1^\circ$

$$\text{Sin } k(\alpha-\beta)' = -\text{Cos } 2\phi_R \text{ Sin } k\beta$$

Same as Condition 1.

Condition 3 $\alpha = \pm 1800''$ $\theta_R = \pm 1^\circ$

The indicated error over the range of $(\alpha-\beta) = \pm 1800''$ is illustrated and compared with Conditions 1 and 2 in figure E-13 for values of $\phi_R = 0.5^\circ$ and 5.0°.

FIGURE E-13 RECEIVER ANGLE SENSING CRYSTAL MISALIGNMENT

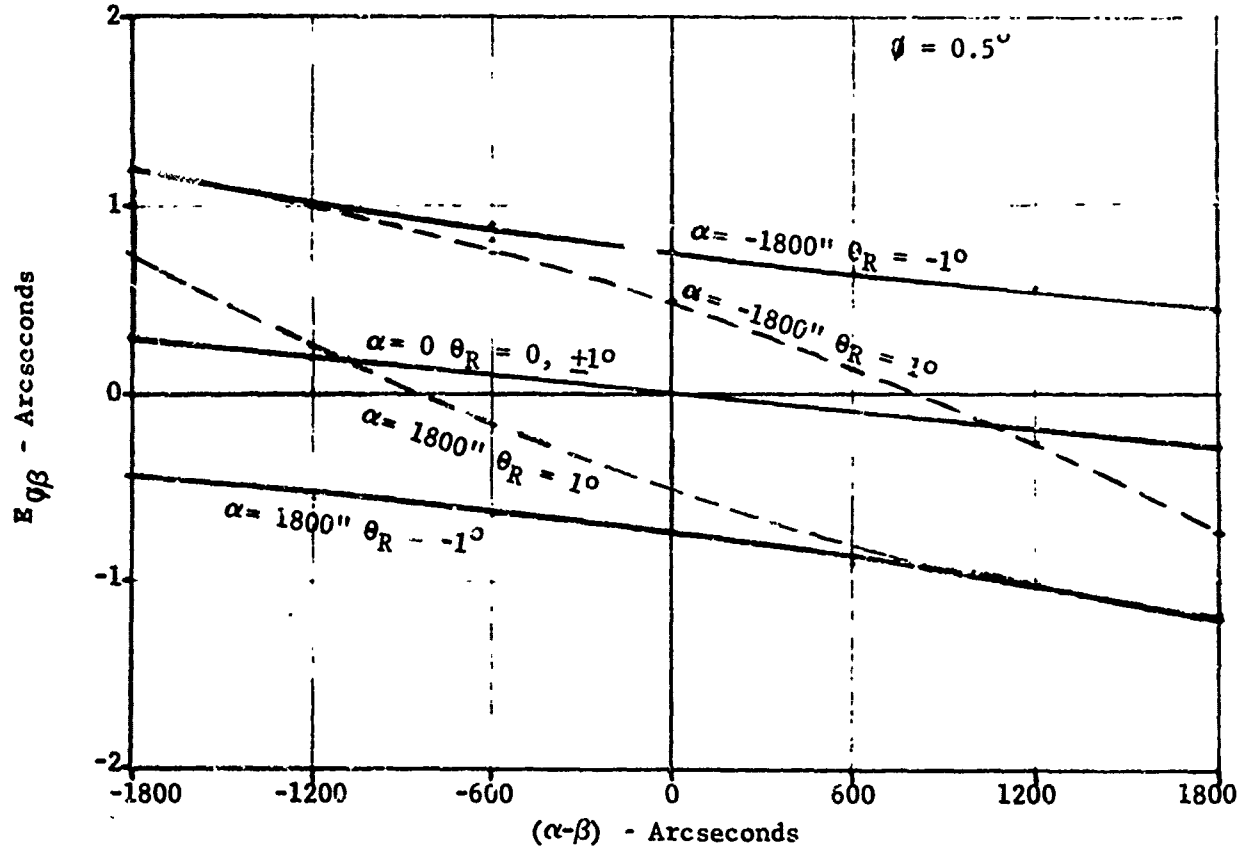

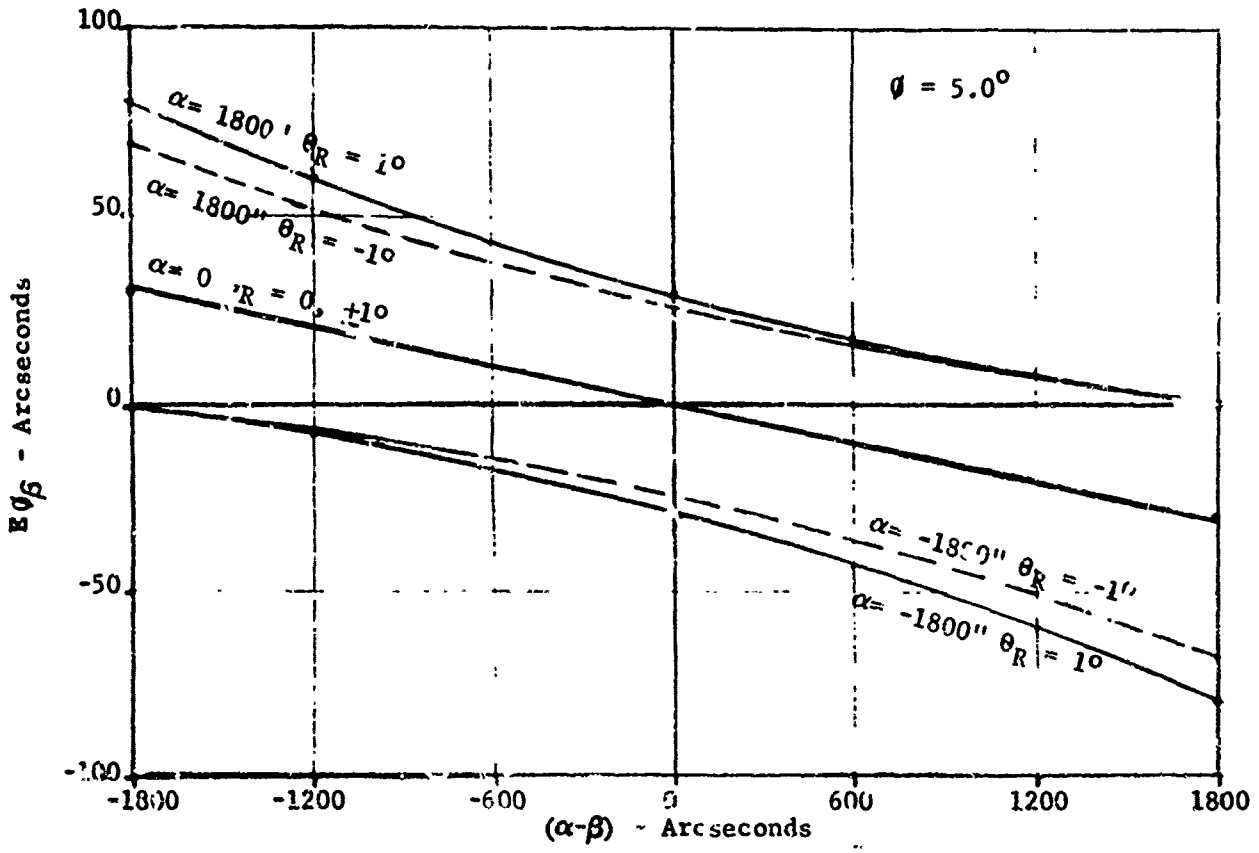

4.2.5 Receiver Wollaston Misalignment

Equation 57 is modified by inserting the rotation matrix $\left|T(\phi)\right|$ between the $\left|W_T\right|$ and $\left|ASC\beta\right|$ matrices representing a wollaston misalignment of ϕ degrees. The error related to this term is,

(73) $E\phi_W = 60 \left| \text{Arc Sin } (\alpha-\beta)' - \text{Arc Sin } (\alpha-\beta) \right| \text{arcseconds}$

where $\text{Sin } k(\alpha-\beta)' = -\text{Sin } k\alpha \text{ Sin } 2\theta_R \text{ Sin } 2\phi_R$

$+ \text{Sin } k\alpha \text{ Cos } k\beta \text{ Cos } 2\theta_R \text{ Cos } 2\phi_R - \text{Cos } k\alpha \text{ Sin } k\beta \text{ Cos } 2\phi_R$

For values of $\phi_R = 0.5^o$ and 5.0^o;

Condition 1 $\alpha = 0 \quad \theta_R = 0$

$\text{Sin } k(\alpha-\beta)' = -\text{Cos } 2\phi_R \text{ Sin } k\beta$

The indicated error over the range of $(\alpha-\beta) = \pm 1800"$ is illustrated in figure E-14 for values of $\phi_R = 0.5^o$ and 5.0^o.

Condition 2 $\alpha = 0 \quad \theta_R = \pm 1^o$

$\text{Sin } k(\alpha-\beta)' = -\text{Cos } 2\phi_R \text{ Sin } k\beta$

Same as Condition 1.

Condition 3 $\alpha = \pm 1800" \quad \theta_R = \pm 1'$

The indicated error over the range of $(\alpha-\beta) = \pm 1800"$ is illustrated and compared with Conditions 1 and 2 in figure E-14 for values of $\phi_R = 0.5^o$ and 5.0^o. The $\theta_R = -1^o$ curves for $\alpha = \pm 1800"$ are not shown because they are within 1" of the $\alpha = 0$ curve.

4.3 Summary

Misalignment of the polarized optical elements will introduce offset and scale factor errors from the ideal case. The type of errors introduced for each condition evaluated are summarized in Table E-4.

E-14 RECEIVER WOLLASTON MISALIGNMENT

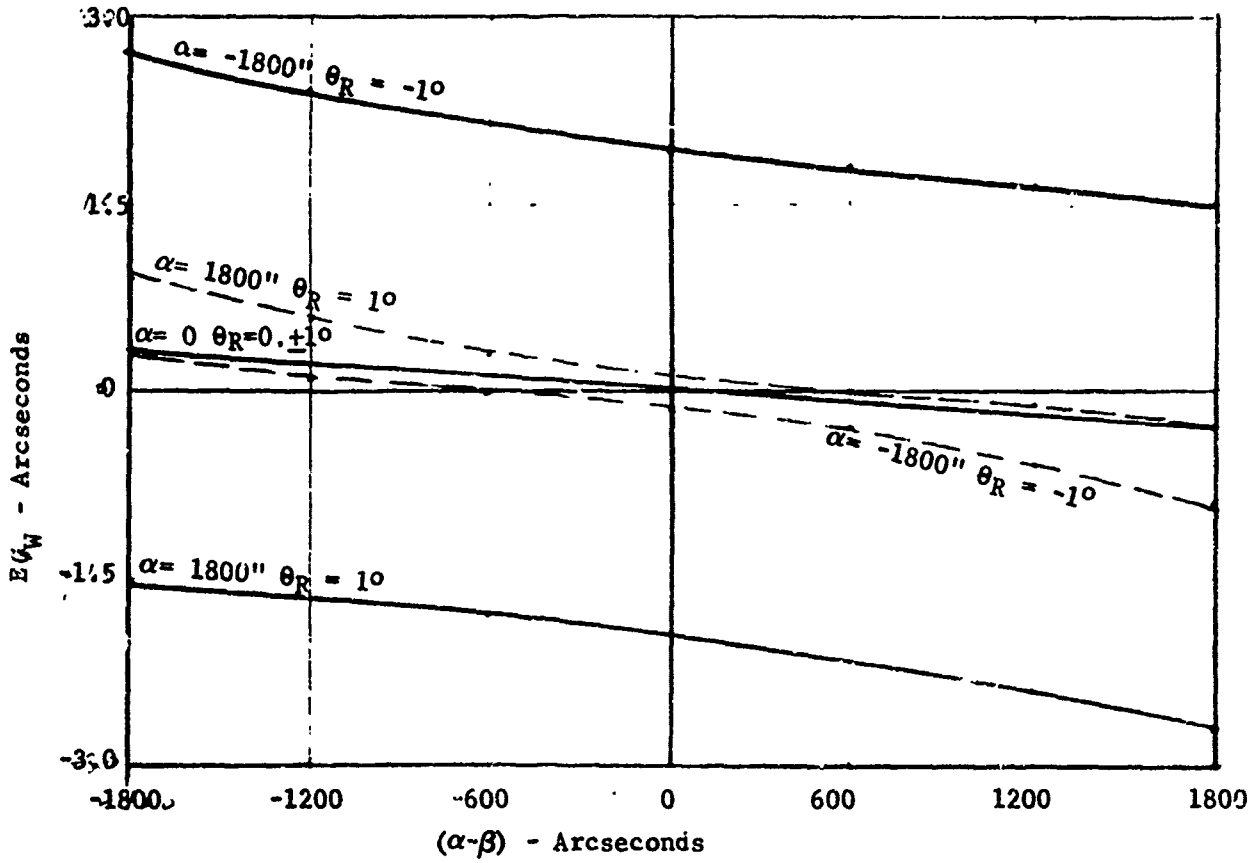

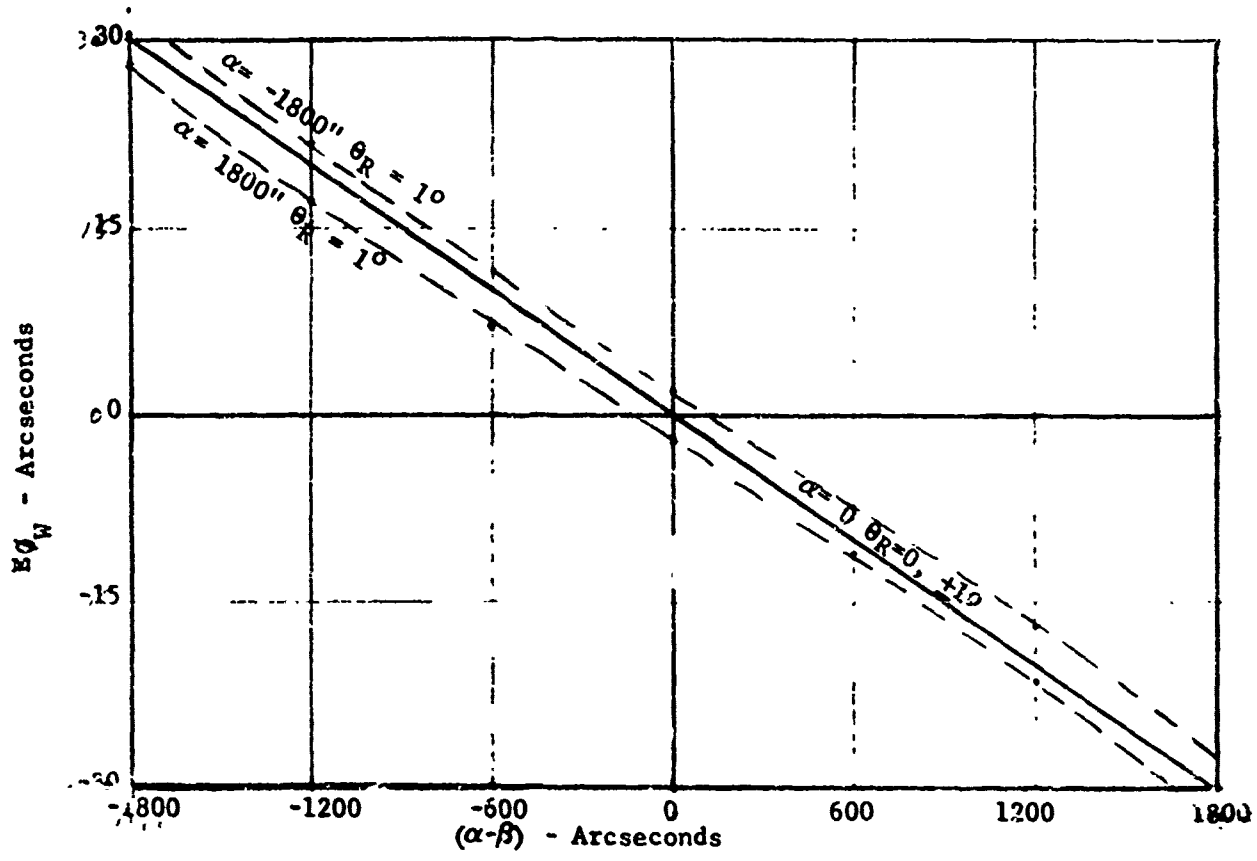

TABLE E-4

OPTICAL ELEMENT	CONDITION		
	1	2	3
$R_{2\theta}$	0	0	X
Q	X	X	X
ASC_{α}	0	0	X
ASC_{α}	S	S	X
W	S	S	X

S - scale factor type error
X - scale factor and offset type error
0 - no error

In all cases, the error terms vary as θ_R and α change over the rotation and translation ranges of $\pm 1^{o}$ and $\pm 1800"$ respectively. Therefore, misalignment of the polarized optical elements cannot be compensated for by calibration and must be controlled during assembly of the optical system.

ANNEX

TECHNICAL REQUIREMENTS

FOR

THE PERFORMANCE AND DESIGN OF THE OPTICAL

ANGULAR MOTION SENSOR

TABLE OF CONTENTS

Section		Page
1.0	SCOPE	1
2.0	REQUIREMENTS	1
	2.1 Performance	1
	2.1.1 Functional Characteristics	1
	2.2 Detailed Interface Definition	4
	2.2.1 Mechanical Interface	4
	2.2.2 Functional Interface	5
	2.2.3 Optical Interface	5
	2.3 General Design Features	5
	2.3.1 Volume	5
	2.3.2 Weight	5
	2.3.3 Multiple Targets	6
	2.3.4 Structure Design	6
	2.3.5 Nuclear Survivability	6

1.0 SCOPE

This specification establishes the requirements and goals for advancing the technology of an Optical Alignment Measurement Sensor (OAMS). Both "requirements" and "goals" are contained in this specification. A requirement must be met in order for the sensor to be acceptable. A goal is not mandatory but would enhance the value of the sensor if it could be met. This method of specifying OAMS parameters is consistent with the intent of a program to advance the state-of-the-art of optical alignment techniques.

2.0 REQUIREMENTS

2.1 Performance

2.1.1 Functional Characteristics

The OAMS unit is a three-axis angular motion sensing device; its electrical output is a function of the angular deflection between a reference object and a remote object at some fixed distance. The OAMS shall consist of two main parts; a transmitter assembly and a target assembly; more than one target assembly may be employed. The main electronics, which interface with other on-board vehicle components, may be integral to the transmitter, or may be in a separate assembly for thermal and electrical isolation.

The design of the OAMS shall be such that it senses relative angular motion (in 3 degrees of rotational freedom) by optical means. Means shall be provided for readily adjusting the OAMS mountings mechanically to achieve an initial three-angle system null; this provision compensates for mounting structure misalignment. Optical surfaces shall be provided on the target assembly for externally monitoring the angular deflection of the assembly.

2.1.1.1 Primary Performance Characteristics

2.1.1.1.1 Measurement Range

As a requirement the OAMS shall have a minimum range of 30 arc minutes for each of three rotational degrees of freedom θ_X, θ_Y, θ_Z, as defined in Figure 1. As goal, a measurement range of 1 degree or more for each axis is desired.

2.1.1.1.2 Calibration

As a goal the output signal of each measurement channel shall be sufficiently linear with deflection that a calibration curve will not be required. If calibration curves are required, each curve shall be defined by a polynomial that expresses the output voltage as a function of angular deflection only. As a requirement, each polynomial shall have not more than 10 terms.

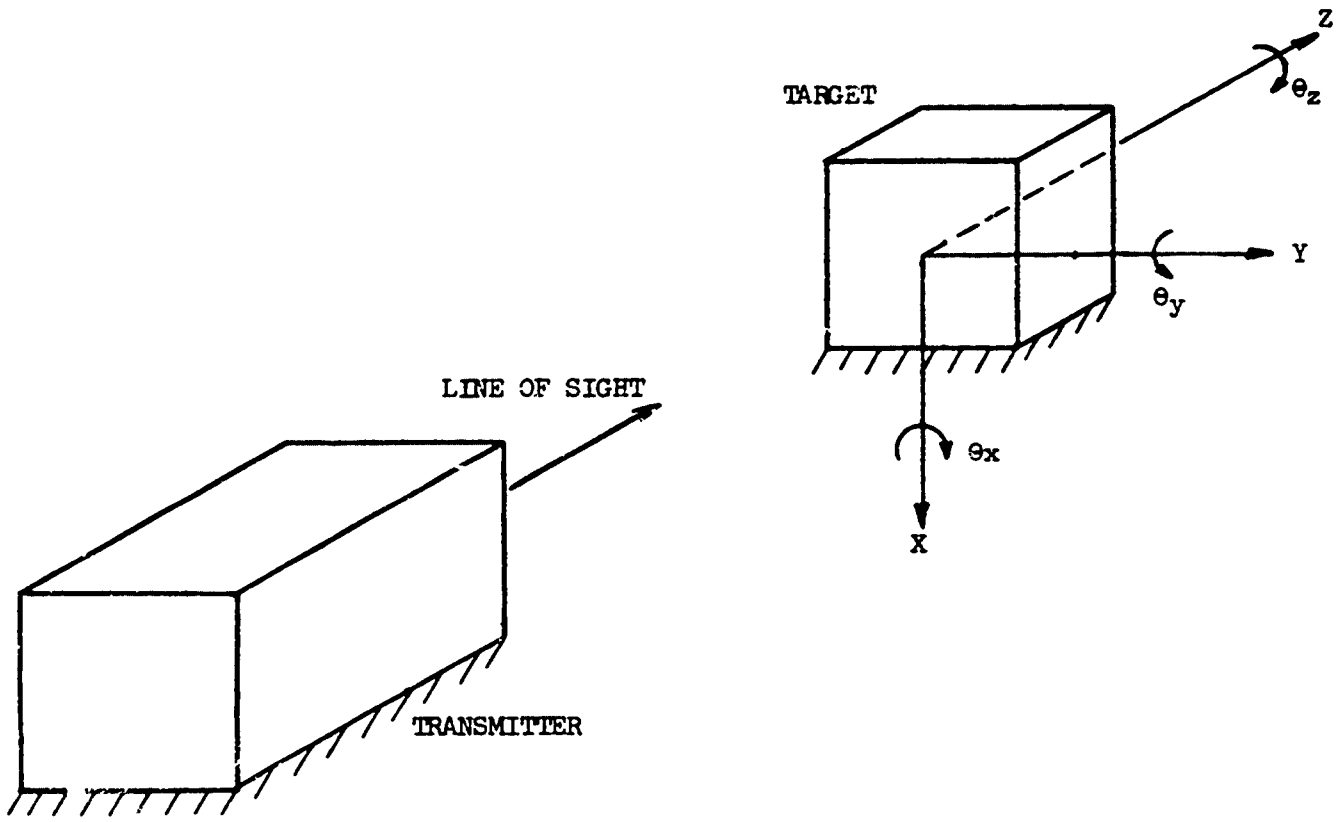

FIGURE 1- GEOMETRIC RELATIONSHIPS

2.1.1.1.3 Accuracy

Specifications are given for allowable systematic and dynamic errors. Systematic errors are those associated with maintaining mounting alignment, calibration and the stability of OAMS output. Dynamic errors are associated with the random variation of the output due to noise within the required system bandwidth

2.1.1.1.3.1 Systematic Errors

As a goal the sum of all systematic errors (mounting alignment, calibration, thermal stability and aging) shall be less than 1 arc second (probability = 0.95, confidence level = 0.95). As a requirement the error shall be less than 5 arc seconds (probability = 0.95, confidence level = 0.95).

2.1.1.1.3.2 Dynamic Error

The dynamic error is stated in terms of the noise equivalent angle (NEA). The NEA is the rms output noise, within the system bandwidth, referenced to the input of the OAMS.

In each of the 3 axes, the NEA, as a goal, shall be less than 1 arc second over the entire measurement range. As a requirement, the NEA shall be less than 5 arc seconds over the entire measurement range.

2.1.1.1.4 Output Signals

Each axis of the OAMS shall provide a bipolar analog readout signal that indicates the direction and magnitude of the angular deflection. The nominal output scale factor shall be less than 1V $\pm$ 5 percent/arc min into a 5-kohm load.

2.1.1.1.5 Saturation Characteristics

For angular deflections greater than full scale, the OAMS shall provide a constant full scale output. Should this condition occur, the unit shall perform within the requirements of this specification within 4 sec after termination of such condition.

2.1.1.1.6 Response Time

The response time (defined as the time to change from 10 to 90 percent of final value) of the OAMS output to a half-scale step angular deflection, in any axis, shall be less than 0.045 sec. In addition, the response to a 10 Hz sinusoidal angular deflection input shall be down by less than 3 db from the response to a 0.1 Hz input.

2.1.1.1.7 Operating Distance

As a goal, the OAMS shall be designed to operate at any selected separation distance up to 50 feet. As a requirement the OAMS shall be designed to operate at any selected separation distance up to 25 feet. Output signal calibration curves shall not be a function of separation distance.

2.1.1.1.8 Temperature Range

The OAMS shall meet the performance requirements specified herein over a temperature range of 0 degrees - 140 degrees F.

2.1.1.1.9 Power Requirements

2.1.1.1.9.1 Input Power

The OAMS shall meet the performance requirements specified herein when supplied with nominal 28 vdc unregulated power from a two-wire, negative-grounded power system having the characteristics described in Paragraph 2.2.2.

2.1.1.1.9.2 Power Consumption

The maximum power required by the OAMS shall be 20 w.

2.1.1.1.9.3 Abnormal Input Power

The OAMS shall not be damaged when subjected to input of from 0 to 24.0 vdc for periods of any duration.

2.1.1.1.9.4 Polarity Reversal

The OAMS shall not be damaged when subjected to normal electrical voltage of reversed polarity.

2.2 Detailed Interface Definition

2.2.1 Mechanical Interface

2.2.1.1 Transmitter Mounting

The transmitter assembly shall be hard mounted to the reference structure.

2.2.1.2 Target Mounting

The target assembly shall be hard mounted to the structure to be monitored. However, the feature of the mounting shall provide for fine adjustments of mounting alignment in order to achieve an initial three-angle system null.

2.2.1.3 Mounting Relationship

The geometrical relationship between the reference and remote monitored structures is shown in Figure 1. The figure also shows the 3 rotational degrees of freedom (roll, pitch and yaw), and defines them as the angular deflections θ_x, θ_y, θ_z, respectively. Rotational and translational motions of the units are defined as follows:

2.2.1.3.1 The transmitter is fixed within the reference system.

2.2.1.3.2 The operating distance between the target and transmitter shall be as defined in paragraph 2.1.1.1.7.

2.2.1.3.3 Maximum operational motions of the target are:

	TRANSLATION			TRANSLATION	
	Goal	Requirement		Goal	Requirement
z	±5.0 in	±1.0 in	z	≥60 arc min	±30 arc min
y	±2.5 in	±0.5 in	y	≥60 arc min	±30 arc min
x	±2.5 in	±0.5 in	x	≥60 arc min	±30 arc min

2.2.2 Functional Interface

2.2.2.1 Input Power

The input power to the OAMS shall have the following characteristics:

2.2.2.1.1 Source Impedance - 0.5 ohm, maximum

2.2.2.1.2 Source Inductance - 2 microhenries, maximum

2.2.2.1.3 Input Voltage - 24.0 to 33.0 vdc

2.2.2.1.4 Ripple Voltage - 0.75v maximum, rms, from 1 Hz to 15 kHz

2.2.2.1.5 Voltage Transients

±56v peak superimposed on the nominal input voltage, 10 sec duration, 1 sec rise time, 5 pps.

2.2.2.2 Output Signals

The OAMS shall provide a bipolar output readout signal for each axis of the OAMS.

2.2.3 Optical Interface

Optically flat alignment surfaces of 1-in-diameter minimum clear aperture shall be provided on the target assembly for external monitoring angular deflection. These surfaces shall be parallel to the target axis planes to within 1 arc min, and orthogonal to each other to within 1 arc min.

2.3 General Design Features

2.3.1 Volume

2.3.1.1 The overall volume of the target assembly shall not exceed 50 cu in as a goal; as a requirement it shall not exceed 150 cu in.

2.3.1.2 The overall volume of the transmitter shall not exceed 200 cu in as a goal; as a requirement it shall not exceed 600 cu in.

2.3.2 Weight

2.3.2.1 The Transmitter Assembly, including electronics, shall not exceed 20 lbs as a goal; as a requirement, the weight shall not exceed 45 lbs.

2.3.2.2 The Target Assembly shall not exceed 3 lbs as a goal; as a requirement it shall not exceed 9 lbs.

2.3.3 Multiple Targets

As a goal, the OAMS shall have the capability to monitor the angular motions of up to 8 equally spaced (angularly) target assemblies with the same capabilities specified for monitoring of a single target.

2.3.4 Structure Design

The OAMS shall be designed with strength adequate to withstand the handling, transportation, and environmental stresses it may be expected to encounter. The structure shall possess sufficient rigidity and stiffness to maintain proper mechanical and optical alignment in relation to its mounting planes.

2.3.5 Nuclear Survivability

The OAMS overall design and major components shall be able to survive in a hostile nuclear space environment according to specifications defined in the JCS Guidelines and SAMSO Exhibit 69-13.